Office de la Propriété Intellectuelle du Canada
Un organisme d'Industrie Canada

Canadian Intellectual Property Office
An agency of Industry Canada

CA 2684052 A1 2008/10/23

(21) 2 684 052

(12) DEMANDE DE BREVET CANADIEN
CANADIAN PATENT APPLICATION

(13) A1

(86) Date de dépôt PCT/PCT Filing Date: 2008/03/12
(87) Date publication PCT/PCT Publication Date: 2008/10/23
(85) Entrée phase nationale/National Entry: 2009/10/09
(86) N° demande PCT/PCT Application No.: US 2008/003422
(87) N° publication PCT/PCT Publication No.: 2008/127532
(30) Priorité/Priority: 2007/04/12 (US60/923,136)

(51) Cl.Int./Int.Cl. *A61K 47/48* (2006.01), *A61K 9/16* (2006.01), *C08G 4/00* (2006.01)

(71) Demandeurs/Applicants:
EMORY UNIVERSITY, US;
GEORGIA TECH RESEARCH CORPORATION, US

(72) Inventeurs/Inventors:
MURTHY, NIREN, US;
DAVIS, MICHAEL, US;
PULENDRAN, BALI, US;
YANG, STEPHEN C., US

(74) Agent: CASSAN MACLEAN

(54) Titre : STRATEGIES INEDITES D'ADMINISTRATION D'AGENTS ACTIFS AU MOYEN DE MICELLES ET DE PARTICULES
(54) Title: NOVEL STRATEGIES FOR DELIVERY OF ACTIVE AGENTS USING MICELLES AND PARTICLES

Polyketals from cyclohexane-dimethanol

A

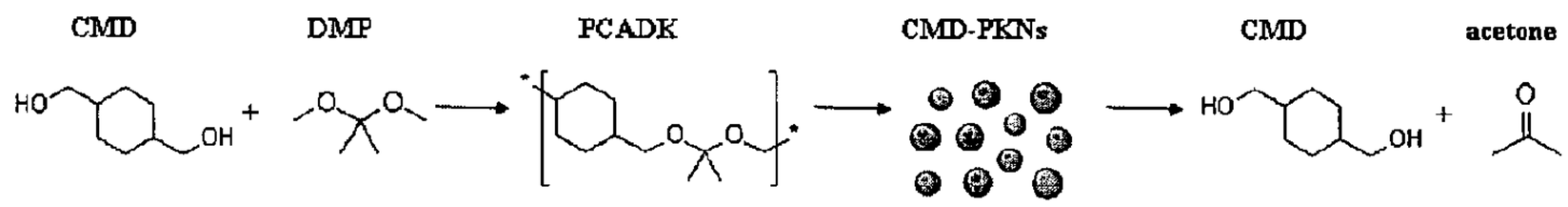

B

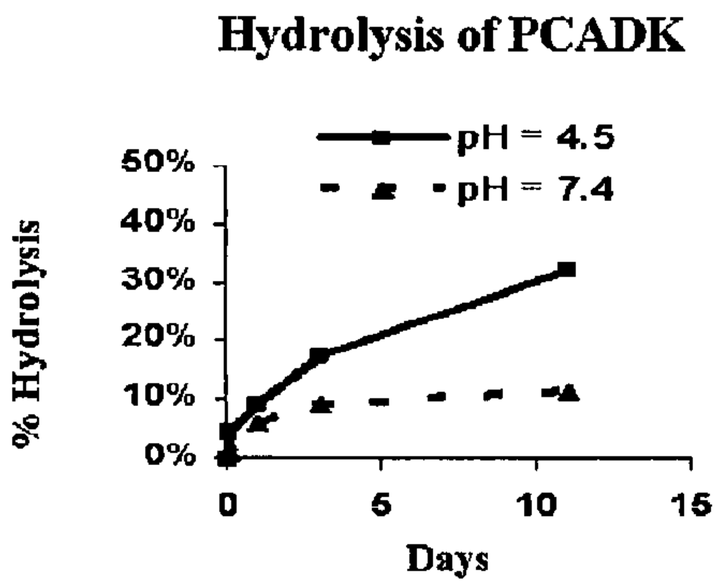

(1) Cyclohexane-dimethanol used in food packaging
(2) Acetone metabolic product of lipids
(3) PCADK Mw = 6,000, PD 1.5
(4) Yield 30-40%

FIG. 19

(57) Abrégé/Abstract:
The present invention provides biodegradable particles (e.g., three-dimensional particles) and micelles which can be used to encapsulate active agents for delivering to a subject. The present invention further provides methods for producing and delivering such particles and micelles. Additionally, the invention provides vaccination strategies that encompass the use of the novel particles and micelles.

(12) INTERNATIONAL APPLICATION PUBLISHED UNDER THE PATENT COOPERATION TREATY (PCT)

(19) World Intellectual Property Organization
International Bureau

(43) International Publication Date
23 October 2008 (23.10.2008)

PCT

(10) International Publication Number
WO 2008/127532 A1

(51) International Patent Classification:
A61K 47/48 (2006.01) *A61K 9/16* (2006.01)
C08G 4/00 (2006.01)

(21) International Application Number:
PCT/US2008/003422

(22) International Filing Date: 12 March 2008 (12.03.2008)

(25) Filing Language: English

(26) Publication Language: English

(30) Priority Data:
60/923,136 12 April 2007 (12.04.2007) US

(71) Applicants *(for all designated States except US)*: **EMORY UNIVERSITY** [US/US]; 1599 Clifton Road NE, 4th Floor, Atlanta, GA 30322 (US). **GEORGIA TECH RESEARCH CORPORATION** [US/US]; 505 Tenth Street, NW, Atlanta, GA 30332-0415 (US).

(72) Inventors; and

(75) Inventors/Applicants *(for US only)*: **MURTHY, Niren** [US/US]; 855 West Peachtree Street, Apt. 1628, Atlanta, GA 30308 (US). **DAVIS, Michael** [US/US]; 1920 Fisher Trail, Atlanta, GA 30345 (US). **PULENDRAN, Bali** [AU/US]; 335 Brook Ford Point, Alpharetta, GA 30322 (US). **YANG, Stephen, C.** [US/US]; 6076 Indian Wood Circle, Mableton, GA 30126 (US).

(74) Agent: **ADRIANO, Sarah**; Mandel & Adriano, 572 E. Green Street, Suite 203, Pasadena, CA 91101 (US).

(81) Designated States *(unless otherwise indicated, for every kind of national protection available)*: AE, AG, AL, AM, AO, AT, AU, AZ, BA, BB, BG, BH, BR, BW, BY, BZ, CA, CH, CN, CO, CR, CU, CZ, DE, DK, DM, DO, DZ, EC, EE, EG, ES, FI, GB, GD, GE, GH, GM, GT, HN, HR, HU, ID, IL, IN, IS, JP, KE, KG, KM, KN, KP, KR, KZ, LA, LC, LK, LR, LS, LT, LU, LY, MA, MD, ME, MG, MK, MN, MW, MX, MY, MZ, NA, NG, NI, NO, NZ, OM, PG, PH, PL, PT, RO, RS, RU, SC, SD, SE, SG, SK, SL, SM, SV, SY, TJ, TM, TN, TR, TT, TZ, UA, UG, US, UZ, VC, VN, ZA, ZM, ZW.

(84) Designated States *(unless otherwise indicated, for every kind of regional protection available)*: ARIPO (BW, GH, GM, KE, LS, MW, MZ, NA, SD, SL, SZ, TZ, UG, ZM, ZW), Eurasian (AM, AZ, BY, KG, KZ, MD, RU, TJ, TM), European (AT, BE, BG, CH, CY, CZ, DE, DK, EE, ES, FI, FR, GB, GR, HR, HU, IE, IS, IT, LT, LU, LV, MC, MT, NL, NO, PL, PT, RO, SE, SI, SK, TR), OAPI (BF, BJ, CF, CG, CI, CM, GA, GN, GQ, GW, ML, MR, NE, SN, TD, TG).

Published:
— *with international search report*

(54) Title: NOVEL STRATEGIES FOR DELIVERY OF ACTIVE AGENTS USING MICELLES AND PARTICLES

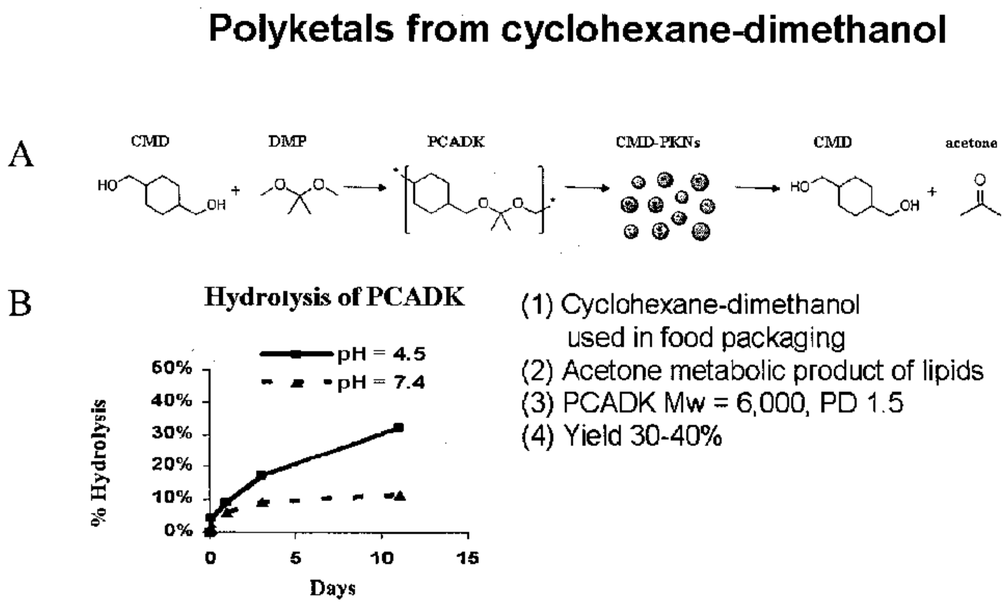

FIG. 19

(57) Abstract: The present invention provides biodegradable particles (e.g., three-dimensional particles) and micelles which can be used to encapsulate active agents for delivering to a subject. The present invention further provides methods for producing and delivering such particles and micelles. Additionally, the invention provides vaccination strategies that encompass the use of the novel particles and micelles.

WO 2008/127532 A1

NOVEL STRATEGIES FOR DELIVERY OF ACTIVE AGENTS USING MICELLES AND PARTICLES

Throughout this application various publications are referenced. The disclosures of these publications in their entireties are hereby incorporated by reference into this application in order to more fully describe the state of the art to which this invention pertains.

This invention was made with government support under NIH/NIAID grant AI048638, AI0564499, AI056947, AI057157, AI05726601, NIH/NIDDK grant DK057665 and Emtech Bio Grant, NIH R01 application. The government has certain rights in the invention.

FIELD OF THE INVENTION

The invention relates to particle and micelle based strategies for delivering active agents, such as (i) vaccines; (ii) immune modulatory agents, (including TLR ligands or synthetic molecules, which modulate the function of innate immune cells such as dendritic cells, or synthetic molecules or siRNA that modulate signaling networks within cells (e.g., dendritic or other antigen presenting cells) and/or; (iii) drugs that target antigen-presenting cells so as to modulate innate and adaptive immunity, in a therapeutic or prophylactic setting.

BACKGROUND OF THE INVENTION

Drug delivery vehicles based on polyesters and polyanhydrides have been widely used for the sustained release of therapeutics because of their excellent biocompatibility profiles and slow hydrolysis rates (Anderson, J.M. et al., *Adv. Drug Delivery Rev.*, 1997,

28:5-24; Jain, R.A., *Biomaterials*, 2000, 21:2475-2490; Mathiowitz, E. et al., *J. Appl. Polym. Sci.*, 1988, 35:755-774; Berkland, C. et al., *J. Controlled Release*, 2004, 94:129-141). However, numerous medical applications, such as targeting the acidic environment of lysosomes and tumors, require drug delivery systems that undergo rapid, pH-sensitive degradation (Stubbs, M. et al., *Mol. Med. Today*, 2000, 6:15-19; Leroux, J.-C., *Adv. Drug Delivery Rev.*, 2004, 56:925-926). The majority of degradable polymers used for drug delivery cannot fulfill this requirement because they are composed of ester linkages, which degrade by base-catalyzed hydrolysis at physiological pH values. Particles made of ester based materials, such as Poly(lactic-glycolic acid) (PLGA), polyorthoesters, and polyanhydrides, all generate high quantities of acid when they degrade. This causes degradation of protein and DNA therapeutics and the degradation also takes weeks to months. Because the life span of mature DCs is around 2 days these materials are not ideal for vaccine development. Recently, pH sensitive hydrophobic microparticles based on poly(orthoesters) and poly(beta-amino esters) have been successfully used for intracellular drug delivery and tumor targeting, thus demonstrating the potential of acid-sensitive biomaterials for drug delivery (Heller, J. et al., *Biomacromolecules*, 2004, 5:1625-1632; Heller, J. et al., *Adv. Drug Delivery Rev.*, 2002, 54:1015-1039; Berry, D. et al., *Chem. Biol.*, 2004, 11:487-498; Potineni, A. et al., *J. Controlled Release*, 2003, 86:223-234). Consequently, there is great interest in developing new strategies for the synthesis of pH-sensitive biodegradable polymers.

Vaccines based on recombinant proteins, peptide antigens, or DNA vaccines encoding such vaccine antigens, have tremendous therapeutic potential against infectious diseases and tumors, in which the antigenic epitopes have been defined. Such vaccines have been capable of generating protective immunity against infectious diseases, in animal models, and numerous clinical trials with such vaccines are currently in progress (van Endert, PM, *Biologicals*, 2001, 29:285-8; Purcell, AW et al., *Journal of Peptide Science*, 2003, 9:255-81; Shirai, M. et al., *Journal of Virology*, 1994, 68:3334-42; Hunziker, IP et al., *International Immunology*, 2002, 14:615-26). However, despite their promise, a major challenge concerns the efficient delivery of peptides, proteins, DNA vaccines and adjuvants, so as to target the appropriate type of antigen presenting cell in order to launch

an effective immune response. Although promising results have been obtained with peptide vaccines composed of lipid conjugates and PLGA microparticles, there is still a great need for the development of new peptide vaccine delivery vehicles (Ertl, HCJ et al., *Vaccine*, 1996, 14:879-85; Jackson, DC et al., *Vaccine*, 1997, 15:1697-705).

Harnessing Innate Immunity for Vaccination

A hallmark of the immune system is its ability to launch qualitatively different types of immune responses. Thus for example, T-helper 1 (or Th1) immune responses stimulate cytotoxic "killer" T cells, which kill virally infected cells or tumors. In contrast, T-helper 2 (or Th2) responses are associated with antibody production, particularly secretion of IgE antibodies, which confer protection against extracellular parasites or bacteria or toxins. Furthermore, T regulatory responses can suppress over exuberant immune responses, and thus limit the immune pathology caused by allergies, autoimmunity, transplant rejection, or sepsis like symptoms. Given the existence of such diverse types of immune responses, and their differential roles in conferring effective protection against viruses, tumors, extracellular parasites and bacteria, and in regulating deleterious immune responses in allergies, autoimmunity, transplantation and sepsis, a "rosetta stone" of modern immunology is to learn how to induce optimally effective immune responses in various clinical settings.

In this context, recent advances in immunology have revealed a fundamental role for the innate immune system in controlling both the quality and quantity of immune responses (Pulendran & Ahmed, Cell, 2006, 124:849-863). Thus, it has long been known that the immune system is unresponsive to most foreign proteins that are injected in a soluble, deaggregated form, but when injected together with immune-stimulating substances called "adjuvants," these foreign proteins can induce robust immunity. In fact it was known that the nature of the adjuvant is what determines the particular type of immune response that follows, which may be biased towards cytotoxic T-cell responses, antibody responses, or particular classes of T-helper responses (Pulendran, Immunol. Rev., 2004, 199:227-250; Pulendran, J. Immunol., 2005, 175:2457-2465; Pulendran & Ahmed, Cell,

2006, 124:849-863). Despite the importance of adjuvants, there is only one adjuvant, alum, licensed for clinical use in the United States, and most other experimental adjuvants consist of crude extracts of microbes or bacteria, which induce potent activation of immune cells, but also result in toxicities. Until recently, the mechanism of action of such adjuvants was not understood. However, recent advances in innate immunity have offered a conceptual framework with which to understand how adjuvants function. Central to this issue is a rare but widely distributed network of cells known as dendritic cells (DCs), which constitute an integral component of the innate immune system. DCs, which have been called 'Nature's adjuvants,' express receptors which can recognize components of microbes and viruses. Such receptors include the Toll-like receptors (TLRs), C-type lectins, and CATTERPILLAR proteins, which can "sense" microbial stimuli, and activate DCs and other immune cells (Pulendran, Immunol. Rev., 2004, 199:227-250; Pulendran, J. Immunol., 2005, 175:2457-2465; Pulendran & Ahmed, Cell, 2006, 124:849-863). It is now clear that DCs play essential roles in orchestrating the quality and quantity of the immune response.

There are currently some 13 TLRs described in mammals. Activating distinct TLRs on DCs induces qualitatively different types of immune responses (Pulendran, et al, 2001, *supra*; Dillon et al, 2004, *supra*; Agrawal et al, J. Immunol., 2003, 171:4984-4989; Dillon et al, J. Clin. Immunol., 2006, 116:916-928). Thus, activating most TLRs can induce Th1 responses; activating TLR3, 7 or 9 can induce cytotoxic T cells that kill virally infected cells and tumors; and emerging evidence suggests that activating TLR2 induces Th2 responses, (which are associated with antibody responses that offer protection against viruses or extracellular bacteria or parasites), or even T regulatory or tolerogenic responses, (which suppress over exuberant immune responses, and thus offer protection against unbridled immunity in allergies, autoimmunity, sepsis, and transplantation). As such, DCs and TLRs and other recognition receptors, represent attractive immune modulatory targets for vaccinologists and drug developers. Thus learning how to exploit fundamental elements of the innate immune system such as DCs and TLRs, is of paramount importance in the development of novel drugs and vaccines.

An important corollary to this notion is that the vast majority of vaccines which have been developed over the past 200 years, (since the first recorded vaccination trial of Edward Jenner), have been developed empirically. Therefore, despite their successes in controlling various scourges such as smallpox, polio, TB and yellow fever, we have no knowledge of the scientific rationale for how these vaccines stimulate such effective immunity. For example, the yellow fever vaccine 17D [YF-17D] is one of the most effective vaccines known. Since its development more than 65 years ago, it has been administered to over 400 million people globally. Despite its success, the mechanism of its action is not known. Therefore, as stated above, the spectacular advances in innate immunity which have occurred in the last six years or so, offer us a new vision with which to understand the modus operandi of such "gold standard" vaccines, with a view to using such knowledge to devising future vaccines against emerging and re-emerging infections of the 21st century. In this context, our recent findings suggest that the highly effective Yellow Fever Vaccine (YF-17D) is a potent stimulator of DCs, and multiple TLRs, including TLR 2, 7, 8 and 9 (Querec et al., J. Exp. Med., 2006, 203:413-421). Given, the different types of immune responses triggered by the distinct TLRs (Pulendran et al., 2001, *supra*; Agrawal et al., J. Immunol., 2003, 171:4984-4989; Dillon et al, 2004, *supra*; Dillon et al, J. Clin. Immunol., 2006, 116:916-928), it was tempting to speculate that by activating multiple TLRs, YF-17D was inducing a broad spectrum of immune responses. Indeed, our data suggests that YF-17D triggers a broad spectrum of innate and adaptive immune responses (Th1, Th2, cytotoxic T cells, neutralizing antibody), and that distinct TLRs control different types of this polyvalent immunity (Querec et al., J. Exp. Med., 2006, 203:413-421). Eliciting such a broad spectrum of immune responses is also likely to be beneficial in designing vaccines against other infections, against which no effective vaccines currently exist, such as HIV, HCV, malaria, TB, influenza, anthrax and Ebola, or against tumors. Thus, strategies for designing future vaccines against emerging or re-emerging infections might benefit from incorporating multiple TLR ligands plus antigens, plus immune modulatory agents, in order to induce multi-pronged immune responses. Therefore, an important challenge is the development of delivery systems which are capable of delivering such immune modulatory agents in vivo.

Congestive heart failure is a leading cause of morbidity and mortality worldwide and effective treatment options are greatly needed. Cardiac dysfunction following myocardial infarction is a progressive disease and any successful therapy is needed over the course of several days/weeks (Anversa, P., Myocyte death in the pathological heart. *Circ Res*, 2000. 86(2): 121-4).

Acute myocardial infarction patients are traditionally treated at the hospital with blood thinning agents and/or angioplasty to try to clear the affected vessels. Local cell death that occurs during this acute period leads to chronic heart failure, marked by increased ventricular size and reduced contractile function (Anversa, P., Myocyte death in the pathological heart. *Circ Res*, 2000. 86(2):121-4). Currently, the only treatment for heart failure is transplantation surgery and it is estimated that less than 30% of transplant patients survive to receive their new heart (Rosamond et al., Heart Disease and Stroke Statistics--2007 Update. A Report From the American Heart Association Statistics Committee and Stroke Statistics Subcommittee. *Circulation*, 2006). A number of processes take place shortly following infarction have been the target of potential therapeutic approaches.

The loss of myocardium is mainly regional and suggests that localized therapy holds the most promise (Anversa, P., Myocyte death in the pathological heart. *Circ Res*, 2000. 86(2):121-4). In recent years, many clinical studies have been initiated to deliver localized therapy in the form of various cell types for reconstitution of the myocardium (Assmus et al., Transplantation of Progenitor Cells and Regeneration Enhancement in Acute Myocardial Infarction (TOPCARE-AMI). *Circulation*, 2002. 106(24): 3009-17; Kang et al., Effects of intracoronary infusion of peripheral blood stem-cells mobilised with granulocyte-colony stimulating factor on left ventricular systolic function and restenosis after coronary stenting in myocardial infarction: the MAGIC cell randomised clinical trial. *Lancet*, 2004. 363(9411):751-6).

Due to the complex nature of direct protein, RNA and DNA injections, efforts have now focused on using biomaterials to deliver therapeutics to the myocardium (Davis et al.,

Custom design of the cardiac microenvironment with biomaterials. *Circ Res*, 2005. 97(1):8-15). While many studies still utilize intravenous injection or oral therapy, the exact mechanism of action remains relatively unknown. Specifically, it is not examined how these molecules/proteins are able to enter orally or intravenously and exert significant effects on solely the heart. Our prior studies have used direct intramyocardial injection for the delivery of biomaterials carrying proteins and drugs (Davis et al., Local myocardial insulin-like growth factor 1 (IGF-1) delivery with biotinylated peptide nanofibers improves cell therapy for myocardial infarction. *Proc Natl Acad Sci U S A*, 2006. 103(21):8155-60; Davis et al., Injectable self-assembling peptide nanofibers create intramyocardial microenvironments for endothelial cells. *Circulation*, 2005. 111(4):442-50; Hsieh et al., Controlled delivery of PDGF-BB for myocardial protection using injectable self-assembling peptide nanofibers. *J Clin Invest*, 2006. 116(1):237-48). While one would think this is detrimental, it is becoming increasingly more popular for human use as several companies have developed catheters capable of delivering cells and drugs to the myocardial wall from the inside of the chamber. Additionally, using new techniques, investigators have been able to deliver microspheres to the myocardial wall of mice in a close-chested procedure (Springer et al., Closed-chest cell injections into mouse myocardium guided by high-resolution echocardiography. *Am J Physiol Heart Circ Physiol*, 2005. 289(3):H1307-14). Thus, there is great interest in the development of small, injectable particles for myocardial therapy.

p38 MAP Kinase

Specific inflammatory cytokines are greatly increased in the myocardium following infarction (Bolli, R., Oxygen-derived free radicals and myocardial reperfusion injury: an overview. *Cardiovasc Drugs Ther*, 1991. 5 Suppl 2:249-68; Bolli, et al., Direct evidence that oxygen-derived free radicals contribute to postischemic myocardial dysfunction in the intact dog. *Proc Natl Acad Sci U S A*, 1989. 86(12):4695-9; Torella, et al., Cardiac stem cell and myocyte aging, heart failure, and insulin-like growth factor-1 overexpression. *Circ Res*, 2004. 94(4):514-24). These cytokines activate specific signaling pathways leading to death of adult cardiac myocytes and the local stem cell populations.

Three distinct mitogen activated protein kinase (MAPK) cascades have been identified and studied as cell signaling pathways. The p38 MAPK cascade has been well characterized in stress and the inflammatory response (Lai et al., The role of MAP kinases in trauma and ischemia-reperfusion. *J Invest Surg*, 2004. 17(1):45-53; Lopez-Neblina and Toledo-Pereyra, Phosphoregulation of signal transduction pathways in ischemia and reperfusion. *J Surg Res*, 2006. 134(2):292-9). Also, the p38 MAPK pathway has been implicated in the death of adult cardiac myocytes by use of transgenic mouse models as well as gene therapy studies (Engel et al., p38 MAP kinase inhibition enables proliferation of adult mammalian cardiomyocytes. *Genes Dev*, 2005. 19(10):1175-87; Awad et al., Obese diabetic mouse environment differentially affects primitive and monocytic endothelial cell progenitors. *Stem Cells*, 2005. 23(4):575-83).

There are 4 distinct isoforms of p38 with p38α being the most studied and implicated in disease processes. Like several MAPK, p38 is activated by dual phosphorylation (using ATP as a phosphate donor) through a variety of upstream mechanisms and its function is conserved across several cell types. Activation of p38 in macrophages leads to superoxide production, as well as increased expression of pro-inflammatory cytokines. In fibroblasts, activation of p38 leads to production of cytokines, as well as activation of pro-fibrotic cascades (Kumar et al., p38 MAP kinases: key signalling molecules as therapeutic targets for inflammatory diseases. *Nat Rev Drug Discov*, 2003. 2(9): 717-26). Finally, in cardiac myocytes, p38 activation leads to apoptosis, as well as release of cytokines (Li et al., Selective inhibition of p38alpha MAPK improves cardiac function and reduces myocardial apoptosis in rat model of myocardial injury. *Am J Physiol Heart Circ Physiol*, 2006. 291(4):H1972-7; Ren et al., Role of p38alpha MAPK in cardiac apoptosis and remodeling after myocardial infarction. *J Mol Cell Cardiol*, 2005. 38(4):617-230). All 3 of these processes play a critical role in the progression of cardiac dysfunction following infarction. Figure 29 shows a general schematic of p38 activation, including activation of upstream effectors and consequences of activation.

Phosphorylation of p38 leads to activation of 2 critical pathways in the disease process, including caspases and nuclear factor kappa B (NFκB) (Chen and Tu, Apoptosis and heart failure: mechanisms and therapeutic implications. *Am J Cardiovasc Drugs*, 2002. 2(1):43-57). During apoptosis, phosphorylation of p38 induces activation of Bax, which eventually leads to mitochondrial permeability, resulting in cleavage of caspases and induction of apoptosis. In an alternate pathway following p38 phosphorylation, the inhibitory protein IκB is phosphorylated, releasing NFκB to the nucleus where activation of inflammatory cytokines can commence (Aggarwal et al., TNF blockade: an inflammatory issue. *Ernst Schering Res Found Workshop*, 2006(56):161-86). Both of these pathways have been targeted for a variety of inflammatory diseases including arthritis, ischemia/reperfusion injury and airway inflammation (Herlaar and Brown, p38 MAPK signalling cascades in inflammatory disease. *Mol Med Today*, 1999. 5(10):439-47; Karin, M., Inflammation-activated protein kinases as targets for drug development. *Proc Am Thorac Soc*, 2005. 2(4):386-90; discussion 394-5; Lee et al., Inhibition of p38 MAP kinase as a therapeutic strategy. *Immunopharmacology*, 2000. 47(2-3):185-201; Peifer et al., New approaches to the treatment of inflammatory disorders small molecule inhibitors of p38 MAP kinase. *Curr Top Med Chem*, 2006. 6(2):113-49; Schieven, G.L., The biology of p38 kinase: a central role in inflammation. *Curr Top Med Chem*, 2005. 5(10):921-8).

Suppression of p38 activation with genetic knockout models, gene therapy and inhibitor administration has had beneficial effects on preventing the contractile dysfunction after myocardial infarction (Engel et al., p38 MAP kinase inhibition enables proliferation of adult mammalian cardiomyocytes. *Genes Dev*, 2005. 19(10):1175-87; Minamino et al., MEKK1 suppresses oxidative stress-induced apoptosis of embryonic stem cell-derived cardiac myocytes. *Proc Natl Acad Sci U S A*, 1999. 96(26):15127-32; Kaiser et al., Inhibition of p38 reduces myocardial infarction injury in the mouse but not pig after ischemia-reperfusion. *Am J Physiol Heart Circ Physiol*, 2005. 289(6):H2747-51; Kumar et al., p38 MAP kinases: key signalling molecules as therapeutic targets for inflammatory diseases. *Nat Rev Drug Discov*, 2003. 2(9): 717-26; Kulik et al., Antiapoptotic signalling by the insulin-like growth factor I receptor, phosphatidylinositol 3-kinase, and Akt. *Mol*

Cell Biol, 1997. 17(3):1595-606; Liu et al., Inhibition of p38 mitogen-activated protein kinase protects the heart against cardiac remodeling in mice with heart failure resulting from myocardial infarction. *J Card Fail*, 2005. 11(1):74-81; See et al., p38 mitogen-activated protein kinase inhibition improves cardiac function and attenuates left ventricular remodeling following myocardial infarction in the rat. *J Am Coll Cardiol*, 2004. 44(8):1679-89). This is widely thought to be due to a variety of mechanisms including inhibition of apoptosis, induction of cardiac myocyte proliferation, reduction in oxidative stress and prevention of pro-fibrotic gene expression. When delivered to mice, the p38 inhibitor SB-282 improved cardiac function in a rat model of cardiac injury (Li et al., Selective inhibition of p38alpha MAPK improves cardiac function and reduces myocardial apoptosis in rat model of myocardial injury. *Am J Physiol Heart Circ Physiol*, 2006. 291(4):H1972-7). Rats that were fed this compound for several days after L-NAME, salt and Angiotensin II treatment showed significant improvements in contractile function and other cardiac parameters. Additionally, in a mouse model of ischemia/reperfusion, SB239063 infused through the tail vein immediately prior to ischemia prevented p38 phosphorylation and reduced the infarct size after 24 hours. It was noted in this study that the findings did not translate to larger animals. Pigs underwent a similar procedure and showed no benefit of p38 inhibition immediately after reperfusion. It is important to understand, however, that in this study the investigators injected the pigs prior to ischemia-reperfusion and gave the inhibitor as a bolus dose in the lumen of the left ventricle (Kaiser et al., Inhibition of p38 reduces myocardial infarction injury in the mouse but not pig after ischemia-reperfusion. *Am J Physiol Heart Circ Physiol*, 2005. 289(6):H2747-51). Thus, it is unlikely that much of the inhibitor was retained within the myocardium in the time frame needed. Interestingly, recent studies performed with the p38 inhibitor SB203580 demonstrated a critical role of p38 inhibition in the modulating the ability of adult cardiac myocytes to re-enter the cell cycle. Treatment with the p38 inhibitor every 3 days resulted in a significant increase in cardiac myocyte proliferation marker staining after myocardial infarction (Engel et al., p38 MAP kinase inhibition enables proliferation of adult mammalian cardiomyocytes. *Genes Dev*, 2005. 19(10):1175-87). While interesting, it is unclear as to the exact benefit as the total amount of cycling myocytes rose less than a percent. Our proposal will examine the

effects of sustained p38 inhibition on cardiac myocyte apoptosis in larger rodents and create a gateway to examining the sustained release of the p38 inhibitor in larger mammals.

Although the p38 kinase inhibitor SB239063 prevented cardiac dysfunction in mice following infarction, this effect was not translated to larger animals (Burnham et al., Increased circulating endothelial progenitor cells are associated with survival in acute lung injury. *Am J Respir Crit Care Med*, 2005. 172(7):854-60). This is most likely due to the small size of the inhibitor and its likely rapid diffusion from the site of injection. Most successful therapeutic outcomes with small molecule inhibitors require multiple injections over longer time periods to recover function, which is not feasible for human intervention. For these reasons, a therapeutic approach that requires only one dose/injection would be largely advantageous to existing treatment options.

As described herein, polyketal (PK) particles are a new class of biomaterials that hydrolyzė in a controllable manner at physiological pH values and degrade into neutral compounds.

SUMMARY OF THE INVENTION

The present invention provides biodegradable particles (e.g., three-dimensional particles) and micelles which can be used to encapsulate active agents for delivering to a subject. The present invention further provides methods for producing and delivering such particles and micelles. Additionally, the invention provides vaccination strategies that encompass the use of the novel particles and micelles.

Hydrophobic Polyketal Particles

The present invention is directed to new type of hydrophobic polymers comprising ketal groups in the polymer backbone wherein the ketal groups are arranged in a way such that both oxygen atoms are located in the polymer backbone.

Further, the ketal polymer can be formed via a ketal exchange reaction between a ketal and a diol. In accordance with the invention, one or more types of the ketals and/or diols can be used for the formation of a homopolymer or copolymer.

Also encompassed by the present invention are polyketal polymers which are joined by other polymers (e.g. PEG, polyesters, polyamides, polysaccharides, polyethers, or polyanhydrides). The resulting polymers can be alternating copolymers, random copolymers, block copolymers, or graft copolymers. Polythioketal polymers, mixed polythio-amine ketals, polythio-hydroxyl ketals and polyhydroxyl-amine ketals are also in the scope of the present invention.

Polyketal polymers of the invention hydrolyze in aqueous solutions into low molecular weight, water soluble alcohols and ketones. The advantage of a ketal linkage in the backbone is that it degrades under acidic conditions of phagosomes, within 1-2 days at pH 5.0. Polyketals can therefore also be used for targeting the acidic environments of tumors, inflammation and phago-lysosomes. The degradation does not generate acidic degradation products. Thus, the ketal polymers are suitable for biological use.

Micelles

The present invention further provides novel biodegradable crosslinked micelles comprising multiple polymers, wherein the polymers are e.g., crosslinked by an external crosslinking agent (i.e., agents which are not introduced into the polymer chain). The advantage of using of external agents is the faster crosslinking reaction compared to a

reaction wherein only crosslinkable moieties within the polymer are used. The external crosslinking agent also decreases the chances that the encapsulated is protein destroyed.

BRIEF DESCRIPTION OF THE FIGURES

Figure 1 is a bar graph showing the fluorescence intensity of filtered and unfiltered PKNs with FITC-Ova (excitation 494 nm, emission 520 nm). The data shown is the average of two samples. The FITC-Ova encapsulation efficiency is 60% (Example 3, *infra*).

Figure 2 is a diagrammatic representation showing the synthesis and degradation of Ketal-backbone polymer (polyketal). (A) Ketal exchange reaction between 1,4-benzenedimethanol and 2,2-dimethoxypropane to produce the ketal intermediate 1. (B) Stepwise polymerization of 1 to produce polyketal 2. Reaction steps A and B are driven forward by distilling off the methanol byproduct. (C) Formation of drug-loaded particles by the solvent evaporation method. Particles exhibit pH-sensitive degradation into low molecular weight excretable compounds (Example 4, *infra*).

Figure 3(A) is a graph showing a GPC trace of polyketal 2 (of Figure 2) in THF (Shimadzu SCL-10A). M_w = 4000, M_w/M_n = 1.54 based on a polystyrene standard (Polymer Laboratories, Inc.). Y-axis indicates relative absorbance at 262 nm. Figure 3(B) shows ^{1}H NMR spectrum of polyketal 2 (of Figure 2) in $CDCl_3$ (Varian Mercury Vx 400); repeating unit peaks at 7.3 ppm (4b), 4.5 ppm (4c), and 1.5 ppm (6a). Peaks at 2.5 and 1.0 are due to triethylamine added to prevent ketal hydrolysis. (Example 4, *infra*)

Figure 4 is a line graph showing the hydrolysis kinetics of polyketal 2 (of Fig. 2) (finely ground powder) at pH 1.0, 5.0, and 7.4. Exponential decay half-lives are 102 h (pH 7.4) and 35 h (pH 5.0). The pH 1.0 control batch was completely hydrolyzed before the first time point. (Example 4, *infra*)

Figure 5 shows SEM images of particles made with polyketal 2 (of Fig. 2). (A,B) Particles using 0.2:1 ratio of PVA to polyketal 2 (particle size: 0.5 – 30 μm). (C) Dexamethasone-loaded particles made using 1:1 PVA:polyketal 2 (particle size: 200 – 500 nm). Scale bars are (A) 80 μm, (B) 3 μm, and (C) 4 μm. (Examples 5 and 6, *infra*)

Figure 6 is a schematic representation showing particle formation. A. Step 1: Dissolve polyketal and drug into chloroform; dissolve polyvinyl alcohol in water. B. Step 2: Add chloroform solution to water and sonicate, generate micron sized droplets. Step 3: Let chloroform evaoporate, generates particles. (Example 6, *infra*)

Figure 7 is a photograph showing polyketal particles loaded with Fluorescein are taken up in the liver. Murine liver tissue slice is shown releaing fluorescein from PKNs following intravenous injection. (Example 6, *infra*)

Figure 8 is a schematic diagram showing a peptide crosslinked micelle design and synthesis. Step 1: ISS DNA and I are mixed to form micelles (uncrosslinked micelle). Step 2: These micelles are then crosslinked with the antigenic peptide (II) to generate a delivery system that can encapsulate both immunostimulatory molecules and peptide antigens. After phagocytosis by APCs, the peptide-crosslinked micelles release their components. (Example 6, *infra*)

Figure 9 shows the synthesis and characterization of PEG-polylysine thiopyridal. A. is a chemical diagram showing the synthesis of PEG-polylysine thiopyridal. B is a 1H-NMR spectrum of PEG-PLL-thiopyridal in D_2O. C./D are graphs depicting the dynamic light scattering analysis of PCMs uncross-linked (C) and peptide cross-linked (D). E is a graph showing the crosslinking reaction of cysteines on peptide anigen II (Fig. 8). F is a graph showing the UV analysis of crosslinking reaction between peptide anigen II (Fig. 8) and block copolymer micelles. (Example 6, *infra*)

Figure 10 shows the effect of GSH on release of peptides and DNA A is a graph showing GSH sensitive peptide release. B is a gel elecrophoresis analysis showing GSH sensitive

DNA release. C is a gel elecrophoresis analysis showing ISS-DNA is protected from serum nucleases in the PCMs. (Example 6, *infra*)

Figure 11 depicts block copolymer micelles. A depicts the chemical structure of PEG-poly(lysine-thio-pyridyl). B is a schematic diagram showing micelle formation. C is a schematic diagram showing crosslinking of micelles. D is a schematic diagram showing reducing of crosslinked micelles. (Example 6, *infra*)

Figure 12 shows the immunology of micelle. A. Confocal microscopic analysis of the uptake of SIINFEKL-CFSE micelles by human monocyte derived DCs. B. FACS analysis of uptake of micelle encapsulated SIINFEKL peptide by human monocyte derived DCs. C. FACS analysis of uptake of micelle encapsulated SIINFEKL peptide by mouse DCs and Macrophages. (Example 6, *infra*)

Figure 13 is a bar graph showing micelle formulated SIINFEKL peptide induces potent T cell responses *in-vitro* (Example 6, *infra*).

Figure 14 shows the immunology of micelle. A shows FACS analysis of efficient uptake of micelle encapsulated OVA protein by mouse DCs and Macrophages. B is a graph showing that micelle encapsulated OVA/CpG activates DCs *in-vitro.* (Example 6, *infra*)

Figure 15 is a graph depicting the immunology of polyketal particles. Uptake of polyketal particle (PKN) encapsulated U0126 by mouse DCs and Macrophages *in-vitro.* (Example 6, *infra*)

Figure 16 is a schematic diagram showing the experimental outline for T cell stimulation in-vitro using OVA-OT/1 transgenic model. (Example 6, *infra*)

Figure 17 shows the immunology of micelle. A. Left panel is the flow cytometery analysis and the right panel is the summary showing that splenocytes pulsed with micelle formulated antigen induces potent antigen-specific CD8+ T cell responses *in-vitro*. B.

Left panel is the flow cytometery analysis and the right panel is the summary showing that DCs pulsed with micelle formulated antigens induce potent antigen-specific CD8+ T cell responses in vitro. C. Flow cytometery analysis showing that micelle formulated antigen activate DCs *in-vivo*. (Example 6, *infra*)

Figure 18 shows the immunology of micelle and polyketal particles. A. Left panel is the flow cytometery analysis and the right panel is the summary showing that micelle formulated vaccines induce strong antigen-specific CD8+ IFN-gamma+ T cell responses *in-vivo*. B. Left panel is the flow cytometery analysis and the right panel is the summary showing that micelle formulated vaccines induce strong antigen-specific $CD8^+$ $TNF\alpha^+$ T cell responses *in-vivo*. C. Line graphs showing the kinetics of specific $CD8^+/IFN\gamma^+$ T cells after OVA/CpG vaccination. D. Line graphs showing the kinetics of specific $CD8^+/IFN\gamma^+$ T cells after OVA + UO126 PKN vaccination. E. Bar graphs showing that micelle formulated vaccines induce strong antigen specific IgG antibody response *in-vivo*. F. Bar graphs showing that micelle formulated vaccines induce antigen specific IgE and IgM antibody response *in-vivo*. (Example 6, *infra*)

Figure 19 shows polyketals from cyclohexane dimethanol (termed PCADK herein with an IUPAC designation poly(cyclohexane-1,4-diyl acetone dimethylene ketal)). A. Chemical representation showing polyketals from cyclohexane dimethanol. B. Line graph showing that PCADK degrades in an acid sensitive manner. (Example 6, *infra*)

Figure 20 shows SEM images depicting that particles from PCADK can encapsulate the hydrophobic compounds and drugs such as rhodhamine red and ebselen. (Example 6, *infra*)

Figure 21 shows line graphs showing that release of rhodhamine red from PCADK is pH sensitive. (Example 6, *infra*)

Figure 22 is a chemical representation showing that polyketals with almost any aliphatic diol can be made. (Example 6, *infra*)

Figure 23 is a photograph showing that FITC labeled polyketals are phagocytosed by liver macrophages. (Example 6, *infra*)

Figure 24A is a schematic diagram showing double emulsion procedure used to encapsulate catalase and super oxide dismutase in polyketal particles. B is a SEM image of catalase containing particles, and fluorescent microscope images of catalase containing particles. C is a graph showing that catalase particles have enzymatic activity. (Example 6, *infra*)

Figure 25 is a chemical representation showing that polyketals made by acyclic diene metathesis (ADMET).

Figure 26 is a schematic diagram for the synthesis and acid degradation of drug loaded particles.

Figure 27 is a table showing the conditions used to make different rhodhamine containing PCADK particles.

Figure 28 is a graph showing that His-GFP stably bound to NTA-Ni for at least 15 hours (Example 9, *infra*).

Figure 29 is a schematic cartoon showing sources of p38 activation as well as downstream effects. (Example 7, *infra*)

Figure 30 is a schematic of the synthesis of Poly(1,4-cyclohexane-acetone dimethylene ketal) (PCADK). PCADK is synthesized using the acetal exchange reaction with 1,4-cyclohexanedimethanol and 2,2 dimethoxypropane as reactants. PCADK hydrolyzes into 1,4-cyclohexanedimethanol and acetone (Example 7, *infra*).

Figure 31 is a graph showing the GPC trace of PCADK in THF, Y-axis indicates relative UV absorbance at 262 nm, Mw = 6,282, polydispersity index (PDI) = 1.54 (Example 7, *infra*).

Figure 32 is a photograph showing a representative SEM image of SB239063-loaded particles (PK-p38$_i$). These images return an approximate particle size of 3-15 μm (Example 7, *infra*).

Figure 33 is a photograph showing that particle size can be easily modified. A) SEM of particles generated with original protocol. B) Higher magnification SEM from particle generated from reduced homogenization speed. C) High magnification image of particle generated from reduced PVA concentration (Example 7, *infra*).

Figure 34 is a photograph showing a representative SEM image of alternative porous particles. Addition of N-hexane to the initial dispersion resulted in formation of porous particles. Approximate size of these particles is 10-25 μm (Example 7, *infra*).

Figure 35 is a photograph showing SEM Images of SOD-PKNs. (A) 6000X magnification. (B) 1000X maginification (Example 7, *infra*).

Figure 36 is a chart showing grouped data from Cultured macrophages pretreated with PK-SOD and stimulated with LPS. Pretreatment of macrophages with SOD-loaded polyketals resulted in a significant decrease in LPS-stimulated superoxide release as compared to empty PK and free SOD (Example 7, *infra*).

Figure 37 is a photograph showing representative fluorescent image of FITC-loaded polyketal incubated with cultured macrophages. Macrophages were incubated with PK-FITC for 2 hours prior to extensive washing and imaging. Arrows denote cells that have taken up FITC dye. Empty particles can also be seen bound to the surface of macrophages (Example 7, *infra*).

Figure 38 shows representative Western blot (top) and grouped densitometric data (bottom) from macrophages pretreated with polyketals for the indicated time (PK time) and stimulated with 10 ng/mL TNF-α for 20 minutes. Macrophages were incubated with empty PK or PK-p38$_i$ for 2-6 hours prior to extensive washing and TNF-α stimulation. While there was no change in p38 phosphorylation with longer empty PK pretreatment, there was significant inhibition of p38 phosphorylation with 4 and 6 hour PK-p38i pretreatment (*$p<0.05$; ANOVA followed by Tukey-Kramer; n=4) (Example 7, *infra*).

Figure 39 is a chart showing grouped data from macrophages pretreated with polyketals for 6 hours, stimulated with 10 ng/mL TNF-α for 20 minutesand dihydroethidium for 20 mins. HPLC data demonstrating a significant increase in extracellular superoxide release by TNF-a treatment. This increase was not blocked by empty PK but completely inhibited by PK-p38$_i$ pretreatment (*$p< 0.05$ ANOVA followed by Tukey-Kramer (Example 7, *infra*).

Figure 40 shows detection of extracellular superoxide production following infarction by DHE-HPLC. Top panel is a representative trace from sham and infarct (MI) samples. Bottom panel is normalized data showing an increase in extracellular superoxide production as detected by this method. Animals were subjected to sham or coronary artery ligation surgery and left ventricular free walls were harvested 3 days following infarction. Pieces were incubated with dihydroethidium in the presence and absence of exogenous SOD and data is represented as SOD-inhibited oxy-ethidium concentration (n=4). These data represent a potential mechanism of post-infarct damage that may be examined in future experiments (Example 7, *infra*).

Figure 41 is a photograph showing representative H&E Stain of leg muscle 3 days following injection. In the left panel, PCADK injected form a defined injection area with little cellular staining outside the borders. PLGA (right) in contrast shows evidence of fibrosis and inflammatory cell population (Example 7, *infra*).

Figure 42 is a photograph showing polyketal injection causes little inflammation. The left panels show 2 representative immunofluoresence stains for CD45, a common inflammatory marker. There is little staining in the sections. In contrast on the right, leg muscle injected with PLGA, a commonly used polymer, generates a robust inflammatory response as measured by CD45 staining (Example 7, *infra*).

Figure 43 shows PK-p38$_i$ treatment inhibits p38 phosphorylation following infarction. Representative Western blots for both phospho- and total-p38 in the infarct zone 3 days following infarction. Grouped data (mean + SEM) demonstrate a significant increase in p38 phosphorylation in MI and MI+PK groups (* $p<0.05$ vs. Sham and MI+PK-p38$_i$; n=13 total mice) (Example 7, *infra*).

Figure 44 shows PK-p38i treatment inhibits IL-5 expression following infarction. Representative Western blots for both IL-5 and β-actin in the infarct zone 3 days following infarction. Grouped data demonstrates a significant increase in normalized IL-5 levels in MI and MI+PK groups (* $p<0.05$ vs. Sham and MI+PK-p38i). Data are represented as mean+SEM (n=13 total mice) (Example 7, *infra*).

Figure 45 is a chart showing polyketal-encapsulated SB239063 inhibits TNF-α production 3 days following infarction. Grouped data demonstrating single injection of PK-p38$_i$ almost normalizes TNF-α levels in post-infarction rats (n=19 total rats). Data are represented as mean + SEM (Example 7, *infra*).

Figure 46 is a chart showing implanted cell death reversed by sustained growth factor treatment. Neonatal cardiac myocytes were stained with a green membrane dye prior to injection, then stained for cleaved caspase-3 14 days following injection. Data are mean $\pm$ SEM from $n\geq4$ animals per group (** $p<0.01$ vs. peptides alone or untethered IGF) (Example 7, *infra*).

Figure 47 shows tracking of cells Using GFP and HA adenoviruses. Cells were incubated in suspension with 100 MOI of GFP or hemagglutanin adenoviruses for 2

hours immediately following isolation. Cells were plated for 24 hours and flow cytometry was performed (Example 7, *infra*).

Figure 48 is a chart showing grouped echocardiographic data 3 days following sham or coronary artery ligation surgery. Fractional shortening measurements made from M-mode, short axis movies after 3 days of ischemia. There was a significant reduction in cardiac function as measured by fractional shortening in rats undergoing this procedure (*$p<0.05$; t-test). These data demonstrate our ability to consistently perform this surgery in rats and induce cardiac dysfunction (Example 7, *infra*).

Figure 49 is a photograph showing cardiac stem cell isolation. Cells were isolated as described, fixed in 4% paraformaldehyde and stained with antibodies against the indicated maker followed by a fluorescent secondary antibody (Example 7, *infra*).

Figure 50 shows H-NMR analysis of PK-3. The H-NMR spectrum was obtained using a Varian Mercury VX 400 MHz NMR spectrometer (Palo Alto, CA) using $CDCl_3$ as the solvent. The molar ratio of 1,5-pentanediol to 1,4-cyclohexanedimethanol was obtained by obtaining the ratio of areas under the peaks a and b, respectively (Example 8, *infra*).

Figure 51 is a schematic showing synthesis of polyketal copolymers from 1,4-cyclohexanedimethanol, a second diol and 2,2-dimethoxypropane. Hydrolysis kinetics of polyketal copolymers can be controlled by copolymerization (Example 8, *infra*).

Figure 52 are graphs showing hydrolysis kinetics of polyketals can be tuned by copolymerization. (A) Hydrolysis profiles of polyketal copolymers PK1 to PK6 in pH 4.5 buffer, and (B) hydrolysis profiles of PK1 to PK6 in pH 7.4 buffer. Data are presented as mean ± standard deviation. All experiments were conducted in triplicates at 37 °C (Example 8, *infra*).

Figure 53 is a photograph showing SEM images of particles formulated with PK3. SEM image of empty particles formulated via double emulsion procedures (Example 8, *infra*).

Figure 54 is a schematic diagram of nitrilotriacetic acid (NTA) which, when loaded with nickel (Ni), binds histidine-tagged proteins (Example 9, *infra*).

Figure 55 is a schematic diagram of a polyketal with a NTA linker forming microspheres where active agents are encapsulated by the microsphere and His-tagged proteins are bound to the surface of the microsphere. B. A diagram of DOGS-NTA (Example 9, *infra*).

Figure 56 is a photograph showing SEM micrographs of 10% NTA PCADK microparticles (Example 9, *infra*).

Figure 57 is a chart showing the spectrophotometric determination of Ni depletion in loading solution. PCADK particle with varying concentrations of NTA-ligand (0%, 1%, 5%, 10%) were loaded in $NiCl_2$ solution. After incubating the particles overnight with agitation, solutions were centrifuged and the supernatants analyzed for Ni content spectrophotometrically. The supernatant particles with no NTA-ligand had a nickel concentration of about 550 mM while 1%, 5%, and 10% NTA particles had approximately 500 mM Ni in their supernants. This data suggests that the surface of the particles is saturated with 1% NTA-ligand inclusion. Further quantative testing is currently underway using atomic absorption spectroscopy (Example 9, *infra*).

Figure 58 are photographs showing that His-tagged Green Fluorescent Protein (GFP) is Ni dependent. 10% NTA particles were charged with Ni, washed extensively and then incubated in a 100 nM solution of His-tagged GFP. Particles were washed extensively with PBS and imaged using fluorescent microscopy. (a) PCADK-NTA particles were loaded in PBS instead of $NiCl_2$. Very little fluorescence from GFP is seen. (b) PCADK-NTA particles loaded with $NiCl_2$ show extensive association with GFP (Example 9, *infra*).

Figure 59 is a graph of the Specific Binding curve for 1% NTA-PCADK particles (On-particle ELISA). 1% NTA-PCADK particles were charged with Ni and loaded with varying concentrations of His-tagged GFP. After extensive washing after GFP loading, horseradish peroxidase (HRP) conjugated GFP antibody (α-GFP Ab) was incubated with the particles (particles suspended at 1 mg particles/ml of PBS-T with a 1:5000 dilution of α-GFP Ab and 1% goat serum) for 2 h at room temperature. Particles were then washed with 3 volumes of PBS-T. Colorimetric determination of HRP activity was done on a plate reader with different amounts of particle per well. 1-step Slow TMB-ELISA substrate (3,3',5,5'-tetramethylbenzidene, Pierce) was used at a substrate and absorbances measured at 370 nm. Readings from 3, 6, and 9 min were compared and shown above. Specific binding curve suggests that 1% NTA particles saturate with GFP when loaded with 60 ng GFP/mg particle (Example 9, *infra*)

Figure 60 is a graph of the Specific Binding curve for 10% NTA-PCADK particles (On-particle ELISA). 10% NTA-PCADK particles were charged with Ni and loaded with varying concentrations of His-tagged GFP. After extensive washing after GFP loading, horseradish peroxidase (HRP) conjugated GFP antibody (α-GFP Ab) was incubated with the particles (particles suspended at 1 mg particles/ml of PBS-T with a 1:5000 dilution of α-GFP Ab and 1% goat serum) for 2 h at room temperature. Particles were then washed with 3 volumes of PBS-T. Colorimetric determination of HRP activity was done on a plate reader with different amounts of particle per well. 1-step Slow TMB-ELISA substrate (3,3',5,5'-tetramethylbenzidene, Pierce) was used at a substrate and absorbances measured at 370 nm. Readings from 3, 6, and 9 min were compared and shown above. Specific binding curve suggests that 10% NTA particles saturate with GFP when loaded with 120 ng GFP/mg particle (Example 9, *infra*).

Figure 61 is a graph showing that GFP Binding is reversible. Particles loaded with GFP were subjected to an spike of imidazole (200 mM final concentration), a competitive binding ligand to the NTA-Ni complex, and the fluorescence intensity of the supernantant measured as a function of time. Data suggests that GFP is maximally dissociated at 30 minutes in the presence of 200 mM imidazole (Example 9, *infra*).

Figure 62 is a chart showing that GFP binding increases with with amount of NTA-Ni (Example 9, *infra*).

DETAILED DESCRIPTION OF THE INVENTION

DEFINITIONS

All scientific and technical terms used in this application have meanings commonly used in the art unless otherwise specified. As used in this application, the following words or phrases have the meanings specified.

As used herein, the term "micelle" refers to a colloidal aggregate of polymer molecules having at least two different moieties which are linked to different properties in a liquid medium. The difference in the properties can occur due to different hydrophobicity/hydrophilicity, polarity, charge or charge distribution or other parameters which influence the solubility of a molecule. Micelles of the present invention are distinguished from and exclude liposomes which are composed of bilayers.

As used herein, the term "polymer" refers to a covalently linked arrangement of monomeric molecules. The arrangement can be realized in a linear chain or in a branched form. The polymer can be a homopolymer which is composed of only one type of monomeric molecules, or it can be a copolymer wherein two or more different types of monomers are joined in the same polymer chain. When the two different monomers are arranged in an alternating fashion, the polymer is called an alternating copolymer. In a random copolymer, the two different monomers may be arranged in any order. In a block copolymer each type of monomer is grouped together. A block copolymer can be thought of as two or more homopolymers joined together at the ends. When chains of a polymer made of one monomer are grafted onto a polymer chain of a second monomer a graft copolymer is formed.

As used herein, the term "particle" or "three-dimensional particle" refers to e.g., nanoparticles and/or microparticles. According to standard definitions, the term "nanoparticle" covers only particle having at least one dimension smaller than 100 nm. Larger particles which do not fulfill this requirement are termed "microparticles". The present invention provides three-dimensional particles sized on the nanometer (nm) and micron (μm) scale. The particles of the invention can range in size from about 50 nm to 1000 μm or from about 200 nm to 600 μm.

The terms "ketals" and "diols" as used herein encompass ketals and diols comprising alkyl, cycloalkyl and aryl groups. "Alkyl group" or "aliphatic group" as used herein, is linear or branched chain alkyl group. In one embodiment a linear alkyl group is preferred. Also included within the definition of alkyl are heteroalkyl groups, wherein the heteroatom can be nitrogen, oxygen, phosphorus, sulfur and silicon.

The term "cycloalkyl group" or "cycloaliphatic group", as used herein describes a ring-structured alkyl including at least three carbon atoms in the ring. In one embodiment, a cycloalkyl group having 5 or 6 carbons is preferred. The cycloalkyl group also includes a heterocyclic ring, wherein the heteroatom can be nitrogen, oxygen, phosphorus, sulfur and silicon.

"Aryl group" or "aromatic group" as used herein, is an aromatic aryl ring such as phenyl, heterocyclic aromatic rings such as pyridine, furan, thiophene, pyrrole, indole and purine, and heterocyclic rings with nitrogen, oxygen, sulfur or phosphorus. Included in the definition of alkyl, cycloalkyl and aryl groups are substituted alkyl, cycloalkyl and aryl groups. These groups can carry one or more substitutions. Suitable substitution groups include but are not limited to, halogens, amines, hydroxyl groups, carboxylic acids, nitro groups, carbonyl and other alkyl, cycloalkyl and aryl groups.

In order that the invention herein described may be more fully understood, the following description is set forth.

COMPOSITIONS OF THE INVENTION

Polyketal Polymers of the Invention

The present invention provides biodegradable hydrophobic polyketal polymers comprising multiple ketal groups, each ketal group having two oxygen atoms within the polymer backbone. In one embodiment, the biodegradable hydrophobic polyketal polymer of the invention is in the form of a solid molecule.

Examples of suitable ketal groups include, but are not limited to, 2,2-dioxypropyl group, 2,2-dioxybutyl group, 1,1-dioxycyclohexyl group or dioxyacetophenyl group. Also in the scope of the invention are ketal polymers including aliphatic, cycloaliphatic or aromatic ketals containing one or more hetero-atom, such as nitrogen, sulfur, oxygen and halides.

In one embodiment of the invention, the polymer further comprises a compound comprising alkyl, aryl, and cycloalkyl groups. In this embodiment, the compound may be directly attached to the ketal group.

Examples of suitable alkyl groups include, but are not limited to, methyl, ethyl and butyl groups. Examples of suitable aryl groups include, but are not limited to, substituted or unsubstituted benzyl, phenyl or naphtyl groups, such as, for example, a 1,4-dimethylbenzene. Examples of suitable cycloalkyl groups include, but are not limited to, substituted or unsubstituted cyclohexyl, cyclopropyl, cyclopentyl groups, such as, for example, 1,4-dimethylcyclohexyl group.

In a preferred embodiment, the polymer may be poly(1,4-phenylene-acetone dimethylene ketal). This polymer can be synthesized of 2,2-dimethoxypropane and 1,4-benzene dimethanol. The polymer may also be a poly(1,4-cyclohexane-acetone dimethylene ketal), which can be synthesized of 2,2-dimethoxypropane and 1,4-cyclohexane dimethanol.

In further embodiment of the invention, the polyketal polymer can be any one or more of PK1, PK2, PK3, PK4, PK5 and PK6 copolymers. These six polyketal copolymers exhibit varied hydrolysis kinetics at different pH levels. For example at pH 4.5, PK4 is the fastest out of the six copolymers to hydrolyze with PK3 having the second faster hydrolysis rate. In turn, PK3 has faster hydrolysis kinetics than PK2 or PK5, while PK2 and PK5 have faster hydrolysis kinetics than PK1 or PK6. However, at pH 7.4, PK3 is hydrolyzed faster than PK4. By altering the copolymer percentage of the polyketals of the invention, the hydrolysis kinetics for controllable release of an active agent can be fine tuned.

In one embodiment, PK1 has a structure as shown in Table 1 (Example 8) and is made up of at least 2 different monomers i.e., repeating units such as random repeating units. In one example of PK1, one type of monomer is 1,4,-cyclohexanedimethoxy with an x value (i.e. percent component of the first monomer incorporated into the polymer) of about 98%, and the second type of monomer is 1,5-pentanedioxy with a y value (i.e. percent component of the second monomer incorporated into the polymer) of about 2%. The n value may be 3. In this embodiment, PK1 is synthesized from two types of starting compounds, namely, 1,4-cyclohexanedimethanol and 1,5-pentanediol. An IUPAC designation for PK1 is poly(cyclohexane-1,4-diyl acetone dimethylene ketal-co-1,5-pentane-acetone dimethylene ketal).

In one embodiment, PK2 has a structure as shown in Table 1 (Example 8) and is made up of at least 2 different monomers i.e., repeating units such as random repeating units. In one example of PK2, one type of monomer is 1,4,-cyclohexanedimethoxy with an x value (i.e. percent component of the first monomer incorporated into the polymer) of about 92%, and the second type of monomer is 1,5-pentanedioxy with a y value (i.e. percent component of the second monomer incorporated into the polymer) of about 8%. The n value may be 3. In this embodiment, PK2 is synthesized from two types of starting compounds, namely, 1,4-cyclohexanedimethanol and 1,5-pentanediol. An IUPAC designation for PK2 is poly(cyclohexane-1,4-diyl acetone dimethylene ketal-co-1,5-pentane-acetone dimethylene ketal).

In one embodiment, PK3 has a structure as shown in Table 1 (Example 8) and is made up of at least 2 different monomers i.e., repeating units such as random repeating units. In one example of PK3, one type of monomer is 1,4,-cyclohexanedimethoxy with an x value (i.e. percent component of the first monomer incorporated into the polymer) of about 87%, and the second type of monomer is 1,5-pentanedioxy with a y value (i.e. percent component of the second monomer incorporated into the polymer) of about 13%. The n value may be 3. In this embodiment, PK3 is synthesized from two types of starting compounds, namely, 1,4-cyclohexanedimethanol and 1,5-pentanediol. An IUPAC designation for PK3 is poly(cyclohexane-1,4-diyl acetone dimethylene ketal-co-1,5-pentane-acetone dimethylene ketal).

In one embodiment, PK4 has a structure as shown in Table 1 (Example 8) and is made up of at least 2 different monomers i.e., repeating units such as random repeating units. In one example of PK4, one type of monomer is 1,4,-cyclohexanedimethoxy with an x value (i.e. percent component of the first monomer incorporated into the polymer) of about 97%, and the second type of monomer is 1,4-butanedioxy with a y value (i.e. percent component of the second monomer incorporated into the polymer) of about 3%. The n value may be 2. In this embodiment, PK4 is synthesized from two types of starting compounds, namely, 1,4-cyclohexanedimethanol and 1,4-butanediol. An IUPAC designation for PK4 is poly(cyclohexane-1,4-diyl acetone dimethylene ketal-co-1,4-butane-acetone dimethylene ketal).

In one embodiment, PK5 has a structure as shown in Table 1 (Example 8) and is made up of at least 2 different monomers i.e., repeating units such as random repeating units. In one example of PK5, one type of monomer is 1,4,-cyclohexanedimethoxy with an x value (i.e. percent component of the first monomer incorporated into the polymer) of about 85%, and the second type of monomer is 1,6-hexanedioxy with a y value (i.e. percent component of the second monomer incorporated into the polymer) of about 15%. The n value may be 4. In this embodiment, PK5 is synthesized from two types of starting compounds, namely, 1,4-cyclohexanedimethanol and 1,6-hexanediol. An IUPAC

designation for PK5 is poly(cyclohexane-1,4-diyl acetone dimethylene ketal-co-1,6-hexane-acetone dimethylene ketal).

In one embodiment, PK6 has a structure as shown in Table 1 (Example 8) and is made up of at least 2 different monomers i.e., repeating units such as random repeating units. In one example of PK6, one type of monomer is 1,4,-cyclohexanedimethoxy with an x value (i.e. percent component of the first monomer incorporated into the polymer) of about 87%, and the second type of monomer is 1,8-octanedioxy with a y value (i.e. percent component of the second monomer incorporated into the polymer) of about 13%. The n value may be 6. In this embodiment, PK6 is synthesized from two types of starting compounds, namely, 1,4-cyclohexanedimethanol and 1,8-octanediol. An IUPAC designation for PK6 is poly(cyclohexane-1,4-diyl acetone dimethylene ketal-co-1,8-octane-acetone dimethylene ketal).

The PK1-PK6 copolymers may be synthesized using the acetal exchange reaction by copolymerizing 1,4-cyclohexanedimethanol with either butanediol, pentanediol, hexanediol or octanediol. As shown in Table 1 of Example 8, *infra*, a PK1 was synthesized with monomer A (1,4-cyclohexanedimethanol) plus monomer B (1,5-pentanediol); a PK2 was synthesized with monomer A (1,4-cyclohexanedimethanol) plus monomer B (1,5-pentanediol); a PK3 was synthesized with monomer A (1,4-cyclohexanedimethanol) plus monomer B (1,5-pentanediol); a PK4 was synthesized with monomer A (1,4-cyclohexanedimethanol) plus monomer B (1,4-butanediol); a PK5 was synthesized with monomer A (1,4-cyclohexanedimethanol) plus monomer B (1,6-hexanediol); a PK6 was synthesized with monomer A (1,4-cyclohexanedimethanol) plus monomer B (1,8-octanediol).

In another embodiment of the invention, the PK1, PK2, PK3, PK4, PK5 and PK6 copolymers of the invention can be intermingled to change or fine tune the release rate profile for attached active agents. For example, a polyketal with fast hydrolysis kinetics (e.g., PK4 or PK3) can be mixed with a polyketal with slower hydrolysis kinetics (e.g.,

PK1 or PK6) and co-administered to a subject. The active agent joined to PK4 or PK3 will be released in a subject quickly to provide the subject with an immediate release (IR) dose of active agent, while the active agent joined to PK1 or PK6 will be released at a slower rate allowing a gradual or extended release (ER) of the active agent in the subject.

In an embodiment of the invention, the biodegradable hydrophobic polyketal polymers comprises (1) multiple ketal groups, each ketal group having two oxygen atoms within the polymer backbone and (2) a linker. The ketal groups may comprise a 2,2-dioxypropyl group.

Biodegradable Polyketal Particles of the Invention

The invention further provides biodegradable particles comprising the polyketal polymers of the invention. The sizes of the particles can vary. For example, biodegradable particles can be made at nanometer (nm) or micron (μm) scale e.g., to form nanoparticles or microparticles. The particles of the invention can range in size from about 50 nm to 1000 μm. In one embodiment, the particles range in size from about 200 nm to 600 μm. In another embodiment, the particles range in size from about 1 μm to 10 μm, 10 μm to 20 μm. 20 μm to 30 μm, 30 μm to 40 μm or 40 μm to 50 μm. In yet another embodiment, the particles range in size from about 1 μm to 50 μm. A preferred particle size is between about 50 and 1000 nm, more preferred between about 200 and 600 nm. Another preferred particle size is about 30 μm.

The preferred size of a suitable polyketal polymer to form the biodegradable particle is between about 0.5 kDa and about 2 MDa, more preferred between 1 and about 150 kDa, most preferred between about 4 and about 6 kDa. In accordance with the invention, the number of the monomers in the polymer can range from about 2 to about 20,000, preferably about 10 to about 1,000, more preferably about 10 to about 50.

Polyketal polymers of the invention hydrolyze in aqueous solutions into low molecular weight, water soluble alcohols and ketones. For example, the degradation of poly(alkyl-

acetone dimethylene ketal) is acid sensitive, with a half-life of 102.0 h at pH 7.4 and 35.0 h at pH 5.0. The advantage of a ketal linkage in the backbone is that it degrades under acidic conditions of phagosomes, within 1-2 days at pH 5.0. Polyketals can therefore also be used for targeting the acidic environments of tumors, inflammation and phago-lysosomes. The degradation also does not generate acidic degradation products. Thus, the ketal polymers are suitable for biological use.

In accordance with the practice of the invention, the polyketal polymer particles can further comprise one or more active agents.

In one embodiment of the invention, the biodegradable particle of the invention comprises: (a) a biodegradable hydrophobic polyketal polymers comprising multiple ketal groups, each ketal group having two oxygen atoms within the polymer backbone and (b) a linker. Suitable polymers to form the particles of the invention include PCADK and PK1-PK6.

In one embodiment of the invention, the polyketal polymer particle can further comprise one or more linkers which can bind an active agent. Multiple linkers of the same or different types can be attached to a polymer particle. The linkers are attached to the surfaces of the the particles i.e., the linkers are exposed to the solvent or aqueous solution surrounding the particles.

In one embodiment, the biodegradable particle of the invention comprises (a) one or more of PK1, PK2, PK3, PK4, PK5 or PK6 (which can optionally comprise a linker), and (b) an active agent. In another embodiment of the invention, the biodegradable particle of the invention comprises (a) PCADK (which can optionally comprise a linker) and (b) an active agent.

In accord with the practice of the invention, the particles can comprise a single population of polyketals or a mixed population.

Active Agents of the Invention

As used herein, the term "active agent" refers to a protein, peptide, nucleic acid (DNA or RNA) or organic molecule, and other synthetic nucleic acid molecules, siRNA molecules, or antisense molecules. The active agent can be a therapeutic, prophylactic or diagnostic agent. The therapeutic agent can be an immunomodulatory agent such as specific ligands for RIG-I or TLRs, or C-type lectins (such as dectin-1 and DC-SIGN) or caterpillar proteins, or combinations of specific TLR ligands, or synthetic molecules or siRNAs which inhibit regulatory signaling networks with DCs and macrophages. The active agent can further include proteins (e.g., recombinant proteins), peptides, carbohydrates, nucleic acids, small molecules (e.g., kinase inhibitors, phosphatase inhibitor, cytokine inhibitors, small molecule antioxidant mimetics, receptor blockers, cytoskeletal rearrangement inhibitors, small molecule receptor activators.), imaging agents, vaccine antigens, DNA vaccines, or vaccines themselves, such as the influenza vaccine. Finally, an active agent can comprise antibodies that target, stimulate, modulate or inhibit subsets of DCs including Langerhans cells, dermal DCs, myeloid DCs, interstitial DCs, plasmacytoid DCs, or subsets of monocytes, and macrophages. Thus surface of these particles can be modified to contain targeting groups such as, for example, antibodies against subsets of dendritic cells, or proteins which stimulate subsets of dendritic cells, or macrophages such as CD40L, DEC-205, CD11c, langerin, MARCO, 33D1 etc.

Examples of suitable active agents include, but are not limited to: (1) agonists and antagonists of TLRs (*e.g.*, TLR-2, TLR-3, TLR-4, TLR-5, TLR-7, TLR-8, TLR-9, TLR-10, and TLR-11), (2) agonists and antagonists of the receptor(s) activated by schistosome egg antigen (SEA), (3) molecules that stimulate or inhibit the expression or activity of a component of an intracellular signaling pathway that transduces the signal generated by activation of either of these types of receptors, (4) agents that stimulate or inhibit a transcription factor that is induced or stabilized by one or more of these signaling pathways, and (5) inhibitors of a regulatory pathway(s) within dendritic cells, macrophages or antigen-presenting cells.

Examples of agonists include, but are not limited to, peptidoglycans (O. Takeuchi, et al., 1999 Immunity 11:443-451) or zymosans (Dillon et al, 2006 *J. Clin. Invest.* 116(4):916-28). A. Ozinsky, et al., 2000 Proc. Natl. Acad. Sci. USA 97:13766-13771). The agonists also include bacterial lipopeptides (e.g., diacylated and triacylated lipopeptides), lipoteichoic acid, lipoarabinomannan, phenol-soluble modulin, glycoinositolphospholipdis, glycolipids, porins, atypical LPS from Leptospira interrogns or Porphyromonas gingivalis, or HSP70 (for a review see K Takeda, et al., 2003 Annu. Rev. Immunol. 21:335-376). The agonists can be isolated and/or highly purified molecules. The agonists include whole molecules or fragments thereof, or naturally-occurring or synthetic. Examples include, but are not limited to, a non-toxic form of cholera toxin (Braun *et al.*, *J. Exp. Med.* 189:541-552, 1999), certain forms of *Candida albicans* (d'Ostiani *et al.*, *J. Exp. Med.* 191:1661-1674, 2000), or *P. gingivalis* LPS (Pulendran *et al.*, *J. Immunol.* 167:5067-5076, 2001).

Examples of bacterial lipopeptides include bacterial cell wall lipopeptides which differ in their fatty acid chain of the N-terminal cysteines, such as diacylated and triacylated lipopeptides. For example, diacylated lipopeptides include Macrophage Activating Lipopeptide 2 kilo-Dalton from *Mycoplasma fermentans* or fragments thereof or synthetic analogues (e.g., MALP2, Pam2CSK4, Pam2CGNNDESNISFKEK, and Pam2CGNNDESNISFKEK-SK4). The triacylated lipopeptides include Pam3cys {S-[2,3-bis(palmitoyloxy)-(2-RS)-propyl]-N-palmitoyl-R-Cys-S-Ser-Lys4-OH)} (Takeuchi, et al., 2001 International Immunology 13:933-940).

In an embodiment, the agonist specifically effects TLR-2 or a receptor(s) bound by SEA (with respect to SEA, *see* MacDonald *et al.*, *J. Immunol.* 167:1982-1988, 2001). Here too, the agonist can be, but is not limited to, a natural ligand, a biologically active fragment thereof, or a small or synthetic molecule. Other useful agonists may include a non-toxic form of cholera toxin (Braun *et al.*, *J. Exp. Med.* 189:541-552, 1999), certain forms of *Candida albicans* (d'Ostiani *et al.*, *J. Exp. Med.* 191:1661-1674, 2000), or *Porphyromonas gingivalis* LPS (Pulendran *et al.*, *J. Immunol.* 167:5067-5076, 2001). These agents fail to induce IL-12(p70) and stimulate Th2-like responses.

The agonists can be agonists of TLR-4 (which bias the immune response toward the Th response, e.g. TH1) include Taxol, fusion protein from Rous sarcomavirus, envelope proteins from MMTV, Hsp60 from *Chlamydia pneumoniae* or Hsp60 or Hsp70 from the host. Other host factors that agonize TLR-3 include the type III repeat extra domain A of fibronectin, oligosaccharides of hyaluronic acid, polysaccharide fragments of heparan sulfate, and fibrinogen. A number of synthetic compounds serve as agonists of TLR-7 (*e.g.*, imidazoquinolin (imiquimod and R-848), loxoribine, bropirimine, and others that are structurally related to nucleic acids).

Additional examples of suitable active agents include inhibitors of ERK, c-Fos, Foxp3, PI3 kinase, Akt, JNK, p38, NF-Kb, STAT 1, STAT2, IRF3, IRF7, IFN-alpha signaling or combinations thereof. Suitable active agents can further include inhibitors of SOCS 1 -7 proteins. Such inhibitors can be a small molecule, or a peptide, protein or nucleic acid (e.g., siRNA or antisense).

The agonist can be an exogenous or endogenous ligand, many of which are known in the art. The novel screening methods described below, particularly those that feature detecting TLR binding or activation, can be used to identify other ligands (whether naturally occurring molecules, fragments or derivatives thereof, antibodies, other peptides or protein-containing complexes, or synthetic ligands). For example, exogenous ligands of TLR-2 include LPS (lipopolysaccharide; a component of the outer membrane of Gram-negative bacteria), yeast-particle zymosan, bacterial peptidoglycans, lipoproteins from bacteria and mycoplasmas, and GPI anchor from *Trypanosoma cruzi*; endogenous ligands include heat shock (or "stress") proteins (*e.g.*, an Hsp60 from, for example, a bacterial or mycobacterial pathogen) and surfactant protein-A. Exogenous ligands of TLR-3 include poly(I:C) (viral dsNRA); exogenous ligands of TLR-4 include LPS, and respiratory syncytial virus (endogenous ligands include stress proteins such as an Hsp60 or Hsp70, saturated fatty acids, unsaturated fatty acids, hyaluronic acid and fragments thereof, and surfactant protein-A). Flagellin is an exogenous ligand of TLR-5. CpG (cytosine-guanine repeat) DNA and dsDNA are exogenous and endogenous ligands,

respectively, of TLR-9. *See* Zuany-Amorim *et al.*, *Nature Reviews* 1:797-807, 2002, and Takeda *et al.*, *Ann. Rev. Immunol.* 21:355-376, 2003.

Additional examples of suitable active agents include (a) an agent that inhibits the expression or activity of an AP-1 transcription factor in a dendritic cell, (b) a dendritic cell treated in culture with an agent that inhibits the expression or activity of an AP-1 transcription factor, or (c) syngeneic T cells stimulated in culture with dendritic cells treated as described in (b). The transcription factor can include c-fos, fos-B, Foxp3, or c-jun, and the agent that inhibits expression (of the transcription factor or of any component of the pathways described herein (these components are known in the art)) can be an antisense oligonucleotide or an RNAi molecule that specifically inhibits c-fos, fos-B, Foxp3, or c-jun expression (or the expression of a kinase, phosphatase, or other component of the signaling pathways). The inhibitory active agents discussed in the context of the present biodegradable particles can also be antibodies (or variants thereof (*e.g.*, single-chain antibodies or humanized antibodies); preferably the antibodies are monoclonal antibodies).

In another embodiment, the active agent is an antagonist (e.g., inhibitor or suppressor) of an intracellular pathway that impairs TLR2 signaling or activation. The antagonists include gram negative LPS, Taxol, RSV fusion protein, MMTV envelope protein, HSP60, HSP70, Type III repeat extra domain A of fibronectin, oligosaccharides of hyaluronic acid, oligosaccharide fragments of heparan sulfate, fibrinogen and flagellin (for a review see K Takeda, et al., 2003 Annu. Rev. Immunol. 21:335-376).

In an additional embodiment, the active agent is an antagonist of an intracellular pathway that impairs SEA signaling or activation. In one other embodiment, the molecule is an antagonist of a JNK 1/2 pathway. In another embodiment, the molecule is CpG DNA which activates p38 and ERK (A-K Yi, et al., 2002 The Journal of Immunolgy 168:4711-4720).

In another embodiment, the active agent is an inhibitor of ERK ½ which can inhibit maturation of dendritic cells and thus enhancing an IL12 and Th1 response. Examples of

the molecule include but are not limited to PD98059 and U0126 (A. Puig-Kroger, et al., 2001 Blood 98:2175-2182).

In another embodiment, the active agent inhibits c-fos signaling thus enhancing an IL12 and Th1 response. Such molecules include a DEF domain mutant of c-fos or any polypeptide having a DEF domain mutation (L.O. Murphy, et al., 2002 Nature Cell Biology 4:556-564 and Supplementary information pages 1-3), including: rat Fra-1, and Fra-2; mouse FosB, JunD, c-Jun, c-Myc, and Egr-1; and human JunB, N-Myc, and mPer1.

Active agents can include nucleic acids such as DNA, RNA, anti-sense oligonucleotide or siRNA. Suitable examples of DNA include therapeutic genes. Examples of therapeutic genes include suicide genes. These are genes sequences, the expression of which produces a protein or agent that inhibits tumor cell growth or tumor cell death. Suicide genes include genes encoding enzymes, oncogenes, tumor suppressor genes, genes encoding toxins, genes encoding cytokines, or a gene encoding oncostatin. The purpose of the therapeutic gene is to inhibit the growth of or kill cancer cell or produce cytokines or other cytotoxic agents which directly or indirectly inhibit the growth of or kill the cancer cell.

Suitable oncogenes and tumor suppressor genes include neu, EGF, ras (including H, K, and N ras), p53, Retinoblastoma tumor suppressor gene (Rb), Wilm's Tumor Gene Product, Phosphotyrosine Phosphatase (PTPase), and nm23. Suitable toxins include Pseudomonas exotoxin A and S; diphtheria toxin (DT); E. coli LT toxins, Shiga toxin, Shiga-like toxins (SLT-1, -2), ricin, abrin, supporin, and gelonin.

Active agents can include enzymes. Suitable enzymes include thymidine kinase (TK), xanthine-guanine phosphoribosyltransferase (GPT) gene from E. coli or E. coli cytosine deaminase (CD), or hypoxanthine phosphoribosyl transferase (HPRT).

Active agents can include cytokines. Suitable cytokines include interferons, GM-CSF, interleukins, tumor necrosis factor (TNF) (Wong G, et al., Science 1985; 228:810); WO9323034 (1993); Horisberger M. A., et al., Journal of Virology, 1990 Mar, 64(3):1171-81; Li YP et al., Journal of Immunology, Feb. 1, 1992, 148(3):788-94; Pizarro T. T., et al. Transplantation, 1993 Aug., 56(2):399-404). (Breviario F., et al., Journal of Biological Chemistry, Nov. 5, 1992, 267(31):22190-7; Espinoza-Delgado I., et al., Journal of Immunology, Nov. 1, 1992, 149(9):2961-8; Algate P. A., et al., Blood, 1994 May 1, 83(9):2459-68; Cluitmans F. H., et al., Annals of Hematology, 1994 Jun., 68(6):293-8; Martinez O. M., et al., Transplantation, 1993 May, 55(5):1159-66.

Active agents can include Growth factors. Growth factors include Transforming Growth Factor-alpha. (TGF-alpha.) and beta (TGF-beta), cytokine colony stimulating factors (Shimane M., et al., Biochemical and Biophysical Research Communications, Feb. 28, 1994, 199(1):26-32; Kay A. B., et al., Journal of Experimental Medicine, Mar. 1, 1991, 173(3):775-8; de Wit H, et al., 1994 Feb., 86(2):259-64; Sprecher E., et al., Archives of Virology, 1992, 126(1-4):253-69).

Active agents can further include the proteins catalase, superoxide dismutase, glutathione peroxidase, nitric oxide synthase.

The active agents of the invention can be can be naturally occurring, synthetic, or recombinantly produced, and includes, but are not limited to, any microbial or viral component or derivative thereof, including any component that is part of the structure of, or is produced by, the microbial cell or virus including, but not limited to, a cell wall, a coat protein, an extracellular protein, an intracellular protein, any toxic or non-toxic compound, a carbohydrate, a protein-carbohydrate complex, or any other component of a microbial cell or virus. The microbial cell or virus can be pathological.

Linkers of the Invention

The polyketals of the invention (e.g., in a particle embodiment) may further comprise one or more linkers. The linkers can be of the same type or can include a mixture of different types attached to the polyketal polymers. The linkers can be attached to the surfaces of the the polyketal polymers e.g., the linkers can be exposed to the solvent or aqueous solution surrounding the particles.

The linker can range in size from 1-1000 nm or 100-200,000 Da. In one embodiment of the invention, the linker can range in size from 1-10 nm, 10-50 nm, 50-100nm, 100-200 nm, 200-300 nm, 300-400 nm, 400-500 nm, 500-600 nm, 600-700 nm, 700-800 nm, 800-900 nm and 900-1000 nm. In another embodiment of the invention, the linker can range in size from 100-10,000 Da, 10,000-50,000 Da, 50,000-100,000 Da, 100,000-150,000 Da and 150,000-200,000 Da. In yet another embodiment of the invention, the linker can be about 200-300 Da, 10,000 Da, 40,000 Da, 64,000 Da or 150,000 Da in size.

The linker can be a protein, polypeptide, nucleic acid or chemical compound. Examples of protein or polypeptide linkers include, but are not limited to, an amino acid sequence such as arginine-aspartic acid-glycine (RDG), hemoglobin, glutathione-S-transferase (GST), streptavidin or an antibody. Examples of nucleic acid linkers include, but are not limited to, RNA, DNA (e.g., ssDNA such as a 4 to 50 nucleic acid long tract of Poly A or Poly T sequence) or synthetic analogues. Examples of chemical compounds that can be used as linkers include, but are not limited to, polycarboxylic acid (e.g., polyacrylic acid) or chelating agents such as nitrilotriacetic acid (NTA) ligand, bipyradol and EDTA. Chelating agents bind to metal ions (e.g., nickel, zinc, copper, etc.) with the metal ions in turn facilitate binding of an active agent to the linker. The linker tethers or joins (e.g., via a noncovalent association) an active agent to the polyketal of the invention.

The linker can bind to active agents including, but not limited to, a protein, peptide, nucleic acid and/or carbohydrate. In one embodiment, the protein, peptide and/or carbohydrate further comprises a histidine tag. The histidine tag can comprise about 2-8

histidines. For example, in one embodiment, the histidine tag comprises about 6 histidines. The protein so bound to the linker can be a therapeutic, prophylactic or diagnostic protein.

In accordance with the practice of the invention, the therapeutic protein can be an immunomodulatory protein. For example, the immunomodulatory protein can include, but is not limited to: (a) a ligand for any of TLR 2, 3, 4, 5, 7, 8, 9, 10 and 11 or combination thereof, (b) an inhibitor of a regulatory pathway within dendritic cells, macrophages or antigen-presenting cells; and (c) a ligand for RIG-1, any C-type lectins including dectin-1 and DC-SIGN, or Caterpillar proteins The inhibitor of a regulatory pathway can include inhibitors of: (a) ERK, c-Fos, Foxp3, PI3 kinase, Akt, JNK, p38, NF-Kb, STAT 1, STAT2, IRF3, IRF7, IFN-alpha signaling; or (b) a SOCS 1, 2, 3, or other SOCS protein.

Additional suitable examples of proteins to bind to the linker include growth factors, cytokines, antioxidant enzymes, antibodies, erythropoietin (EPO), receptor ligand.

In one embodiment, a polyketal of the invention (e.g., PCADK or any of PK1 to PK6) comprises a NTA linker. The NTA linker can be loaded with nickel ions to produce a NTA-Ni linker that binds histidine tagged proteins.

Micelles of the Invention

The present invention further provides a biodegradable crosslinked micelle comprising multiple polymers of the invention. The polymers can be crosslinked by an external crosslinking agent. External crosslinking agents as used herein are agents which are not introduced into the polymer chain. The advantage of using of external agents is the faster crosslinking reaction compared to a reaction wherein only crosslinkable moieties within the polymer are used. The external crosslinking agent also reduces the probability that the encapsulated protein will be destroyed.

In one aspect of the present invention, suitable crosslinking agents are compounds which comprise at least two thiol groups. Examples of suitable crosslinking agents include, but are not limited to, ethylene glycol dithiol, aliphatic dithiols, dithiols which are connected by ketal linkages, and diamine containing molecules. The advantage of thiol groups is the sensitivity to reducing conditions, thus enabling an easy degradation of the micelle. Other crosslinking strategies include, but are not limited to, crosslinking by amines, esters, carbonates, thioesters, Schiff bases, vicinal diols, alkenes and alkynes, ketals, ketals orthoesters, thio-ketals, thio-orthoesters, sily-ketals, phenyl boronic acid-diol complexes, carbon-carbon bonds, sulfones, phosphate containing functional groups, azides, enzyme cleavable linkages, and urethanes, with Schiff bases, thiols and ketones being preferred in one embodiment of the present application (O'Reilly et al., 2005 *Chem. Mater.*, 17(24):5976-5988; Hanker et al., 2005 *Science* 309(5738):1200-05; Le, Z. et al., 2005 *Langmuir* 21(25):11999-12006; Example 1, Figure 9).

In another aspect of the present invention, the external crosslinking agent comprises an antigen. Examples of suitable antigens include, but are not limited to, proteins or peptides. The antigens can be naturally occurring, chemically synthesized or recombinantly made. Specific examples of suitable protein or peptide antigens include, but are not limited to, HIV antigens such as gp120 protein (or fragment thereof), TAT protein (or fragment thereof), NEF protein (or fragment thereof), HCV protein (or fragment thereof), and env protein (or fragment thereof). A preferred antigen includes a gp120 peptide antigen chemically synthesized and modified to contain four additional cysteine residues to create therein additional disulfide bonds. Any antigen having crosslinkable groups can be used. Antigens not having or having few crosslinkable groups can be modified (e.g., chemically modified) to comprise crosslinkable thiol groups, azides, alkynes, amines, maleimides, vinyl sulfones, ketones, hydrazines and thioesters.

Polymers to be used for micelle formation can be homopolymers or copolymers, such as block copolymers or graft polymers. Examples of suitable polymers include, but are not limited to, PEG block copolymers, such as PEG-polyamino acids, for example, PEG-

polylysine, PEG-polyglutamic acid, PEG-polyaspartic acid or PEG-polyarginine; PEG-polyesters, PEG-polyurethane, PEG-PPO, modified or unmodified, PEG-polyacrylate or PEG-polymethacrylate, synthesized by atom transfer polymerization, where the PEG acts as an initiator. To facilitate polymer crosslinking, the polymer can be modified to include chemical groups including, but not limited to, amines, esters, carbonates, thioesters, Schiff bases, vicinal diols, alkenes and alkynes, ketals, ketals orthoesters, thio-ketals, thio-orthoesters, sily-ketals, phenyl boronic acid-diol complexes, carbon-carbon bonds, sulfones, phosphate containing functional groups, azides, enzyme cleavable linkages, and urethanes, with Schiff bases, thiols and ketones being preferred in one embodiment of the present invention. These groups can be introduced via chemical reactions known in the art, such as, among others, Michael addition or acylation (Example 1, Figure 9). In one preferred embodiment the modified polymer is PEG-polylysine thiopyridal (Figure 9).

The polymethacrylate or polyacrylate block can contain modifications to allow for assembly with vaccine components and crosslinking. For example a polyacrylate block can be a block copolymer consisting of polydimethylamino-acryalte-poly-glycidyl acrylate. Homopolymer of random copolymers composed of various acrylate or methacrylate monomers capable of forming micelles with vaccine components are also in the scope of the present invention.

In another aspect of the present invention the micelle can further comprise one or more active agents. Examples of suitable active agents are found herein, *supra*.

In accordance with the practice of the invention, the interaction between the micelle and the active agent can be electrostatic or hydrophobic or can occur due to hydrogen bond formation or molecular recognition depending on the type of polymer and agent. The surface of this micelle can be modified to contain targeting groups such as, for example, antibodies against dendritic cells, or proteins which stimulate subsets of dendritic cells, or macrophages such as CD40L, DEC-205, CD11c, langerin, MARCO, 33D1 etc.

In one embodiment, the micelle is designed to deliver peptide antigens and immunomodulatory molecules to antigen-presenting cells (APCs). In this embodiment, the micelle comprises immunomodulatory molecules, peptide antigens and a copolymer. The peptide antigen acts as a crosslinker which allows the peptide antigen to be efficiently encapsulated into the peptide crosslinked micelles (PCMs) and also stabilizes them against degradation by serum components

In another embodiment, the micelle can be used to encapsulate peptide or protein antigens together with immunomodulatory agents including multiple TLR ligands, or molecules such as synthetic compounds or siRNA that modulate signaling networks within cells (e.g., dendritic cells or other antigen presenting cells). The micelle targets dendritic cells and macrophages through their nanometer dimensions, as such cells robustly internalize nanometer sized materials, through phagocytosis. The micelles are crosslinked by crosslinking agents comprising disulfide linkages, which should stabilize them against decomposition induced by serum proteins. In the further embodiment of the invention, the micelle has a size of 5 to 50 microns.

After phagocytosis, the biodegradable particles and micelles of the invention will break down, and the encapsulated material such as peptide or antigens, and immune stimulatory agents [e.g: ISS DNA, TLR 7/8, TLR 3 ligands such as ss RNA, TLR 2 ligands, and inhibitors of regulatory pathways such as the ERK, c-Fos or Foxp3 pathway], will be released into the dendritic cell, or macrophage, and the immunomodulatory agent will induce the antigen-presenting cells, to secrete a variety of cytokines. This combination of signals will result in the optimal activation of T cells, and inhibition of regulatory T cells and dendritic cells.

The micelles of the invention can include active agents such as vaccines composed of antigens from the relevant pathogen, together with immune modulatory agents [e.g: ISS DNA, TLR 7/8 ligands such as ss RNA, TLR 2 ligands, and inhibitors of regulatory pathways such as inhibitors of ERK, c-Fos or Foxp3, PI3 kinase, Akt, SOCS 1-7 proteins, or siRNA molecules or antisense molecules that inhibit such regulatory pathways].

The invention also provides methods for reversibly modifying proteins so that they have the appropriate charge to be encapsulated in the micelles. This strategy is based on reacting the amine groups of said protein with a compound, generating additional negative charges for every amine group, and rendering the protein negative. The modified protein will then be encapsulated in the micelle, crosslinked and then the pH will be reduced in order to remove the inserted compound form the protein. In one embodiment of the invention, the compound is amine groups is cis-aconityl. This group adds to negative charges to each amine group and can be released at ph 4.0.

Examples for targeting strategies include synthesizing a heterobifunctional PEG that has a DNA binding domain at one end and another end that can attached to a protein. This PEG chain is then attached to a protein and then assembled into a preformed micelles that contains immunostimulatory DNA. Examples of DNA binding domains include acridine or polyacridines. Examples of targeting ligands include galactose, mannose phosphate, mannose, peptides, and antibodies.

Further Modifications of the Biodegradable Particles and Micelles of the Invention

The biodegradable particle or micelles can be further modified to incorporate antibodies or other molecules which target (1) specific receptors on particular subsets of DCs or macrophages or monocytes, including Langerhans cells, dermal DCs, myeloid DCs, plasmacytoid DCs or (2) specific receptors on antigen-presenting cells, such as DEC205, Langerin, DC-SIGN, dectin-1, 33D1, MARCO.

Pharmaceutical Compositions of the Invention

The present invention provides a pharmaceutical composition comprising the polymer (which can optionally comprise a linker) of the invention. In one embodiment, the present invention provides a pharmaceutical composition comprising the particle (which can optionally comprise a linker) of the invention. In another embodiment, the present

invention provides a pharmaceutical composition comprising the micelle (which can optionally comprise a linker) of the invention. The polymer of the invention, whether in the form of a particle or micelle, can further comprise an active agent. For example, in one embodiment, the present invention provides a pharmaceutical composition comprising PCADK, PK1, PK2, PK3, PK4, PK5 and/or PK6 particles with a linker bound to an active agent.

METHODS OF THE INVENTION

Methods of Producing the Particles and Micelles of the Invention

The invention provides methods for producing the particles of the invention. In one embodiment, the method comprises the steps of a) forming a hydrophobic polymer of a ketal and a diol or an unsaturated alcohol; b) forming a polymer particle of the polymer of a) in the presence of one or more active agents and thereby encapsulating the agent(s). Examples of suitable chemistries for forming the hydrophobic polymer of a ketal and a diol or an unsaturated alcohol include acetal exchange reaction using single or double emulsions and acyclic diene metathesis (Heffernan MJ and Murthy N., 2005 *Bioconjug. Chem.* 16(6):1340-2; Jain RA., 2000 Biomaterials. 21(23):2475-90; Wagener K. B. and Gomez F. J., "ADMET Polymerization", in Encyclopedia of Materials: Science and Technology, E.J. Kramer and C. Hawker, Editors, Elsevier, Oxford, **5**, 48 (2002)).

Suitable examples of ketals for this method include, but are not limited to, 2,2-dimethoxypropane, 2,2-dimethoxybutane, 1,1-dimethoxycyclohexane or dimethoxyacetophenole. Also in the scope of the invention are ketal polymers including aliphatic, cycloaliphatic or aromatic ketals containing one or more hetero-atom, such as nitrogen, sulfur, oxygen and halides.

In accordance with the practice of the invention, the diol can be any of alkyl, aryl and cycloalkyl diols.

Suitable examples of diols include, but are not limited to, 1,4-benzenedimethanol, 1,4-cyclohexanedimethanol, 1,5-pentane diol, 1,4-butane diol or 1,8-octane diol.

In one embodiment, the invention provides a method for producing the particles of the invention comprising the steps of (a) forming PCADK polymer; and (b) forming a particle of PCADK in the presence of one or more active agents, thereby producing the particle of the invention. The PCADK polymer can optionally comprise a linker.

In one embodiment, the invention provides a method for producing the particles of the invention comprising the steps of (a) forming PK1, PK2, PK3, PK4, PK5 and/or PK6 polymer; and (b) forming a particle of one or more of PK1, PK2, PK3, PK4, PK5 and/or PK6 in the presence of one or more active agents, thereby producing the particle of the invention. The PK1-PK6 polymers can optionally comprise a linker.

The micelles of the invention can be produced in a two step process. First, the polymers of interest can be contacted with a liquid (polar or nonpolar liquid depending on the polymer to be used) under appropriate conditions so as to form a micelle. After micelle formation, the micelle can be crosslinked with an external crosslinking agent to produce the biodegradable micelle of the invention.

Methods for Using the Compositions of the Invention

The invention further provides methods for delivering the active agents of the invention, via the particles of the invention or the micelles of the invention, to a subject in order to, for example, deliver active agents so as to treat the subject suffering from a disease (e.g. alleviate symptoms associated with the disease) or disorder. The particles (e.g., made of PCADK, PK1, PK2, PK3, PK4, PK5 or PK6 polymer) or micelles may then be degraded or dissolved in the subject so as to release the active agent for delivery to the subject. The particles or micelles of the invention have variable degradation rates at various pH ranges and can be designed to release an active agent according to a desired profile. For

example, particles formed from PK3 polymers would degrade and release an active agent faster than particles formed from PK6 polymers.

In one embodiment of the invention, the particles or micelles of the invention used for delivering active agents further comprise a linker. In a further embodiment, a particle formed of the PCADK polymer further comprises a linker (e.g., NTA) bound to an active agent is used for delivery of the active agent to a subject.

The disease or disorder suffered by the subject can be any of HIV, malaria, TB, SARS, anthrax, Ebola, influenza, avian influenza and HCV. Further disease or disorder can be any of an infectious disease, autoimmune disease, allergic disease, disorder or complications associated with transplantation, diabetes and cancer. Examples of autoimmune disease include lupus, rheumatoid arthritis, psoriasis, asthma and COPD.

The active agents are delivered through the particles of the invention by various administration means including, but not limited to, intravenous, subcutaneous, intramuscular, oral and inhalation means. The most effective mode of administration and dosage regimen for the compositions of the present invention depends upon the exact location of the disease or disorder being treated, the severity and course of the disease or disorder, the subject's health and response to treatment and the judgment of the treating physician. Accordingly, the dosages of the molecules should be titrated to the individual subject.

The interrelationship of dosages for animals of various sizes and species and humans based on mg/m^2 of surface area is described by Freireich, E. J., et al. Cancer Chemother., Rep. 50 (4):219-244 (1966). Adjustments in the dosage regimen maybe made to optimize the tumor cell growth inhibiting and killing response, e.g., doses may be divided and administered on a daily basis or the dose reduced proportionally depending upon the situation (e.g., several divided dose may be administered daily or proportionally reduced depending on the specific therapeutic situation). It would be clear that the dose of the

compositions of the invention required to achieve treatment may be further reduced with schedule optimization.

As used herein, the term "subject" may include a human, any animal such as equine, porcine, bovine, murine, canine, feline, and avian subject, a cell or a cell tissue. In accordance with the practice of the invention the active agents can be delivered or administered to the subject (using the compositions of the invention) before, after, or during the onset of the disease or disorder.

The invention provides methods for regulating an immune response by administering active agents via the particles or micelles of the invention. In one embodiment of the invention, the particles or micelles used in the methods of the invention further comprise a linker. For example, in the methods of the invention, an immune response can be biased towards a Th immune response in a TLR-dependent manner by delivering or administering to a subject a particle or micelle of the invention containing a desired active agent. In one embodiment, a TLR-expressing cell is contacted with an agent (delivered by the particle or micelle of the invention) that effects a bias towards a Th immune response (e.g., a Th0, Th2 or T regulatory cell immune response). For example, the agent (*e.g.*, a natural ligand, a biologically active fragment thereof, or a small or synthetic molecule) that activatesTLR-2, ERK ½, or c-fos.

As noted above, the immune response can be regulated or modulated (e.g., increase biasing or decrease biasing toward a Th immune response) at a point in the signaling pathway downstream from receptor activation (*e.g.*, downstream from TLR binding or downstream from TLR activation or recognition). Thus, the patient can also be treated with an active agent or combination of active agents (delivered using the compositions of the invention) that bias the immune response by acting intracellularly on the elements of the downstream signaling pathway.

The present invention provides methods for biasing towards a Th2 immune response by inducing cell signaling (e.g., activation) of any of the MAP kinase pathways, including an

ERK ½ pathway using a desired active agent delivered using the compositions of the invention. An induced MAP kinase pathway can be characterized by an increase in the amount and/or duration of phosphorylated components of the MAP kinase pathways, including ERK ½.

In another embodiment of the methods of the invention, an active agent can be delivered, via the compositions of the invention, which modulates an ERK ½ MAP kinase pathway so as to regulate a TH2 immune response. In this embodiment, as an example, an agonist of a TLR (e.g., TLR-2) induces phosphorylation of ERK ½ so as to enhance a TH2 immune response. In yet another embodiment of the methods of the invention, an active agent can be delivered via the compositions of the invention so as to modulate a c-FOS pathway in the cell thereby regulating a TH2 immune response. In this embodiment, as an example, an agonist of a c-fos pathway induces expression of c-fos and/or phosphorylation of c-fos so as to enhance a TH2 immune response. Additionally, in yet a further embodiment of the methods of the invention, an active agent can be delivered via the compositions of the invention, so as to modulate a Th2 immune response by affecting TLR2 or its downstream signaling pathway elements such as ERK ½ MAP kinase pathway and a c-FOS pathway. For example, the active agent, delivered via the compositions of the invention, can be used to modulate production or activity of IL-10 (for example increase production or upregulate of IL-10).

In one embodiment, the methods for biasing towards a Th2 immune response includes decreasing or inhibiting signaling of p38 and/or JNK pathway(s) which mediate (e.g., inhibit) IL12 production and thus biasing against a Th1 response by administering an active agent delivered via the compositions of the invention. In another embodiment, the methods for biasing towards a Th2 immune response includes decreasing or inhibiting the amount of phosphorylated p38 and/or JNK, or decreasing or inhibiting the duration of phosphorylation of p38 and/or JNK which mediate (e.g., inhibit) IL12 production and thus biasing against a Th1 response by administering micelles or particles of the invention containing a desired active agent (or combination thereof).

The present invention also provides methods for biasing towards a Th1 immune response by inducing cell signaling (e.g., activation) of any of the MAP kinase pathways, including a p38 and/or JNK pathway by administering an active agent delivered via the compositions of the invention. An induced p38 and/or JNK pathway can be characterized by an increase in the amount and/or duration of phosphorylated components of the MAP kinase pathways, including p38, and/or JNK.

In one embodiment, the methods for biasing towards a Th1 immune response includes decreasing or inhibiting signaling of ERK ½ and/or c-fos pathway(s) by administering an active agent delivered via the compositions of the invention. In another embodiment, the methods for biasing towards a Th1 immune response includes decreasing or inhibiting the amount of phosphorylated ERK ½ and/or c-fos, or decreasing or inhibiting the duration of phosphorylation of ERK ½ and/or c-fos by administering an active agent delivered via the compositions of the invention.

Additionally, the invention provides methods for regulating a TH2 immune response which comprises contacting a T cell (e.g., a naïve T cell) with a TLR-positive cell (such as a DC) treated in culture with a TLR agonist (e.g., TLR-2 agonist), delivered via the compositions of the invention, which activates an ERK ½ pathway and/or which activates c-fos or c-fos pathway.

Additionally, the invention provides methods for regulating a TH1 immune response which comprises contacting a T cell (e.g., a naïve T cell) with a TLR-positive cell treated in culture with a TLR agonist (e.g., TLR-4 agonist), delivered via the compositions of the invention, which activates a p38 pathway and/or a JNK pathway.

The present invention provides methods for treating a subject having an immune-related condition or disease (e.g., allergies, autoimmune disease, and other immune-related conditions including cancer), comprising administering to the subject any of the agents of the invention, delivered via the compositions of the invention, in an amount effective to

bias towards or against a Th1, Th2 or Th0 immune response. The subject can be bovine, porcine, murine, equine, canine, feline, simian, human, ovine, piscine or avian.

In one embodiment, a subject having a condition or disease associated with an exhuberant Th2 response is treated with an agent of the invention, delivered via the compositions of the invention, that activates cell signaling in the subject so as to bias towards a Th1 immune response. Diseases characterized by exhuberant Th2 response include, but are not limited to allergy, asthma, and chronic obstructive pulmonary disease (COPD (*e.g.*, emphysema or chronic bronchitis).

In another embodiment, a subject having a condition or disease associated with an exhuberant Th2 response is treated with a molecule that inhibits biasing towards a Th2 immune response, delivered via the compositions of the invention.

In one embodiment, a subject having a condition or disease associated with an exuberant Th1 response is treated with agents of the invention, delivered via the compositions of the invention, that activate cell signaling in the subject so as to bias towards a Th2 immune response. Disease characterized by exhuberant Th1 response include, but are not limited to diabetes, rheumatoid arthritis, multiple sclerosis, psoriasis, and systemic lupus erythematosis.

In another embodiment, a subject having a condition or disease associated with an exuberant Th1 response is treated with an active agent, delivered via the compositions of the invention, that inhibits biasing towards a Th1 immune response.

ADVANTAGES OF THE INVENTION

Polyketal particles of the invention comprise, or are capable of encapsulating, a wide range of active agents, from small inhibitors to large proteins, and can be used to deliver

the active agents to a subject suffering from a disease or condition or as a preventative measure.

In one embodiment, the active agents joined to or encapsulated by the polyketals can retain activity for several weeks in a subject. Additionally, the polyketals with the active agents can be freeze-dried, and are capable of being stored for months without degradation. The polyketals have a controllable degradation profile at various pH ranges, and if necessary can be fine tuned for precision release of active agents.

The polyketal polymer of the invention should overcome problems associated with administering active agents in areas around e.g., cardiac myocytes, namely, that the increased blood supply in areas surrounding the myocytes makes it highly likely that active agents will be immediately carried away following administration. The larger, micron-scale polyketals of the invention should overcome this obstacle and allow the polyketals comprising or encapsulating active agents to remain in the local microenvironment.

The polyketals of the invention have several unique properties that make them ideal as a delivery vehicle of active agents for the treatment of a disorder or disease (e.g., myocardial treatment) or as a preventative measure: (1) they can degrade on a time scale that can be easily manipulated from 1-2 days to weeks at a variety of pH values; (2) they can hydrolyze into neutral excretable compounds, and should therefore cause less degradation and denaturation of proteins than polyester-based microparticles; (3) the polyketals can be solid particles and may be stable for extended periods after formulation; and (4) the properties of polyketals can be easily manipulated to alter particle size, shape and porosity.

In one embodiment of the invention, altering the copolymer percentage of the polyketals can change or fine tune the hydrolysis kinetics of the polyketals in order to provide controllable release of active agents joined to or encapsulated by polyketals. For example, the monomer composition of PK4 provides for faster hydrolysis kinetics than

PK3 at pH 4.5. In turn, PK3 has faster hydrolysis kinetics than PK2 or PK5, while PK2 and PK5 have faster hydrolysis kinetics than PK1 or PK6. Thus, active agents joined to PK4 will be released faster than active agents joined to PK3; active agents joined to PK3 will be released faster than active agents joined to PK2 or PK5; and active agents joined to PK2 or PK5 will be released faster than active agents joined to PK1 or PK6.

In another embodiment of the invention, the polyketals of the invention can be mixed in order to change or fine tune the release rate for active agents joined to or encapsulated by polyketals. For example, a polyketal with fast hydrolysis kinetics (e.g., PK4 or PK3) can be mixed with a polyketal with slower hydrolysis kinetics (e.g., PK1 or PK6) and co-administered to a subject. The active ingredient joined to PK4 or PK3 will be released in a subject quickly to provide the subject with an immediate release (IR) dose of active agent, while the active agent joined to PK1 or PK6 will be released at a slower rate allowing a gradual or extended release (ER) of the active agent in the subject.

Another advantage of the invention is that in one embodiment, a linker can be attached to the polyketal polymer. The polyketal polymers may then be used to form particles with linkers. Particles with linkers allow dual delivery of one or more active agents to a subject, namely, via encapsulation of the active agents by the particle and attachment of the active agent to the particle to the linker. In one embodiment, this dual mode of delivery for active agents provides for dual release times for the active agents, with the linker bound active agents released faster than the encapsulated active agents.

The following examples are presented to illustrate the present invention and to assist one of ordinary skill in making and using the same. The examples are not intended in any way to otherwise limit the scope of the invention.

EXAMPLES

EXAMPLE 1: Synthesis of Antigen Containing Crosslinked Micelles

Crosslinked micelles that contain the protein antigen Ovalbumin and immunostimulatory DNA were synthesized in a two step process. First, micelles were formed between the cationic block copolymer, PEG-polylysine-thiopyridal and negatively charged FITC-Ovalbumin (FITC-OVA) and immunostimulatory DNA (ISS-DNA). These micelles contained a 10mg/ml concentration of PEG-polylysine-thiopyridal, a 0.5 mg/ml concentration of FITC-OVA and a 0.5 mg/ml concentration of ISS-DNA. The micelles were allowed to form for one hour and were then crosslinked with 0.4mg/ml of dithio-ethylene glycol. The crosslinking reaction was monitored by U.V. activity (342nm), and indicated that the thiopyridal groups had been quantitatively reacted after 1 hour at room temperature. The encapsulation efficiency of FITC-OVA in the micelles was determined by centrifuging the micelles through a 100kD spin-filter (centricon) and analyzing the recovered solution for FITC fluorescence (excitation 494nm, emission 510nm). This indicated that over 95% of the FITC-OVA was encapsulated in the micelles.

EXAMPLE 2: Synthesis of Polyketal Particles (Single Emulsion Method for Delivery of Hydrophobic Drugs)

Particles were synthesized with poly(1,4-phenylene-acetone dimethylene ketal) using an oil-in-water emulsion method. Briefly, 10 mg of 2, 1mg of the ERK inhibitor UO126 and 0.1 g of chloro-methyl fluorescein diacetate (CMFDA), were dissolved in 0.5 mL of $CHCl_3$ (with 0.1% triethylamine). This solution was then added to 5 mL of pH 9 buffer (10 mM $NaHCO_3$) containing 2mg/ml polyvinyl alcohol (PVA, 31–50 kDa, Aldrich). The oil-water mixture was shaken briefly and then sonicated for 2 to 3 min at 40 watts (Branson Sonifier 250) to form a fine oil/water emulsion. The emulsion was stirred under N_2 flow for at least 3 h to evaporate the solvent and produce a particle suspension. Particle sizes were analyzed by dynamic light scattering (DLS) and indicated that the average diameter was 282 nm.

EXAMPLE 3: Synthesis of Polyketal Particles Encapsulating Ovalbumin (Double Emulsion Method for Synthesis of Hydrophilic Drugs)

Synthesis of polyketal particles

Polyketal particles (PKNs) containing FITC-ovalbumin were fabricated using a double emulsion method. First, 20 mg of poly(1,4-phenylene acetone dimethylene ketal) (PPADK) dissolved in 500 μL of chloroform was added to 100 μL of FITC-Ova solution (~0.7 mg). This mixture was sonicated at 40 watts for 1 minute to form the primary emulsion. Next, 5 mL of 0.2% w/v polyvinyl alcohol (PVA, Aldrich) in 10 mM pH 9 sodium phosphate buffer was added, and this mixture was sonicated at 40 watts for at least 1 minute to form the secondary emulsion. The emulsion was mixed under nitrogen ventilation for 4 hours, after which the volume was made up to 5 mL with buffer. Two batches of PKNs containing FITC-Ova were prepared in this manner, as well as two batches of plain PKNs (without FITC-Ova). The PKN suspensions were stored at 4°C.

Particle sizing was determined by dynamic light scattering (DLS). The two batches of FITC-Ovalbumin-loaded PKNs had effective diameters of 426 nm and 462 nm, and the empty PKN batches were 321 nm and 347 nm.

Labeling of FITC-Ova

Chicken egg albumin (ovalbumin) was labeled with fluorescein as follows. Ovalbumin was dissolved at 10 mg/mL in 200 mM pH 9 $NaHCO_3$ buffer. Fluorescein isothiocyanate (FITC) was dissolved at 10 mg/mL in DMSO. Next, 2.5 mL of ovalbumin solution (25 mg, 0.56 mmol) was mixed with 50 μL of FITC/DMSO (0.5 mg, 1.28 mmol) for at least 1 hour at 30°C. The product was filtered in a Sephadex PD-10 column to remove the free dye; the column was loaded with 2.5 mL of product and was eluted with 2.5 mL water. The resulting ovalbumin concentration was approximately 7 mg/mL. The degree of labeling was calculated to be 1.09 by measuring the absorbance of FITC at 497 nm and using the estimated concentration of ovalbumin.

Determination of FITC-Ova encapsulation in PKNs

The two FITC-Ova PKN batches were diluted by 5-fold in water, and a portion of each diluted sample was filtered through a 0.1 μm Supor syringe filter (Pall Acrodisc). The filtered and unfiltered samples were further diluted by 10-fold into pH 9 sodium phosphate buffer, and the fluorescence was measured with 494 nm excitation wavelength and 520 nm emission wavelength. (Figure 1)

The encapsulation efficiency was calculated using the fluorescence intensity of the filtered and unfiltered samples, as follows:

$$EncapsulationEfficiency = \left(1 - \frac{Filtered}{Unfiltered}\right) \times 100\% = \left(1 - \frac{189.5}{476.7}\right) \times 100\% = 60\%$$

EXAMPLE 4: Synthesis and Degradation of Ketal-Backbone Polymer (Polyketal)

Figure 2 shows: (A) Ketal exchange reaction between 1,4-benzenedimethanol and 2,2-dimethoxypropane to produce the ketal intermediate 1. (B) Stepwise polymerization of 1 to produce polyketal 2. Reaction steps A and B are driven forward by distilling off the methanol byproduct. (C) Formation of drug-loaded particles by the solvent evaporation method. Particles exhibit pH-sensitive degradation into low molecular weight excretable compounds.

Synthesis

The Polyketals are synthesized via a new polymerization strategy based on the ketal exchange reaction (Lorette, N. B.; Howard, W. L. *J. Org. Chem.* 1960, *25*, 521-525). This reaction is generally used to introduce protecting groups onto low molecular weight alcohols and has not been used previously to synthesize polymers. However, we demonstrate here that the ketal exchange reaction can be used to synthesize an acid sensitive polymer by simply reacting 2,2-dimethoxypropane (DMP) with a diol. We propose that the polymerization occurs through the reaction mechanism in Figure 2. The

ketal exchange reaction is an equilibrium reaction involving protonation of DMP followed by nucleophilic attack by the alcohol. This equilibrium is shifted toward formation of the ketal intermediate 1 by distilling off the methanol byproduct. As the reaction proceeds, molecules of 1 combine in a stepwise manner to form polyketal 2.

A representative polymerization of DMP and 1,4-benzenedimethanol (BDM) gave the polyketal 2 with a 48% yield. The polymerization was carried out in a 25 mL two-necked flask connected to a short-path distilling head. BDM (1.0 g, 7.3 mmol, Aldrich) dissolved in 10 mL warm ethyl acetate was added to 10 mL distilled benzene kept at 100°C. Re-crystallized *p*-toluene sulfonic acid (5.5 mg, 0.029 mmol, Aldrich) dissolved in 550 μL ethyl acetate was then added. After allowing the ethyl acetate to distill off, distilled DMP (900 μL, 7.4 mmol, Aldrich) was added to initiate the reaction. Additional doses of DMP were added via a metering funnel, with each dose consisting of 2 mL benzene plus 300 to 500 μL DMP. Each dose was added over a 30 to 40 min period with a 30 min interval in between. The total duration of the reaction was 7 h. The reaction was stopped with the addition of 100 μL triethylamine and was precipitated in cold hexanes. The crude product was vacuum filtered, rinsed with ether and hexanes, and vacuum dried to yield 600 mg of white solid product (48% yield). The recovered polymer was analyzed by GPC and ^{1}H NMR.

Figure 3A shows the GPC trace from one batch in which M_w = 4000 was obtained, corresponding to a degree of polymerization of 22.5 repeating units, with a polydispersity index of 1.54. The ^{1}H NMR spectrum (Figure 3B) confirms that the repeating unit of 2 contains a dimethyl ketal group ('6a'). Together, the GPC and ^{1}H NMR data provide evidence for the successful synthesis of polyketal 2.

Hydrolysis

The hydrolysis kinetics of 2 were measured at pH values corresponding to lysosomes (pH 5.0) and the bloodstream (pH 7.4). The hydrolysis rates were measured by grinding polyketal 2 into a fine powder and adding it to deuterated solutions at pH 7.4 (phosphate

buffer), pH 5.0 (acetate buffer), and pH 1.0 (DCl). The suspensions were stirred at 37°C and data points were taken at 3 h, 24 h, 48 h, and 72 h. Each suspension was centrifuged for 4 min at 1800 *g*, and the supernatant was analyzed by ^{1}H NMR. The spectra contained peaks for BDM (7.24 and 4.47 ppm) and acetone (2.05 ppm). The average of the two BDM peak integrals was used to determine the relative degree of hydrolysis. The percent hydrolysis was calculated as the BDM peak average of the pH 7.4 or 5.0 sample divided by the BDM peak average of the pH 1.0 control batch.

Exponential decay half-lives were calculated to be 102 h at pH 7.4 and 35 h at pH 5.0, representing a 3-fold rate increase from pH 7.4 to 5.0 (Figure 4). The pH sensitivity of 2 is significantly less than that reported by Kwon, et al. (Kwon, Y. J.; Standley, S. M.; Goodwin, A. P.; Gillies, E. R.; Fréchet, J. M. J. *Mol. Pharm.* 2005, *2*, 83-91) for a water-soluble ketal. We hypothesize that the lower pH sensitivity of 2 is due to its water insolubility, which limits the diffusion of water and creates another rate limiting step that is insensitive to pH. The diffusion kinetics of water into materials made of 2 will be dependent on the size of the particles and we would expect smaller particles to have greater pH sensitivity than ground particles.

EXAMPLE 5: Synthesis of Micron Sized Particles

Polyketal 2 (from Example 4, *supra*) was also used to synthesize micron sized particles. An oil-in-water emulsion method (Panyam, J.; Williams, D.; Dash, A.; Leslie-Pelecky, D.; Labhasetwar, V. *J. Pharm. Sci.* 2004, *93*, 1804-1814) was used to form the particles. Briefly, 50 mg of 2 dissolved in 1 mL $CHCl_3$ (with 0.1% triethylamine) was added to 5 mL of 10 mM $NaHCO_3$ pH 9 buffer containing various amounts of polyvinyl alcohol (PVA, 31–50 kDa, Aldrich) as the emulsifier. The oil-water mixture was shaken briefly and then sonicated for 2 to 3 min at 40 watts (Branson Sonifier 250) to form a fine oil/water emulsion. The emulsion was stirred under N_2 flow for at least 3 h to evaporate the solvent and produce a particle suspension.

Particle sizes were analyzed by dynamic light scattering (DLS) and SEM. DLS samples were prepared by diluting the particle suspension in 10 mL pH 9 buffer and allowing the larger particles to settle out. An aliquot from the liquid portion of each vial was then diluted for DLS particle sizing (Brookhaven 90Plus particle sizer). An SEM sample was made with the 0.2:1 ratio of PVA:polyketal by centrifuging the particle suspension for 10 min (5000 g, 4°C), washing with distilled water, and lyophilizing the recovered pellet.

As expected, the particle size was sensitive to the ratio of PVA to polyketal. The DLS particle diameters were 520 nm, 290 nm, and 280 nm for samples containing 0.2:1, 0.8:1, and 2:1 ratios of PVA:polyketal, respectively. The SEM images of the 0.2:1 batch (Figures 5A and 5B) confirm that the polyketal does form micron sized particles, with particle size distribution ranging from 0.5 to 30 μm in diameter.

EXAMPLE 6: Synthesis and Characterization of Micelles and Polyketal Particles

Materials and Methods

Encapsulation of Dexamethasone in Polyketal Particles

The anti-inflammatory drug dexamethasone (Dex, Sigma) was encapsulated into particles made with polyketal 2 described above. Dex-loaded particles were formulated using the same procedure as that described above, except that the oil phase contained a 5 mg/ml concentration of Dex and a 1:1 ratio of PVA:polyketal was used. SEM images of these particles demonstrate that they are 200-600 nm in diameter (Figure 5C). Particle sizing by DLS indicated an effective diameter of 250 nm for the Dex-loaded particle batches. The Dex encapsulation efficiency ranged between 43-53%. Control batches were prepared with polyketal/PVA only and Dex only. To measure Dex encapsulation, each particle batch was re-suspended in pH 9 buffer, and an aliquot was then further diluted. A portion was filtered through a 0.1 μm Supor membrane Acrodisc syringe filter (Pall Corp.), and the 242 nm absorbance of the filtrate was recorded with a Shimadzu UV-1700 spectrophotometer. The encapsulation efficiency was calculated as (A_{Dex} –

$A_{DexPoly}$)/(A_{Dex} – A_{Poly}), where A is the absorbance at 242 nm and the subscripts 'Poly', 'Dex', and 'DexPoly' refer to the 'Polyketal only', 'Dex only', and 'Dex + Polyketal' samples, respectively. These calculations resulted in a Dex encapsulation efficiency of 43% to 53% for various samples.

Micelle Formation

Figure 8 is a schematic representation showing peptide crosslinked micelle design and synthesis. Step 1: ISS DNA and I are mixed to form micelles (uncrosslinked micelle). Step 2: These micelles are then crosslinked with the antigenic peptide (II) to generate a delivery system that can encapsulate both immunostimulatory molecules and peptide antigens. After phagocytosis by APCs, the peptide-crosslinked micelles release their components.

An HIV peptide vaccine was synthesized using the PCM strategy with the peptide CGCRIQRGPGRAFVTIGKCGCG (II). The peptide II comes from the GP-120 protein and contains the sequence RIQRGPGRAFVTIGK, which is both a class I and II antigen. First, micelles were formed between I and ISS-DNA by mixing 0.5 mg of I with 0.1 mg of ISS DNA (5-TCCATGACGTTCCTGACGTT-3) (charge ratio was 1 to 15 (-/+)) in 0.5ml of 50mM PBS. Dynamic light scattering of these micelles using the Cumulants method indicated that they had an average diameter of 57.0 nm. These micelles were then crosslinked by adding 0.1 mg of II to the micelles (equal molar ratio of cysteines on II to thiopyridal groups on I). The peptide II was incorporated into the micelles through a disulfide exchange reaction.

Figure 9 shows synthesis and characterization of PEG-polylysine thiopyridal. A. Synthesis of PEG-polylysine thiopyridal (I). 44 μmole of PEG-Poly-*l*-lysine (with PEG = 5kd and Poly-*l*-lysine = 5,000) was dissolved in 1ml of DMF, in a 5ml round bottom flask, fitted with a stir bar (overnight stirring at room temperature was required to completely dissolve the polymer). 415 μmole of hydroxyl-ethyl thiopyridal acrylate and 58μl of triethylamine were then added to the PEG-poly-*l*-lysine solution and the reaction was allowed to run for 24 hours at room temperature. The product was isolated by

precipitating the reaction solution into 15 ml of ice cold diethyl ether. The yield was 88.2%. B. 1H-NMR spectrum of PEG-PLL-thiopyridal in D_2O. The product of A) was analyzed by ^1H NMR in D_2O. The percentage of amines alkylated was determined by comparing the peak intensity ratio of pyridine protons (-NC_5H_4: δ=7.101ppm, 7.629ppm, 8.187ppm) versus α, β, γ-methylene protons of poly-*l*-lysine (-$CH_2CH_2CH_2$: δ=1.122ppm, 1.285ppm, 1.553ppm), this indicated that a 100 % of the amines had been reacted. C./D. Dynamic light scattering analysis of PCMs uncross-linked (C) and peptide cross-linked (D). A 50mM PBS buffer solution, at pH 7.4, containing 0.06 mg/ml of PEG-polylysine thiopyridal and 20μg/ml of ISS DNA was made and filtered through a 200nm syringe filter. This solution was then analyzed by dynamic light scattering (Zetasizer Nano ZS, Malvern Instruments), using the Cumulant method (C). This solution was then crosslinked by adding 0.12 mg of peptide antigen (II), after 3 hours of reaction the solution was analyzed by DLS as described above, the size and the size distribution of the crosslinked micelles are shown in D). E. Crosslinking reaction of cysteines on peptide anigen (II). F. UV analysis of crosslinking reaction between peptide anigen (II) and block copolymer micelles. Block copolymer micelles were formed between I and ISS DNA by mixing 0.5 mg of I with 0.1 mg of ISS DNA (representing a 15/1 amine to phosphate ratio), in 0.5 ml of 50mM NaH_2PO_4 buffer (pH 7.4), in an eppendeorf tube. After incubation for 2 hours at room temperature, 0.1mg of II (representing a 1:1 cysteine to thiopyridal ratio) was added to the micelles. The crosslinking reaction between the cysteines on II with the thiopyridal groups in the micelles was determined by UV analysis at 342nm (representing the released thiopyridone). The percent of cysteine groups reacted was determined by the following formula:

$$reacted\ peptide\ (\%) = \frac{ABS_1 - ABS_2}{ABS_o} \times 100\%$$

where: ABS_1 = UV absorption at 342nm for the peptide-crosslinked micelles reaction (filled circles); ABS_2 = UV absorption at 342nm for the uncrosslinked micelles, without peptide (empty squares); ABS_o = UV absorption at 342nm when all of the thiopyridone groups have been reacted (by addition of DTT) (empty circles).

Figure 10 shows the effects of GSH on release of peptides and DNA.A. GSH sensitive peptide release. The stimuli responsive release of peptides from the PCMs due to the presence of GSH was investigated to determine if the PCMs will release peptide antigens after phagocytosis. The PCMs were incubated with different concentrations of GSH, for 24 hours in 50mM pH 7.4 PBS buffer, and then analyzed by HPLC to determine the release of peptides. This figure demonstrates that the release of peptides is triggered by the presence of GSH. Incubation of the PCMs with 10mM GSH (intracellular levels) induces the release of 71% of peptide, whereas incubation of the PCMs with just buffer causes the release of only 10% of peptides. B. GSH sensitive DNA release. The ability of the PCMs to protect encapsulated ISS-DNA from degradation by serum nucleases was investigated. PCMs were synthesized (as described above) and incubated with 10% serum for 12 hours, these PCMs were then examined by gel electrophoresis to determine the stability of the encapsulated ISS-DNA. As a control, ISS-DNA by itself was incubated with serum. This figure demonstrates that ISS-DNA, by itself, is completely hydrolyzed in 10% serum (Lane 2), in contrast ISS-DNA encapsulated in the PCMs is protected from serum nucleases, presumably because of the effects of the crosslinking (Lane 3), which should prevent nucleases from entering the micelle. C. ISS-DNA is protected from serum nucleases in the PCMs. A key advantage of the PCM strategy is that it generates a crosslinked delivery system. This crosslinking should stabilize the PCMs in vivo. The stability of the PCMs to decomposition was investigated by mixing the negatively charged polymer, poly(vinyl sulfate) (PVS) with the PCMs, this mixture was then analyzed by gel electrophoresis to determine the quantity of ISS-DNA displaced by the PVS. As a control, PVS was also incubated with uncrosslinked micelles that were just composed of II and ISS-DNA. Figure A, lane 4, demonstrates that PVS can disrupt uncrosslinked micelles that are just composed of ISS-DNA and II. In contrast, A, lane 5 demonstrates that PVS cannot displace ISS-DNA from the PCMs, presumably because the peptide crosslinking prevents the PVS from diffusing into the micelles and displacing the ISS-DNA. Importantly, after incubation of the PCMs with intracellular concentrations of GSH, the PCMs release encapsulated ISS-DNA, in the presence of PVS, demonstrating that the micelles should release their contents after phagocytosis. (lanes 2 and 3 in b). Charge ratio of ISS-DNA to I is 1 to 15 (-/+); 1μg of DNA was

loaded in each lane; GSH (100μM) was added to lane 3 to induce release of encapsulated ISS-DNA. All samples were incubated with 10% serum at room temperature for 12 h.

Figure 11 depicts block copolymer micelles: A. Chemical structure of PEG-poly(Lysine-Thio-Pyridyl). PEG chain gives stability to the micelles, Polylysine segment is used for electrostatic interactions with proteins and DNA or RNA. Thiopyridal group is for subsequent crosslinking via a disulfide bond. B. Step I: Mix PEG-poly(Lysine-thio-pyridal) with DNA and protein, form micelles, with PEG on the outside. C. Step II: Crosslink micelles with a di-thiol containing molecule, such as di-thioethylene glycol. D. Crosslinked micelles are reduced by Glutathione, which has a much higher concentration in the cell than in the blood.

Figure 12 shows the immunology of micelles. A. Uptake of SIINFEKL-CFSE micelles by human monocyte derived DCs. Human PBMC derived DCs (day 6 of culture) were pulsed with SIINFEKL/CFSE micelles for 4h in 37°C at the concentration of 10µg/ml, 5x10*5 cell/well, 96-U wells, RPMI/10% FCS. Cells were washed, fixed on the figures and prepared for confocal microscope imaging. B. Efficient uptake of micelle encapsulated SIINFEKL peptide by human monocyte derived DCs. Human PBMC derived DCs (day 6 of culture) were pulsed with SIINFEKL/CFSE plain (1) or micelle formulated (2,3) for 4h in 37°C at the concentration of 10µg/ml, 5x10*5 cell/well, 96-U wells, RPMI/10% FCS. Cells were washed, stained for CD11c and HLADR. Cells were gated for CD11c+, HLADR+ cells and analysed for CFSE fluorescence. C. Efficient uptake of micelle encapsulated SIINFEKL peptide by mouse DCs and Macrophages. Total mouse C57Bl/6J FLT3-L splenocytes were pulsed with 1 or 10 µg/ml of CFSE labeled plain SIINFEKL (1) or micelle formulated peptide (2,3) for 4 hours (blue line), or remained untreated (red line) at 37°C at the concentration 1x10*6 cell/well, 96-U wells, RPMI/10% FCS. Cells were stained for CD11c and CD11b and analyzed for CFSE positive fluorescence.

Figure 13 is a bar graph showing that micelle formulated SIINFEKL peptide induces potent T cell responses *in-vitro*. Purified $CD11c^+$ cells from a syngeneic C57Bl/6J H-2^b

FLT3-L treated mouse were pulsed for 4 hours with indicated concentrations and combinations of plain or micelle formulated SIINFEKL peptide. Cells were washed and cocultured with total OT-1 splenocytes for 20h (left panel) or 96h (right panel). Cells were stained for CD8 and intracellular IFNγ and analyzed on a flow cytometer. Graphs represent: micelle SIINFEKL 213.3 (black bar), micelle SIINFEKL 213.2 (grey bar), plain SIINFEKL (empty bar), medium (dotted bar) stimulated CD11c+ DCs.

Figure 14 shows the immunology of micelles. A. Efficient uptake of micelle encapsulated OVA protein by mouse DCs and Macrophages. Total mouse C57Bl/6J FLT3-L splenocytes were pulsed with 1 or 10 μg/ml of FITC labeled plain ovalbumin (1) or micelle formulated protein (2) for 1 hour (black line), 5 hours (dotted line) or remained untreated (shaded). 37°C at the concentration 1x10*6 cell/well, 96-U wells, RPMI/10% FCS. Cells were stained for CD11c and CD11b and analyzed for FITC positive fluorescence. B. Micelle encapsulated OVA/CpG activates DCs *in-vitro*. Total mouse C57Bl/6J FLT3-L splenocytes were pulsed with 1 μg/ml of plain OVA (1) plain OVA + 1ug of CpG (2) or micelle formulated OVA (3) or micelle OVA + 1ug of CpG (4) for 24 hours. CD11c+ cells were analysed for and CD80 or CD86 markers. Data represent isotype control (shaded), untreated (grey line) or stimuli treated (black line) cells.

Figure 15 is a graph depicting the immunology of polyketal particles. Uptake of polyketal particle (PKN) encapsulated U0126 by mouse DCs and Macrophages *in-vitro*. Total mouse C57Bl/6J FLT3-L splenocytes were pulsed with 1 or 10 μg/ml of CMFDA labeled Polyketal Particle carrying U0126 ERK inhibitor for 5 hours at 37°C, 1x10*6 cell/well, 96-U wells, RPMI/10% FCS. Cells were stained for CD11c and CD11b and analyzed for CMFDA positive fluorescence. Data represent medium treated cells (shaded line) or 5 hours uptake (black line).

Figure 16 is a schematic diagram showing the experimental outline for T cell stimulation in-vitro using OVA-OT/1 transgenic model.

Figure 17 shows the immunology of micelles. A. Micelle formulated antigen induces potent T cell responses *in-vitro*. Purified CD11c^{+} cells from a syngeneic C57Bl/6J H-2^{b} mouse were pulsed for 4 hours with indicated concentrations and combinations of ovalbumin and CpG plain or micelle formulated. Cells were washed and 1x10*5 of CD11c+ were cocultured with 1x10*6 of total OT-1 (SIINFEKL specific) splenocytes for 5 days. After 5 days cells were restimulated with a SIINFEKL peptide (1ug/ml) with BFA (5ug/ml) for 6 hours and stained for CD8 and intracellular IFNγ. Left panel represents the Flow Cytometer analysis; right panel shows the summary of the data. B. Micelle formulated antigens overcome CD4+ dependent mechanisms of CD8+ T cells induction. Purified CD11c^{+} cells from a syngeneic C57Bl/6J H-2^{b} mouse were pulsed for 4 hours with indicated concentrations and combinations of ovalbumin and CpG plain or micelle formulated. Cells were washed and 1x10*5 of CD11c were cocultured with 5x10*5 of CD8+ MACS purified OT-1 splenocytes (purity of ~90%) for 5 days. After 5 days cells were restimulated with a SIINFEKL peptide (1ug/ml) with BFA (5ug/ml) for 6 hours and stained for CD8 and intracellular IFNγ. Left panel represents the Flow Cytometer analysis; right panel shows the summary of the data. C. Micelle formulated antigen activate DCs *in-vivo*. C57Bl/6J mice (2/group) were injected i.v. with 5 μg/mouse of ovalbumin/CpG as plain or micelle formulated in 500ul PBS. Spleens were harvested at 4 and 24 hours post injection, treated with collagenase (30min/37C), homogenized, and treated with erythrocyte lysis buffer. CD11c+ cells were stained for CD80 or CD86 markers and analyzed with a flow cytometer. Data represent isotype control (shaded), nontreated mouse (grey line) or antigen injected mouse (black line).

Figure 18 shows the immunology of micelles and polyketal particles. A. Micelle formulated vaccines induce strong T cell responses *in-vivo* - CD8^{+} IFNγ^{+}. Cohorts of 4 C57Bl/6J mice were vaccinated s.c. with 5 μg/mouse of OVA (1) or OVA + CpG (2), micelle OVA (3), micelle OVA/CpG (4). Animals were boosted at day 36 (BOOST 1) and 84 (BOOST 2) using the same antigen formulations. Blood was harvested at days 6 post BOOST 2 and PBMCs were isolated using Histopaque gradient method, and restimulated with SIINFEKL peptide (1ug/ml) and BFA (5ug/ml) for 6 hours and stained for CD8 and intracellular IFNγ. Left panel represents the Flow Cytometry analysis and

gating strategy for selected mice; right panel shows the summary of the data as a % of $CD8^+$ $IFN\gamma^+$ cells of total $CD8^+$ T cells. B. Micelle formulated vaccines induce strong T cell responses *in-vivo* - $CD8^+$ $TNF\alpha^+$. Cohorts of 4 C57Bl/6J mice were vaccinated s.c. with 5 μg/mouse of OVA (1) or OVA + CpG (2), micelle OVA (3), micelle OVA/CpG (4) micelle. Animals were boosted at day 36 (BOOST 1) and 84 (BOOST 2) using the same antigen formulations. Blood was harvested at days 6 post BOOST 2 and PBMCs were isolated using Histopaque gradient method. PBMCs from 4 mice were pooled and restimulated with SIINFEKL peptide (1ug/ml) and BFA (5ug/ml) for 6 hours and stained for CD8 and intracellular TNFα and IL-10. Left panel represents the Flow Cytometer analysis and gating strategy for selected mice; right panel shows the summary of the data as a % of $CD8^+$ $TNF\alpha^+$ cells of total $CD8^+$ T cells. C. Kinetics of specific $CD8^+/IFN\gamma^+$ T cells after OVA/CpG vaccination. Cohorts of 4 C57Bl/6J mice were vaccinated s.c. with 5 μg/mouse of OVA + CpG (grey line) and micelle OVA/CpG (blue line). Animals were primed at day 0 and boosted at day 36 (BOOST 1) and 84 (BOOST 2) using the same antigen formulations. Blood was harvested at distinct days post priming and boosts and PBMCs were isolated using Histopaque gradient method. PBMCs from 4 mice were restimulated with SIINFEKL peptide (1ug/ml) and BFA (5ug/ml) for 6 hours and stained for CD8 and intracellular IFNγ. Panels represent the summary of the data as % of $CD8^+$ $IFN\gamma^+$ cells of total $CD8^+$ T cells including SEM error bars. D. Kinetics of specific $CD8^+/IFN\gamma^+$ T cells after OVA + UO126 PKN vaccination. Cohorts of 4 C57Bl/6J mice were vaccinated s.c. with 5 μg/mouse of OVA (grey line) micelle OVA (blue line) and micelle OVA + 10ug UO126 PKN(red line). Animals were primed at day 0 and boosted at day 36 (BOOST 1) and 84 (BOOST 2) using the same antigen formulations. Blood was harvested at distinct days post priming and boosts and PBMCs were isolated using Histopaque gradient method. PBMCs from 4 mice were restimulated with SIINFEKL peptide (1ug/ml) and BFA (5ug/ml) for 6 hours and stained for CD8 and intracellular IFNγ. Panels represent the summary of the data as % of $CD8^+$ $IFN\gamma^+$ cells of total $CD8^+$ T cells including SEM error bars. E. Micelle formulated vaccines induce strong antigen specific IgG antibody response *in-vivo*. Cohorts of 4 C57Bl/6J mice were vaccinated s.c. with 5 μg/mouse of OVA (1) or OVA + CpG (2), micelle OVA (3), micelle OVA/CpG (4) micelle OVA+ 10ug of PKN U0126 (5) or micelle OVA/CpG + 10ug of PKN U0126

(6). Animals were boosted at days 36 and 84 using the same antigen formulations. Bleedings were performed at week 4 post priming (PRIME), week 6 post 1st boost (BOOST 1) and week 7 post 2nd boost (BOOST 2). Sera from individual mice were pooled and tested for OVA specific IgG total, IgG1, IgG2a and IgG2b antibody reactivity using plate ELISA. Antibody reactivity was measured in 450nm absorbance of serum serial dilution. Data are represented as a reciprocal of specific anti-OVA antibody. F. Micelle formulated vaccines induce antigen specific IgE and IgM antibody response *in-vivo*. Cohorts of 4 C57Bl/6J mice were vaccinated s.c. with 5 μg/mouse of OVA (1) or OVA + CpG (2), micelle OVA (3), micelle OVA/CpG (4) micelle OVA+ 10ug of PKN U0126 (5) or micelle OVA/CpG + 10ug of PKN U0126 (6). Animals were boosted at days 36 and 84 using the same antigen formulations. Bleeding was performed and week 7 post 2nd boost. Sera from individual mice were pooled and tested for OVA specific IgE and IgM antibody reactivity using plate ELISA. Antibody reactivity was measured in 450nm absorbance of serum serial dilution. Data are represented as a reciprocal of specific anti-OVA antibody.

Polyketal PCADK Characterization

Figure 19 shows polyketals from cyclohexane dimethanol A. Polyketals from cyclohexane dimethanol (termed PCADK) degrade into cyclohexane dimethanol and acetone, both have FDA approval for human use. B. PCADK degrades in an acid sensitive manner. The ketal linkages in PCADK hydrolyze on the order of weeks under physiologic pH conditions. The hydrolysis of the ketal linkages in PCADK were measured by H-NMR at the pHs of 4.5 and 7.4. At the phagosomal pH of 4.5, the ketal linkages of PCADK are approximately 30% hydrolyzed after 10 days. Based on this result, we anticipate that CAT-PKNs should be completely hydrolyzed, within 4-5 weeks after phagocytosis by macrophages.

Figure 20 shows SEM images depicting that particles from PCADK can encapsulate the hydrophobic compounds and drugs such as rhodhamine red and ebselen.

Figure 21 shows line graphs showing that release of rhodhamine red from PCADK is pH sensitive.

Synthesis and Characterization of Polyketals and Particles Thereof

Figure 6 is a schematic representation showing the steps of particle formation. A. Step 1: Dissolve polyketal and drug into chloroform; dissolve polyvinyl alcohol in water. B. Step 2: Add chloroform solution to water and sonicate, generate micron sized droplets. Step 3: Let chloroform evaoporate, generates particles.

Figure 7 shows polyketal particles loaded with Fluorescein are taken up in the liver. Murine liver tissue slice showing release of fluorescein from PKNs following intravenous injection.

Figure 22 is a chemical representation showing that polyketals with almost any aliphatic diol can be made. The hydrophobicity of the polyketal determines its hydrolysis kinetics.

Figure 23 is a photograph showing that FITC labeled polyketals are phagocytosed by liver macrophages. Phagocytosis of PKNs in vivo by Kupffer cells. Mice were injected with either FITC-PKNs or Empty PKNs. The livers of these mice were analyzed by histology. Left: FITC-PKNs are abundantly present in Kupffer cells, as evidenced by the punctate green fluorescence (100x magnification). Middle: empty PKNs generate very little background green fluorescence (100x magnification). Right: immunohistochemistry (IHC) for FITC (red) confirms uptake by Kupffer cells (400x magnification).

Figure 24. A. Double emulsion procedure used to encapsulate catalase and super oxide dismutase in polyketal particles. A 50 μL aqueous solution of catalase (1 mg/ml) was dispersed into an organic phase, consisting of 75 mg of PCADK, dissolved in 1mL of dichloromethane, using a homogenizer, generating a water in oil (w/o) emulsion. This w/o emulsion was then dripped into 25mL of a 4% PVA solution, which was mechanically stirred with a homogenizer. The resulting w/o/w emulsion was then poured

into 225mL of a 4% PVA solution and mechanically stirred for several hours until the methylene chloride evaporated. The resulting particles were isolated by centrifugation, freeze-dried and examined by SEM (B) The protein encapsulation efficiency was 35%. The CAT-PKNs have an average diameter of approximately 8 microns. B. SEM image of catalase containing particles, and fluorescent microscope images of catalase containing particles. C. Catalase particles have enzymatic activity, as evidenced by their ability to decrease the absorbance at 240nm of hydrogen peroxide.

References for Examples 4-6:

Ahsan, F.; Rivas, I. P.; Khan, M. A.; Torres-Suárez, A. I. *J. Controlled Release* 2002, *79*, 29-40.

Prior, S.; Gander, B.; Blarer, N.; Merkle, H. P.; Subirá, M. L.; Irache, J. M.; Gamazo, C. *Eur. J. Pharm. Sci.* 2002, *15*, 197-207.

Hahn, S. K.; Jelacic, S.; Maier, R. V.; Stayton, P. S.; Hoffman, A. S. *J. Biomater. Sci. Polymer Edn.* 2004, *15*, 1111-1119.

Walter, E.; Dreher, D.; Kok, M.; Thiele, L.; Kiama, S. G.; Gehr, P.; Merkle, H. P. *J. Controlled Release* 2001, *76*, 149-168.

van Apeldoorn, A. A.; van Manen, H.-J.; Bezemer, J. M.; de Bruijn, J. D.; van Blitterswijk, C. A.; Otto, C. *J. Am. Chem. Soc.* 2004, *126*, 13226-13227.

Fu, K.; Pack, D. W.; Klibanov, A. M.; Langer, R. *Pharm. Res.* 2000, *17*, 100-106.

Shenderova, A.; Burke, T. G.; Schwendeman, S. P. *Pharm. Res.* 1999, *16*, 241-248.

Fife, T. H.; Jao, L. K. *J. Org. Chem.* 1965, *30*, 1492-1495.

Kwon, Y. J.; Standley, S. M.; Goodwin, A. P.; Gillies, E. R.; Fréchet, J. M. J. *Mol. Pharm.* 2005, *2*, 83-91.

Murthy, N.; Campbell, J.; Fausto, N.; Hoffman, A. S.; Stayton, P. S. *Bioconjugate Chem.* 2003, *14*, 412-419.

Murthy, N.; Xu, M.; Schuck, S.; Kunisawa, J.; Shastri, N.; Fréchet, J. M. J. *Proc. Natl. Acad. Sci. U. S. A.* 2003, *100*, 4995-5000.

Standley, S. M.; Kwon, Y. J.; Murthy, N.; Kunisawa, J.; Shastri, N.; Guillaudeu, S. J.; Lau, L.; Fréchet, J. M. J. *Bioconjugate Chem.* 2004, *15*, 1281-1288.

Gillies, E. R.; Goodwin, A. P.; Fréchet, J. M. J. *Bioconjugate Chem.* 2004, *15*, 1254-1263.

Lorette, N. B.; Howard, W. L. *J. Org. Chem.* 1960, *25*, 521-525.

Panyam, J.; Williams, D.; Dash, A.; Leslie-Pelecky, D.; Labhasetwar, V. *J. Pharm. Sci.* 2004, *93*, 1804-1814.

EXAMPLE 7A: Synthesis and Characterization of PK Particles for Treatment of Myocardial Infarction

In this example, the use of polyketal (PK) particles for the delivery of a small molecule inhibitor to the myocardium is described. The PKs are designed to deliver therapeutics to the heart and treat acute myocardial infarction. The PKs are formulated from a new class of polymers, the polyketals, which contain ketal linkages in their backbone (Figure 30).

Materials and Methods

Synthesis of Poly(cyclohexane-1,4-diyl acetone dimethylene ketal) (PCADK)

PCADK was synthesized in a 50 mL two-necked flask, connected to a short-path distilling head. First, 5.5 mg of re-crystallized p-toluenesulfonic acid (0.029 mmol, Aldrich), dissolved in 6.82 mL of ethyl acetate, was added to a 30 mL benzene solution (kept at 100°C), which contained 1,4-cyclohexanedimethanol (12.98 g, 90.0 mmol, Aldrich). The ethyl acetate was allowed to boil off, and distilled 2,2-dimethoxypropane (10.94 mL, 90.0 mmol, Aldrich) was added to the benzene solution, initiating the polymerization reaction. Additional doses of 2,2-dimethoxypropane (5 mL) and benzene (25 mL) were subsequently added to the reaction every hour for 6 hours via a metering funnel to compensate for 2,2-dimethoxypropane and benzene that had been distilled off. After 8 hours, the reaction was stopped by addition of 500 μL of triethylamine. The polymer was isolated by precipitation in cold hexane (stored at -20°C) followed by vacuum filtration. The molecular weight of PCADK was determined by gel permeation chromatography (GPC) (Shimadzu) equipped with a UV detector as shown in Figure 31. THF was used as the mobile phase at a flow rate of 1 ml/min. Polystyrene standards from Polymer Laboratories (Amherst, MA) were used to establish a molecular weight calibration curve. This compound was used to generate the PCADK particles in all subsequent experiments.

Particles can be fabricated with SB239063 joined to PCADK

SB239063 is an inhibitor of p38. Figure 29 shows a general schematic of p38 activation, including activation of upstream effectors and consequences of activation.

An experimental protocol was developed based on procedures used to formulate SOD into PLGA-based microparticles (Hayashi et al., Entrapment of proteins in poly(L-lactide) microspheres using reversed micelle solvent evaporation. *Pharm Res*, 1994. 11(2):337-40). Briefly, a 500 μL solution of SB239063 (1 mg/mL) was added to 1.0 mL of methylene chloride, containing 75 mg of PCADK. This mixture was then dripped into 5 mL of 4% (w/v) aqueous polyvinyl alcohol (PVA) solution and was stirred with a

homogenizer at 6,000 rpm for 1 min. The resulting w/o emulsion was then poured into 25 mL of pH 7.4 buffer, and this mixture was stirred for several hours, evaporating the methylene chloride. The resulting particles were isolated by centrifugation and freeze-dried, generating a white solid powder. The protein encapsulation efficiency of the SB293063 microparticles was 25-50%, as determined by U.V. absorbance at 320 nm using a standard curve for SB239063 alone. An SEM image of the SB239063-PCADK particles, shown in Figure 32, demonstrates that they are 3 to 15 μm in diameter, which is suitable for both intracellular and extracellular delivery. These data demonstrate that SB239063 can be successfully loaded in PK particles and that particles can be hydrolyzed for measurement of encapsulation efficiency.

Particle size can be easily altered

In order to demonstrate the feasibility of making larger particles, we performed an emulsion with the original protocol (above), one with a reduced homogenization speed or one with reduced PVA percentage. We then stirred for 4 hours at room temperature to evaporate the methylene chloride, and after several washes freeze dried the polyketals and examined them for size with SEM. As Figure 33 shows, the original protocol gave us particles in the range of <10 μm. However, by reducing the homogenization speed (15,000 RPM for 60 seconds), or by reducing the PVA percentage from 8% to 4%), we were able to generate particles 20 μm and larger. The data show that larger particles can be generated by reducing the speed of homogenization or reducing the percentage of aqueous solution. This shows the feasibility of generating larger particles as an alternative approach should we not get sufficient myocardial retention.

Porous PCADK microparticles can be synthesized

Porous microparticles 20-30 microns in size have recently attracted interest for lung drug delivery because their low density gives them the aerodynamic properties to be inhaled, via a spinhaler, yet their large size prevents them from being phagocytosed by macrophages. Studies by Langer et al., with PLGA, have demonstrated that 20-30 micron sized particles are optimal for delivering therapeutics to the extracellular space of the alveolar region of the lung (Cheng et al., Formulation of functionalized PLGA-PEG

nanoparticles for in vivo targeted drug delivery. *Biomaterials*, 2007. 28(5):869-76; Edwards et al., Large porous particles for pulmonary drug delivery. *Science*, 1997. 276(5320):1868-71; Perez et al., Poly(lactic acid)-poly(ethylene glycol) nanoparticles as new carriers for the delivery of plasmid DNA. *J Control Release*, 2001. 75(1-2):211-24).

We therefore developed an experimental protocol to generate protein loaded, porous PCADK microparticles. This protocol was adapted from a procedure used to formulate porous polylactide microspheres by Hong et al. Briefly, 100 mg of PCADK polymer was dissolved in 2.55 ml of methylene chloride. Then 0.45 ml of n-hexane was added to the polymer/methylene chloride solution and homogenized at 21,500 rpm for 30 seconds to generate the "oil phase". Next, a water-in-oil emulsion was created by added 200 µl of aqueous FITC-labeled OVA solution (25 mg/ml) to the oil phase and dispersing the aqueous phase in the oil phase via homogenation at 21,500 rpm for 90 seconds. The turbid w/o emulsion was then poured into 20 ml of 2% (w/v) aqueous polyvinyl alcohol solution and homogenized at 17,000 rpm for 60 seconds to generate the final water-in-oil-in-water emulsion. The w/o/w emulsion was then decanted into 100 ml of 2% PVA solution and stirred at 500 rpm for 3 hours at 25 °C in order to evaporate the methylene chloride in the oil phase causing the polymer to harden around the encapsulated OVA. The hardened particles are then stirred at 500 rpm for 72 hours at 40 °C to remove the hexane from the particles leaving pores in the interior and on the surface of the particles. An SEM image of OVA-PCADK is shown in Figure 34 demonstrating that porous particles were synthesized. These data support our alternative plan should there be issues with the release of SB239063 in vivo.

Release kinetics can be altered with co-polymer addition.

In this study, the influence of hydrophobicity on the hydrolysis kinetics of the polyketal copolymers was investigated. Two sets of copolymers were synthesized and their hydrolysis rates were investigated. First a series of polyketal copolymers, consisting of 1.4-cyclohexanedimethanol and 1,5-pentanediol, were synthesized, which contained varying ratios of 1,5-pentandiol. The hydrophilicity of these copolymers scales with their 1,5 pentane diol content, based on the large difference in hydrophobicity between 1,5-

pentandiol and 1,4-cyclohexanedimethanol, their respective Log P values are 0.27 and 1.75. We demonstrate that 1,5-pentandiol dramatically accelerates the hydrolysis kinetics of 1,4-cyclohexanedimethanol based polyketals. For example, at pH 4.5, PCADK has a hydrolysis half life of 20 days, however PK1, a copolymer which contains 2% pentane diol has a half life of 12.5 days at pH 4.5, and PK3, a copolymer containing 13% mole of 1.5-pentanediol, has a hydrolysis half life of only 2 days. A second series of copolymers, based on 1.4-cyclohexanedimethanol, were also synthesized, which contained diols of vary hydrophilicity. In summary, the data in Table 3 demonstrate that the hydrolysis kinetics of polyketals can be tuned by varying their hydrophilicity and suggests that diffusion of water into the polymer matrix is the rate determining step governing ketal hydrolysis. These co-polymers of PCADK will be used for our study as they have a "tunable" hydrolysis rate, and particles that slowly hydrolyze over the course of several weeks are optimal for cardiac regeneration.

Polymer composition				Half life at pH 4.5	Estimated half life at pH 7.4	Log P of diol B
Diol A	**Percent diol A**	**Diol B**	**Percent diol B**			
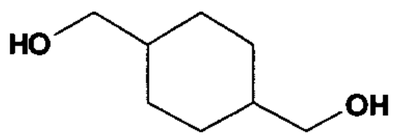 1,4-cyclohexane dimethanol	97%	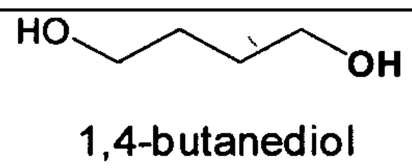 1,4-butanediol	3%	1.0 day	54 days	-0.83
	87%	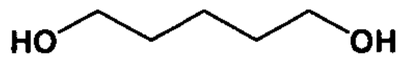 1,5-pentanediol	13%	1.8 days	39 days	0.27
	85%	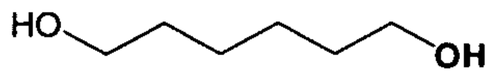 1,6-hexanediol	15%	4.4 days	53 days	0.76
	87%	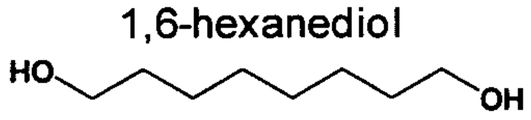 1,8-octanediol	13%	18.6 days	360 days	1.75

Table 3. Hydrolysis half-lives of polyketal copolymers with varying doil selections at pH 4.5 and pH 7.4.

Protein-loaded polyketals can be generated

An experimental protocol was developed based on procedures used to formulate SOD into PLGA-based microparticles. Briefly, a 100 μL aqueous solution of SOD (40 mg/mL) was dispersed by homogenization (21,500 rpm, 30 sec) into 1.0 mL of

methylene chloride, containing 125 mg of PCADK, generating a water in oil (w/o) emulsion. This w/o emulsion was then dripped into 5 mL of 8% (w/v) aqueous polyvinyl alcohol (PVA) solution and was stirred with a homogenizer at 6,000 rpm for 5 min. The resulting w/o/w emulsion was then poured into 25 mL of pH 7.4 buffer, and this mixture was stirred for several hours, evaporating the methylene chloride. The resulting particles were isolated by centrifugation and freeze-dried, generating a white solid powder. The protein encapsulation efficiency of the SOD-PCADK microparticles was 36.7%, as determined by U.V. absorbance at 280 nm. An SEM image of the SOD-PCADK microparticles, shown in Figure 35, demonstrates that they are 3 to 15 μm in diameter, which is suitable for both intracellular and extracellular delivery. This may be beneficial in the case of SOD delivery, because superoxide causes both intracellular toxicity and extracellular tissue damage during inflammation. These data demonstrate the versatility of the polyketals in their ability to encapsulate larger, hydrophilic proteins, in addition to small molecule inhibitors for our alternative approaches.

PCADK enhances the delivery of SOD to macrophages

The ability of SOD-PCADK microparticles to scavenge superoxide from macrophages was investigated in cell culture. TIB-186 macrophages ($1x10^5$ cells/well, 96 well plate) were incubated with either 0.1 mg/mL SOD-PCADK microparticles, free SOD (1.14 μg/mL SOD), or empty PCADK microparticles for 2 hours and then stimulated with 0.2μg/mL phorbol myristate acetate (PMA) for 30 min. The superoxide production from these macrophages was then measured using 20 nmol cytochrome c (absorbance at 550 nm). Figure 36 demonstrates that free SOD by itself causes very little inhibition of superoxide production, whereas SOD-PCADK microparticles caused a 60% reduction in superoxide production. Empty microparticles also reduced superoxide production by macrophages by approximately 20%. These data show that enzymatic proteins can retain their activity when encapsulated for cellular delivery. While formulated for another project, these data demonstrate feasibility of polyketal-mediated delivery of proteins to cells as an alternative method.

Polyketals are retained by macrophages in culture

Generally, macrophages will engulf foreign particles via phagocytosis, however our polyketals containing SB239063 are likely too large (> 5 μm) to undergo phagocytosis and the main method of release will likely be uptake of the small moleculars following hydrolysis of the particles by macrophages. To determine if polyketals are retained by macrophages, we incubated FITC-loaded polyketals with RAW macrophages for 2 hours, washed 3 times with PBS and imaged using fluorescence microscopy. As Figure 37 shows, FITC-loaded polyketals (and non-loaded polyketals) can be seen on the outside of cells. Additionally, Figure 37 shows cells (arrows) that have taken up the FITC. These data demonstrate that polyketals "stick" to cultured macrophages and their contents may be released following hydrolysis for uptake.

SB239063 particles inhibit p38 phosphorylation in TNF-α-stimulated macrophages

To determine the effects of PK-$p38_i$ on cytokine mediated p38 phosphorylation and superoxide release, RAW macrophages were plated at confluency in serum-free medium, and switched to serum-free medium containing empty PK or PK-$p38_i$ for 2, 4 or 6 hours, prior to 20 minutes TNF-α stimulation. Proteins were harvested in sample buffer and 20 μg run on a 12% SDS-polyacrylamide gel for Western analysis. Proteins were transferred to a PVDF membrane and were probed with an antibody to phospho-specific p38 (Cell Signaling). Blots were scanned and quantified using Quantity One software from Bio-Rad. As Figure 38 demonstrates, PK-$p38_i$ (0.1 mg/mL or 2 μM) prevented p38 phosphorylation by TNF-α in a time dependent manner. While there was no effect of empty PK at various time points, treatment of macrophages for 4 or 6 hours with PK-$p38_i$ completely prevented p38 phosphorylation by TNF-α. These data suggest that PK-$p38_i$ is capable of preventing cytokine-mediated p38 activation and superoxide production in macrophages.

SB239063 particles inhibit superoxide production in TNF-α-stimulated macrophages

Increased superoxide production following myocardial infarction may play a role in post-infarction cardiac apoptosis and dysfunction. TNF-α stimulation can lead to extracellular superoxide production in macrophages and this response was shown to be p38 dependent.

To determine whether polyketals loaded with SB239063 could inhibit extracellular superoxide production, we adapted a published method for using high performance liquid chromatography to measure accumulation of oxidized dihydroethidium in the media of stimulated cells (Fernandes et al., Analysis of dihydroethidium-derived oxidation products by HPLC in the assessment of superoxide production and NADPH oxidase activity in vascular systems. *Am J Physiol Cell Physiol*, 2006; Fink et al., Detection of intracellular superoxide formation in endothelial cells and intact tissues using dihydroethidium and an HPLC-based assay. *Am J Physiol Cell Physiol*, 2004. 287(4):C895-902). Of importance to note is that once dihydroethidium is oxidized, it can no longer cross the cell membrane, thus any oxy-ethidium formed in the extracellular space will remain there for measurement. Oxy-ethidium is stable and values can be quantified using the extinction coefficient and moles of superoxide are estimated to be the same as moles of oxy-ethidium as they react in a 1:1 ratio. Macrophages were plated at 10^6 cells/well in serum-free medium the night before experiments. Cells were then switched to serum-free medium containing buffer, empty PK, or PK-p38$_i$ for 6 hours and extensively washed prior to stimulation with TNF-α. TNF-α (10 ng/mL) was added to the cells in a Krebs-Hepes buffer for 15 minutes prior to the addition of dihydroethidium (25 μM) for 20 minutes. 100 μL of media was collected in 300 μL of methanol for HPLC with a fluorescence detector. As the data in Figure 39 demonstrate (n=4), there was a significant increase in extracellular superoxide production in macrophages stimulated with TNF-α that was completely inhibited by pretreatment with PK-p38$_I$ and not affected by empty polyketals. Exogenously added superoxide dismutase (50 U/mL) completely abolished the signal. Given that extracellular superoxide release is greatly increased in response to myocardial infarction (Figure 40), this may represent a potential mechanism to be investigated in future studies. These data do demonstrate however, that polyketals can deliver SB239063 to cells and inhibit not only TNF-α-induced p38 phosphorylation, but a downstream consequence as well.

Polyketals are retained in muscle 3 days following injection

To determine whether the polyketals can be detected in vivo after several days, we injected the leg muscle of C57BL/6J mice with 25 mg/mL of empty polyketals or

poly(lactic-co-glycolic acid) (PLGA). Three days following injection, muscles were isolated, fixed in 4% paraformaldehyde and embedded for histology. Hematoxylin & Eosin staining was performed on 5 μm sections and images captured using light microscopy. As the representative images in Figure 41 demonstrate, the particles were detectable 3 days following injection. Interestingly, despite the unusually high concentration of particles (25 mg/mL is 25-250-fold higher than our proposed experiments), there appeared to be very little inflammation around the particles. In contrast, leg muscles injected with PLGA particles showed intense fibrosis and possible inflammatory cell infiltration as examined in the subsequent figure. Note, the dark staining in the PCADK samples are most likely particles and not cells as confirmed by DAPI staining. These data demonstrate a critical proof of principle, in that injection of PCADK particles can be confirmed by light microscopy and doesn't appear to result in an intense inflammatory response.

Polyketal injection does not induce inflammatory response

To determine the effect of polyketal injection on inflammation, sections from the leg injection experiment above were stained with a fluorescent antibody against CD45, a common inflammatory cell marker. Specifically, after paraffin removal and rehydration, sections were incubated with proteinase K for antigen retrieval. Following retrieval, sections were blocked in 10% horse serum, then incubated with a fluorescently tagged anti-mouse CD45 antibody (eBioscience). After extensive washing, sections were incubated with DAPI (1 μg/mL) and coverslipped. The proper FITC-conjugated isotype was used as a control and no staining was evident. Images were taken with the exact same exposure times and merged using Matlab software. As the images in Figure 42 demonstrate, there was robust staining throughout the injection area in PLGA treated muscle, as compared to polyketal-injected muscle on the left. We confirmed this data with staining for CD14, another marker of inflammatory cells. While there was an intense cellular response in the PLGA treated muscle, we believe that much of the DAPI staining in the PCADK treated muscle is non-specific. These data are essential to the proposal, demonstrating little inflammatory response to a large concentration of polyketal injection. Even though the concentrations used in this experiment were likely orders of

magnitude above our proposed injections, there was little inflammatory cell response as measured by CD45 and CD14 staining. These data will provide confidence that any decrease we see in inflammation related to PK-p38$_i$ will not be due to offsetting any inflammation caused by the particles themselves.

SB239063 within polyketals inhibits p38 phosphorylation within the infarct zone

To determine whether polyketals encapsulating SB239063 are active in vivo, C57BL/6 mice underwent coronary artery ligation and immediately following infarction, were given either empty polyketals (PK) or polyketals containing SB239063 (PK-p38$_i$ 0.1 mg/mL) intramyocardially in a double-blinded manner. Hearts were excised 3 days following infarction and the infarct zone of the left ventricular free wall was isolated and homogenized in a Triton-X buffer containing protease and phosphatase inhibitors. 500 μg of protein was incubated overnight with a polyclonal p38 antibody (Cell Signaling) prior to incubation with protein-A agarose. Beads were washed and incubated with sample buffer before being run on 12% gel. Proteins were transferred to a PVDF membrane and were probed with a phospho-specific p38 antibody (Cell Signaling). After development, membranes were stripped and re-probed with a total p38 antibody. Blots were scanned and quantified using Quantity One software and data expressed as a ratio of phospho- to total p38 and compared statistically using ANOVA. As the blots and data in Figure 43 demonstrate, there was a significant increase in left ventricular phospho-p38 3 days following infarction. This increase was not inhibited by empty PK, but was completely abolished by PK-p38$_i$ treatment. These data demonstrate that SB239063 encapsulated within polyketals is active in vivo and significantly reduces p38 phosphorylation within the infarct zone following acute myocardial infarction.

SB239063 within polyketals inhibits IL-5 increase following myocardial infarction

Protein homogenates (50 μg) from the above double-blinded experiment were run on a 12% gel and transferred to a PVDF membrane for Western analysis. Membranes were incubated with an antibody against interleukin-5 (IL-5; AbCam), a pro-inflammatory cytokine associated with post-infarct cardiac dysfunction (Wei et al., Subacute and chronic effects of quinapril on cardiac cytokine expression, remodeling, and function

after myocardial infarction in the rat. *J Cardiovasc Pharmacol*, 2002. 39(6):842-50). Membranes were then stripped and re-reprobed with an antibody against β-actin for normalization. As the representative blots and grouped data show in Figure 44, there was a significant increase in IL-5 expression 3 days following infarction. This increase was not blocked by empty PK treatment, but completely abolished by PK-p38$_i$ treatment. These data demonstrate the potential of SB239063 within polyketals to inhibit pro-inflammatory cytokine production following acute myocardial infarction.

SB239063 within polyketals inhibits TNF-α increase following myocardial infarction in rats

Much of the above data was gathered using a mouse model, however we have begun to analyze data from our double-blinded studies in rats. To determine TNF-α release, adult male Sprague-Dawley rats underwent sham or coronary artery ligation surgery, and were injected with 50 μL of either 0.5 mg/mL empty PK, PK-p38$_i$, or free SB239063 (1 μM; corresponding to 0.5 mg/mL PK-p38$_i$). Left ventricular free walls were harvested and homogenized 3 days following ligation, and protein levels were determined by Bradford assay (Bio-Rad). Samples were then analyzed for TNF-α content using a commercially available ELISA kit (eBioscience). Data were expressed as pg/mg protein following correction. As the data in Figure 45 show, there was a two-fold increase in TNF-α production in infarcted animals 3 days following ligation. While not statistically significant because of low numbers (n=3-4 per group), there was a trend for inhibition by PK-p38$_i$ (~33% decrease). Also, there was no apparent effect of empty polyketals (PK) or injection of a comparable amount of free SB239063. These data support our initial positive findings in mice, and suggest that SB239063 encapsulation within polyketals may inhibit production of pro-inflammatory cytokines following myocardial infarction in rats.

Results and Discussion

In this example we have presented data consisting of both particle synthesis and testing, as well as some cellular and post-infarction effects. Our data show that the particles encapsulating the p38 inhibitor SB239063 can be generated from relatively simple single

emulsion protocols. Furthermore, out data clearly show the properties of the particles can be easily altered. Specifically, by altering the homogenization speed or the aqueous solution, particle size can be increased to ensure myocardial retention. Additionally, by addition of various copolymers, we can fine-tune the hydrolysis kinetics to match the needs of the post-infarct healing process. Finally, in addition to encapsulation of small molecule inhibitors, we can also encapsulate large, enzymatic proteins should our needs call for it.

When these particles are delivered to cultured macrophages, they are large enough to be retained outside the cell, while clearly the contents of the polyketal particles are delivered intracellularly. This occurs in a time-dependent manner, as incubation of macrophages with PK-$p38_i$ took at least 4 hours to significantly inhibit p38 phosphorylation in response to TNF-α stimulation. This inhibition was translated in to a downstream effect, as PK-$p38_i$ pretreatment inhibited TNF-α-induced extracellular superoxide production.

When delivered to leg muscle, the particles were easily distinguishable from the surrounding tissue and were retained for several days following injection. In comparison to PLGA particles, which degrade in to acidic products, PCADK caused very little inflammation as measured by CD45 and CD14 staining. When delivered intramyocardially, PK-$p38_i$ reduced left ventricular p38 phosphorylation in response to myocardial infarction. In addition, PK-$p38_i$ treatment reduced left ventricular levels of IL-5 and TNF-α, two pro-inflammatory cytokines. In contrast, there was no effect of empty PK, or even free SB239063.

In summary, this example shows that retention of compound SB239063, a p38 inhibitor, within the infarct area after a single injection will inhibit endogenous cardiac myocyte cell death, restore cardiac function following myocardial infarction and improve cell therapy in larger rodents.

The data herein demonstrated our ability to create small micron-scale polyketal (PK) particles that encapsulate SB239063 and TNF-α-induced p38 activation and superoxide

formation in cultured cells. Our data also showed that these particles can be delivered to the myocardium following infarction, and reduce p38 phosphorylation within the infarct region in mice.

EXAMPLE 7B: Future Studies

Polyketals (PK) containing the p38 inhibitor SB239063 may inhibit p38 phosphorylation, pro-inflammatory cytokine production and apoptosis in cultured cells.

PK-encapsulated SB239063 may be used to inhibit TNF-α-induced p38 phosphorylation and apoptosis in rat neonatal cardiac myocytes in a dose-dependent manner over the course of several days.

Experimental design: PK-$p38_i$ will be generated as described in the methods section above. We will isolate rat neonatal cardiac myocytes as described in the methods and incubate them with 0, 0.1, 0.5 and 1 mg/mL of empty PK or PK-$p38_i$ for 6 hours, based on the time course shown in Figure 38. Following PK-$p38_i$ incubation, TNF-α (10 ng/mL) will be added to the cells for 30 minutes and proteins will be harvested in SDS-sample buffer. This dose of TNF-α should be sufficient for activation of p38 in most cell types. Samples will be run on an SDS-PAGE gel and probed with antibodies recognizing either the phosphorylated or total p38 protein. This experiment will be repeated with addition of the TNF-α occurring at 24, 48 and 72 hours following PK-$p38_i$ treatment and washing. Free SB293063 will be used as a positive control for inhibition. Densitometry will be performed and groups will be compared statistically by ANOVA. Each experiment will be repeated at least 3 times for statistics.

To determine the effect on cardiac myocyte apoptosis, rat neonatal cardiac myocytes will be incubated with 0, 0.1, 0.5 and 1 mg/mL of empty PK or PK-$p38_i$ for 6 hours. Following PK-$p38_i$ incubation, TNF-α (10 ng/mL) will be added to the cells for 18 hours and proteins will be harvested in SDS-sample buffer. We will examine apoptosis by

Western analysis using antibodies against cleaved caspase-3, as well as cleaved PARP, two well known apoptosis pathway signaling molecules. Groups will be quantified using densitometry and compared using ANOVA. In addition to the above experiment, cells will also be harvested with trypsin and Annexin V staining will be performed followed by flow cytometry. Data will be collected and represented as a percentage of cells undergoing apoptosis and will be compared for statistical significance using ANOVA and Graphpad Prism software. These experiments will be repeated with addition of the TNF-α occurring at 24, 48 and 72 hours following PK-p38$_i$ treatment and empty particles (negative control), as well as the non-encapsulated form of SB239063 (positive control) will be used as controls. In addition to measuring pro-apoptosis markers, we will also examine TNF-α-stimulated myocytes for apoptosis using TUNEL staining followed by fluorescent imaging.

<u>PK-encapsulated SB239063 may inhibit p38 phosphorylation and inflammatory cytokine production in both RAW and isolated primary macrophages.</u>

Experimental design: PK-p38$_i$ will be generated as described in the methods section. We will perform these experiments using cultured RAW cells stimulated with TNF-α (10ng/mL) following incubation with 0, 0.1, 0.5 and 1 mg/mL of empty PK or PK-p38$_i$ for 6 hours. In one set of experiments, total proteins will be extracted following 30 minutes of stimulation and Western analysis will be performed for phosphorylated and total p38. Additionally, downstream effectors of p38 such as the transcription factor NFκB may be examined for activation. To measure cytokine production, we will stimulate cells with LPS and TNF-α following 6 hours of PK incubation. Media will be isolated and cytokine production will be measured using the Bio-Plex cytokine assay from Bio-Rad. Selected cytokines to be measured include, TNF-α, several members of the interleukin family, interferon-γ, and several other well known inflammatory cytokines. Specifically, IL-1, IL-5, IL-6 and IL-8 have been implicated in cardiac dysfunction following myocardial infarction. Thus, the above Bio-Plex assay may be followed up with Western analysis for confirmation. In addition to measuring pro-inflammatory cytokine production, mRNA from cultured and isolated cells will be

isolated and we will perform real-time PCR for the same cytokines and using either 18S or a housekeeping gene (β-tubulin) as a control.

We expect that PK-p38$_i$ will inhibit TNF-α-induced p38 phosphorylation in a dose-dependent manner. Additionally, we expect that this inhibition will be evident whether the PK-p38$_i$ is incubated for 6, 24, 48 or 72 hours before addition of TNF-α. In comparison, empty PK should have no effect on phosphorylation of p38, and free SB293063 should be a suitable positive control. It is possible that encapsulation may cause some of the inhibitor to be less active. If this is the case, we can either increase the starting amount of SB293063, or choose a replacement inhibitor. We also expect that PK-p38$_i$ treatment will reduce apoptosis induced by TNF-α. Many studies have shown a direct link between this pathway and activation of cleaved caspase-3 followed by additional apoptosis signals. We expect that PK-p38$_i$ will dose-dependently decrease cleavage of caspase-3 and PARP, as well as prevent Annexin V exposure. There are also several other methods of detecting apoptosis that can be examined if any difficulties arise including TUNEL, DNA fragmentation and cytochrome c release. It is possible that p38 inhibition is not sufficient to prevent apoptosis induced by TNF-α, despite the extensive literature history. In this case, we may examine the possibility of adding other inhibitors to the encapsulation procedure such as c-jun-N-terminal kinase (JNK) and stress activated protein kinase (SAPK) pathway inhibitors. This would not preclude us from our in vivo work, as TNF-α is not the only cytokine produced following infarction and preliminary studies from other laboratories suggest a strong role for p38 in vivo.

In addition to the effects on cardiac myocytes, we expect that PK-p38$_i$ treatment will dose-dependently inhibit phosphorylation of p38 and inflammatory cytokine production in cultured and isolated macrophages stimulated with TNF-α.

For all Western studies, developed film will be scanned and quantified using Bio-Rad's Quantity One software. All experiments will be repeated at least 3 separate times and means will be compared using ANOVA followed by the appropriate post-test. Cytokine

production will be expressed as pg/mL and data compared across all groups using ANOVA followed by the appropriate post-test.

PKs containing the p38 inhibitor SB239063 may inhibit p38 phosphorylation, cardiac myocyte apoptosis, prevent inflammatory marker expression, and improve cardiac function following myocardial infarction.

PK-encapsulated SB239063 may inhibit p38 phosphorylation and apoptosis within the infarct zone for up to 7 days following myocardial infarction in rats, rescuing cardiac function.

Experimental design: PK-p38$_i$ will be generated as described in the methods section. Adult male Sprague-Dawley rats will undergo sham surgery or coronary artery ligation as described in the methods and injected in a randomized and blinded manner with administration of empty PK, PK-p38$_i$ or free SB293063. At 3 and 7 days following surgery, animals will be subjected to echocardiography and MRI by a trained technician under light anesthesia, and hearts will either be harvested for protein ($n \geq 5$) or immunohistological studies ($n \geq 5$) at the indicated time point. For protein studies, the left ventricular free wall will be cut out and homogenized in a detergent buffer and proteins will be run on an SDS-PAGE gel and probed with antibodies recognizing both the phospho and total levels of p38. This method has been used by our laboratory and others to reliably detect phospho-proteins in vivo following infarction (Hsieh et al., Controlled delivery of PDGF-BB for myocardial protection using injectable self-assembling peptide nanofibers. *J Clin Invest*, 2006. 116(1):237-48). Protein samples will also be examined for cleaved caspase-3 levels to determine levels of apoptosis. In addition to phospho-p38 measurements, blots will also be probed with antibodies against pro-inflammatory cytokines such as TNF-α and several members of the interleukin family, including IL-1, IL-5, IL-6, and IL-8 Densitometry will be performed using Quantity One software from Bio-Rad, and data compared statistically using ANOVA followed by the appropriate post-test. Our animal numbers are justified in the subsequent vertebrate animal section, but power analysis with our published variability has determined these numbers.

Immunohistologically, sections will be probed with antibodies recognizing both phospho-p38 as well as a reliable cardiac myocyte marker (troponin I, α-sarcomeric actinin). We have published several papers using our standard protocol for immunohistochemistry. Briefly, tissue will be fixed in 4% paraformaldehyde, dehydrated and embedded in paraffin for sectioning. A standard microtome will be used to make 5 μm sections for all studies. For staining, following rehydration, antigen retrieval will be performed with proteinase K (20 μg/mL). After washing, sections will be blocked with 10% serum prior to incubation with the indicated primary antibody and appropriate fluorescent-tagged secondary antibody. Finally, sections will be incubated with DAPI (1 μg/mL) for visualization of nuclei. Both phospho-p38 staining intensity and double-positive cells will be quantified using ImagePro software. Intensity per unit area and percentage of double-positive cells will be compared statistically by ANOVA. To measure apoptosis, tissue sections will subjected to TUNEL staining per manufacturers protocol to determine a percentage of cardiac myocytes undergoing apoptosis. Data will be analyzed using ImagePro software and percentage of apoptotic cells will be counted and compared statistically with ANOVA followed by the appropriate post-test.

<u>PK-encapsulated SB239063 may prevent long-term cardiac dysfunction and development of fibrosis.</u>

In addition to the above experiments, we will also subject adult male rats ($n \geq 10$) to sham surgery or coronary artery ligation prior to injection of empty PK, PK-$p38_i$ or free SB239063 in a randomized and double-blinded manner. Rats will undergo echocardiography and MRI by a trained technician under light anesthesia at 28 and 90 days following infarction to determine if the recovery is evident in the chronic phase. At the indicated time points, hearts will be harvested in paraformaldehyde for immunohistological evaluation. Fibrosis will be determined by picrosirius red staining, followed by quantification of staining using a special program written in Matlab software. The program examines pixel intensity over several areas and is designed to reduce background in the sample. Groups will be compared statistically using ANOVA

followed by the appropriate post-test. In addition to fibrosis staining, immunohistochemistry will be performed for common markers of cardiac fibrosis, including connective tissue growth factor and transforming growth factor.

Following myocardial infarction, we expect an increase in phosphorylated p38 that will be inhibited by PK-p38$_i$ but not empty PK or free SB293063. We expect to see this with both extracted protein, as well as both cardiac myocyte- and macrophage-specific inhibition with immunohistochemistry. It is possible that p38 inhibition will not occur in vivo following PK-p38$_i$ administration. We may also examine encapsulation of an alternate inhibitor or increasing the loading of SB239063. Additionallywe can vary the porosity and hydrolysis kinetics of the particles to improve the delivery kinetics if needed. In addition to the above, we may also consider a second injection after several weeks as a booster. Thus, we can achieve chronic p38 inhibition by a second injection. We expect this inhibition of p38 activation following myocardial infarction to result in a significant decrease in cardiac myocyte apoptosis. This will be evident by staining for apoptosis markers including cleaved caspase-3, and TUNEL labeling. We expect that administration of PK-p38$_i$ will also reduce pro-inflammatory cytokine production in the infarct region, as compared with empty PK or SB239063 alone. This will be evident by Western analysis for the specific cytokines, including TNF-α, specific members of the interleukin family, and interferon-γ. It is possible that Western analysis may not be sensitive enough to detect differences in these markers in vivo, in which case we can use the Bio-Plex cytokine assay from Bio-Rad, or real-time PCR for the indicated markers. It is also possible that treatment with PK-p38$_i$ will not inhibit cytokine production after myocardial infarction. In either case, these data will give valuable information as to the contribution of local post-infarction signals transducing to more global signals in the progression of the disease.

We expect that these potential beneficial effects by PK-p38$_i$ outlined above will result in an improvement in cardiac function as compared to empty PK and free SB239063. This should be evident by a significant increase in fractional area of shortening, as well as decreases in end diastolic ventricular diameter and volume in the PK-p38$_i$ group as

compared to MI alone, with empty PK, or free SB239063. Echocardiographic measurements will be made by our technician during M-mode from short-axis images, and volumetric measurements will be made from long-axis measurements in a blinded manner. Additionally, cardiac MRI will be performed to confirm these data. It is possible that despite the reduction in pro-inflammatory cytokine production and apoptosis, the positive effect on cardiac function may not be evident at this early time point. For this reason, we have proposed performing the experiments again with longer time points (>28 days).

Finally, the beneficial effect may be evident on a prevention of fibrosis, as several studies have shown the p38 cascade to be a critical mediator of cardiac fibrosis. Therefore, in the future we may examine markers of cardiac fibrosis, such as the release of pro-inflammatory cytokines by ELISA or expression of pro-inflammatory genes by real time PCR. Published data also demonstrated a significant increase in adult cardiac myocyte proliferation after infusion of a p38 inhibitor (Engel et al., p38 MAP kinase inhibition enables proliferation of adult mammalian cardiomyocytes. *Genes Dev*, 2005. 19(10):1175-87). While the rates of proliferation even with p38 inhibitor were quite low, we may examine this by staining with Ki67 or by injection of BrdU prior to sacrifice. Our laboratory and others have developed protocols for BrdU injection for measurement of myocyte proliferation following injury (Hsieh et al., Controlled delivery of PDGF-BB for myocardial protection using injectable self-assembling peptide nanofibers. *J Clin Invest*, 2006. 116(1):237-48).

PKs containing the p38 inhibitor SB239063 may improve cardiac stem cell survival and efficacy both in culture and in vivo.

<u>PK-p38$_i$ may improve cultured cardiac stem cell survival and differentiation.</u>

Experimental design: We will isolate cardiac stem cells as described in the methods at the end of this section. Our preliminary isolation has demonstrated a high purity of c-kit$^+$ cardiac stem cells as shown in the methods. Cultured cardiac stem cells will be plated in

serum-free medium at confluency and incubated with 0, 0.1, 0.5 and 1 mg/mL of empty PK or PK-$p38_i$ for 6 hours. Following PK incubation, cells will be washed and incubated with TNF-α for 30 minutes. Proteins will be harvested in sample buffer and Western analysis will be performed for phospho- and total-p38. In addition, cells will be incubated for 18 hours with TNF-α and cells will be stained for common markers of apoptosis including cleaved caspase-3 and cleaved poly (ADP-ribose) polymerase (PARP). Apoptosis will also be measured using TUNEL and Annexin-V staining. All images will be quantified using a Matlab program and expressed as percent-positive. Western blots will be scanned and quantified using Quantity One software from Bio-Rad. All experiments will be repeated at least 3 times before statistical comparison between groups with ANOVA followed the appropriate post-test.

To determine whether improved survival can enhance differentiation, cells will be treated with 10% calf serum and 10 nM dexamethasone to induce differentiation in the presence and absence of empty PK or PK-$p38_i$ pretreatment. This combination of calf serum and dexamethasone should be sufficient to induce differentiation in cardiac stem cells as described by Linke et al. previously (Linke et al., Stem cells in the dog heart are self-renewing, clonogenic, and multipotent and regenerate infarcted myocardium, improving cardiac function. *Proc Natl Acad Sci U S A*, 2005. 102(25):8966-71). The same experiment will be performed in the presence of TNF-a (10 ng/mL) to determine whether the improvement in survival confers an additional benefit on differentiation. Following calf serum and dexamethasone treatment, cells will be fixed in 80% methanol for permeabilization and subsequent staining with cardiac-specific markers including the transcription factor Nkx2.5, cardiac myosin, α-sarcomeric actinin, connexin-43 and troponin T. These are all markers of cardiac maturation that we have used previously to determine cardiac phenotype in progenitor population. In addition to cardiac marker-specific staining, we will also harvest cellular RNA for measurement of the above proteins using real-time PCR.

PK-p38$_i$ may improve endogenous cardiac stem cell survival, growth and maturation.

Experimental design: PK-p38$_i$ will be generated as described in the methods. Adult male Sprague-Dawley rats will be subjected to coronary artery ligation followed by immediate injection of empty PK, PK-p38$_i$ or SB239063 alone. At 1, 7, 14 and 28 days following coronary artery ligation, rats will be sacrificed and hearts fixed in 4% paraformaldehyde and embedded for immunohistological evaluation ($n \geq 5$). The presence, as well as the size, of c-Kit positive and Sca-1 positive cells in the infarct zone will be analyzed using immunofluorescence and imaging software and performed in a blinded and randomized fashion. Double staining for the cardiac stem cell markers c-Kit or Sca-1 and the survival factor phospho-Akt will be examined as well using double immunofluorescence. Additionally, TUNEL and cleaved caspase-3 staining will also be co-localized with c-Kit and Sca-1 to determine if PK-p38$_i$ delivery improves survival of these endogenous stem cells. To measure maturation/differentiation, we will examine these progenitor cells for the expression of the cardiac markers α-sarcomeric actinin, troponin T, and for the presence of sarcomeres. Finally, to measure replication, we will examine BrdU incorporation and Ki67 staining of c-kit and sca-1 positive stem cells. Our prior studies demonstrate a single bolus injection of BrdU 2 hours prior to sacrifice is sufficient for measuring proliferating cells. For the above immunohistological evaluation, positive cells will be counted manually and with a program written in Matlab and expressed as percent positive. In addition, we have generated a program for counting cell size in Matlab that we have used previously for measuring implanted cell size (Davis et al., Local myocardial insulin-like growth factor 1 (IGF-1) delivery with biotinylated peptide nanofibers improves cell therapy for myocardial infarction. *Proc Natl Acad Sci U S A*, 2006. 103(21):8155-60). In our published studies, this method has been reliable with little variability in standardized assays. Groups will be compared statistically by using ANOVA comparison with the appropriate post-test. All animal numbers were justified by performing power analysis using our previously published standard deviations for immunohistochemical staining followed by cell counting.

PK-p38$_i$ may improve implanted cardiac stem cell survival, growth and maturation.

Experimental design: Cardiac stem cells will be isolated and cultured as described in the methods section. Prior to use, cells will be infected with an adenovirus encoding hemagglutanin for tracking. In a randomized and double-blinded manner, immediately following coronary artery ligation in adult male Sprague-Dawley rats ($n \geq 5$ per group), cells alone, cells with empty PK, cells with free SB239063, or cells with PK-p38$_i$ will be injected in to the infarct zone as inspected visually. In all studies, 500,000 cells per injection will be used as we have had success with injection of this amount previously (Davis et al., Local myocardial insulin-like growth factor 1 (IGF-1) delivery with biotinylated peptide nanofibers improves cell therapy for myocardial infarction. *Proc Natl Acad Sci U S A*, 2006. 103(21):8155-60). Echocardiography and cardiac MRI will be performed at 3, 14 and 28 days following infarction by a trained technician under light anesthesia in a double-blinded manner. In addition to cardiac function, hearts will be harvested at 3 and 28 days, fixed with 4% paraformaldehyde and embedded for immunohistological evaluation ($n \geq 5$ per group, per time point). Sections will be co-stained for hemagglutanin, as well as cleaved caspase-3 and TUNEL for assessment of apoptosis. We have used hemaglutanning and GFP adenoviruses to track cells previously and are able to stain greater than 95% of cells (Figure 47). Data will be expressed as percentage of implanted stem cells positive for these markers. In addition to measurement of apoptosis markers, we will also stain for cardiac maturation markers including cardiac myosin, α-sarcomeric actinin, and troponin T to determine differentiation/maturation. Finally, sections will be stained with hemagglutanin and size will be measured with a program written in Matlab. All data will assessed for statistical significance using ANOVA followed by the appropriate post-test. We expect that PK-p38$_i$ will significantly inhibit activation of cleaved caspase-3 in TNF-α-treated cells as compared to empty PK, whereas free SB239063 should be a suitable control. This should be evident in other markers for apoptosis including TUNEL and Annexin-V staining. In addition to the effects on survival, we also expect that this protection will translate into an increase in calf serum/dexamethasone-induced differentiation as measured by mature cardiac marker staining.

In addition to the effects on cultured cells, we expect that PK-p38$_i$ will enhance endogenous stem cell survival following myocardial infarction. By allowing more adult and stem cells to survive following infarction, we believe this will also result in increased stem cell maturation as measured by staining for specific markers over time. We expect that rats receiving cells implanted with PK-p38$_i$ will show improved cardiac function as compared to as measured by echocardiography and MRI when compared to cells with empty PK or free SB239063.

Close attention will be paid to the characterization of the cells by staining with specific lineage markers we have described in the methods. In addition to the magnetic bead separation we have used for our preliminary isolation, fluorescence activated cell sorting method has also been published for isolation of c-kit$^+$ stem cells. Original cardiac stem cells with be frozen, and cultures will be routinely checked for lineage markers to ensure proper cell type.

Polyketal synthesis- Poly(1,4-cyclohexane-acetone dimethylene ketal) (PCADK) will be synthesized, by reacting 1,4-cyclohexanedimethanol with 2,2-dimethoxypropane. PKs generated from PCADK should degrade in vivo to 1,4-cyclohexanedimethanol and acetone. PCADK will be synthesized in a 25 mL two-necked flask, connected to a short-path distilling head. 1,4-cyclohexanedimethanol (1.0 g, Aldrich), dissolved in 10 mL of warm ethyl acetate, will be added to 10 mL of distilled benzene kept at 100°C. Re-crystallized p-toluenesulfonic acid (5.5 mg, 0.029 mmol, Aldrich) dissolved in 550 µL of ethyl acetate will then be added to the benzene solution. The ethyl acetate will be allowed to distill off, and distilled 2,2-dimethoxypropane (900 µL, 7.4 mmol, Aldrich) will be added to initiate the reaction. Additional doses of 2,2-dimethoxypropane will be added via a metering funnel, to compensate for 2,2 dimethoxypropane that has distilled off. The reaction will be stopped with the addition of a 100 µL triethylamine and will be precipitated in cold hexanes. The crude product will be vacuum filtered, rinsed with ether and hexanes, and vacuum dried, generating PCADK. The recovered polymer will be analyzed by GPC and ^{1}H NMR.

Copolymers of polyketals, consisting of cyclohexane-dimethanol and butane diol will also be synthesized, using the methodology described above, to manipulate the hydrophobicity and hydrolysis kinetics of polyketal microparticles. Copolymers with 3, 5 and 10 mole percent of butane diol will be synthesized, we anticipate that these polymers will hydrolyze and release SB239063 significantly faster at pH 7.4 than PCADK, due to their greater hydrophilicity.

Encapsulation of SB239063- The SB239063 encapsulation experiments will be performed using a single emulsion procedure, using dichloromethane as the oil phase and PVA as the surfactant stabilizer. A representative procedure is described below. A 500 μL solution of SB239063 (1 mg/ml) will be dispersed into an organic phase, which consists of 75 mg of PCADK dissolved in 1mL of dichloromethane. This solution will be homogenized in 4% PVA at the lowest setting for 1 minute, and should generate a water-in-oil (w/o) emulsion. The resulting w/o emulsion will then be poured into 30 mL of a 1% PVA solution and mechanically stirred for several hours until the organic solvent evaporates. The resulting particles will be isolated by centrifugation, washed extensively, and freeze-dried. Particles can be assayed for inhibitor content by A320 using empty polyketals as a control. We have generated standard curves for SB239063 concentrations that can be applied. The resulting polyketals will also be dried and examined with SEM.

Myocardial injection/infarction- Adult male Sprague-Dawley rats weighing 250 grams will be subjected to myocardial infarction or injection surgeries as described. Briefly, the animals will be anesthetized (1-3% isoflurane) and, following tracheal intubation, the heart will exposed by separation of the ribs. Myocardial infarction will be performed by ligation of the left anterior descending coronary artery. For PK injection or cell therapy studies, immediately after coronary artery ligation, treatment (50-100 μL) will be injected into the infarct zone through a 30-gauge needle while the heart is beating. Following injection, the chests will be closed and animals will recover on a heating pad. Echocardiograms will be performed when described in the experimental design. I have

experience in this animal model and we have obtained reproducible infarcts as measured by echocardiography. We have performed several experiments in rats and Figure 48 shows a graph of grouped data from 10 animals undergoing sham or coronary artery ligation surgery. On the Y-axis is %fractional shortening after 3 days, a common measurement of cardiac function using echocardiography.

Neonatal cardiac myocyte isolation- By following this protocol, we have been able to recover neonatal cardiac myocytes with 95-99% purity (Davis et al., Local myocardial insulin-like growth factor 1 (IGF-1) delivery with biotinylated peptide nanofibers improves cell therapy for myocardial infarction. *Proc Natl Acad Sci U S A*, 2006. 103(21):8155-60; Davis et al., Injectable self-assembling peptide nanofibers create intramyocardial microenvironments for endothelial cells. *Circulation*, 2005. 111(4):442-50; Narmoneva et al., Endothelial cells promote cardiac myocyte survival and spatial reorganization: implications for cardiac regeneration. *Circulation*, 2004. 110(8):962-8). One-day-old pups from Sprague-Dawley rats (Charles River Laboratories) will be killed; hearts will be excised, washed in Hanks' buffered salt solution, and, after mincing, placed in trypsin (1 mg/mL) for 6 hours at 4°C. The resulting pellet will then be dissolved in collagenase type 2 (0.8 mg/mL) for 1 hour at 37°C. Following light centrifugation, the resulting pellet will be resuspended in Medium 199 containing 20% fetal bovine serum and plated for 2 hours. The nonadherent cells will be plated on fibronectin coated dishes for experiments or collected and analyzed by flow cytometry with the use of an antibody to α-sarcomeric actin to determine myocyte composition.

Cardiac stem cell isolation- Hearts of adult Sprague-Dawley rats will be isolated, minced, and incubated with collagenase Type 2 (0.8 mg/ml) for 1 hour at 37°C. The supernatant will be isolated by centrifugation and then incubated with a c-Kit antibody conjugated to magnetic beads (Dynal). A second selection step will take place after cells reach confluency with an antibody directed against Sca-1. Cell phenotype will be determined with flow cytometry against c-Kit, Sca-1, and lineage markers. Lineage markers to be used are CD34, CD45, CD31, connexin43, cardiac myosin and von Willebrand factor. With this process, several investigators have been able to maintain a

line of cardiac stem cells that continuously renew and can be kept in culture (Beltrami et al., Adult cardiac stem cells are multipotent and support myocardial regeneration. *Cell*, 2003. 114(6):763-76). Additionally, as Figure 49 demonstrates, our preliminary isolation procedures have begun and are quite effective. We have been able to maintain a line of c-kit$^+$ stem cells that do not stain for other lineage markers, including CD45. Additional studies are underway to determine absence of other markers, as well as sensitivity to pro-death stimuli.

Western analysis and real-time PCR- Western analysis in cultured cells and protein extracted from the infarct region and will be performed as previously described (Hsieh et al., Controlled delivery of PDGF-BB for myocardial protection using injectable self-assembling peptide nanofibers. *J Clin Invest*, 2006. 116(1):237-48). Antibodies to CTGF, TGF-β, collagen type 1 and MMP-2 are commercially available. RNA will be extracted from the infarct zone using Tri-Reagent and following manufacturer's protocol. Western analysis will performed from cell homogenates or tissue homogenates. Cells will be harvested in a Tris/EDTA buffer containing 0.1% Triton-X, protease and phosphatase inhibitors. Tissue homogenates will be made with similar buffers (unless specific protocol calls for a different buffer) and homogenized using a PowerGen homogenizer (Fisher) with a saw-tooth generator.

Immunostaining- Hearts will be isolated at the indicated time point and fixed in 4% paraformaldehyde for 6 hours at room temperature. Following dehydration, hearts will be embedded in paraffin and 5 μm sections will be made for immunohistochemistry. Paraffin will be removed by immersion in Xylene and sections will be probed with antibodies as described in the methods. Antibodies to cardiac markers (troponin T, α-sarcomeric-actin, cardiac myosin) are commercially available and have been used in our laboratory.

Echocardiography/MRI- Echocardiography and MRI will be performed under light anesthesia by an experienced technician. All measurements will be taken and analyzed in

a double-blinded manner. Left ventricular end systolic and diastolic measurements will be taken from M-mode short-axis images, and confirmed in long-axis views.

EXAMPLE 8: Synthesis of Polyketal Copolymers and Formation of Particles

In this example a strategy is presented for manipulating the hydrolysis kinetics of poly(cyclohexane-1,4-diyl acetone dimethylene ketal) (PCADK) by controlling its hydrophilicity through copolymerization with other diols, of varying hydrophilicity. Six polyketal copolymers PK1 to PK6, based on PCADK, were synthesized.

Materials and Methods

Polyketal copolymers were synthesized in a 25 mL two-necked flask, connected to a short-path distilling head. The diols, 1,4-cyclohexanedimethanol (1.04 g, 7.25 mmol) and, either 1,4-butanediol, 1,5-pentanediol, 1,6-hexanediol, or 1,8-octanediol were dissolved in 20 mL of distilled benzene and kept at 100°C. Re-crystallized p-toluenesulfonic acid (5.5 mg, 0.029 mmol), dissolved in 550 μL of ethyl acetate, was added to the benzene solution. The ethyl acetate was distilled off, and distilled 2,2-dimethoxypropane (equal molar quantity as the two diols combined) was added to initiate the reaction. Additional doses of 2,2-dimethoxypropane (500 μL) and benzene (2 mL) were subsequently added to the reaction, every hour for 6 hours, via a metering funnel, to compensate for 2,2-dimethoxypropane and benzene that had distilled off. After 24 hours, the reaction was stopped by adding 100 μL of triethylamine. The polymer was isolated by precipitation into cold hexanes and analyzed by ^{1}H-NMR and GPC, in general the resulting polymers had number average molecular weights between 2000 to 4000 Da. Table 1 lists the compositions and molecular weights of the polyketal copolymers synthesized. ^{1}H NMR spectra were obtained using a Varian Mercury VX 400 MHz NMR spectrometer (Palo Alto, CA) using $CDCl_3$ as the solvent, the H-NMR spectra of the polyketal copolymers are summarized below, as a representative example, the ^{1}H-NMR of PK3 is shown in Figure 50. The molar ratio of 1,5-pentanediol to 1,4-

cyclohexanedimethanol was obtained by obtaining the ratio of areas under the peaks a and b, respectively.

PK1. ^{1}H NMR ($CDCl_3$) δ = 3.4 – 3.18 (m, 4H), 1.66 (s, 1.9H), 1.85 – 0.93 (m, 8H), and 1.32 (s, 6H).

PK2. ^{1}H NMR ($CDCl_3$) δ = 3.4 – 3.18 (m, 4H), 1.66 (s, 1.8H), 1.85 – 0.93 (m. 8H), and 1.32 (s, 6H).

PK3. ^{1}H NMR ($CDCl_3$) δ = 3.4 – 3.18 (m, 4H), 1.64 (s, 1.7H), 1.85 – 0.93 (m, 8.2H), and 1.32 (s, 6H).

PK4. ^{1}H NMR ($CDCl_3$) δ = 3.4 – 3.18 (m, 4H), 1.68 (s, 2H), 1.85 – 0.93 (m, 8H), and 1.32 (s, 6H).

PK5. ^{1}H NMR ($CDCl_3$) δ = 3.4 – 3.18 (m, 4H), 1.67 (s, 1.8H), 1.85 – 0.93 (m, 8H), and 1.32 (s, 6H).

PK6. ^{1}H NMR ($CDCl_3$) δ = 3.4 – 3.18 (m, 4H), 1.68 (s, 1.8H), 1.85 – 0.93 (m, 8H), and 1.32 (s, 6H).

The molecular weight of the polyketal copolymers was determined by gel permeation chromatography (GPC) using a Shimadzu system (Kyoto, Japan) equipped with a UV detector. THF was used as the mobile phase at a flow rate of 1 mL/min. Polystyrene standards (Peak Mw = 1060, 2970, and 10680) from Polymer Laboratories (Amherst, MA) were used to establish a molecular weight calibration curve.

The hydrolysis of the polyketal copolymers was measured in buffered water at pH values of 1.0 (.1M HCL), 4.5 (100 mM AcOH) and 7.4 (100 mM) at 37°C. Briefly, 20mg of the polymer samples were placed in a 5 ml vial, 1 mL of buffer solution was added to each

vial, and mixed with a magnetic stir bar. At specific time points, 1 mL of CDCl3 was added to each vial and shaken vigorously, the $CDCl_3$ phase was isolated and analyzed by ^1H NMR, to determine the percent hydrolysis the of ketal linkages in polyketal copolymer.

Results and Discussion

Six polyketal copolymers PK1 – PK6 (Table 1, *infra*), based on PCADK, were synthesized using the acetal exchange reaction. The copolymers of PCADK were synthesized by copolymerizing 1,4-cyclohexanedimethanol with either butanediol, pentanediol, hexanediol, and octanediol. The hydrophilicity of these diols are different from that of 1,4-cyclohexanedimethanol (log P = 1.46), as evidenced by their respective log P values (Table 2, *infra*). Figure 51 shows a synthetic scheme of the acetal-exchange reaction used to make the polyketals and the degradation products generated from their hydrolysis. The synthesis of all the polyketal copolymers was accomplished in one step, on a multi-gram scale, and with yields of 50 – 60%. In general, the introduction of diols other than CDM did not cause any complications in the synthesis, and procedures developed for the synthesis of PCADK were suitable for the synthesis of the copolymers. Importantly, all the copolyketals synthesized were crystalline, and therefore have the potential for formulation into microparticles.

Table 1. Compositions and molecular weight of polyketal copolymers synthesized.

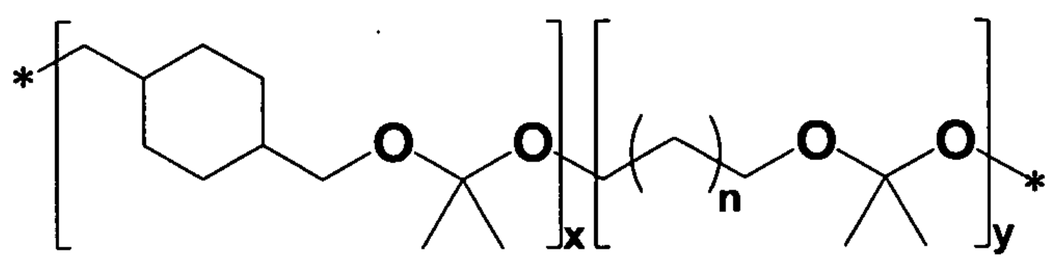

n = 2, 3, 4, and 6

Polymer ID	Polymer composition		M_n	DPI
	Monomer A	Monomer B		
PK1	1,4-cyclohexanedimethanol	1,5-pentanediol	2149	1.742

	(x=98.03%)	(y=1.93%)		
PK2	1,4-cyclohexanedimathanol (x=92.46%)	1,5-pentanediol (y=7.56%)	2530	1.629
PK3	1,4-cyclohexanedimathanol (x=86.70%)	1,5-pentanediol (y=13.30%)	2596	1.432
PK4	1,4-cyclohexanedimathanol (x=96.75%)	1,4-butanediol (y=3.25%)	2637	1.553
PK5	1,4-cyclohexanedimathanol (x=85.32%)	1,6-hexanediol (y=14.68%)	2122	1.538
PK6	1,4-cyclohexanedimathanol (x=87.31%)	1,8-octanediol (y=12.69%)	2181	1.786

The hydrolysis kinetics of PK1 to PK6 was measured at the pH values of 4.5 and 7.4 to determine their behavior in the acidic environment of phagosomes and in the blood. Figure 52 demonstrates that all polyketal copolymers undergo acid-catalyzed hydrolysis and that their hydrolysis kinetics scale inversely with their hydrophobicity. PK1, PK2, and PK3 were copolymers synthesized from 1,4-cyclohexanedimethanol and 1,5-pentanediol. Their hydrophilicity scales with their 1,5-pentanediol content, due to the large difference in hydrophobicity between 1,5-pentanediol and 1,4-cyclohexanedimethanol, their respective Log P values are 0.27 and 1.46. Figure 52A demonstrates that 1,5-pentanediol dramatically accelerates the pH 4.5 hydrolysis kinetics of 1,4-cyclohexanedimethanol based polyketals. For example, only 30% of PK1, a copolymer containing 2% pentanediol, was hydrolyzed after 10 days at pH 4.5. On the other hand, at the same pH condition PK2, which contains 7.5% pentanediol, was 75% hydrolyzed after 7 days, and PK3, containing 13% pentanediol, was 50% hydrolyzed after 2 days and completely hydrolyzed after 5 days. For all three polyketals, less than 15% of the polymers were hydrolyzed in pH 7.4 within the duration of the experiments (Figure 52B).

Table 2. Hydrolysis half-lives of polyketal copolymers at pH 4.5 and pH 7.4, at 37°C.

PK ID	Polymer composition				Half life at pH 4.5	Estimated half life at pH 7.4	Log P of diol B
	Diol A	Percent diol A	Diol B	Percent diol B			
PK4		96.75%	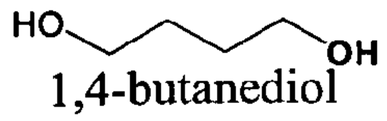 1,4-butanediol	3.25%	1.0 day	54 days	-0.83
PK3	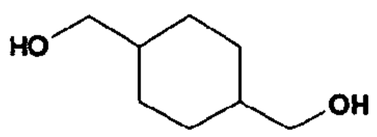	86.70	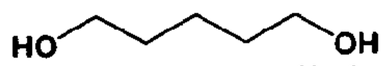 1,5-pentanediol	13.30%	1.8 days	39 days	0.27
PK5	1,4-cyclohexane dimethanol	85.32%	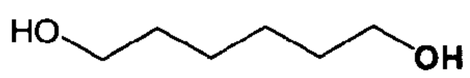 1,6-hexanediol	14.68%	4.4 days	53 days	0.76
			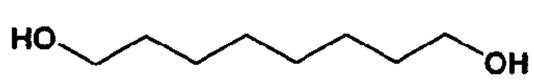 1,8-octanediol				
PK6		87.31%		12.69%	18.6 days	360 days	1.75

To determine if this was a broader phenomenon, extending beyond copolymers of pentane diol, polyketal copolymers PK4, PK5, and PK6 were also synthesized from butanediol, hexanediol, and octanediol, which have differing hydrophobicity from pentanediol, and their hydrolysis kinetics were investigated. Table 2 demonstrates that this set of copolymers also has an inverse relationship between hydrophobicity and hydrolysis kinetics. For example, PK4, a copolymer synthesized using 1,4-cyclohexanedimethanol and 1,4-butanediol, has the faster hydrolysis kinetics of all the copolyketals synthesized, having a hydrolysis half-life of 1 day at pH 4.5, which is predicted based on the hig hydrophilicity of butanediol in comparison to the other diols. On the other hand, PK6, synthesized using 1,4-cyclohexanedimethanol and a more

hydrophobic monomer, 1,8-octanediol, had a pH 4.5 hydrolysis half-life of 18.6 days. In summary, these data demonstrate that the hydrolysis kinetics of polyketals can be tuned by varying their hydrophobicity and suggests that diffusion of water into the polyketals is the rate determining step governing hydrolysis. Importantly, the hydrolysis kinetics of all the polyketal copolymers was pH sensitive; in general they hydrolyzed at least one order of magnitude faster at pH 4.5 than at pH 7.4.

One of the polyketal copolymers synthesized (termed PK3 in Table 1), consisting of cyclohexane-dimethanol and pentane diol, had a hydrolysis half life of 2 days at pH 4.5 but several weeks at pH 7.4. This polyketal may be useful for delivering therapeutic drugs to a subject because it should hydrolyze rapidly after phagocytosis; however it is relatively stable at physiological pH. Additionally, PK3 may be suitable for microparticle drug delivery because of its rapid hydrolysis kinetics and biocompatible degradation products, which are 1,5-pentanediol, 1,4-cyclohexanedimethanol, and acetone.

To further the study of using PK3 for delivery of drug therapies, microparticles were formulated from PK3 using a solvent evaporation procedure. Figure 53 demonstrates that microparticles can be formed with PK3, and that the particles have a size between 1-5 microns, which suitable for phagocytosis by macrophages. Thus, therapeutic drugs may be encapsulated into PK3 microparticles (for example by using a water/oil/water double emulsion procedure or other method) for adminstration into a subject.

Microparticles loaded with active agents will be formulated from the polyketal copolymers using a modified water/oil/water emulsion method (Ando et al., *Journal of Pharmaceutical Sciences* 1999, *88*, 126-130). For example, PK3 (100mg) will be dissolved in 1 mL of dichloromethane, in a separate vial, 40 mg of the active agent will be dissolved in 400μL of D.I. water. The aqueous solution of the active agent will be mixed with the PK3 solution, and sonicated for 60 seconds (Misonix Incorporated, Farmigdale, NY). The sonicated mixture will then immersed in liquid nitrogen for 15 sec, and 12 mL of a 5% w/w PVA solution (pH 7.45) will be added to it. This mixture

will be homogenized for 120 seconds with a Powergen 500 homogenizer (Fisher Scientific, Waltham, MA), and then transferred to a beaker containing 40 mL of 1% w/w PVA (pH 7.45). This solution will then be stirred for 3 hours with a magnetic stir bar to evaporate the organic solvent. The particles will be isolated by centrifuging at 10,000 rmp for 15 min, washed twice with 15 mL of PBS buffer and freeze dried.

References for Example 8:

Cordes, E. H.; Bull, H. *Chemical Reviews* **1974**, *74*, 581.

Gopferich, A. *Biomaterials* **1996**, *17*, 103.

Gopferich, A.; Tessmar, J. *Advanced Drug Delivery Reviews* **2002**, *54*, 911.

Kumar, N.; Langer, R. S.; Domb, A. J. *Advanced Drug Delivery Reviews* **2002**, *54*, 889.

EXAMPLE 9: Formation of Particles with Linkers

In this example, a polyketal molecule of the invention was modified with a linker that can bind an active agent. Specifically, a nitrilotriacetic acid (NTA) linker was added to PCADK. The NTA linker, when loaded with nickel (Ni) allowed the binding of histidine-tagged proteins (Figure 54). The modified PCADK then formed microspheres ideal for rapid delivery of active agents (e.g. growth factors) (Figure 55).

Materials and Methods

Synthesis of PCADK Particles with NTA Linker

PCADK was synthesized as previously described above (see also Lee S et al. Polyketal microparticles: a new delivery vehicle for superoxide dismutase. Bioconjug Chem. 2007 Jan-Feb;18(1):4-7 and Heffernan MJ and Murthy N. Polyketal nanoparticles: a new pH-sensitive biodegradable drug delivery vehicle. Bioconjug Chem. 2005 Nov-Dec; 16(6):1340-2, herein incorporated by reference).

After synthesis of the polyketal, 90 mg of PCADK was dissolved in 1 mL of a 10 mg/mL solution of DOGS-NTA (Avanti Polar Lipids) in dichloromethane (final concentration of 10% DOGS-NTA). To ensure solubility, the mixture was sonicated for several seconds/minutes in a water bath sonicator. The polymer solution was then poured into a vial containing 5 mL of PVA (2%) and homogenized for 60 seconds. The resulting solution was stirred over 40 mL of 0.5% PVA for 4-6 hours. The particles were then spun down and washed several times in deionized water and frozen in liquid nitrogen for lyophilization. The resulting freeze-dried particles were imaged using SEM and shown in Figure 56.

Nickel loading of PCADK-NTA

In order to get particles capable of binding to His-tagged proteins, particles needed to be loaded with nickel. Thus, particles were incubated with 50 mM $NiCl_2$ at 10 mg/mL and agitated for 2 hours at room temperature. To determine nickel uptake, we incubated the particles overnight with $NiCl_2$, spun down the particles, and measured the unbound nickel in the supernatant spectrophotometrically. As the data in Figure 57 demonstrate, at varying NTA loading there was a decrease in free nickel in the solution, indicating the particles had been loaded with nickel.

Binding of His-tagged Proteins to PCADK-NiNTA

To determine if NiNTA on particles was capable of binding His-tagged proteins, varying concentrations of His-GFP were incubated with PCADK-NiNTA (1% solution w/v) overnight at 4 degrees Celsius. Particles were centrifuged out and washed several times in PBS before resuspension for analysis. Figure 58 is a representative fluorescent stain for GFP that was converted to grayscale for presentation. As the image shows, the particles retained GFP on their surface. To further quantify the amount of His-GFP bound, particles were loaded with increasing amounts of His-GFP, washed several times, and ELISA was run on the particles to determine levels of binding. As the data in

Figures 59 (1% NTA) and 60 (10% NTA) show, PCADK-NiNTA dose-dependently bound the His-tagged protein. At 1% NTA, the particles saturated binding at a loading of 60 ng His-GFP, while at 10% NTA, saturation was reached at 120 ng His-GFP loading. At most points in the linear range, binding was roughly 50% efficient. The data in Figure 62 shows that the percent binding of His-GFP encreases with the amount of NTA. Figure 28 shows that His-GFP binding to NTA is stable for at least 15 hours.

To determine if the binding was reversible, various NTA concentration His-GFP-loaded particles were incubated with imidazole (200 mM), a competitive agent for the Ni-NTA complex. Supernatants were collected at various time points and assayed for GFP fluorescence. As the data in Figure 61 demonstrate, the His-GFP was released from the particles rather rapidly, with most of the protein released at 30 minutes. This suggests that the protein is not irreversibly bound to the particle and should have good bioavailability.

What is claimed is:

1. A polyketal polymer which is PK1, PK2, PK3, PK4, PK5 or PK6.

2. A biodegradable particle comprising the polyketal polymer of Claim 1.

3. The particle of Claim 2, further comprising one or more active agents.

4. A biodegradable particle comprising
(a) one or more of PK1, PK2, PK3, PK4, PK5 or PK6, and
(b) an active agent.

5. The particle of Claim 2 or 4, wherein the particle is a nanoparticle or microparticle.

6. The particle of Claim 2 or 4, wherein the particle is from about 50 nm – 1000 μm in size or from about 200 nm – 600 μm in size.

7. The particle of Claim 3 or 4, wherein said active agent is a therapeutic, prophylactic or diagnostic agent.

8. The particle of Claim 7, wherein said therapeutic agent is an immunomodulatory agent.

9. The particle of Claim 8, wherein said immunomodulatory agent is selected from a group consisting of
a. a ligand for any of TLR 2, 3, 4, 5, 7, 8, 9, 10 and 11 or combination thereof, and
b. an inhibitor of a regulatory pathway within dendritic cells, macrophages or antigen-presenting cells.

c. a ligand for RIG-1, any C-type lectins including dectin-1 and DC-SIGN, or Caterpillar proteins.

10. The particle of Claim 9, wherein said inhibitor is selected from the group consisting of inhibitors of (a) ERK, c-Fos, Foxp3, PI3 kinase, Akt, JNK, p38, NF-Kb, STAT 1, STAT2, IRF3, IRF7, IFN-alpha signaling; or (b) a SOCS 1, 2, 3, or other SOCS protein.

11. The particle of Claim 3 or 4, wherein said active agent is a protein, peptide, carbohydrate, nucleic acid, small molecule, imaging agent, vaccine antigen, and/or vaccine.

12. The particle of Claim 11, wherein said protein is a growth factor, cytokine, antoxidant protein, antibody, erythropoietin (EPO), receptor ligand.

13. The particle of Claim 11, wherein said nucleic acid is DNA, RNA, anti-sense oligonucleotide or siRNA.

14. The particle of Claim 11, wherein said small molecule is a kinase inhibitor, phosphatase inhibitor, receptor blocker, small molecular antioxidant mimetic, cytoskeletal rearrangement inhibitor, receptor ligand.

15. The particle of Claim 2 or 4, further comprising a linker.

16. The particle of Claim 15, wherein the linker is streptavidin, RDG, GST, ssDNA, hemoglobin, an amino acid sequence, an antibody, a polycarboxylic acid and/or a chelating agent.

17. The particle of Claim 16, wherein the chelating agent is nitrilotriacetic acid (NTA) ligand, bipyradol or EDTA.

18. The particle of Claim 15, wherein the linker binds a protein, peptide and/or carbohydrate.

19. The particle of Claim 18, wherein the protein, peptide and/or carbohydrate comprises a histidine tag.

20. The particle of Claim 19, wherein the histidine tag comprises about 2-8 histidines.

21. The particle of Claim 19, wherein the histidine tag comprises about 6 histidines.

22. The particle of Claim 18, wherein the protein is a therapeutic, prophylactic or diagnostic protein.

23. The particle of Claim 22, wherein the therapeutic, prophylactic or diagnostic protein is a growth factor, cytokine, antioxidant enzyme or antibody, erythropoietin (EPO), receptor ligand.

24. A pharmaceutical composition comprising the polyketal polymer of Claim 1.

25. A pharmaceutical composition comprising the particle of Claim 3 or 4.

26. A method for delivering of active agents to a subject, comprising administering the particle of Claim 3 or 4 into the subject, said particle being degraded in the subject so that the active agent is released and delivered to the subject.

27. A method of treating a subject suffering from a disease or disorder by delivering active agents that can affect the disease or disorder by the method of Claim 26.

28. The method of Claim 27, wherein the disease or disorder is selected from the group consisting of autoimmune diseases, allergic diseases, infectious diseases, disorder or complications associated with transplantation, diabetes and cancer.

29. The method of Claim 28, wherein the infectious disease is selected from the group consisting of HIV, malaria, TB, SARS, anthrax, Ebola, influenza, avian influenza and HCV.

30. The method of Claim 28, wherein the autoimmune disease is selected from the group consisting of lupus, rheumatoid arthritis, psoriasis, asthma and COPD.

31. A method for delivering of a protein, peptide and/or carbohydrate to a subject, comprising administering the particle of Claim 18 into the subject, said particle being degraded in the subject so that the protein, peptide and/or carbohydrate is released and delivered to the subject.

32. A method of treating a subject suffering from a disease or disorder by delivering a protein, peptide and/or carbohydrate that can affect the disease or disorder by the method of Claim 31.

33. The method of Claim 32, wherein the disease or disorder is selected from the group consisting of autoimmune diseases, allergic diseases, infectious diseases, disorder or complications associated with transplantation, diabetes and cancer.

34. The method of Claim 33, wherein the infectious disease is selected from the group consisting of HIV, malaria, TB, SARS, anthrax, Ebola, influenza, avian influenza and HCV.

35. The method of Claim 33, wherein the autoimmune disease is selected from the group consisting of lupus, rheumatoid arthritis, psoriasis, asthma and COPD.

36. A method for producing the particle of Claim 3 or 4 comprising the steps of

a. forming PK1, PK2, PK3, PK4, PK5 and/or PK6 polymer; and

b. forming a particle of one or more of the polymer of a) in the presence of one or more active agents,

thereby producing the particle of Claim 3 or 4.

37. The method of Claim 36, wherein the active agent is a therapeutic, prophylactic or diagnostic agent.

38. The method of Claim 37, wherein said therapeutic agent is an imunomodulatory agent.

39. The method of Claim 38, wherein said immunomodulatory agent is selected from a group consisting of

a. a ligand for any of TLR 2, 3, 4, 5, 7, 8, 9, 10 and 11 or combination thereof,
b. an inhibitor of a regulatory pathway within dendritic cells, macrophages or antigen-presenting cells,
c. a ligand for RIG-I, any C-type lectins such as dectin-1 and DC-SIGN, or any Caterpillar proteins

40. The method of Claim 39, wherein said inhibitor is selected from the group consisting of inhibitors of (a) ERK, c-Fos, Foxp3, PI3 kinase, Akt, JNK, p38, NF-Kb, STAT 1, STAT2, IRF3, IRF7, IFN-alpha signaling; or (b) a SOCS 1, 2, 3 or other SOCS protein.

41. The method of Claim 36, wherein the active agent is a protein, peptide, carbohydrate, nucleic acid, small molecule, imaging agent, vaccine antigens and/or vaccines.

42. The method of Claim 41, wherein said protein is a growth factor, cytokine, antoxidant protein, antibody, erythropoietin (EPO), or receptor ligand.

43. The particle of Claim 41, wherein said nucleic acid is DNA, RNA, anti-sense oligonucleotide or siRNA.

44. The particle of Claim 41, wherein said small molecule is a kinase inhibitor, phosphatase inhibitor, receptor blocker, small molecular antioxidant mimetic, cytoskeletal rearrangement inhibitor or receptor ligand.

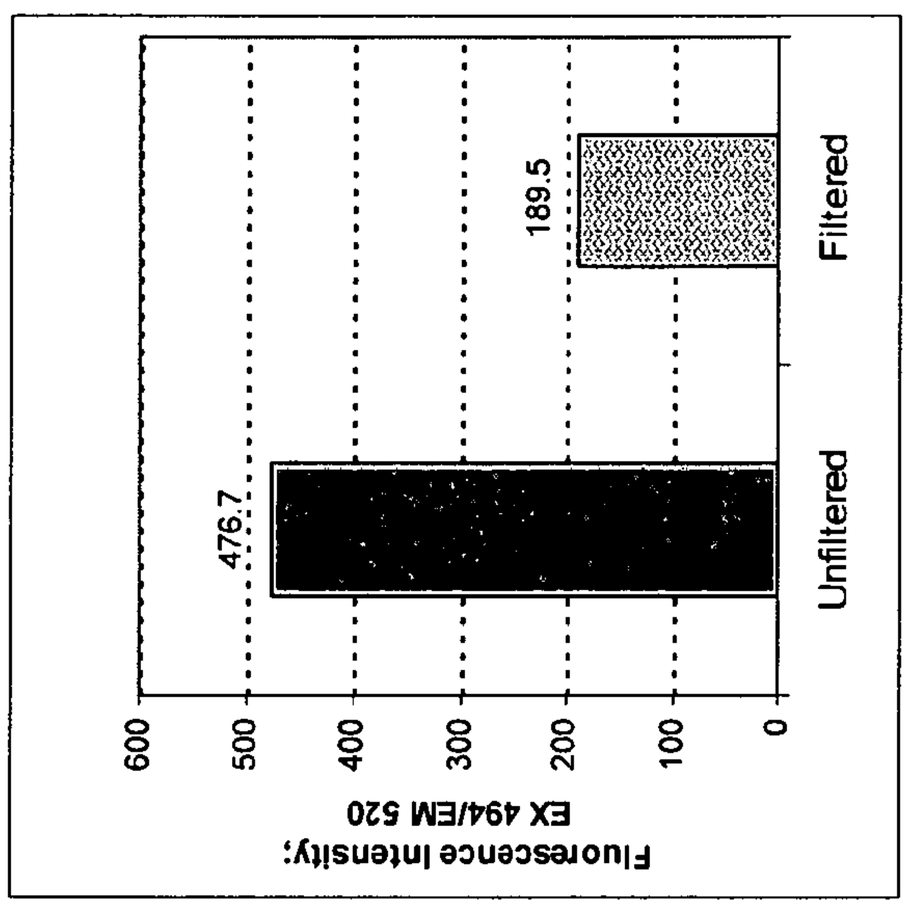
Fluorescence Intensity;
EX 494/EM 520
600
500
400
300
200
100
0
476.7
189.5
Unfiltered
Filtered

FIG. 1

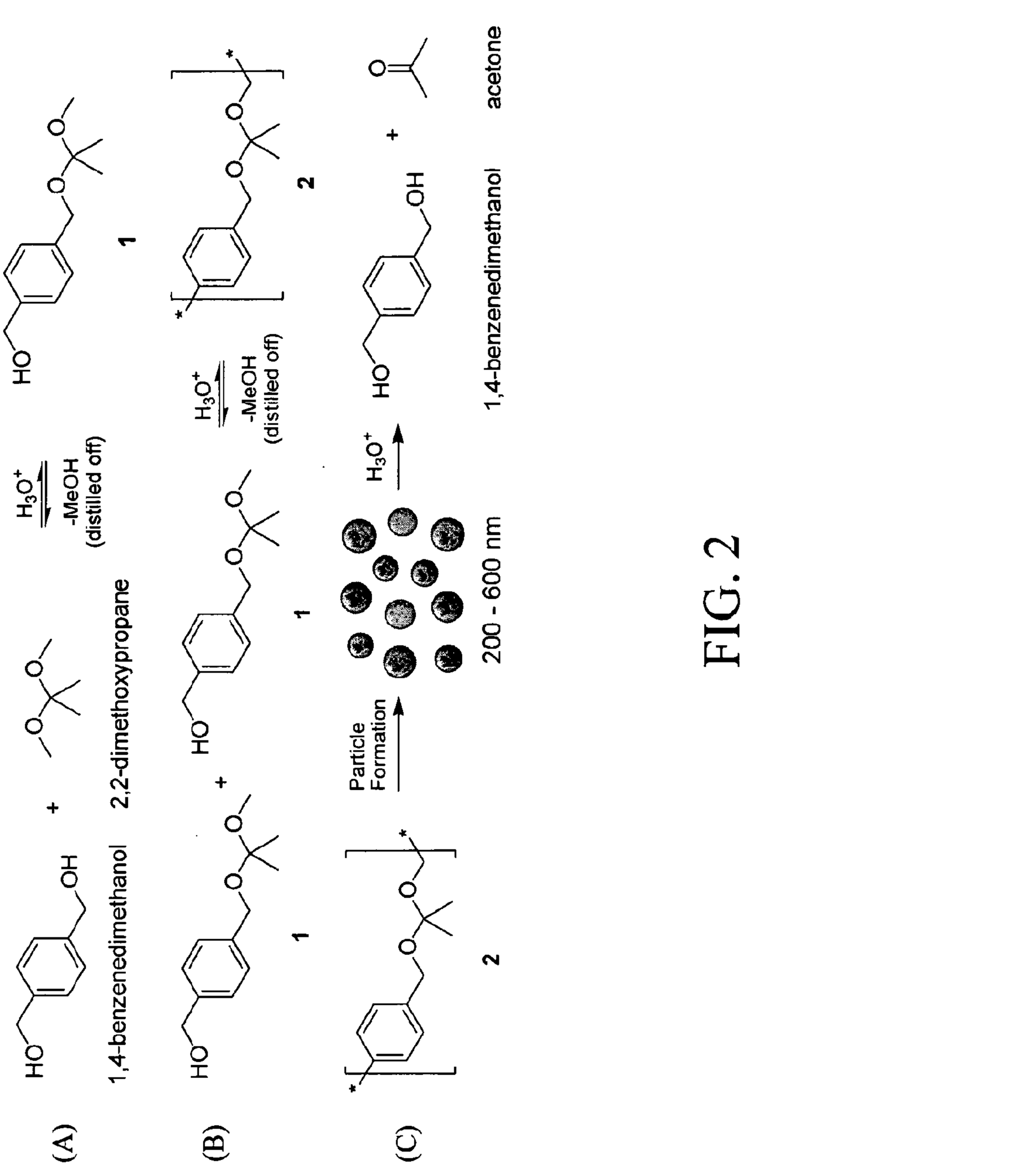
1,4-benzenedimethanol
2,2-dimethoxypropane
H_3O^+
-MeOH
(distilled off)
1
2
200 - 600 nm
acetone
Particle Formation
(A)
(B)
(C)

FIG. 2

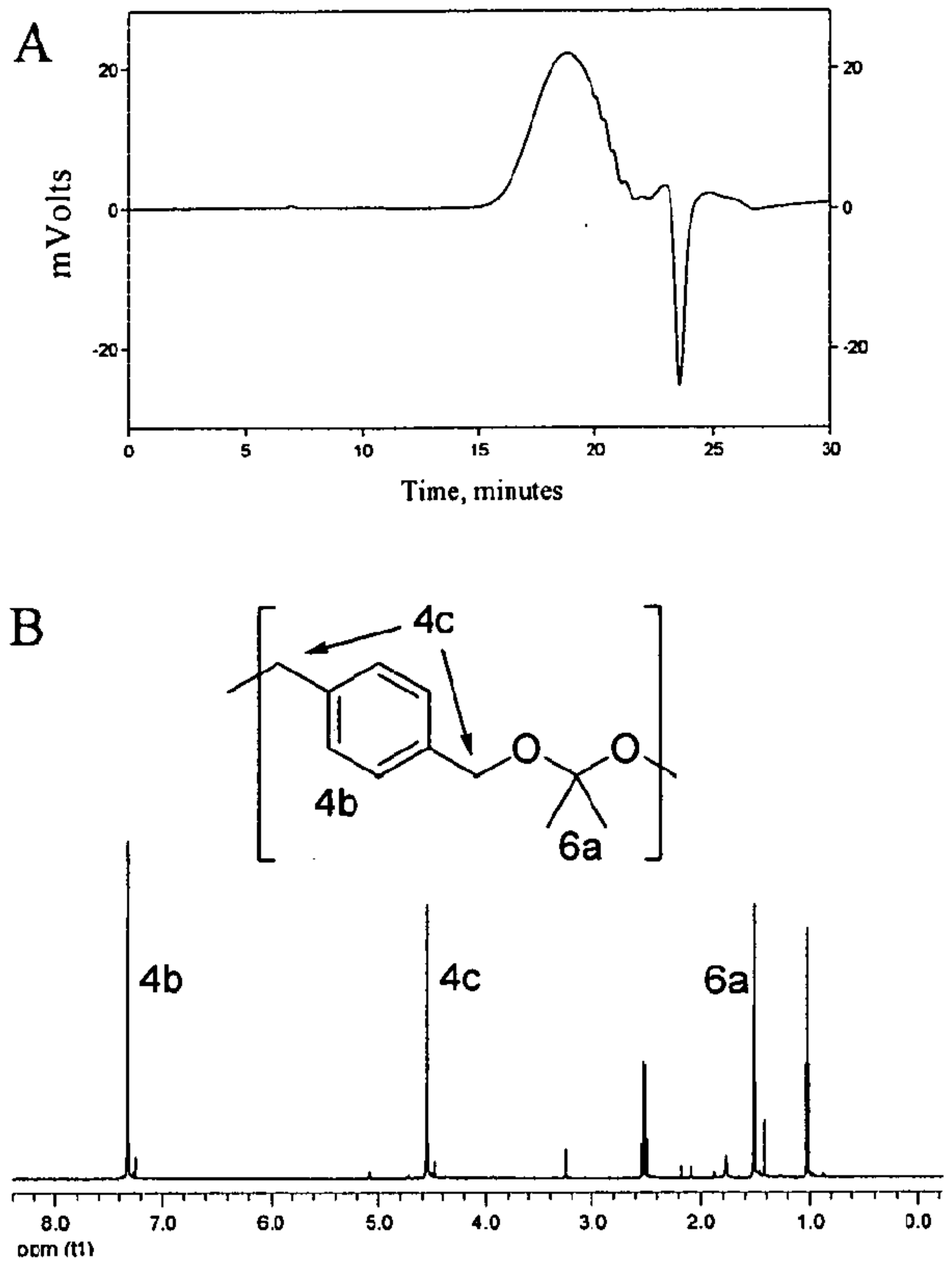
A
mVolts
20
0
-20
0
5
10
15
20
25
30
Time, minutes
B
4c
4b
6a
O
O
4b
4c
6a
8.0
7.0
6.0
5.0
4.0
3.0
2.0
1.0
0.0
ppm (t1)

FIG. 3

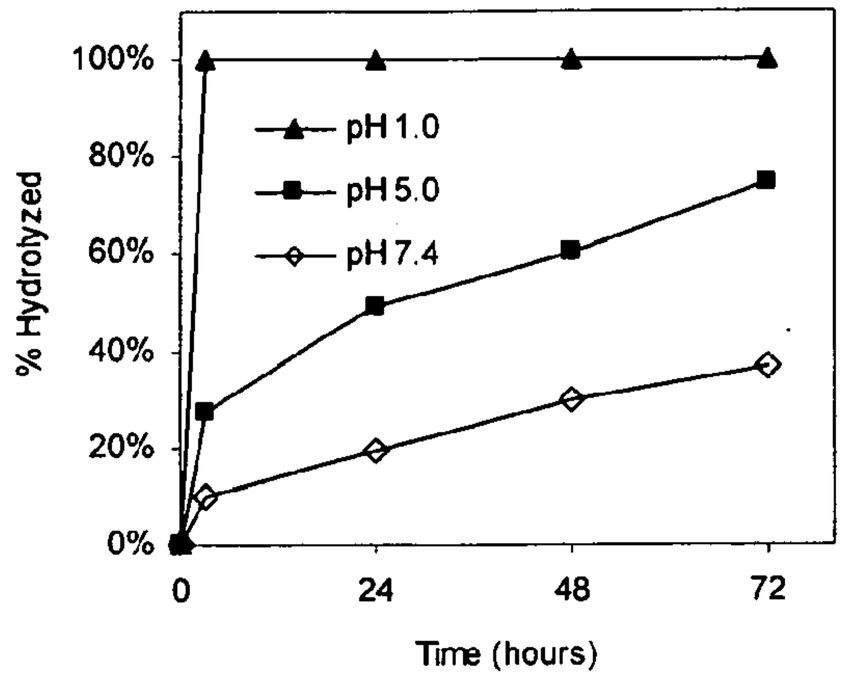
100%
80%
60%
40%
20%
0%
% Hydrolyzed
pH 1.0
pH 5.0
pH 7.4
0
24
48
72
Time (hours)

FIG. 4

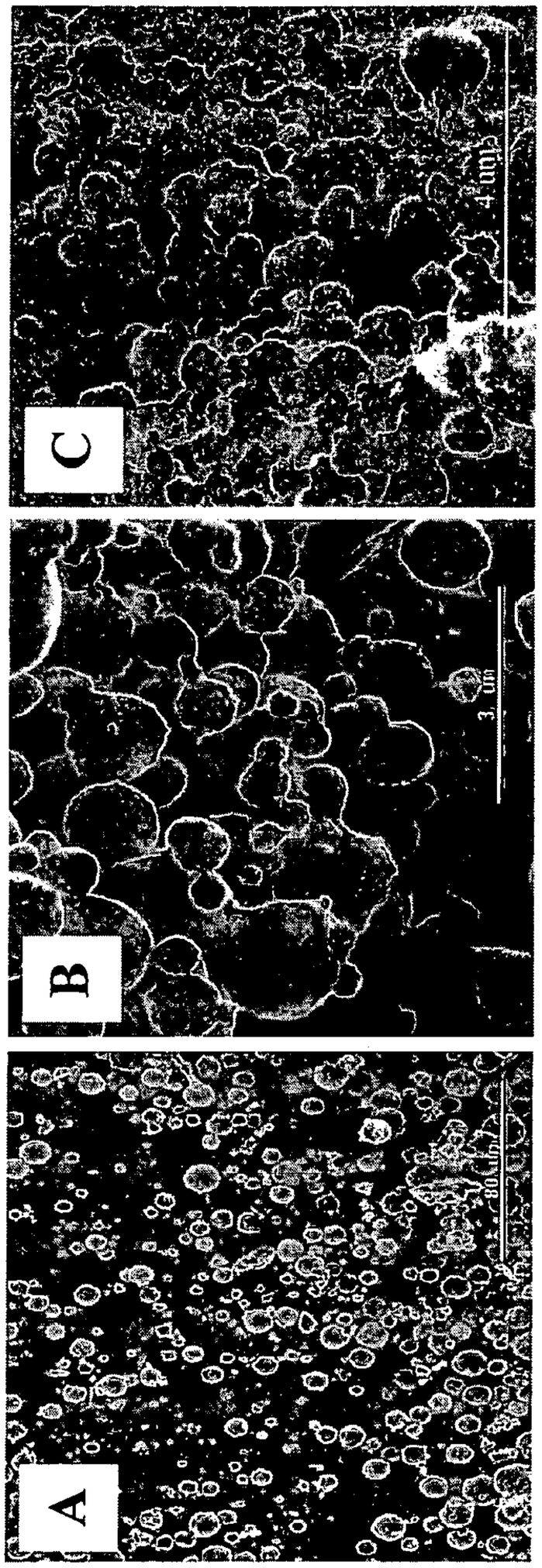

FIG. 5

Particle Formation

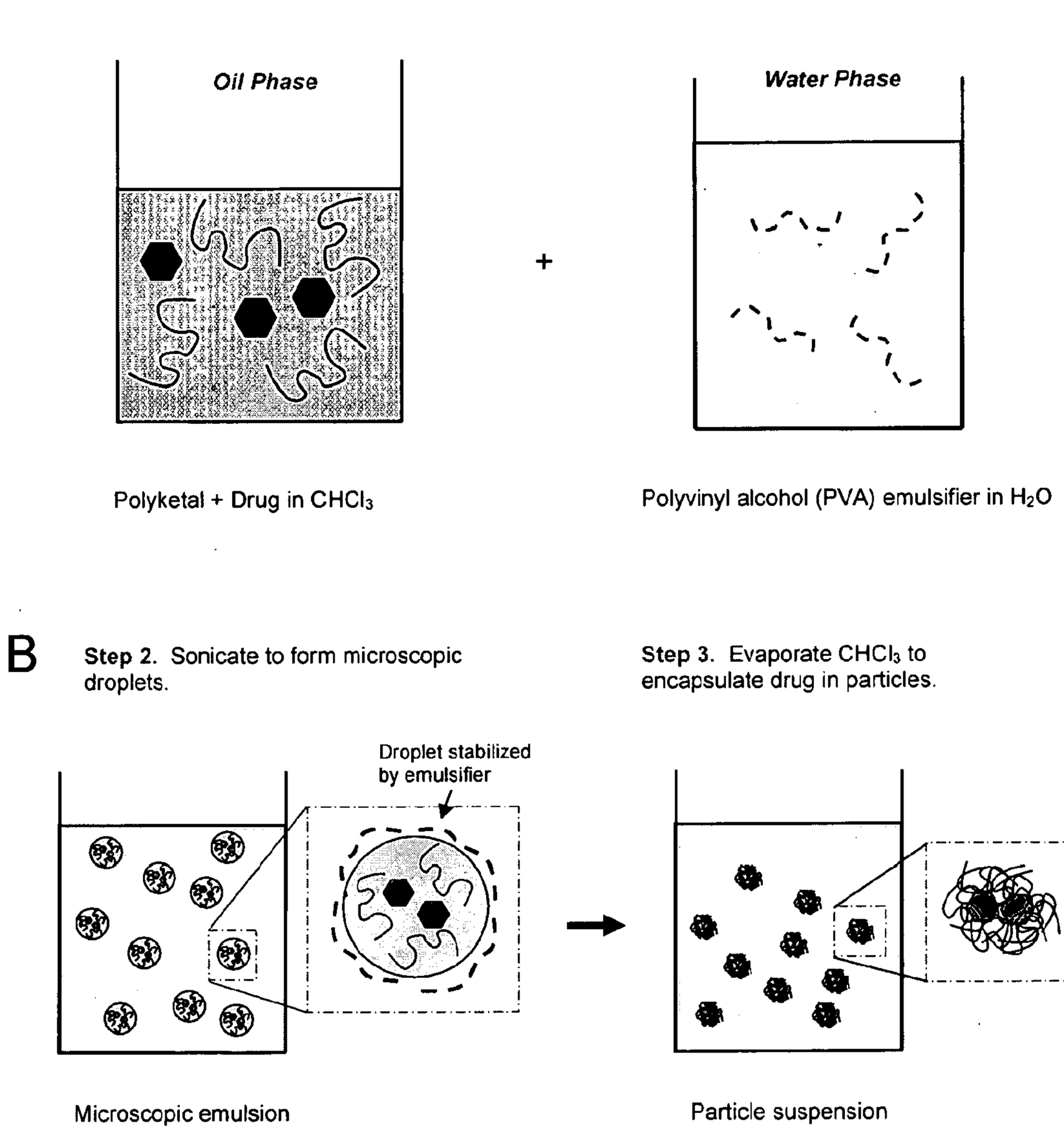

FIG. 6

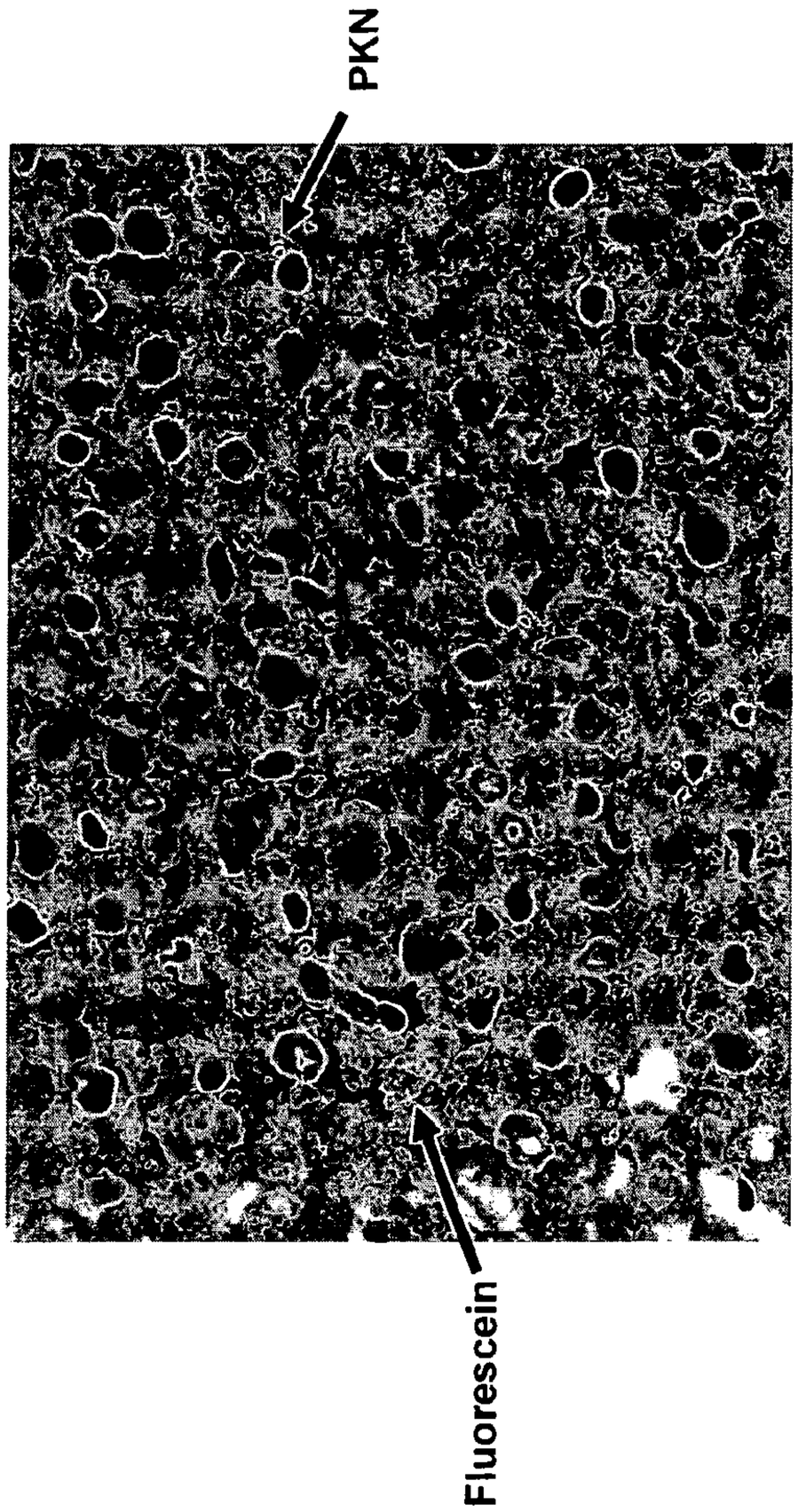

FIG. 7

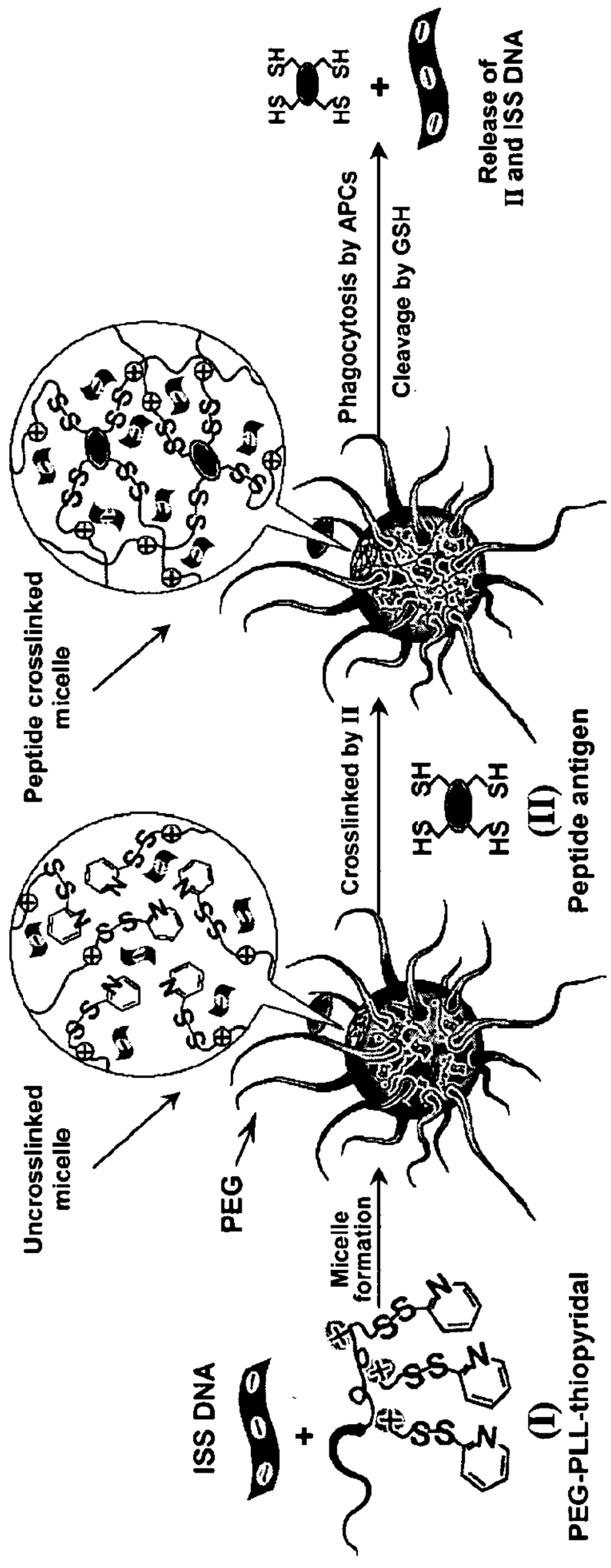
ISS DNA
+
(I)
PEG-PLL-thiopyridal
Micelle formation
PEG
Uncrosslinked micelle
Crosslinked by II
(II)
Peptide antigen
Cleavage by GSH
Phagocytosis by APCs
Release of II and ISS DNA
Peptide crosslinked micelle

FIG. 8

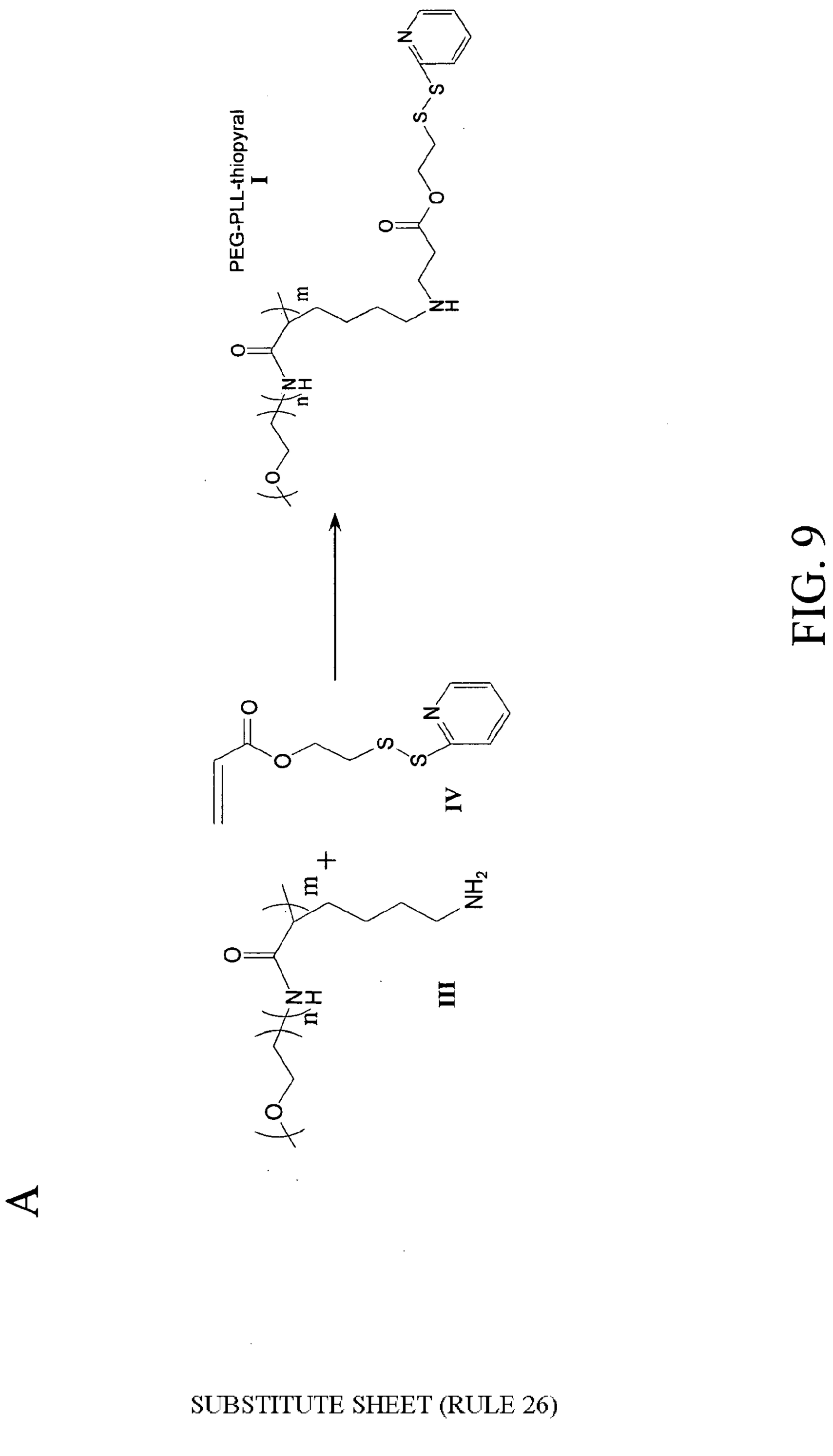

FIG. 9

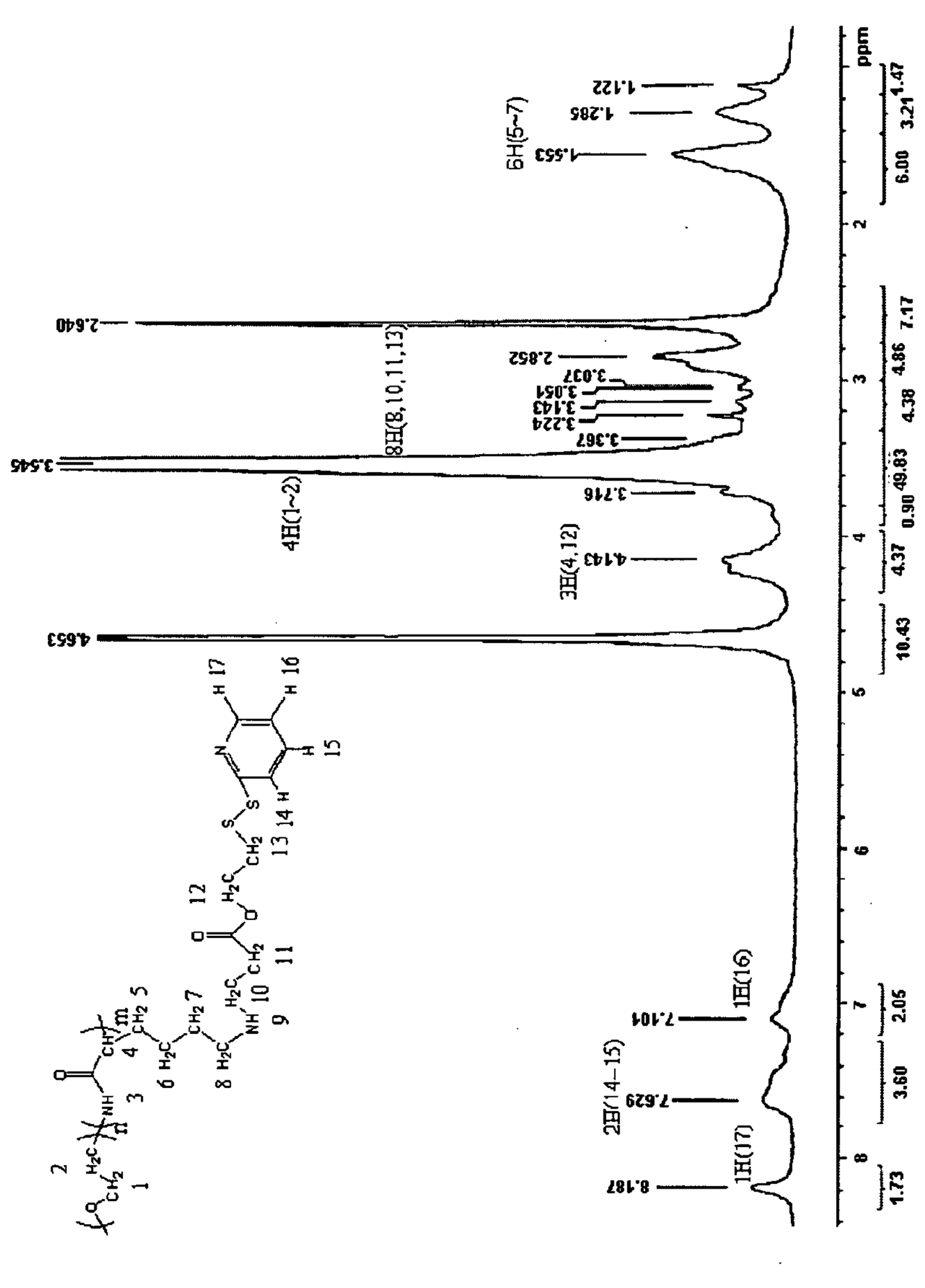

FIG. 9 continued

B

C

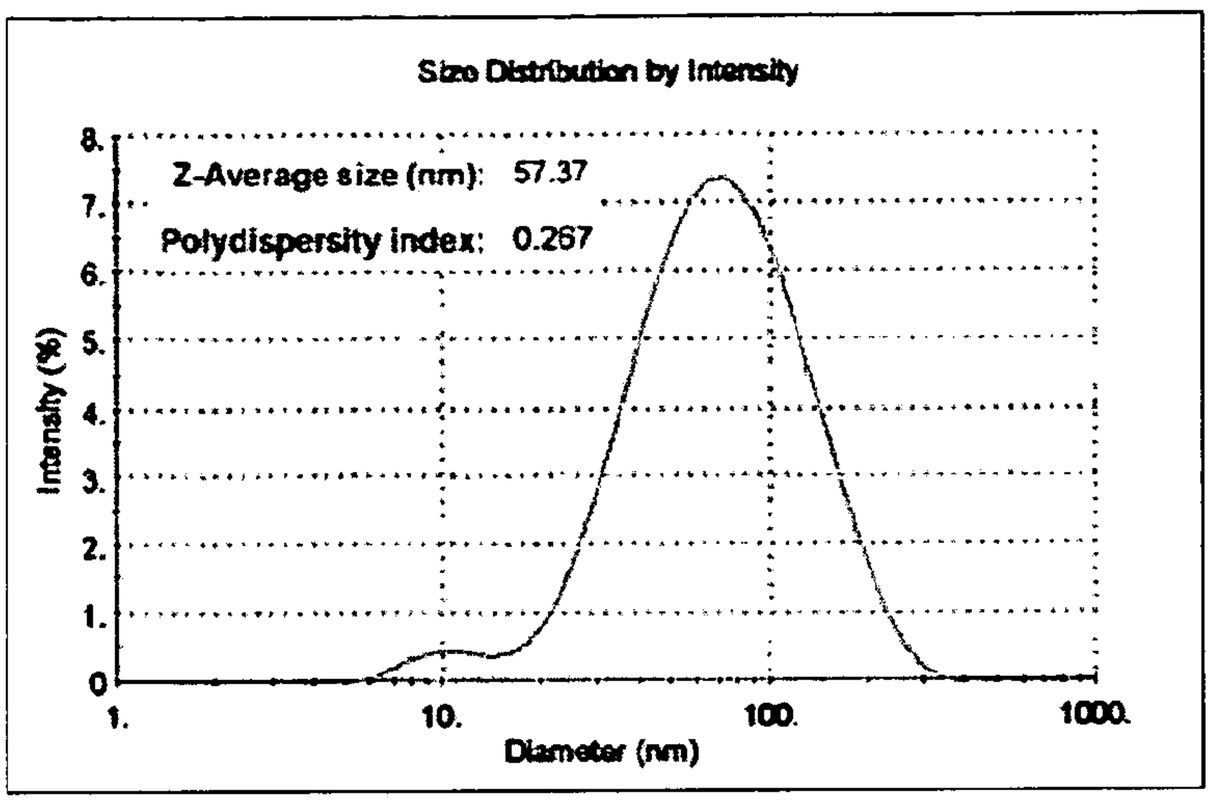

D

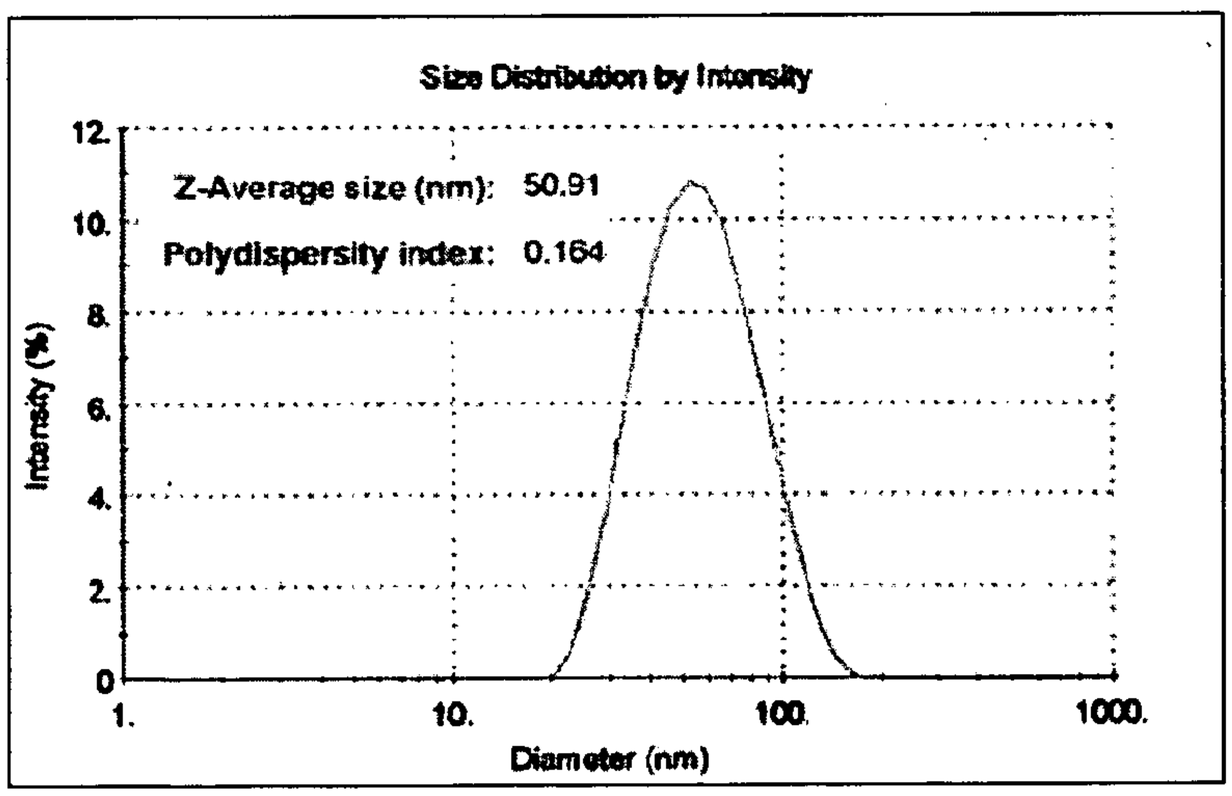

FIG. 9 continued

E

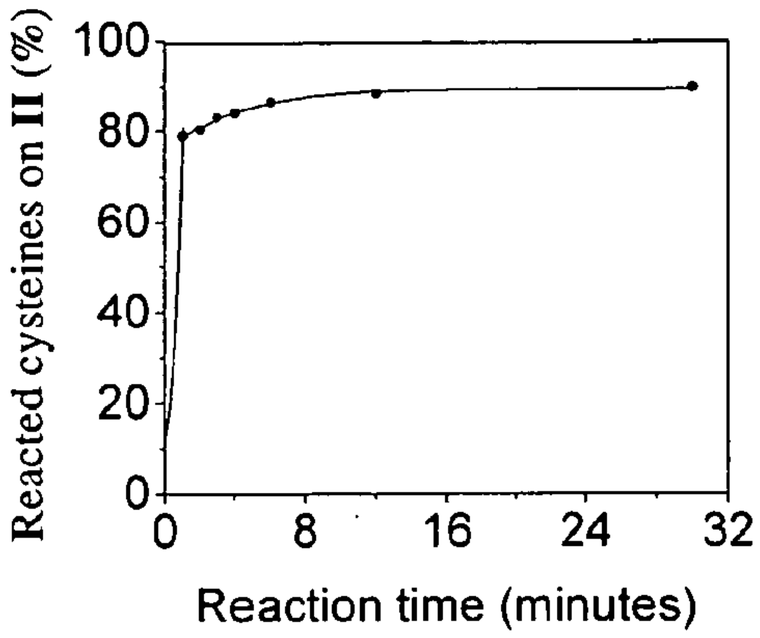

F

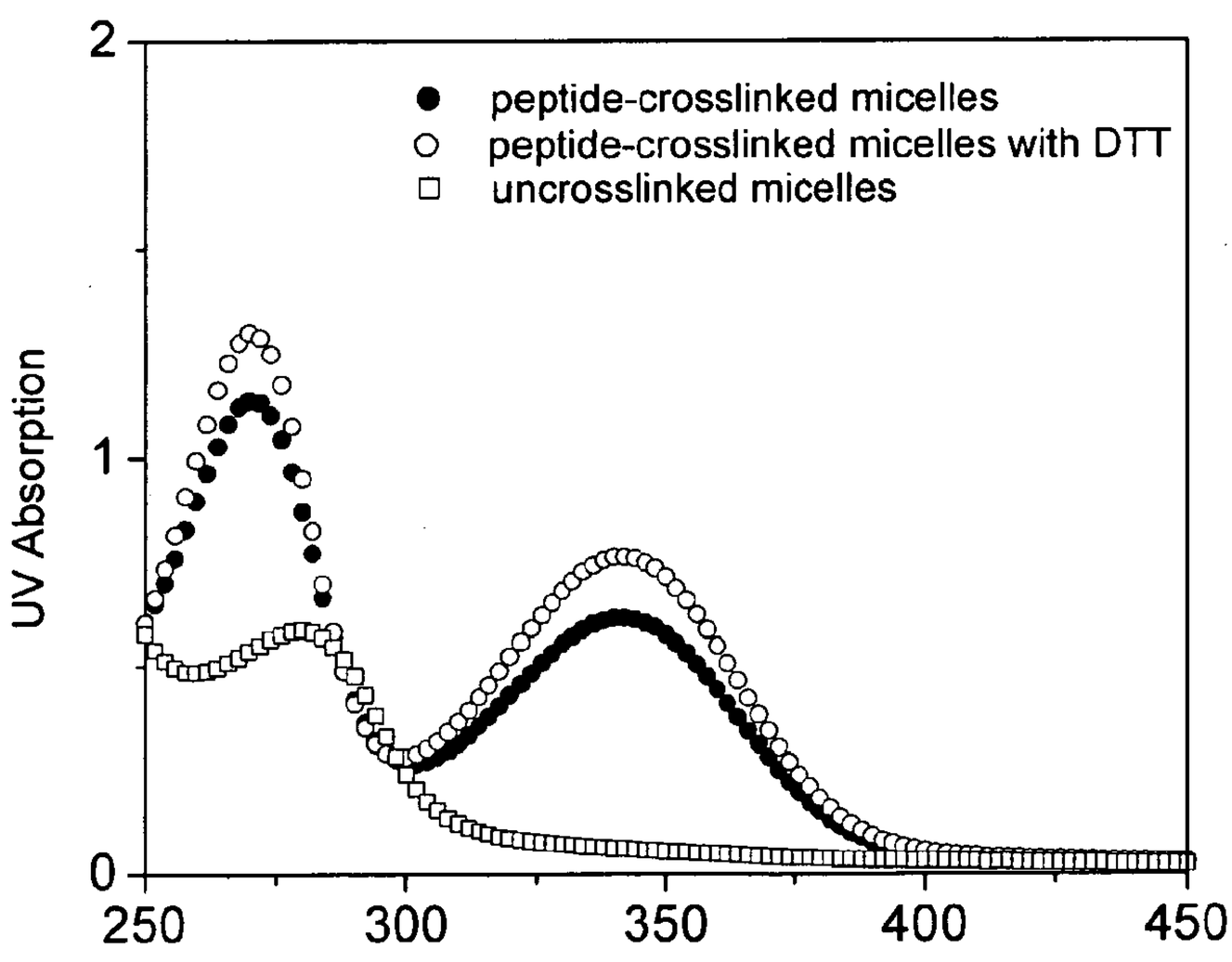

FIG. 9 continued

A

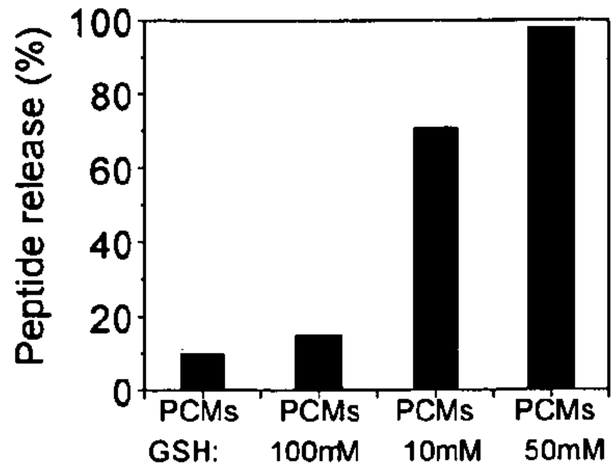

B

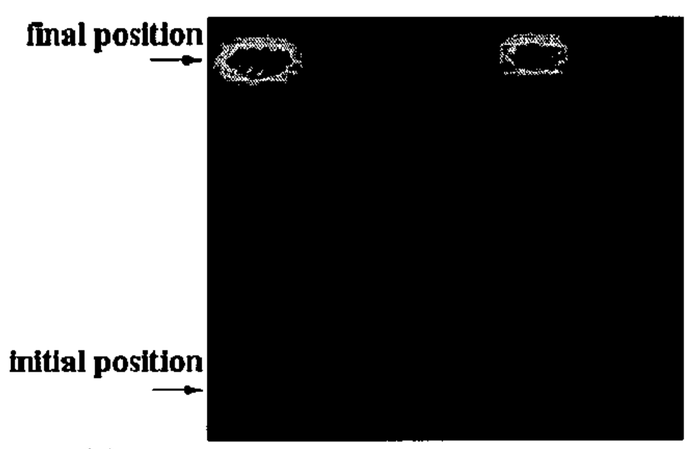

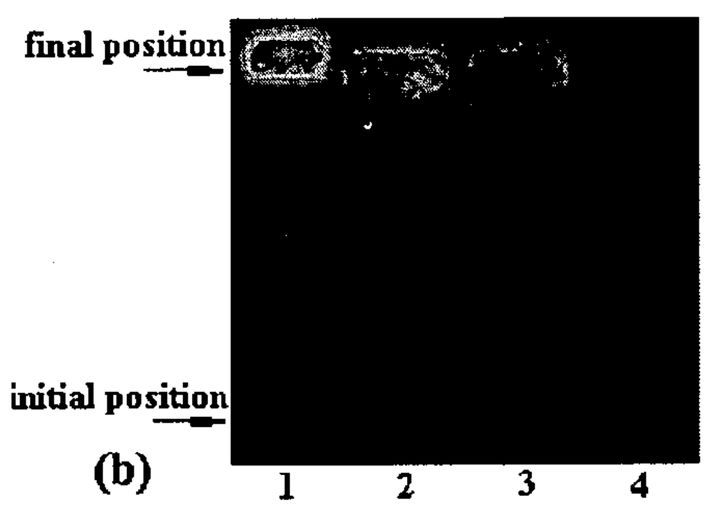

(a): lane 1: DNA alone;
lane 2: DNA, copolymer (II);
lane 3: DNA, II, peptide;
lane 4: DNA, II, PVS;
lane 5: DNA, II, peptide, PVS.

(b): lane 1: DNA alone;
lane 2: DNA, II, peptide, PVS, glutathione (10mM);
lane 3: DNA, II, peptide, PVS, glutathione (15mM);
lane 4: DNA, II, peptide, PVS.

C

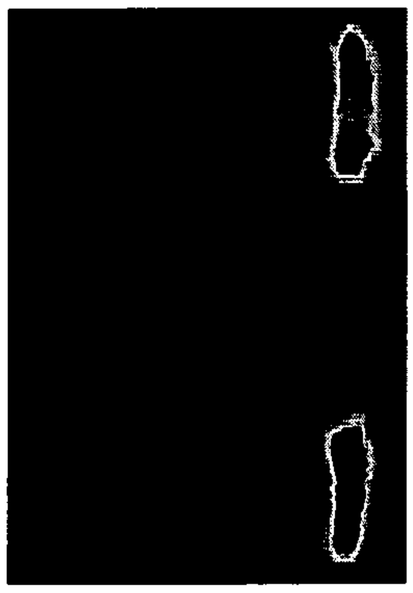

lane 1: DNA alone;

lane 2: DNA, Serum;

lane 3: DNA, II, peptide, GSH, Serum.

FIG. 10

A

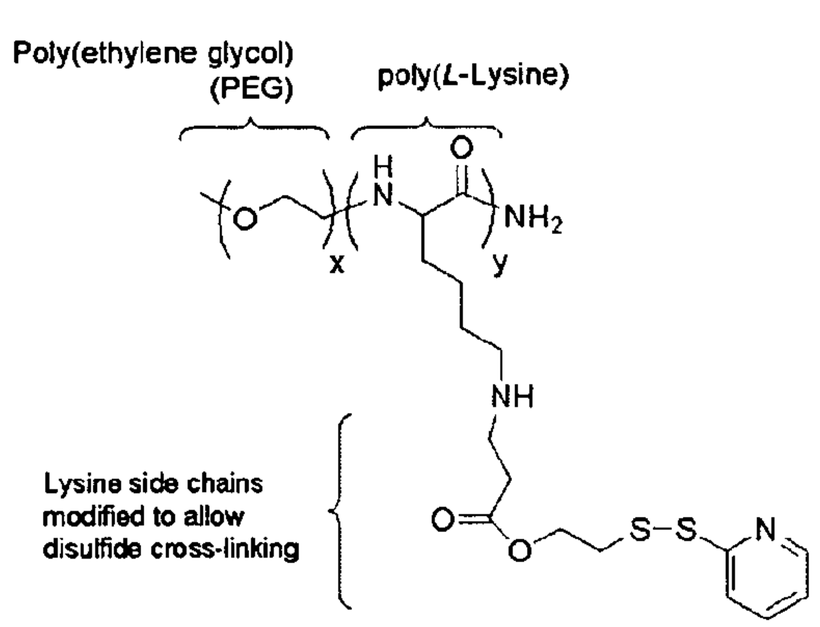
PEG-poly(Lysine-Thio-Pyridyl):
Poly(ethylene glycol) (PEG)
poly(L-Lysine)
Lysine side chains modified to allow disulfide cross-linking

B

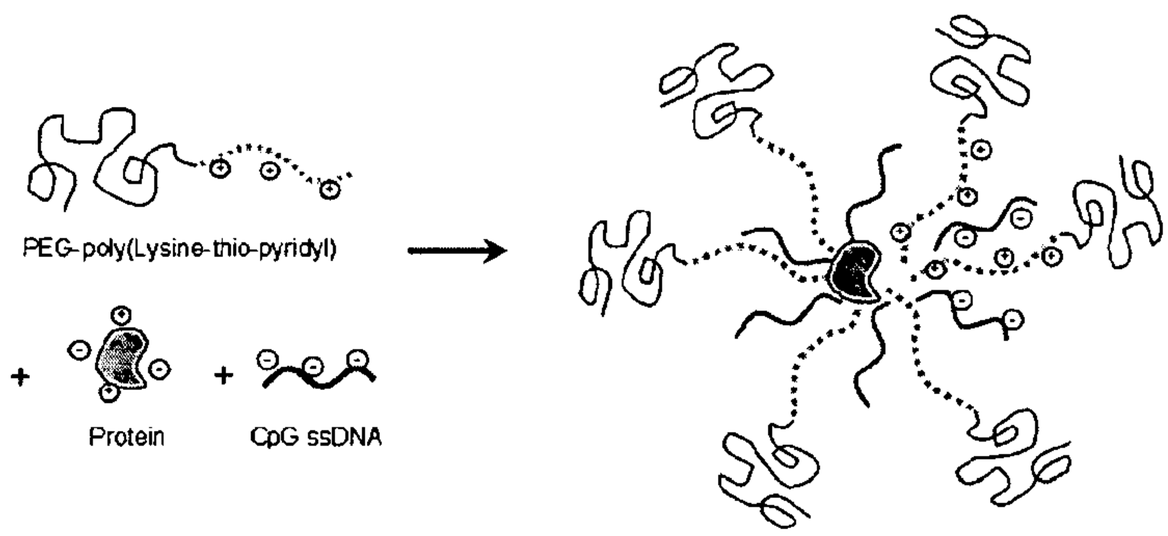
PEG-poly(Lysine-thio-pyridyl)
Protein
CpG ssDNA
Mix co-polymer with protein and DNA
Components self-assemble into a micelle

FIG. 11

C

Disulfide cross-linking:

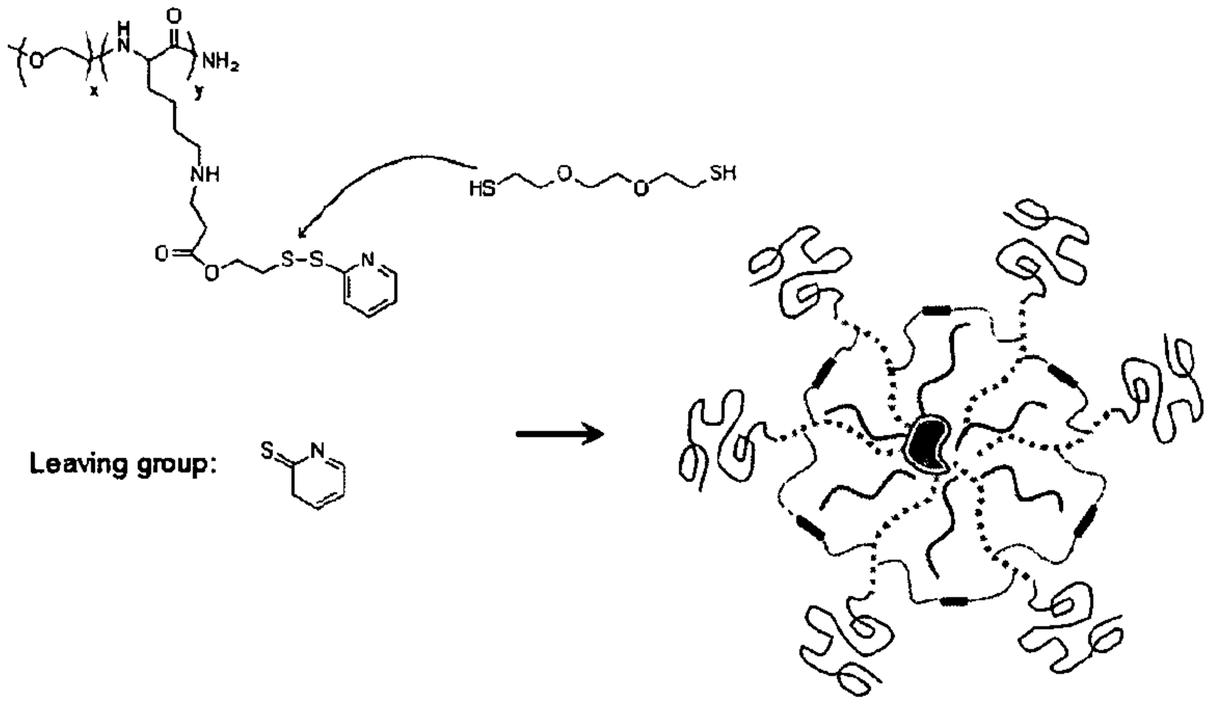

D

Glutathione reduces disulfide cross-linking:

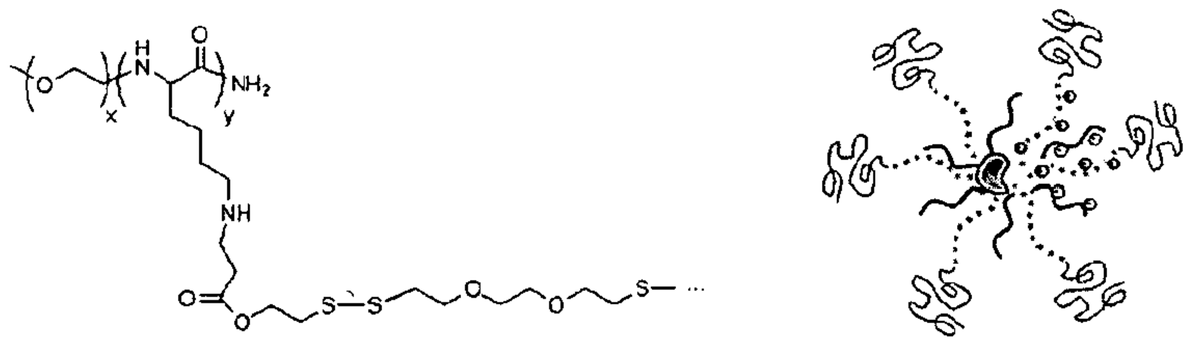

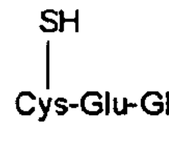

Glutathione (reducing agent):

100 uM in blood

10 mM in cytosol

FIG. 11 continued

A

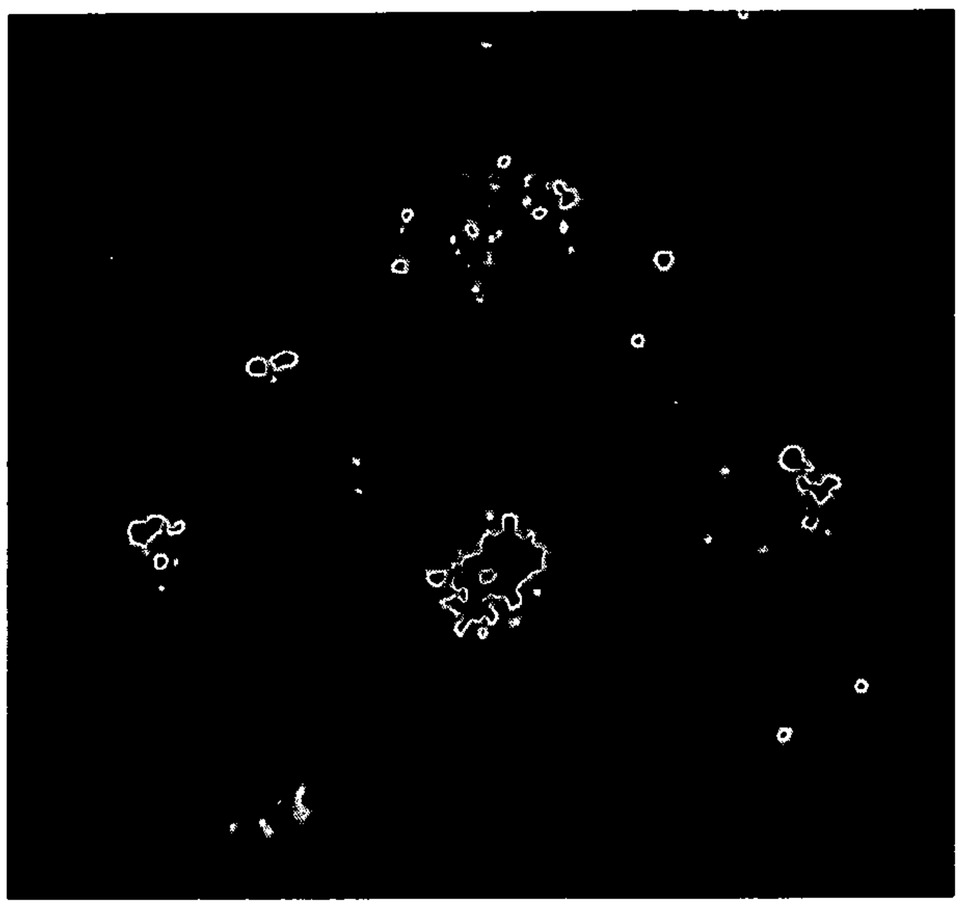

FIG. 12

B

1. SIINFEKL-CFSE

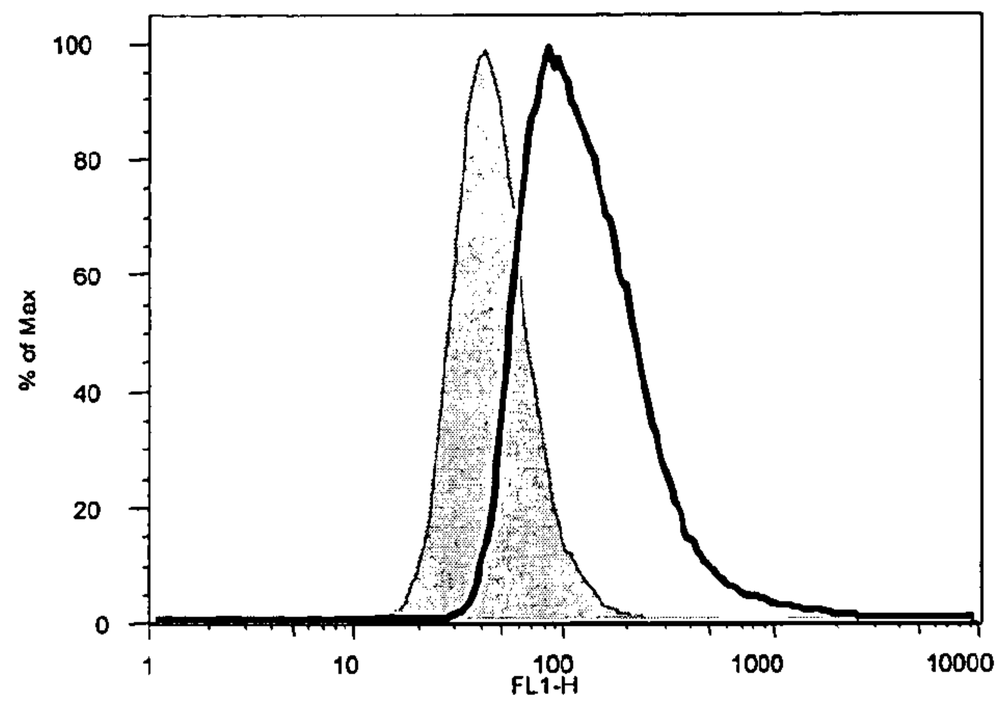

2. SIINFEKL-CFSE micelle 213.2

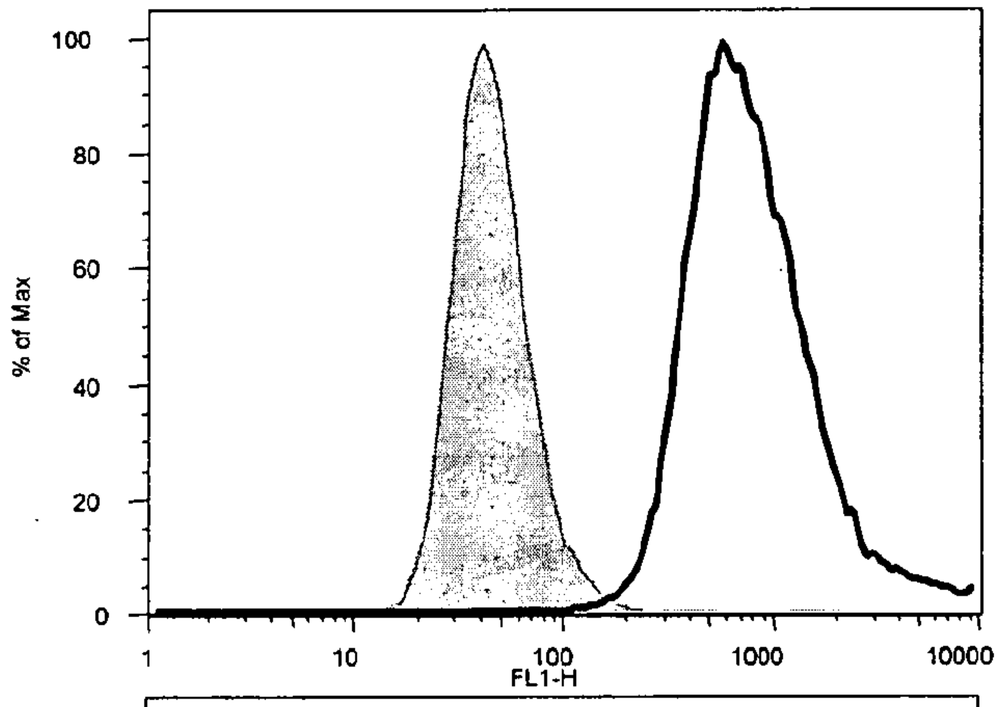

3. SIINFEKL-CFSE micelle 213.3

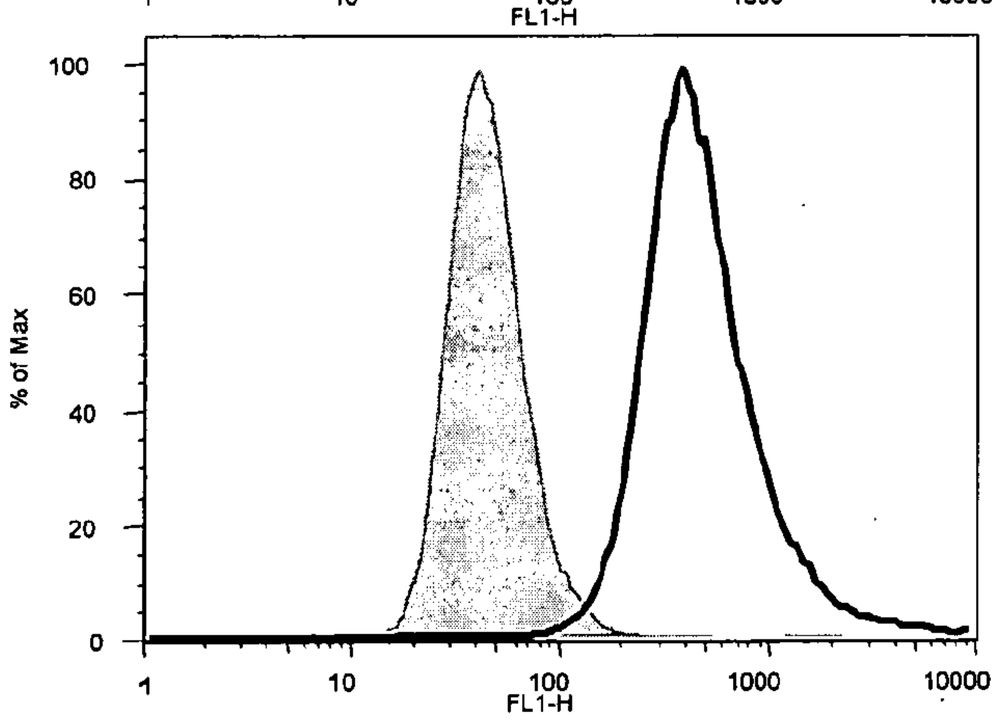

FIG. 12 continued

C

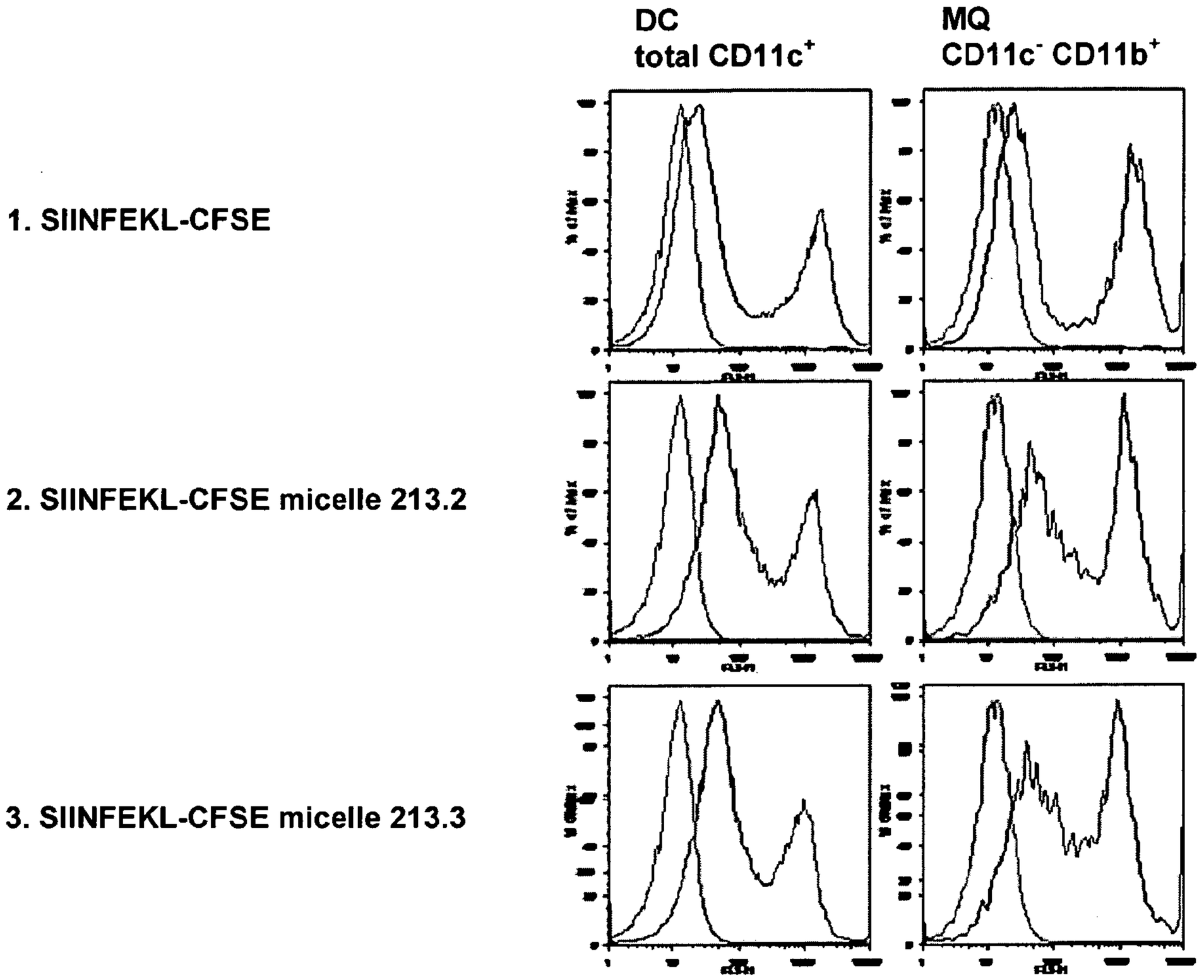

FIG. 12 continued

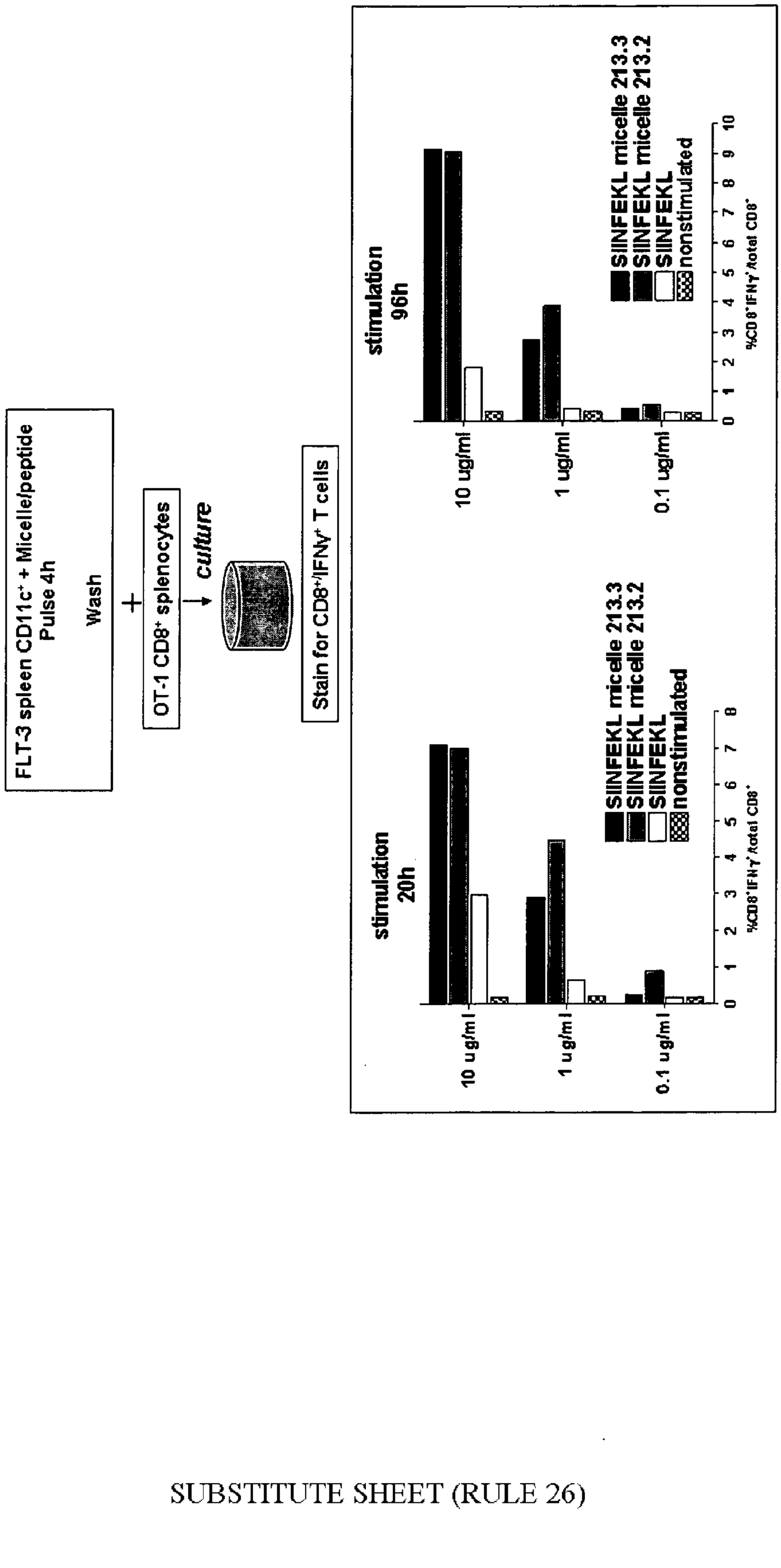
FLT-3 spleen CD11c+ + Micelle/peptide
Pulse 4h
Wash
+
OT-1 CD8+ splenocytes
culture
Stain for CD8+/IFNγ+ T cells
stimulation
96h
SIINFEKL micelle 213.3
SIINFEKL micelle 213.2
SIINFEKL
nonstimulated
%CD8+IFNγ+/total CD8+
10 ug/ml
1 ug/ml
0.1 ug/ml
stimulation
20h
SIINFEKL micelle 213.3
SIINFEKL micelle 213.2
SIINFEKL
nonstimulated
%CD8+IFNγ+/total CD8+
10 ug/ml
1 ug/ml
0.1 ug/ml

FIG. 13

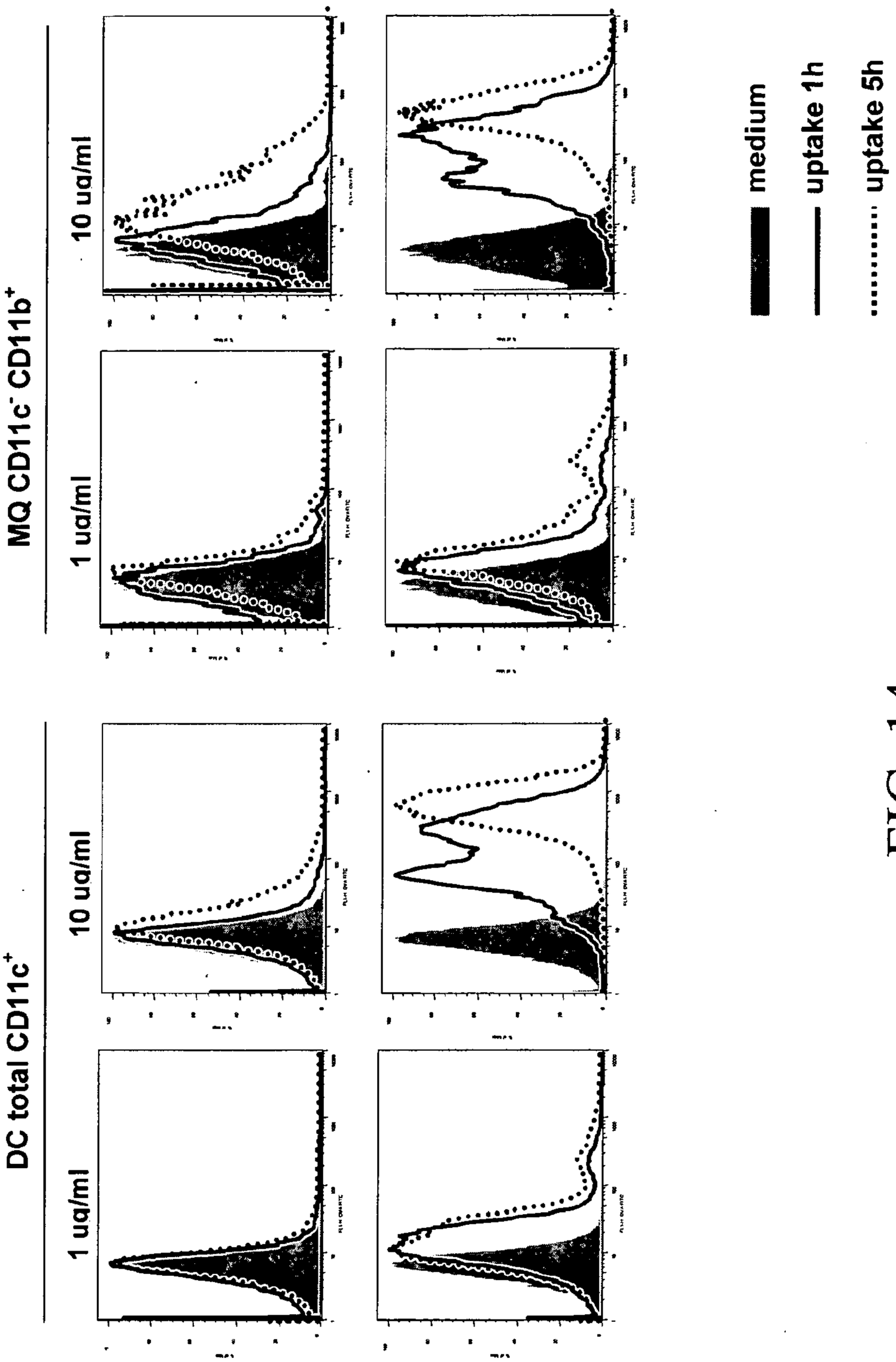
MQ CD11c⁻ CD11b⁺
DC total CD11c⁺
10 ug/ml
1 ug/ml
medium
uptake 1h
uptake 5h
A
1. OVA
2. Micelle OVA-FITC

FIG. 1

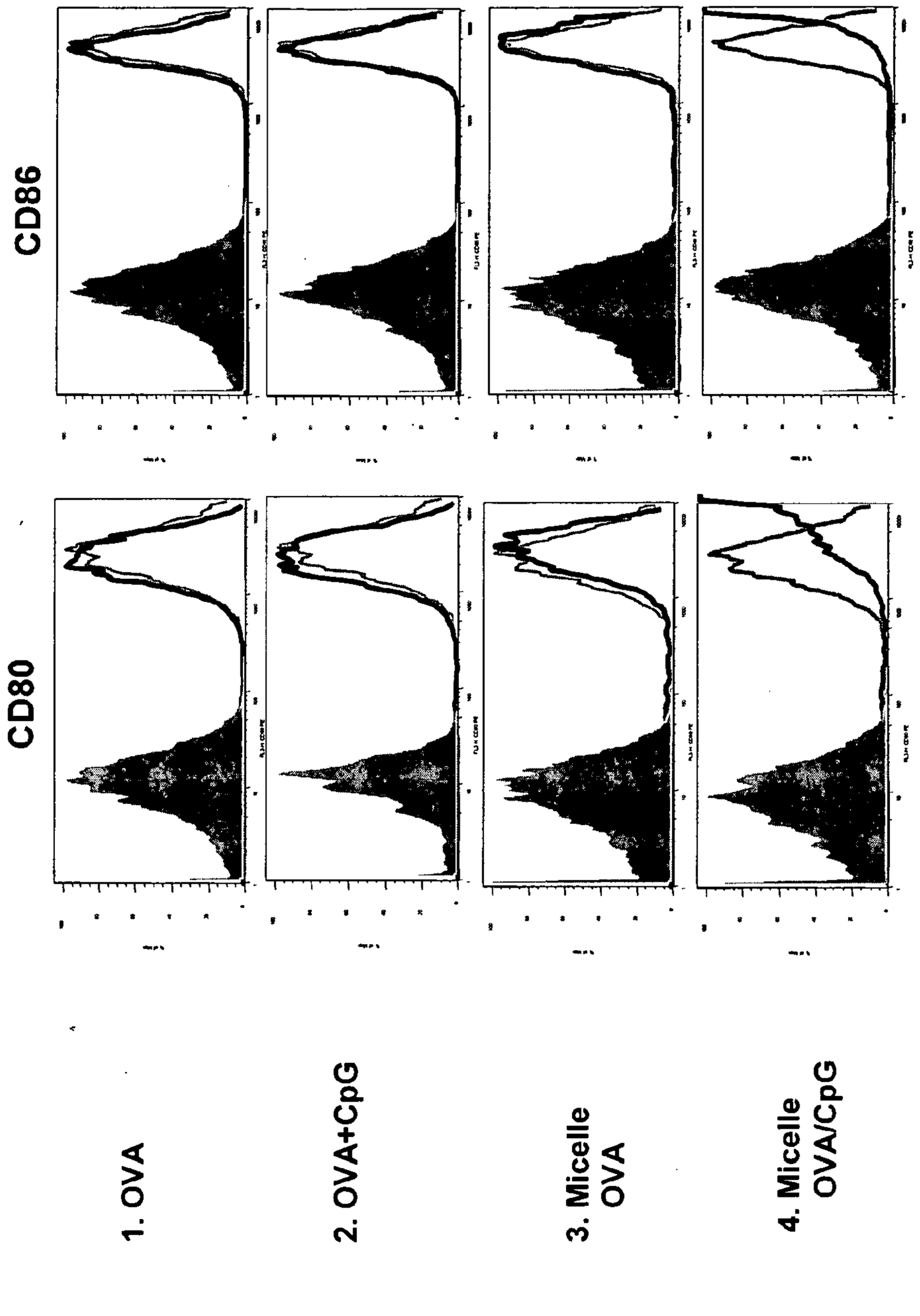

FIG. 14 continued

B

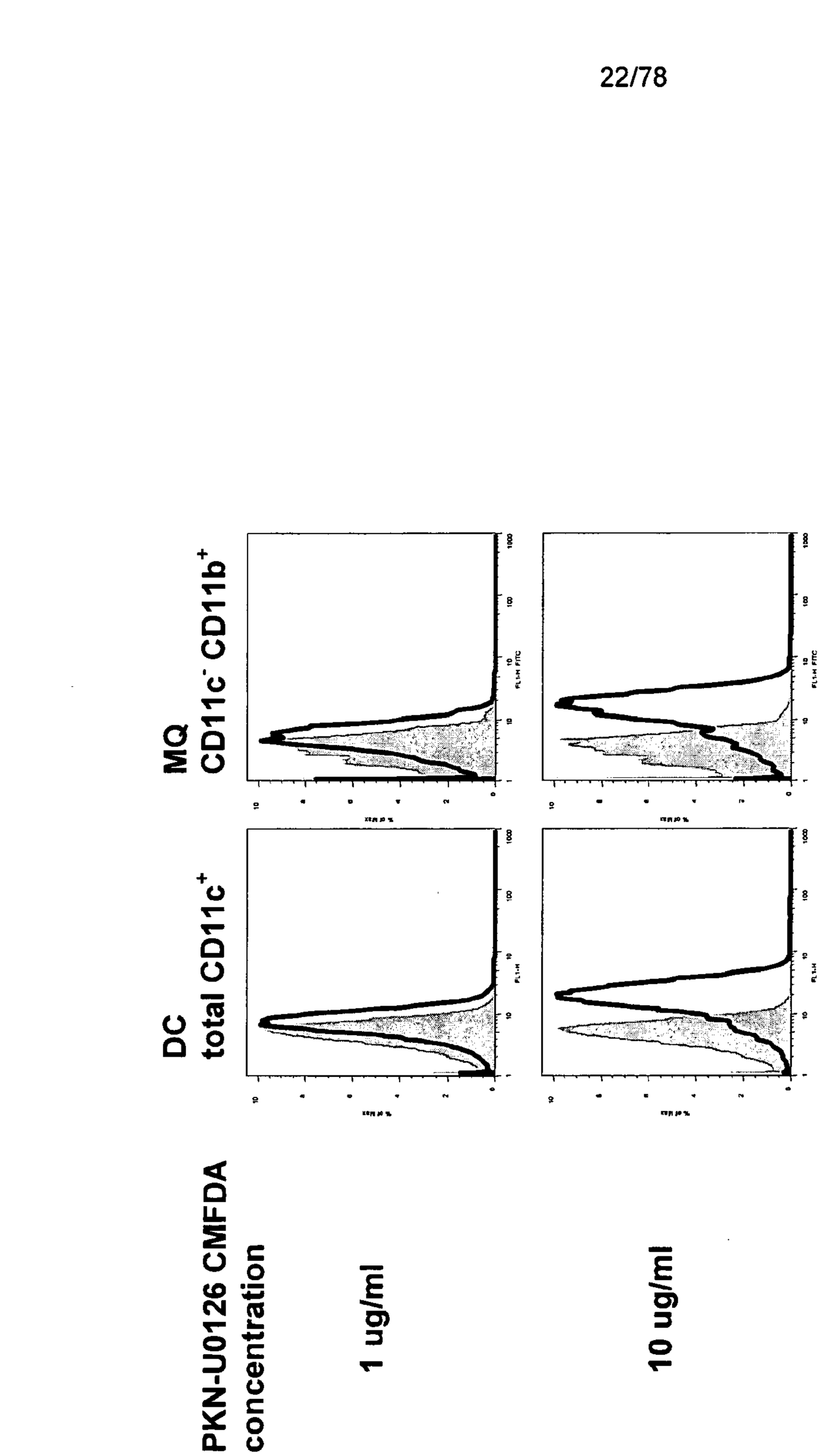
PKN-U0126 CMFDA
concentration
1 ug/ml
10 ug/ml
MQ
CD11c- CD11b+
DC
total CD11c+
FL1-H FITC
medium
uptake 5h

FIG. 15

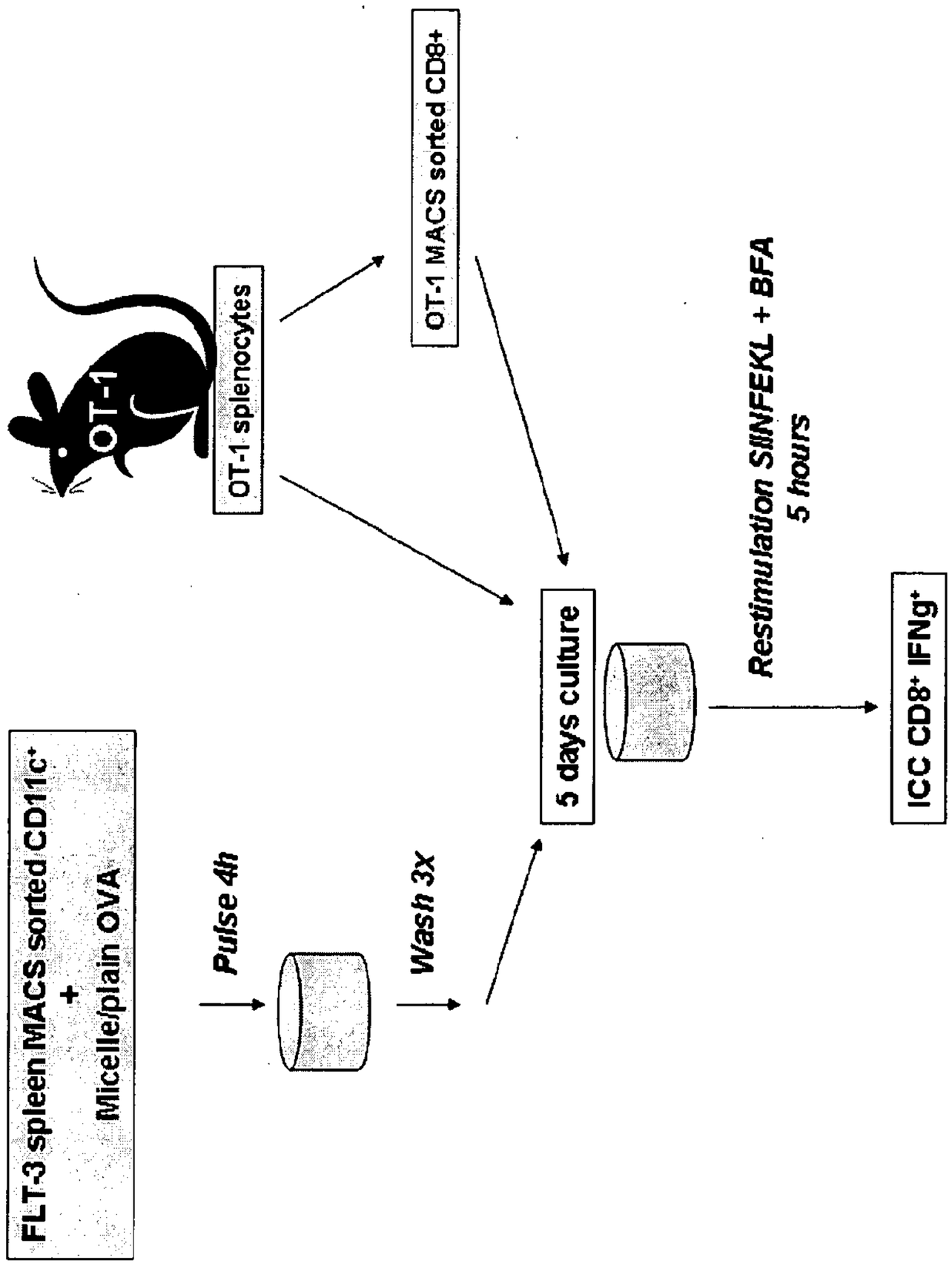
OT-1
OT-1 splenocytes
OT-1 MACS sorted CD8+
FLT-3 spleen MACS sorted CD11c+
+
Micelle/plain OVA
Pulse 4h
Wash 3x
5 days culture
Restimulation SIINFEKL + BFA
5 hours
ICC CD8+ IFNg+

FIG. 16

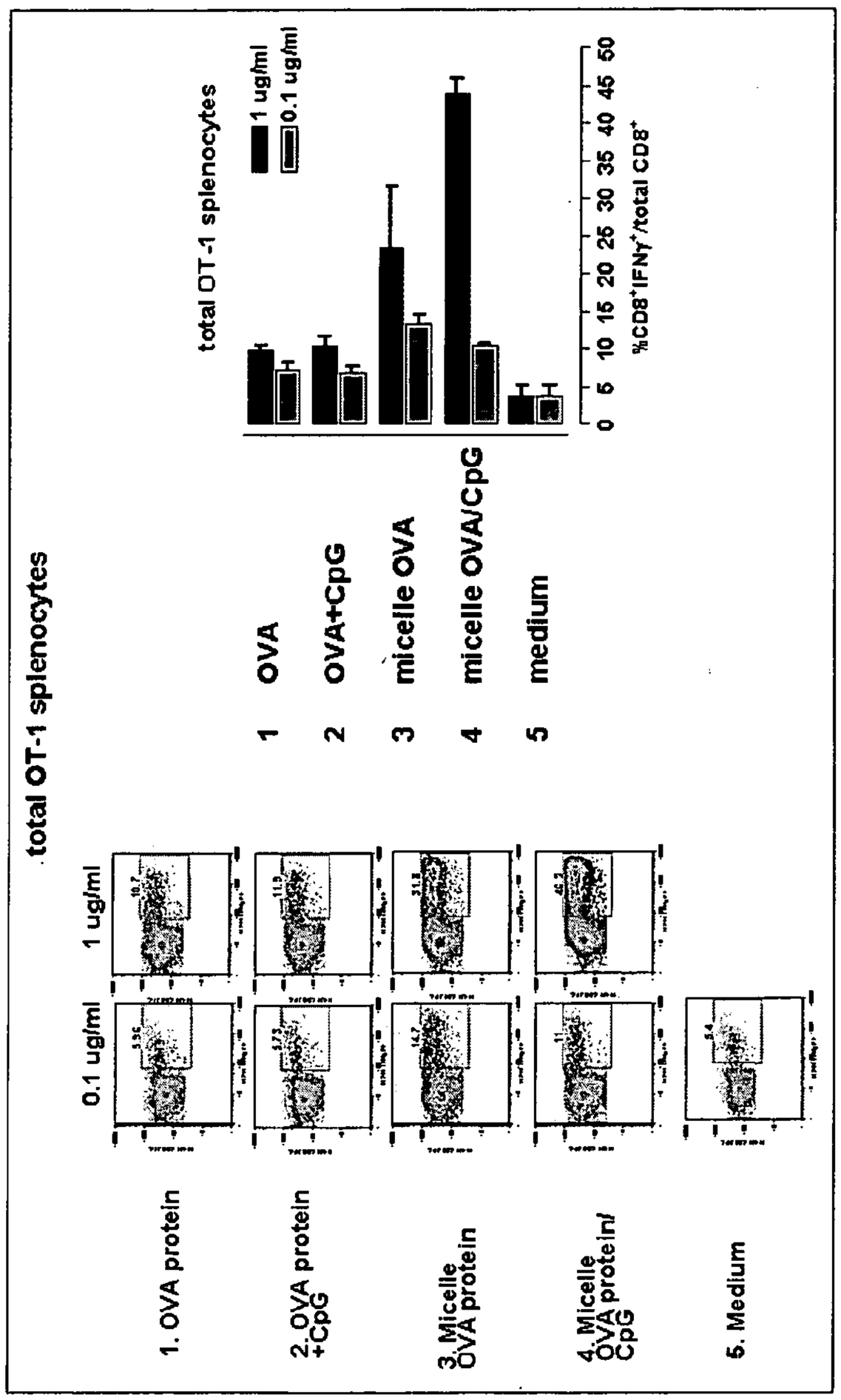
A
total OT-1 splenocytes
1 OVA
2 OVA+CpG
3 micelle OVA
4 micelle OVA/CpG
5 medium
1 ug/ml
0.1 ug/ml
%CD8+IFNγ+/total CD8+
0 5 10 15 20 25 30 35 40 45 50
total OT-1 splenocytes
0.1 ug/ml
1 ug/ml
1. OVA protein
2. OVA protein +CpG
3. Micelle OVA protein
4. Micelle OVA protein/ CpG
5. Medium

FIG. 17

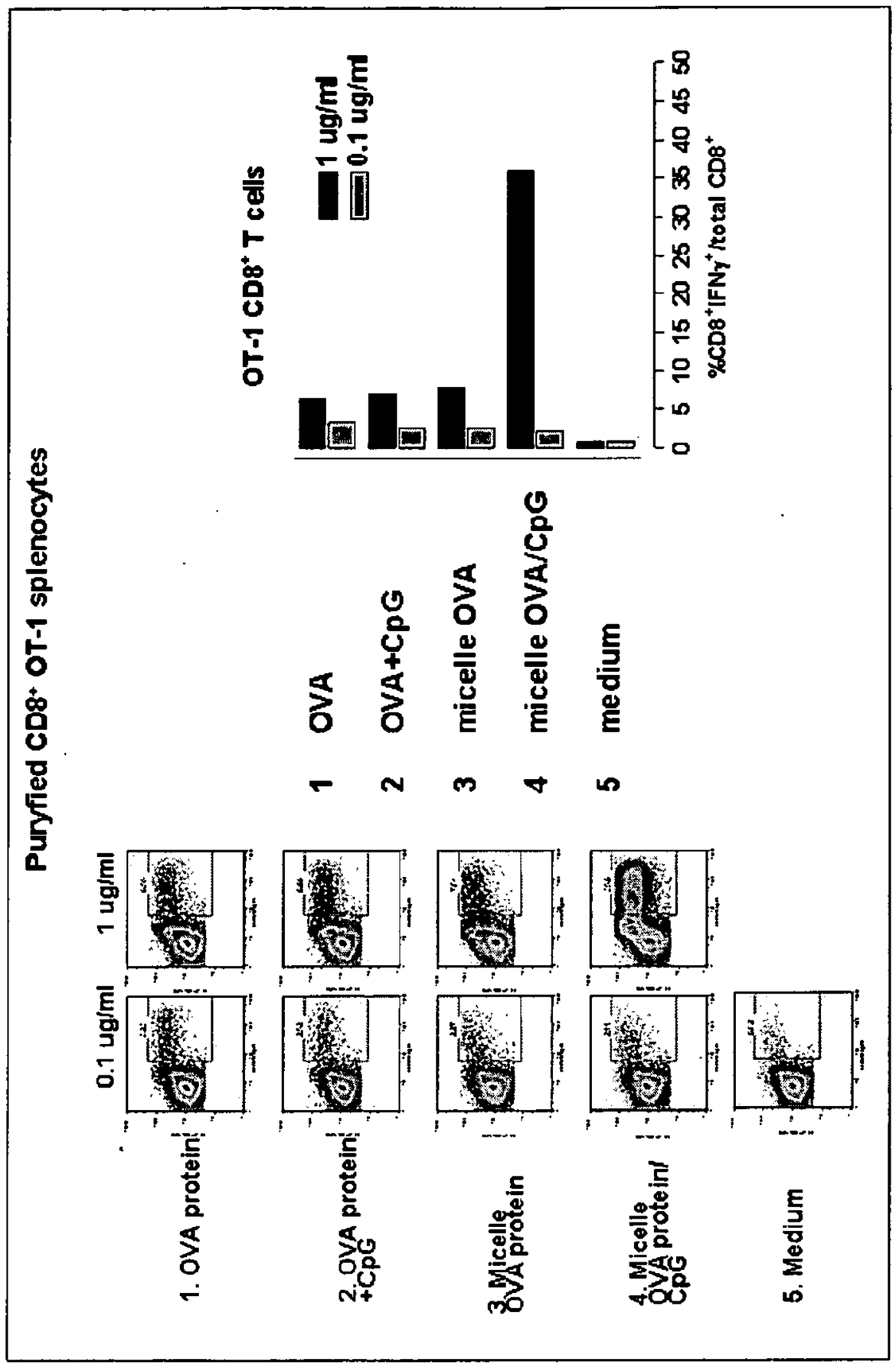

FIG. 17 continued

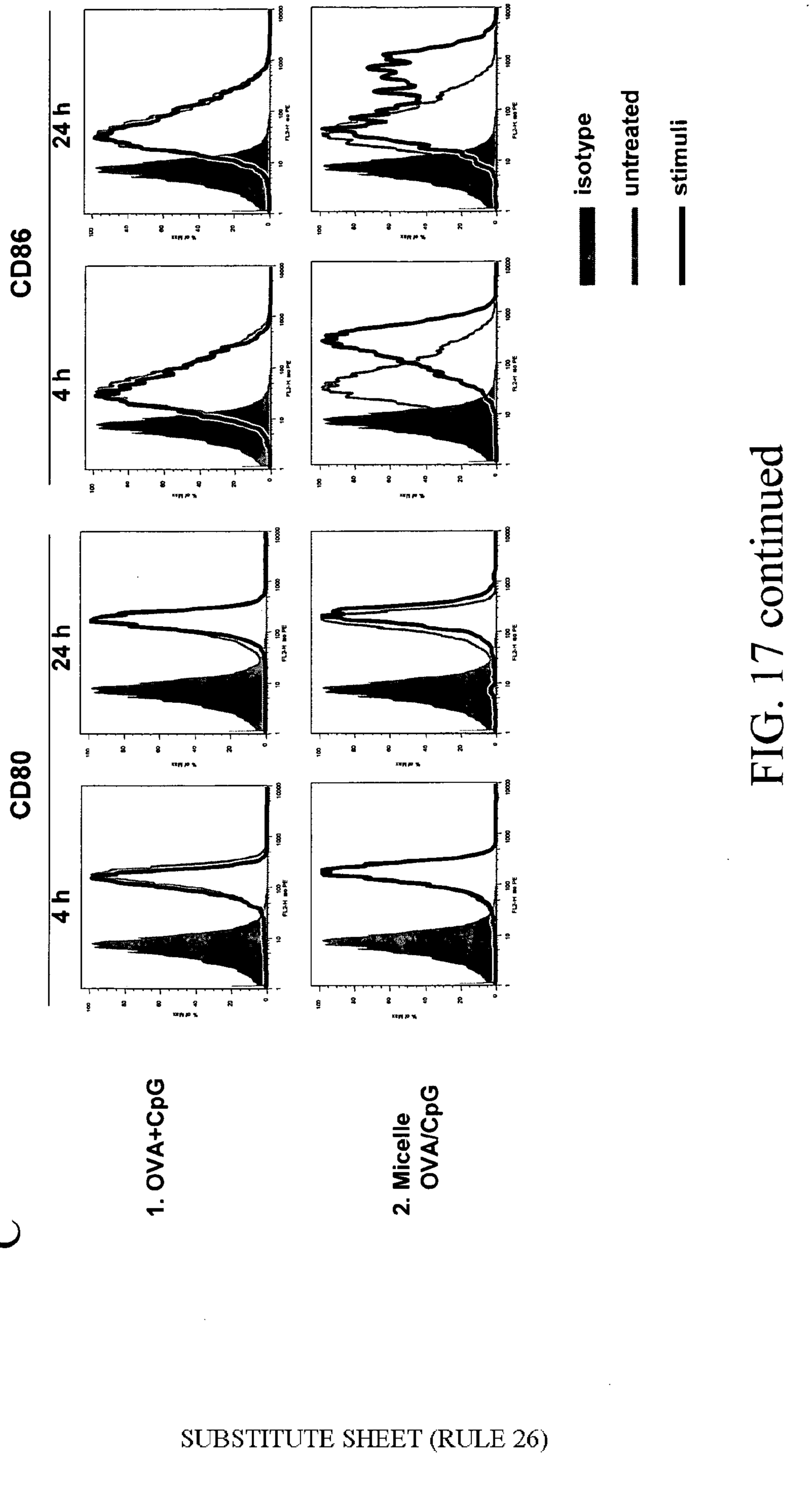

FIG. 17 continued

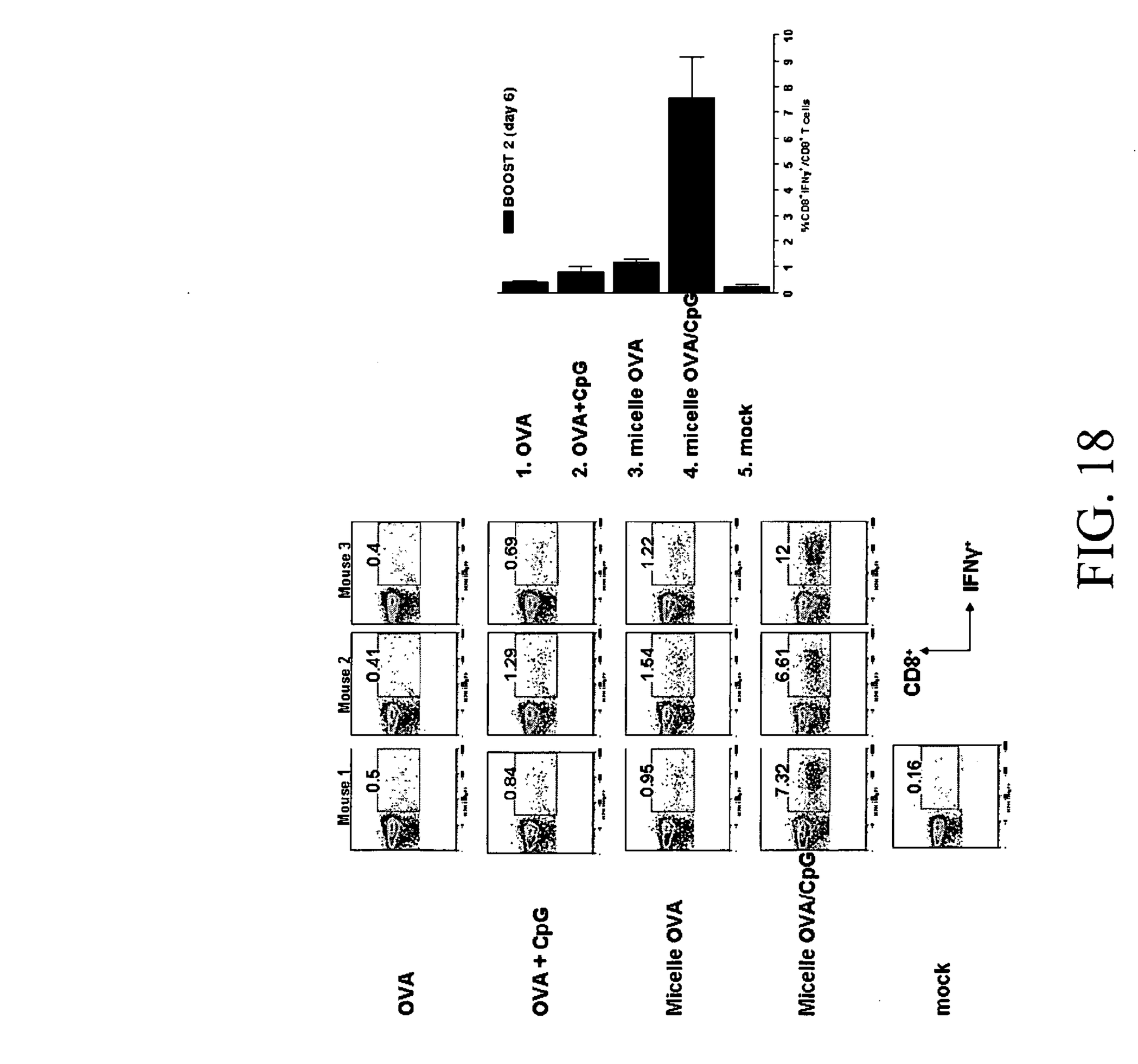
BOOST 2 (day 6)
1. OVA
2. OVA+CpG
3. micelle OVA
4. micelle OVA/CpG
5. mock
% CD8+IFNγ+/CD8+ T cells
0 1 2 3 4 5 6 7 8 9 10
Mouse 1
Mouse 2
Mouse 3
0.5
0.41
0.4
0.84
1.29
0.69
0.95
1.54
1.22
7.32
6.61
12
0.16
OVA
OVA + CpG
Micelle OVA
Micelle OVA/CpG
mock
CD8+
IFNγ+

FIG. 18

FIG. 18 continued

FIG. 18 continued

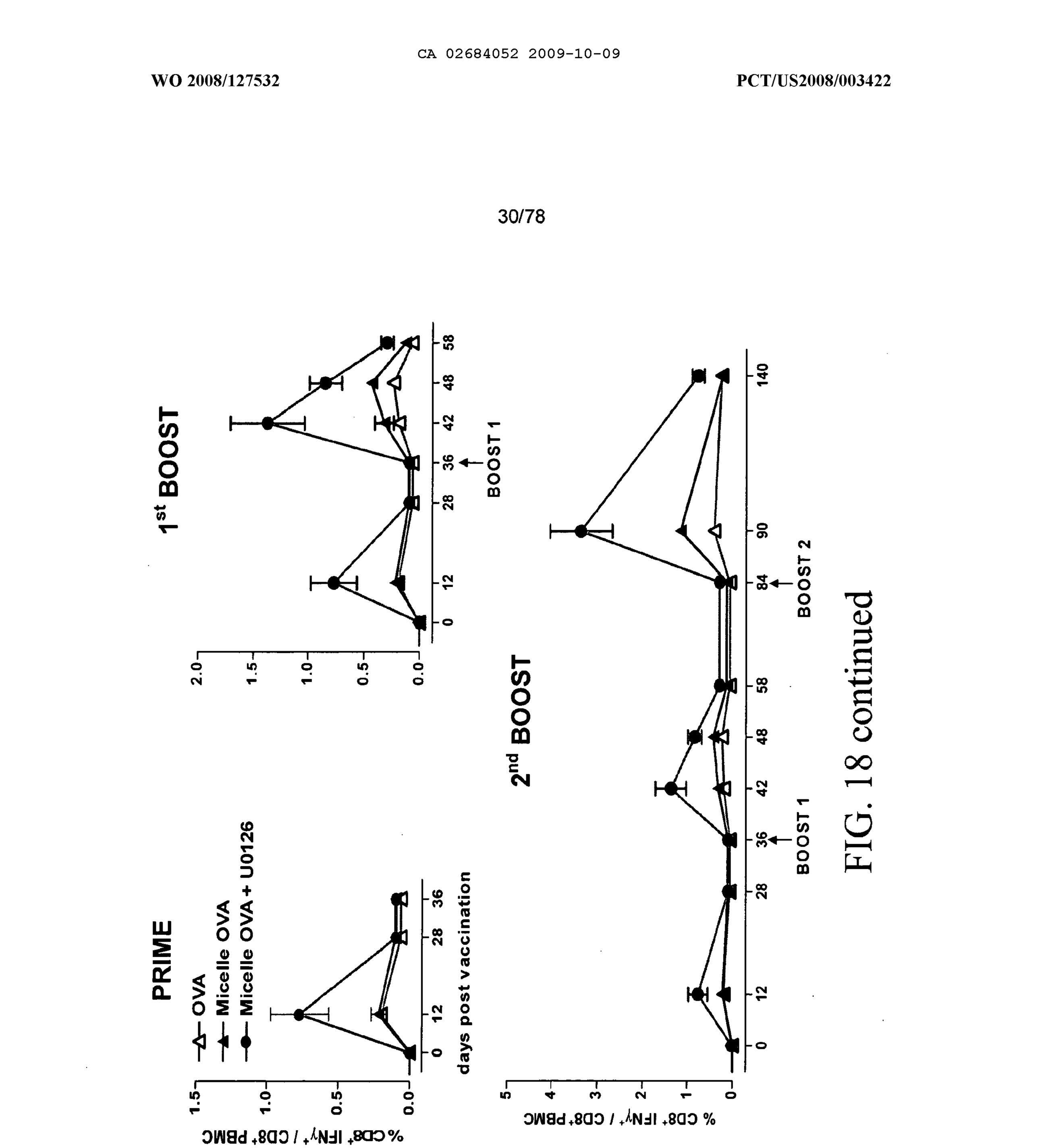

FIG. 18 continued

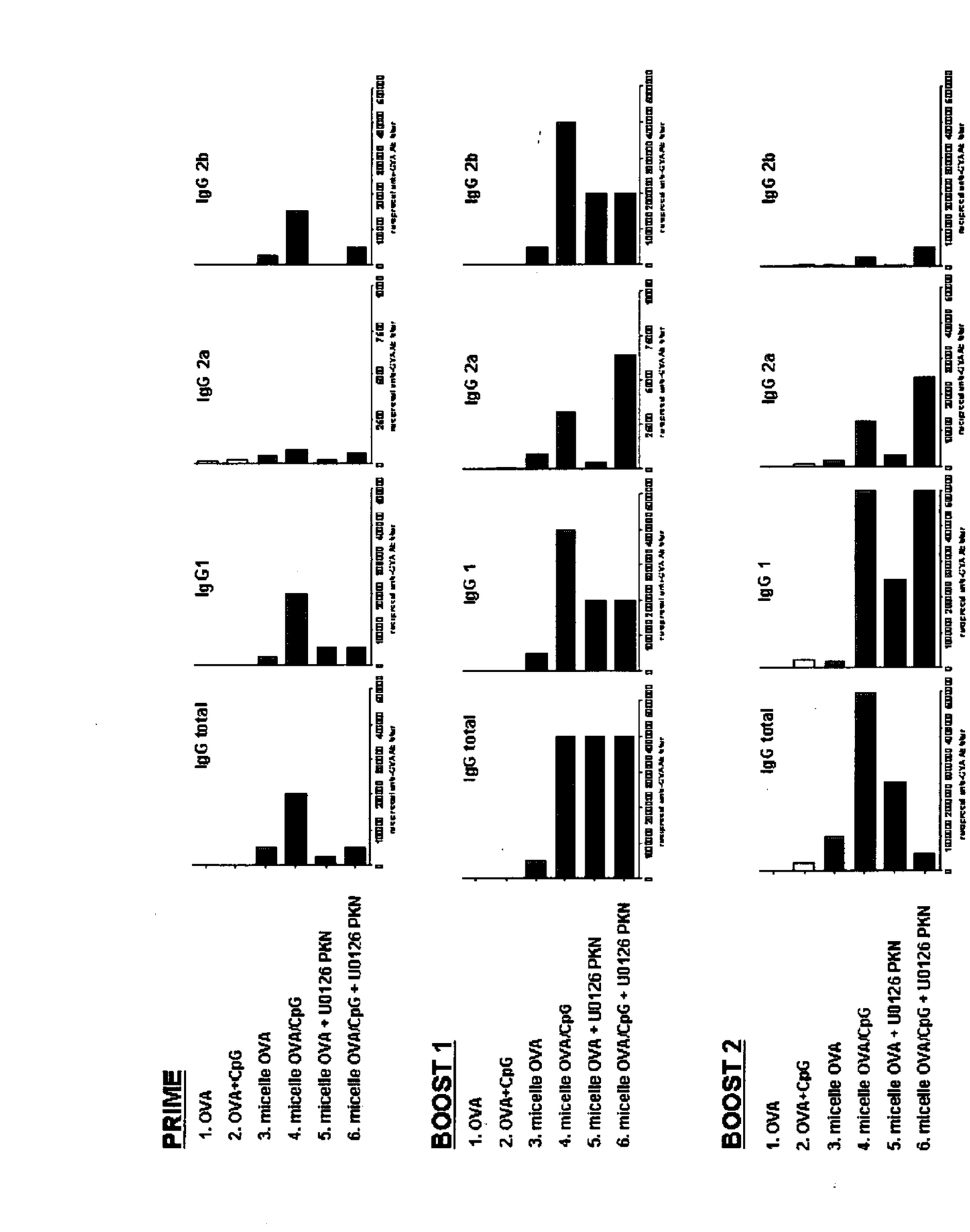

FIG. 18 continued

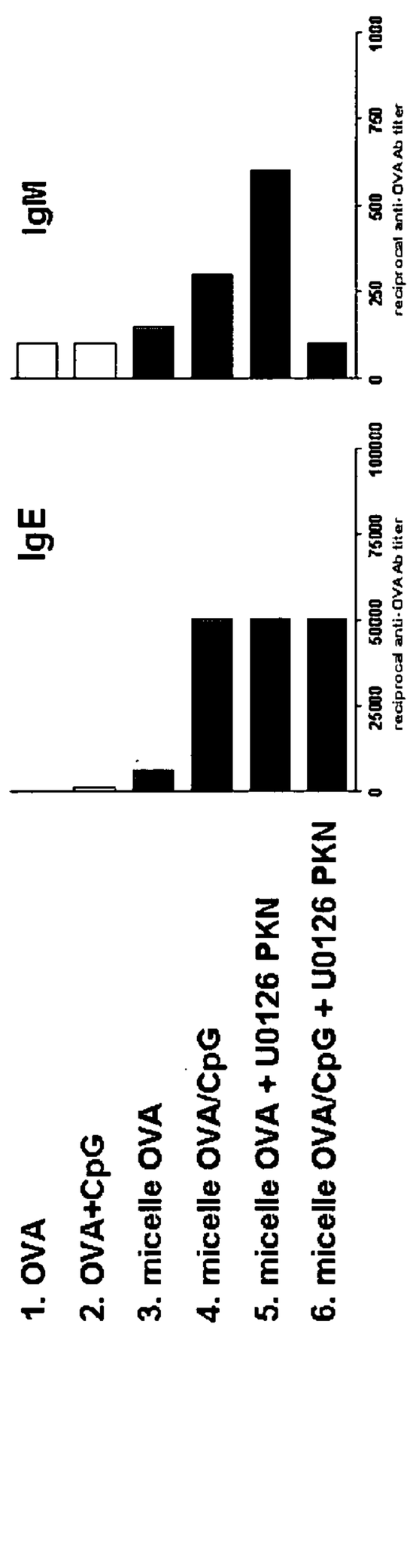

FIG. 18 continued

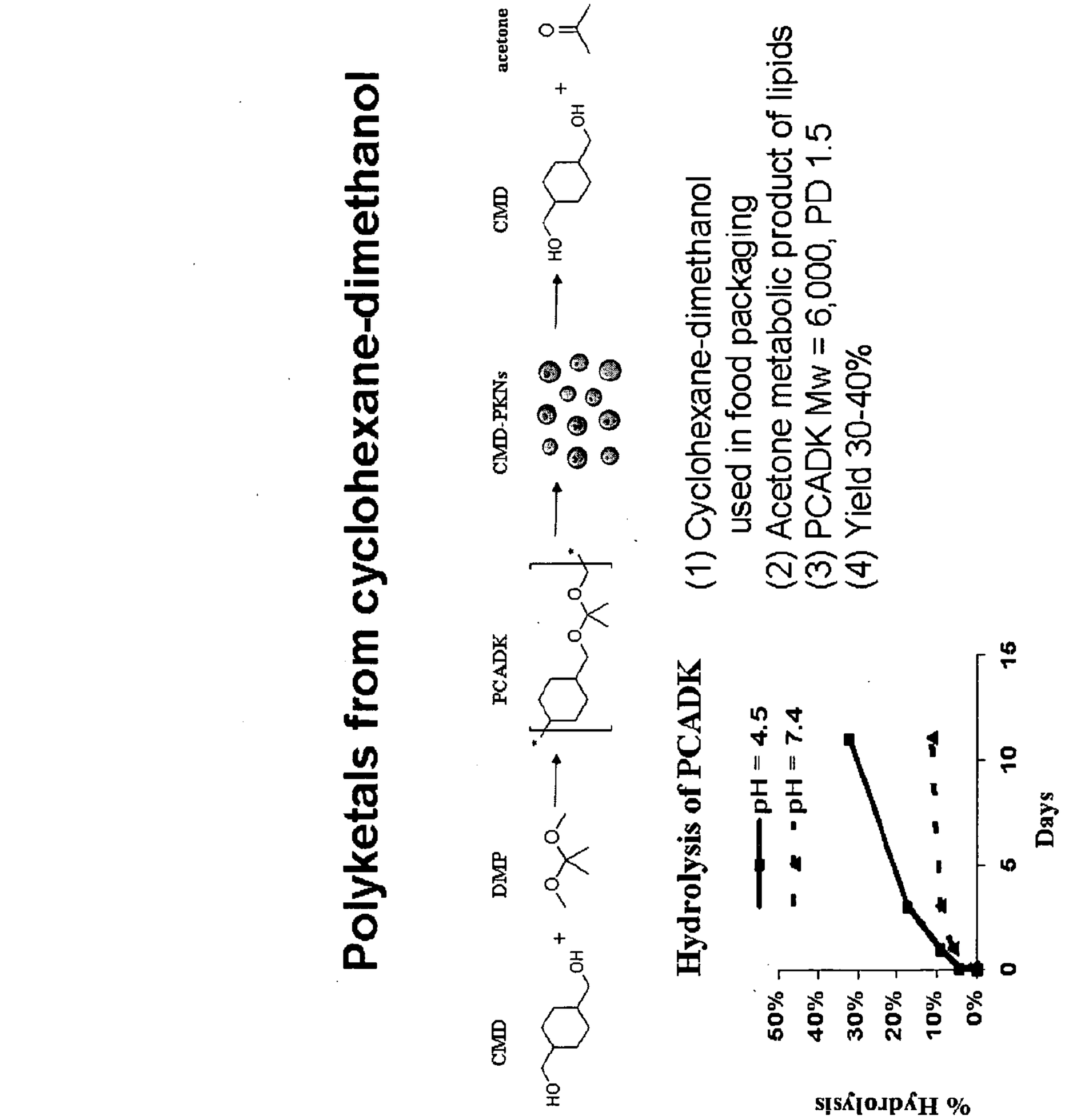
Polyketals from cyclohexane-dimethanol
CMD
DMP
PCADK
CMD-PKNs
CMD
acetone
(1) Cyclohexane-dimethanol used in food packaging
(2) Acetone metabolic product of lipids
(3) PCADK Mw = 6,000, PD 1.5
(4) Yield 30-40%
Hydrolysis of PCADK
pH = 4.5
pH = 7.4
% Hydrolysis
Days
A
B

FIG. 19

SEM Images of PCADK-particles
(using sonication)

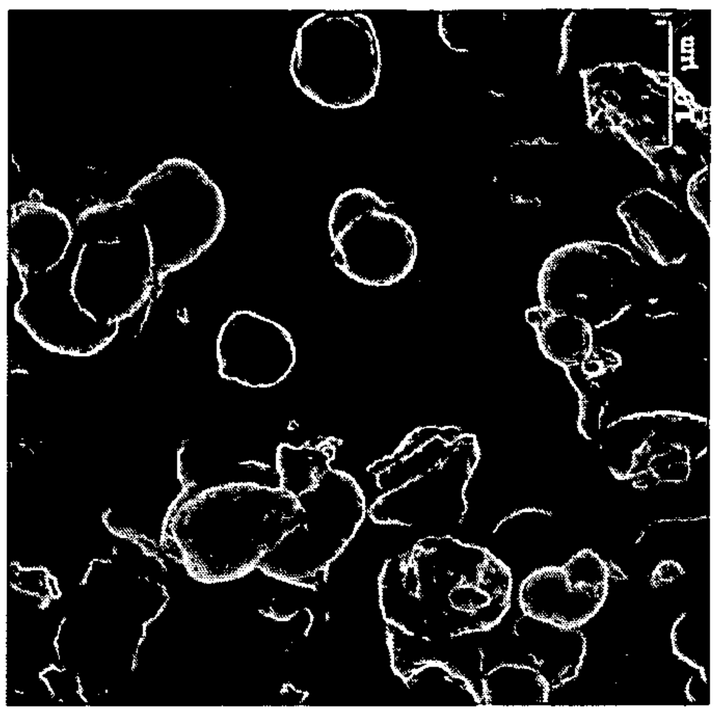

Ebselen

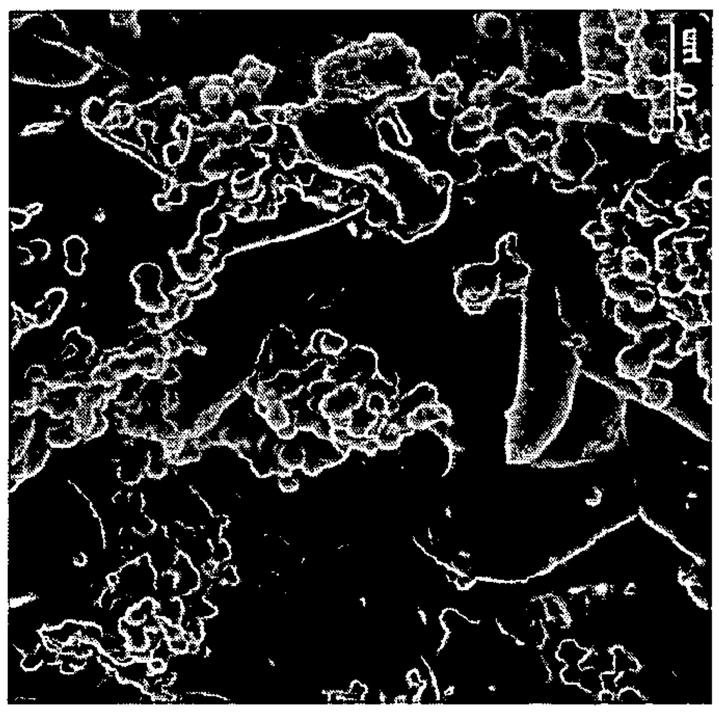

Rhodhamine

FIG. 20

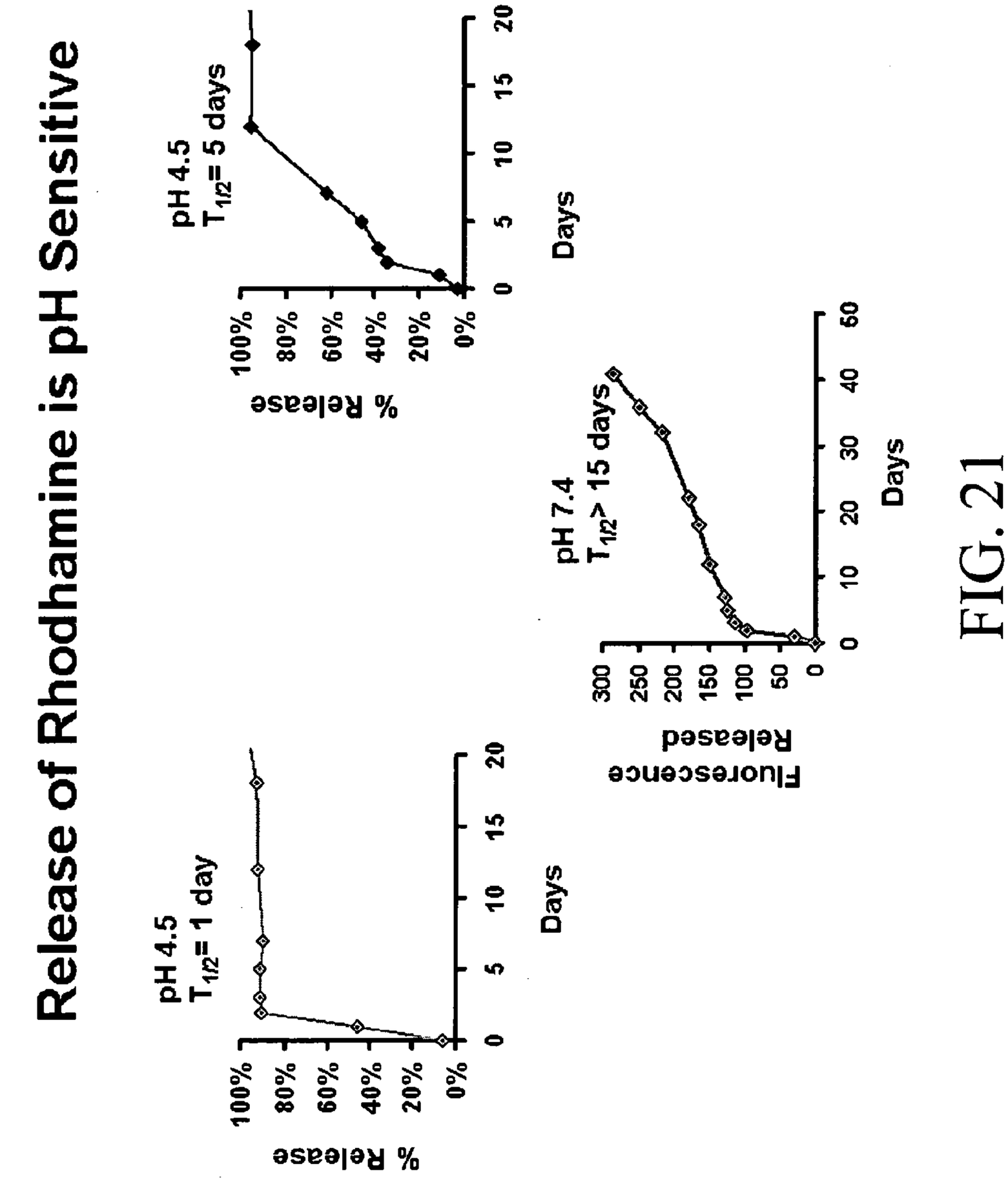
Release of Rhodhamine is pH Sensitive
pH 4.5
$T_{1/2}$= 5 days
% Release
100%
80%
60%
40%
20%
0%
0
5
10
15
20
Days
pH 7.4
$T_{1/2}$> 15 days
Fluorescence Released
300
250
200
150
100
50
0
10
20
30
40
60
Days
pH 4.5
$T_{1/2}$= 1 day
% Release

FIG. 21

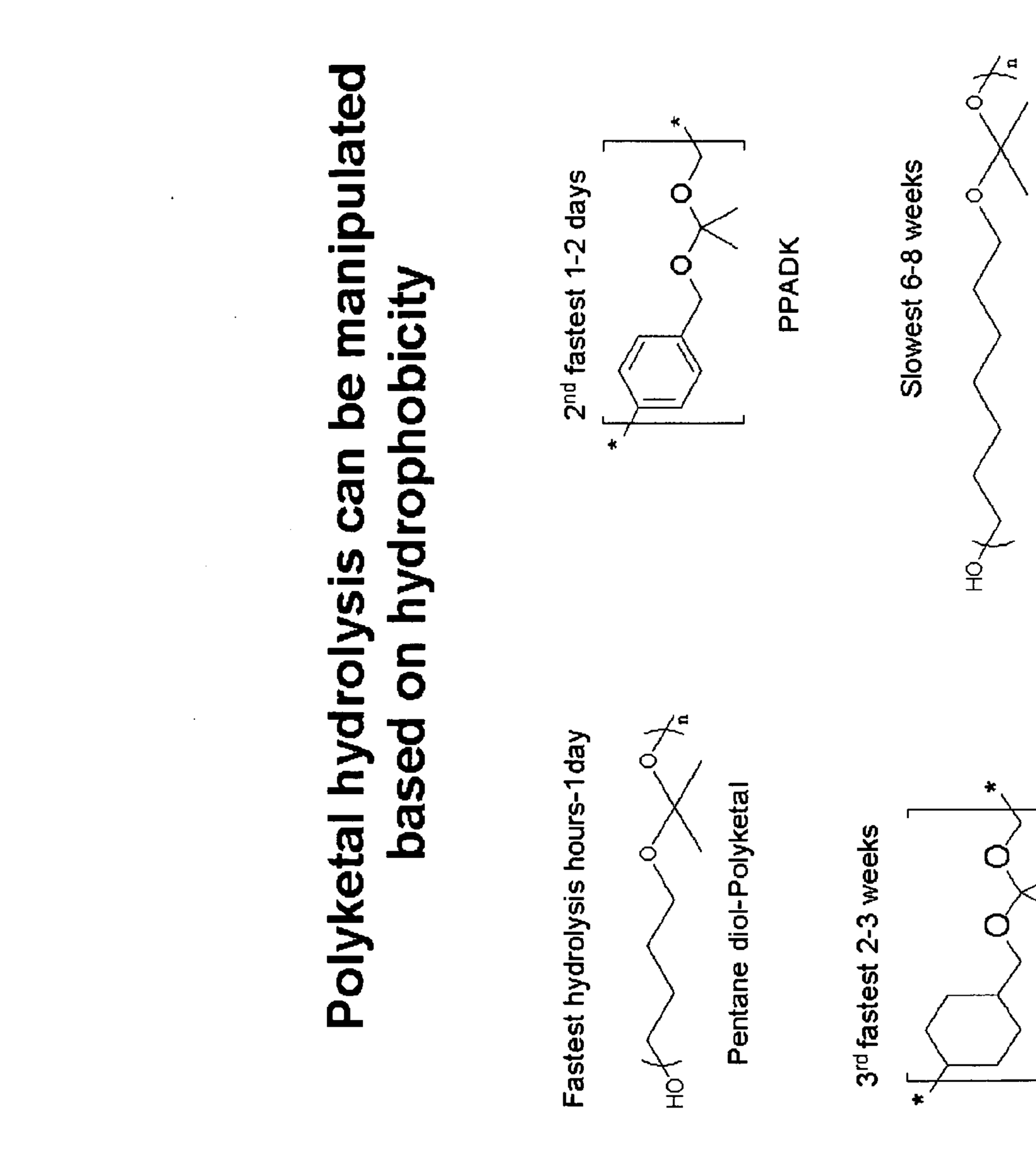
Polyketal hydrolysis can be manipulated based on hydrophobicity
2nd fastest 1-2 days
PPADK
Slowest 6-8 weeks
Octane-diol Polyketal
Fastest hydrolysis hours-1day
Pentane diol-Polyketal
3rd fastest 2-3 weeks
PCADK

FIG. 22


Phagocytosis of PKNs in vivo by liver macrophages
Injected FITC-PKNs into mice, isolated liver
Empty PKNs
IHC FITC-PKNs
FITC-PKNs
Green dots are FITC-PKNs
Red stain is macrophage specific antibody

FIG. 23

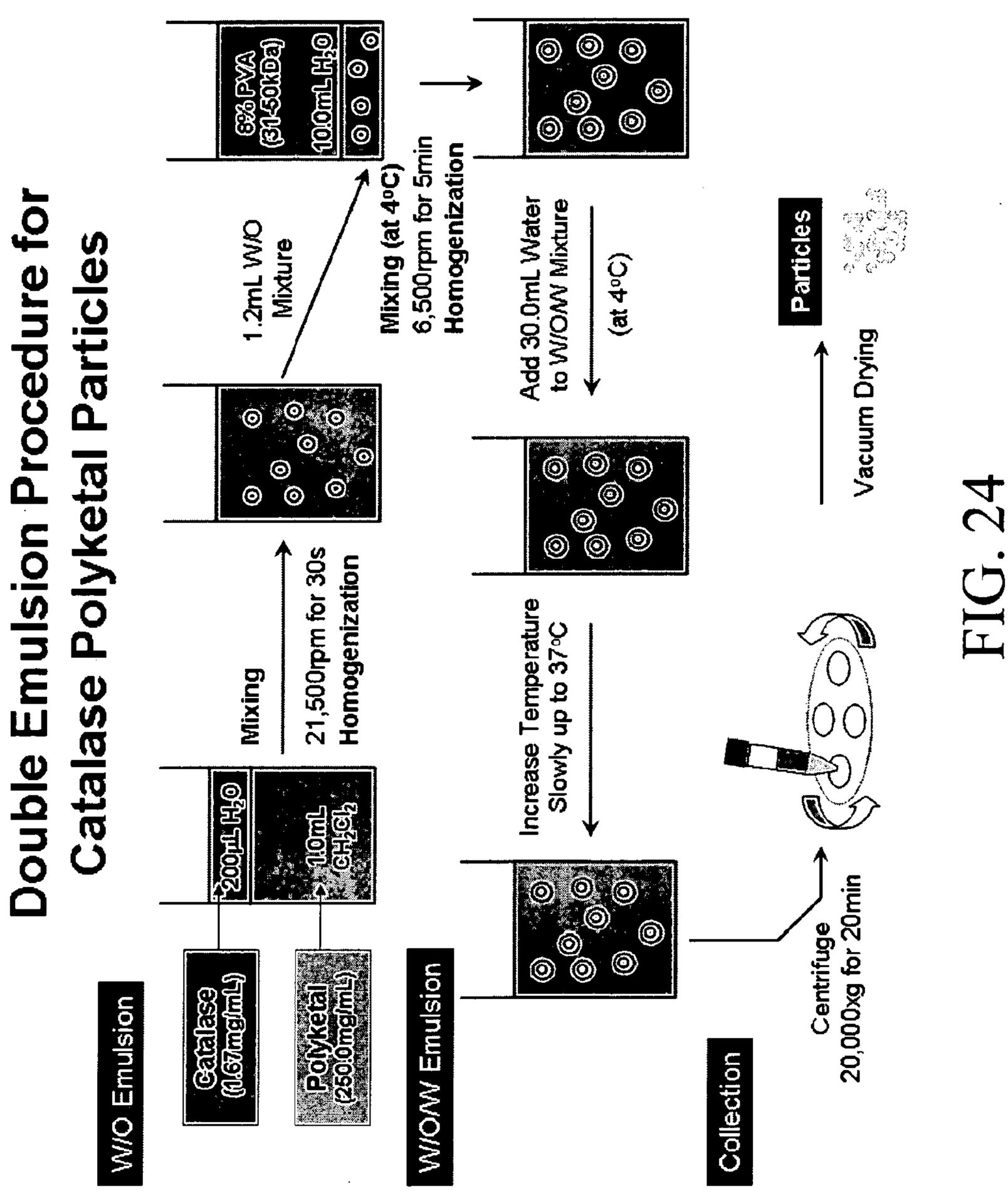
Double Emulsion Procedure for Catalase Polyketal Particles
W/O Emulsion
Catalase (1.67mg/mL)
200μL H_2O
Polyketal (250.0mg/mL)
10mL CH_2Cl_2
Mixing
21,500rpm for 30s
Homogenization
W/O/W Emulsion
1.2mL W/O Mixture
8% PVA (31-50kDa)
10.0mL H_2O
Mixing (at 4°C)
6,500rpm for 5min
Homogenization
Add 30.0mL Water to W/O/W Mixture
(at 4°C)
Increase Temperature Slowly up to 37°C
Collection
Centrifuge
20,000xg for 20min
Vacuum Drying
Particles

FIG. 24

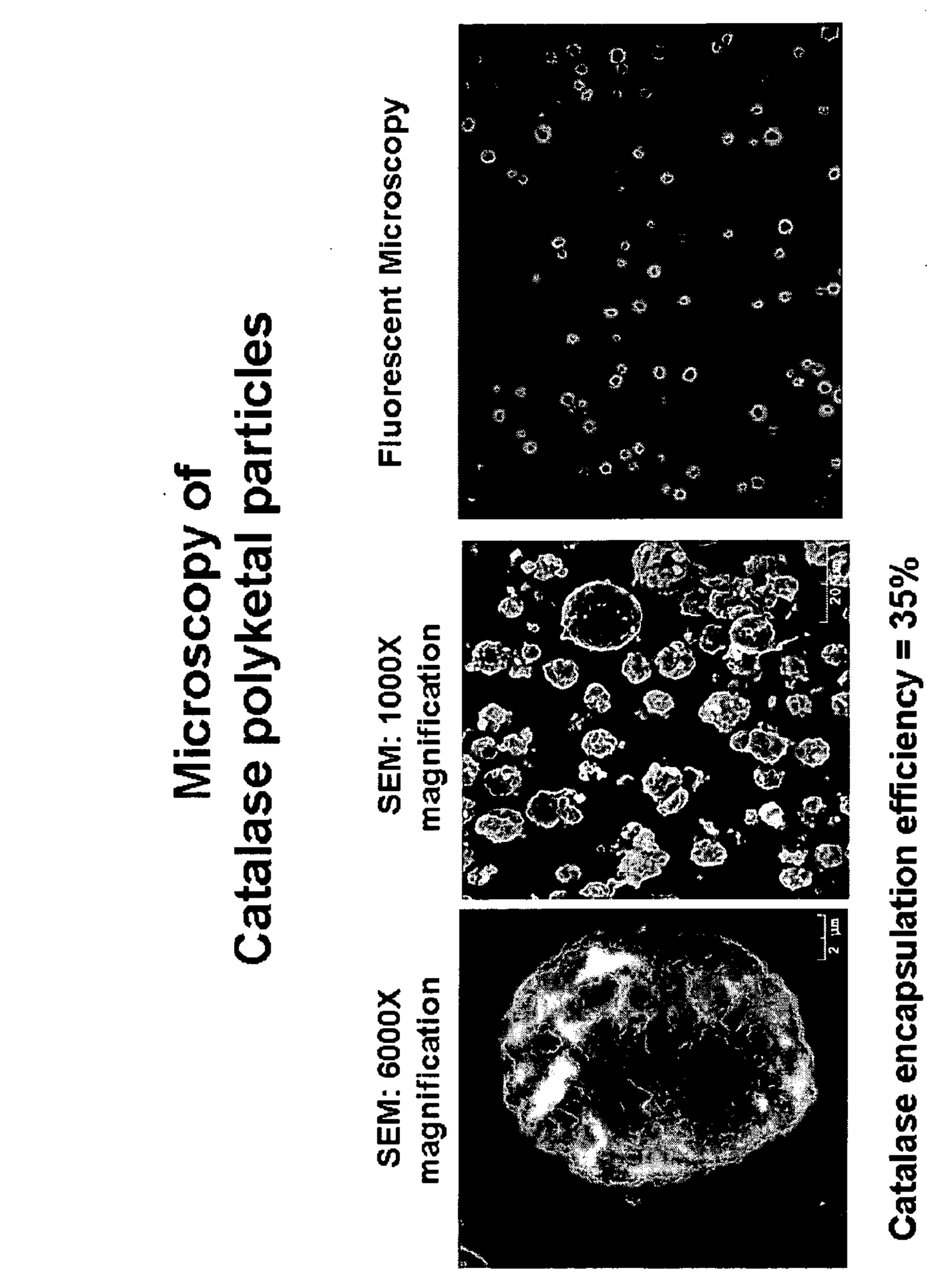

B

FIG. 24 continued

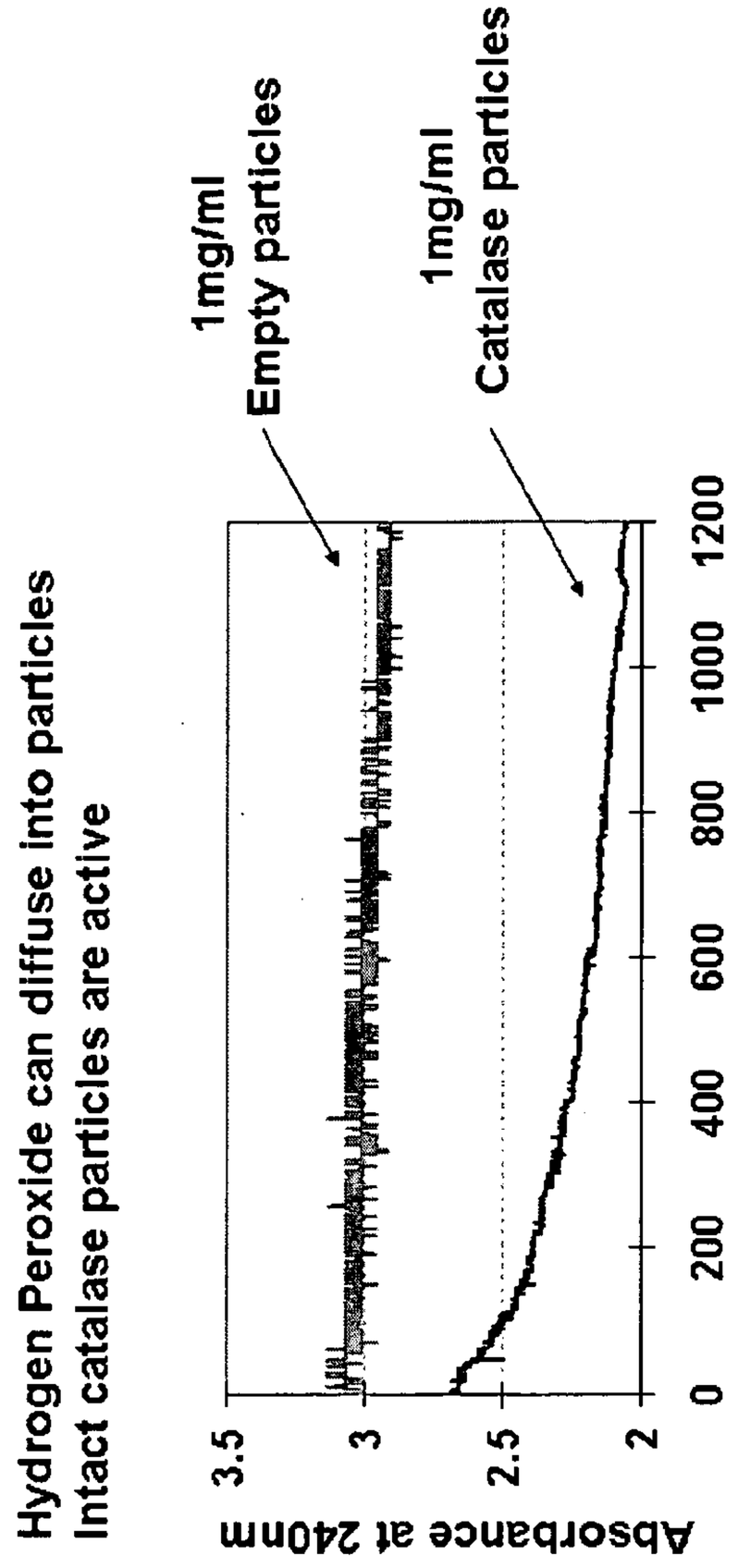

FIG. 24 continued

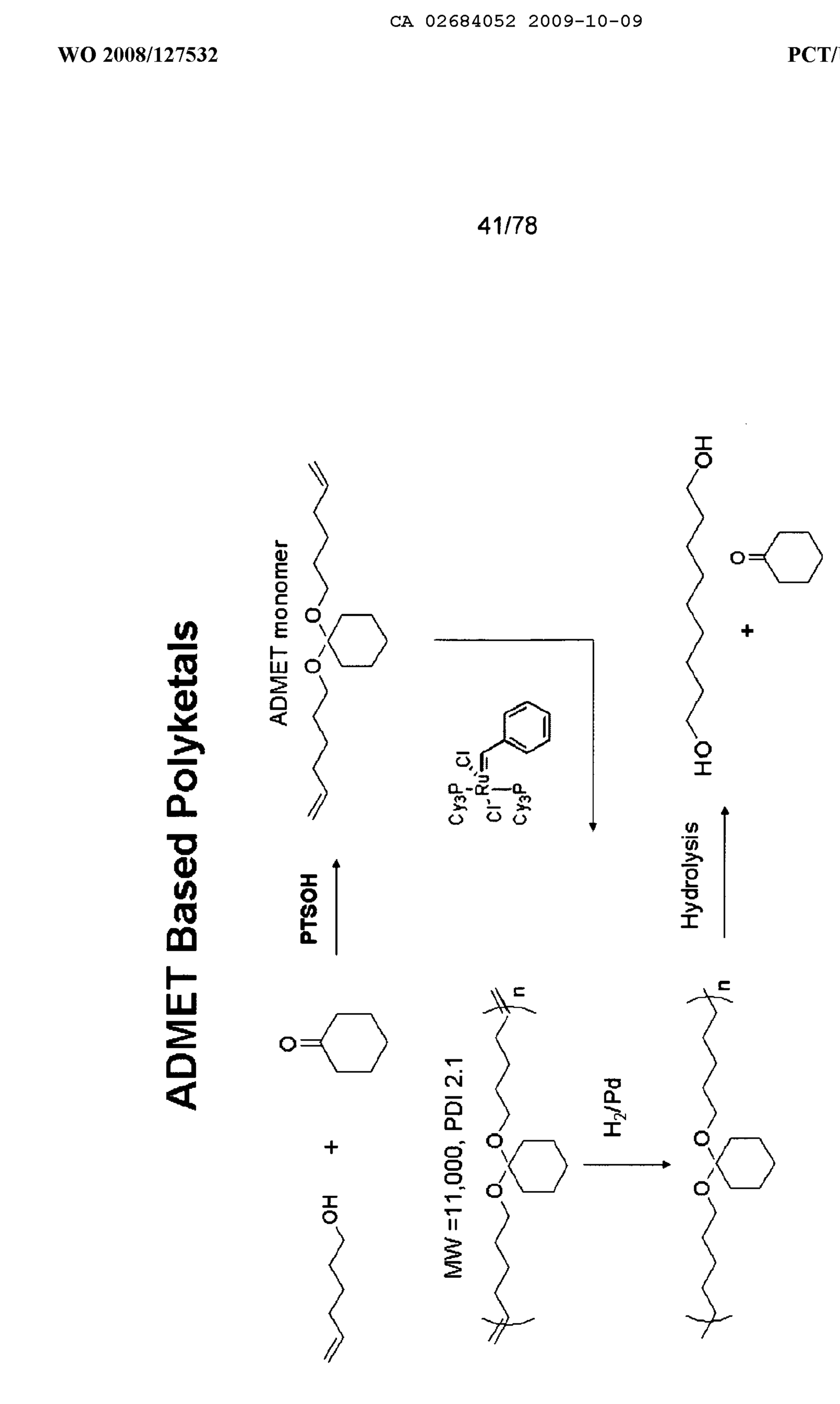
ADMET Based Polyketals
ADMET monomer
PTSOH
Hydrolysis
MW =11,000, PDI 2.1
H2/Pd
HO
OH
O
Cl
Ru
Cy3P
PCy3

FIG. 25

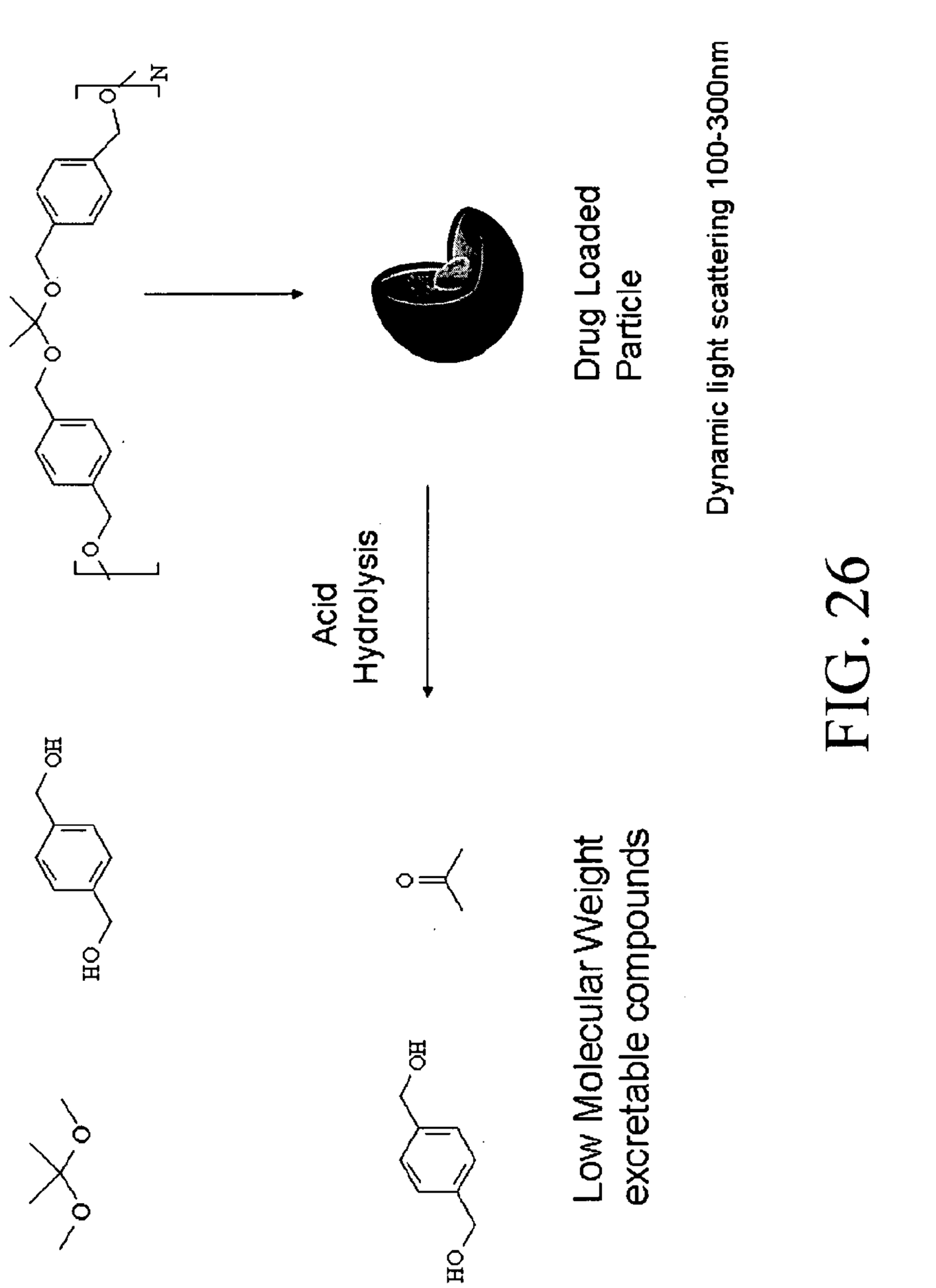
Acid
Hydrolysis
Drug Loaded
Particle
Dynamic light scattering 100-300nm
Low Molecular Weight
excretable compounds

FIG. 26

Nanoparticles Formed with PCADK (using sonication)

- Nanoparticles formed by Solvent Evaporation (Single Emulsion)

Batch	Polymer (mg)	PVA (mg)	CH_3Cl (ul)	Buffer (ml)	Effective Diameter (nm)
1	20	10	500	5	**361.3**
2	40	10	500	5	**367.8**
3	10	10	500	5	**307.8**
4	20	5	500	5	**457.5**
5	20	20	500	5	**307.4**
6	20	10	250	5	**331.2**
7	20	10	1000	5	**378.2**

- Conclusion: Particles formed are in 200-300nm range

FIG. 27

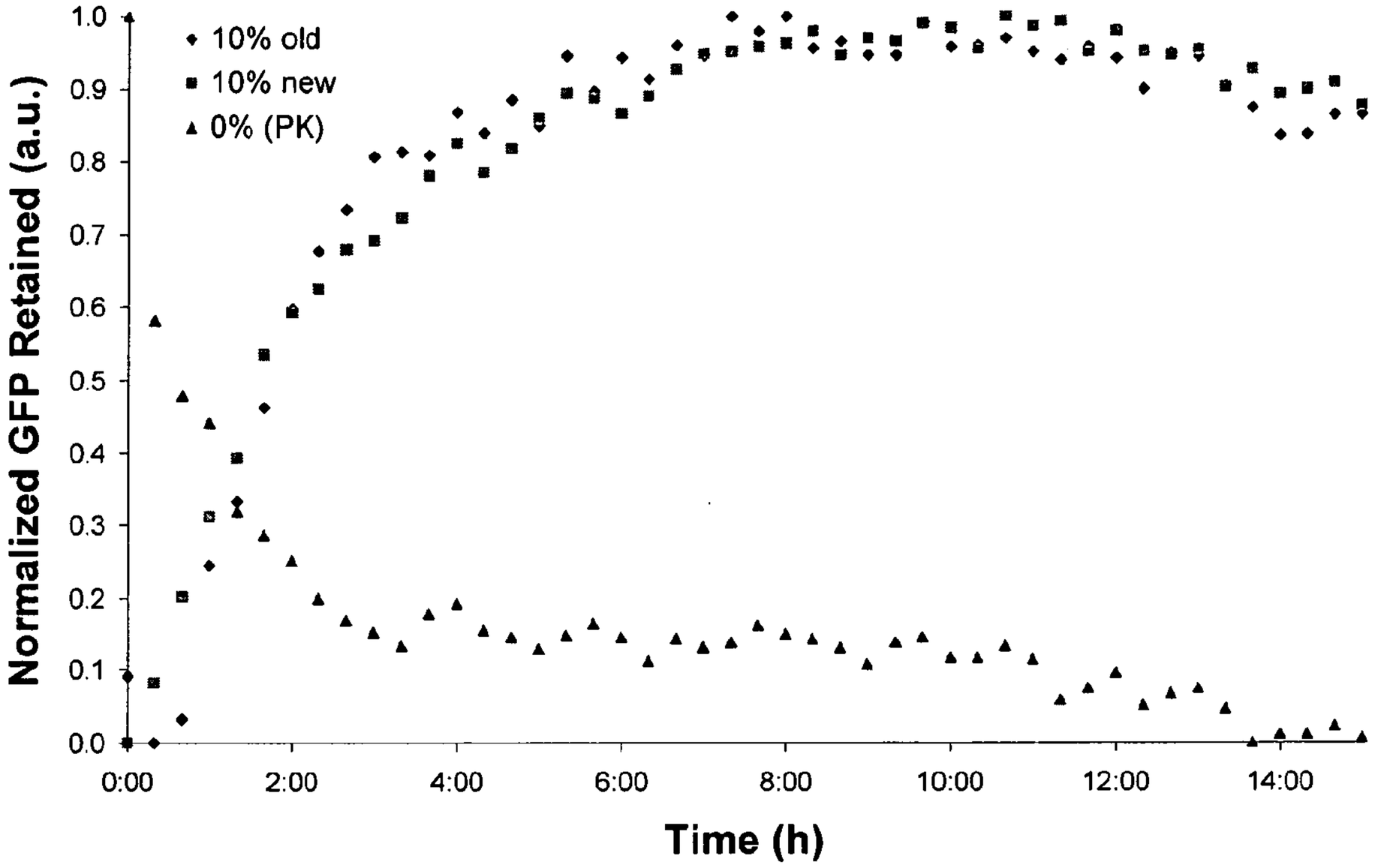
10% old
10% new
0% (PK)
Normalized GFP Retained (a.u.)
1.0
0.9
0.8
0.7
0.6
0.5
0.4
0.3
0.2
0.1
0.0
0:00
2:00
4:00
6:00
8:00
10:00
12:00
14:00
Time (h)

FIG. 28

FIG. 29

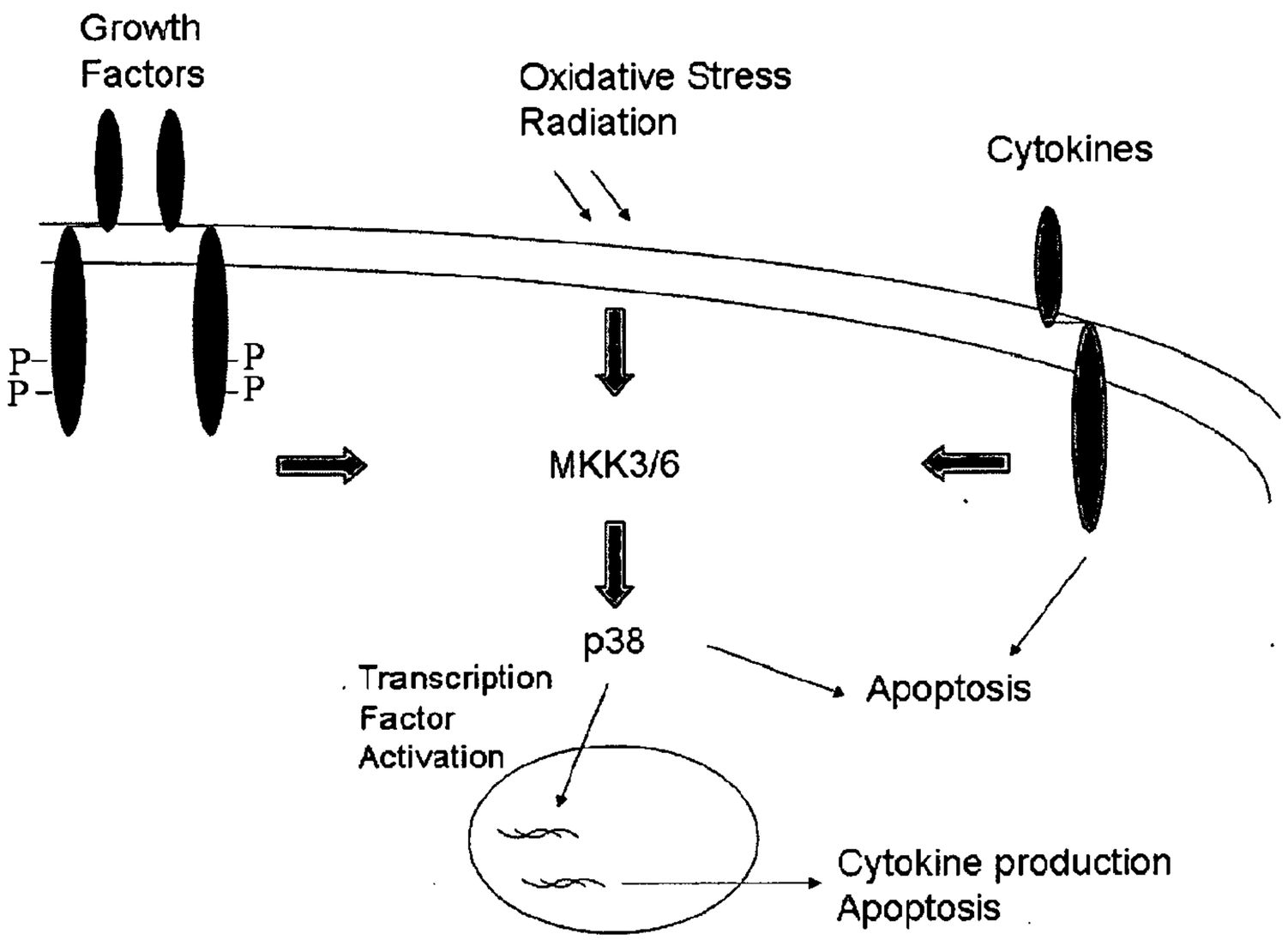

Schematic cartoon showing sources of p38 activation as well as downstream effects.

FIG. 30

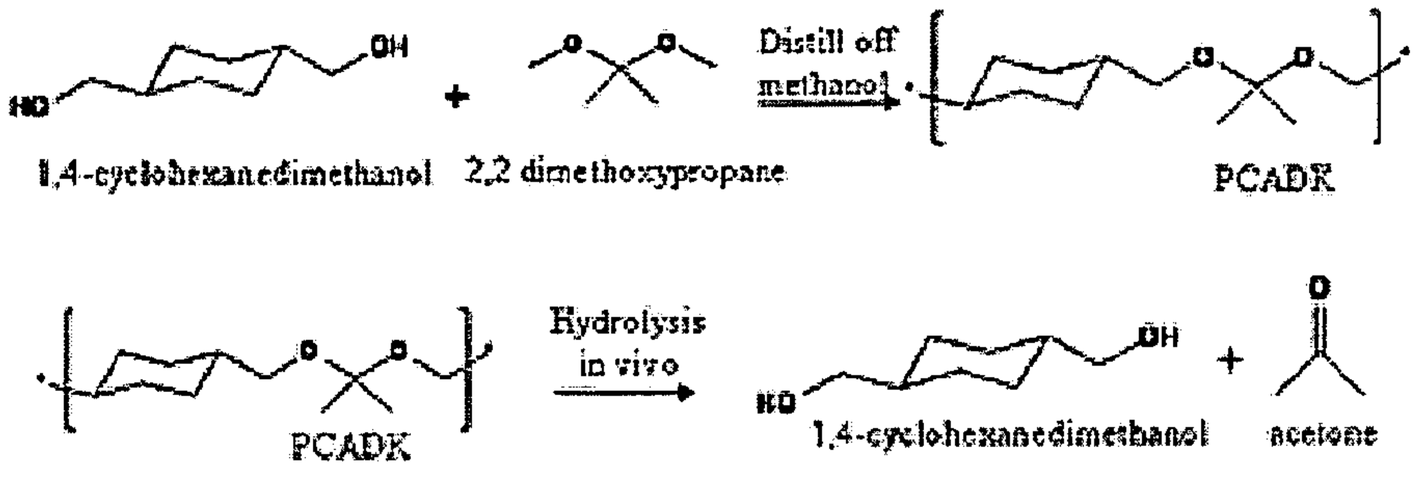

Synthesis of Poly(1,4-cyclohexane-acetone dimethylene ketal) (PCADK). PCADK is synthesized using the acetal exchange reaction with 1,4-cyclohexanedimethanol and 2,2 dimethoxypropane as reactants. PCADK hydrolyzes into 1,4-cyclohexanedimethanol and acetone.

FIG. 31

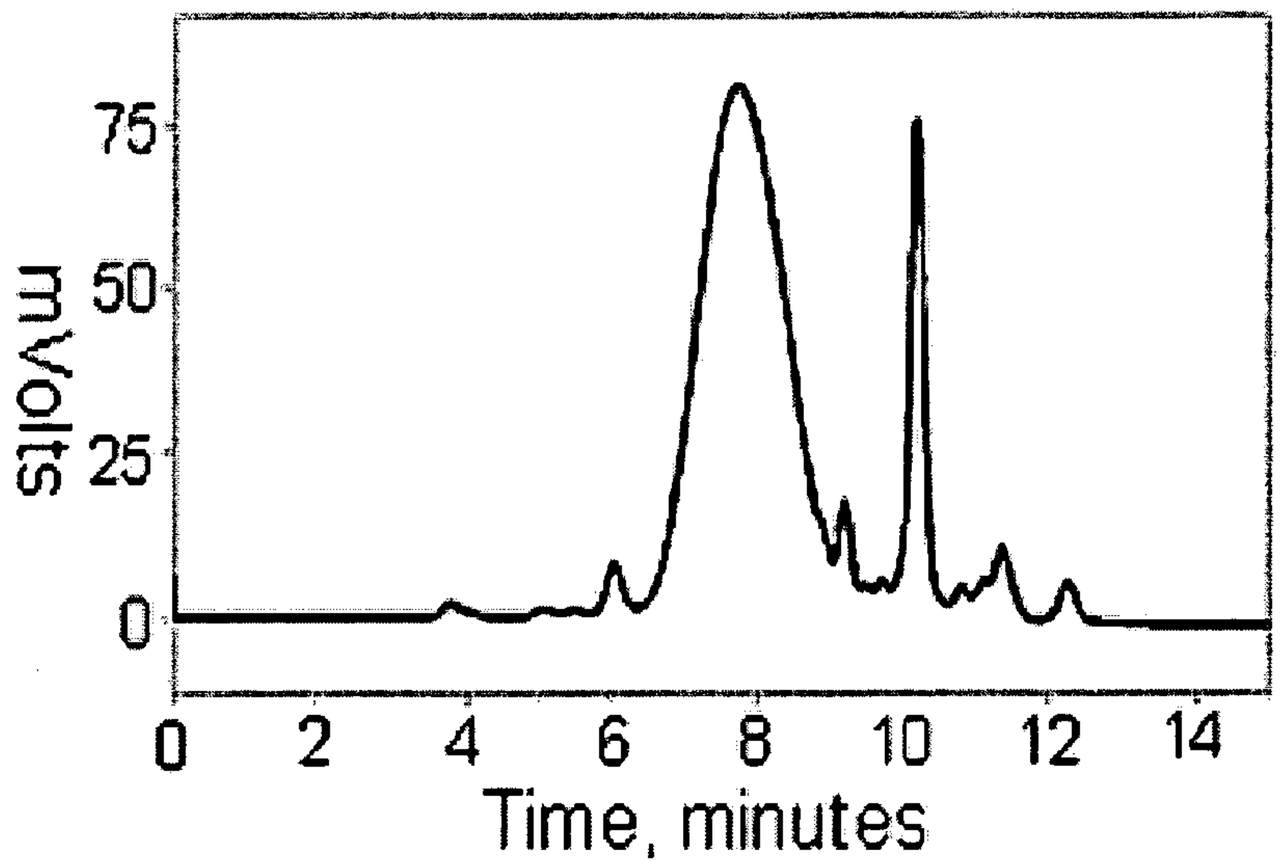

GPC trace of PCADK in THF, Y-axis indicates relative UV absorbance at 262 nm, Mw = 6,282, polydispersity index (PDI) = 1.54.

FIG. 32

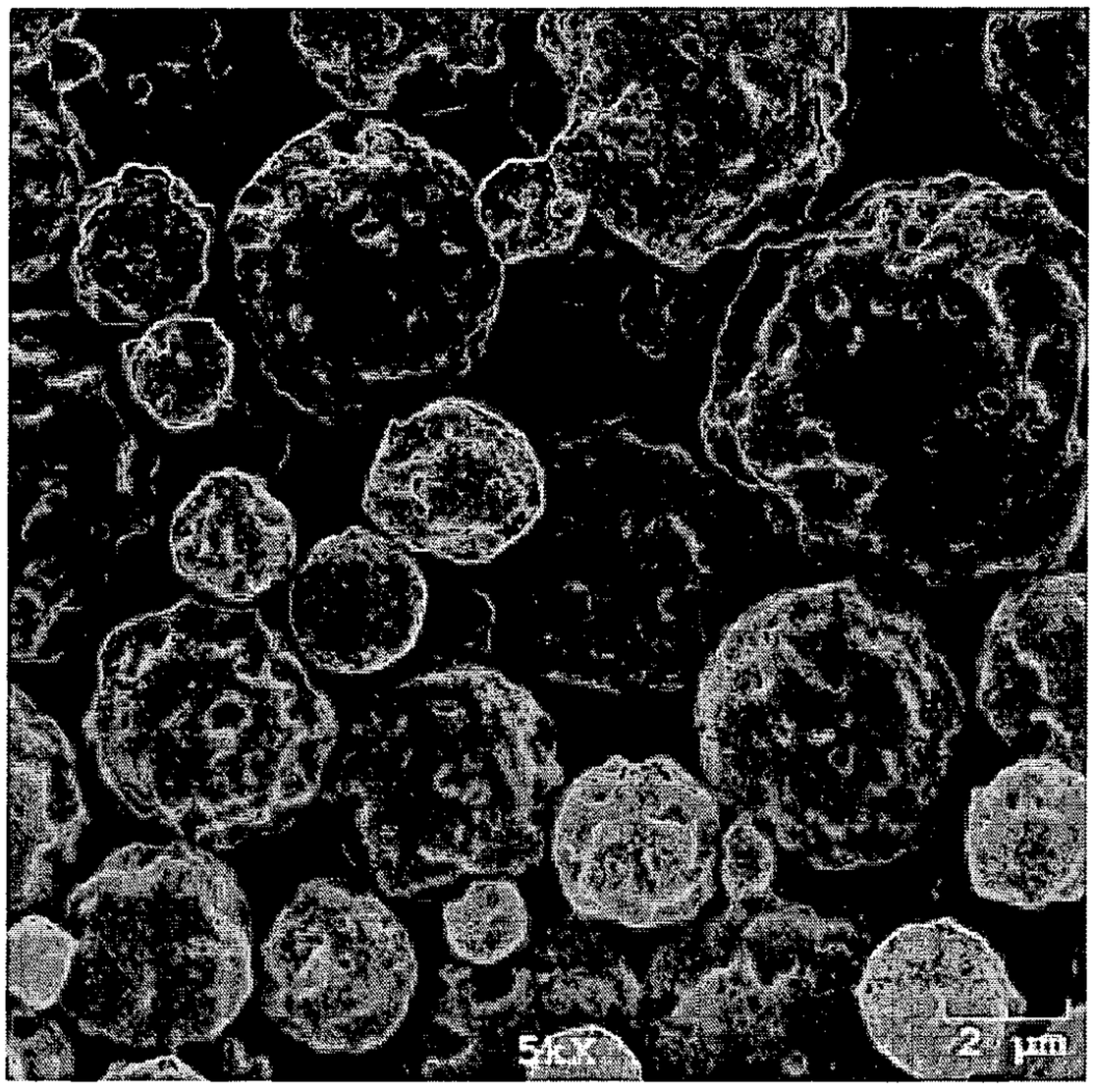

Representative SEM image of SB239063-loaded particles (PK-p38$_i$). These images return an approximate particle size of 3-15 μm.

FIG. 33

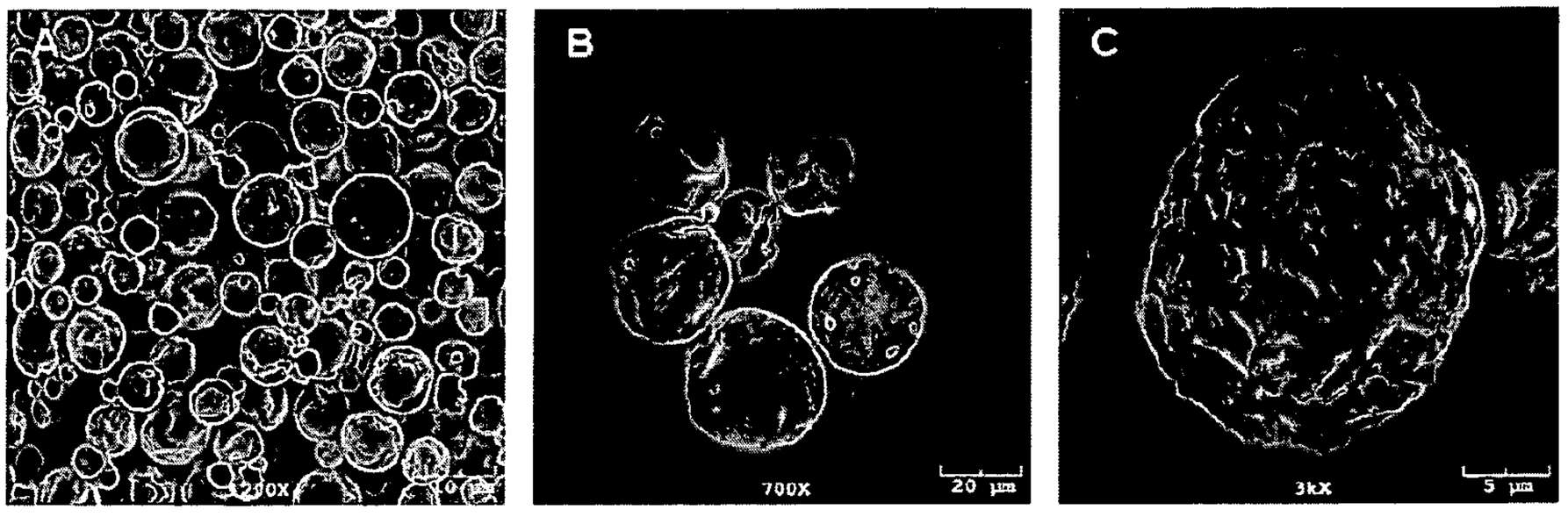

Particle size can be easily modified. A) SEM of particles generated with original protocol. B) Higher magnification SEM from particles generated from reduced homogenization speed. C) High magnification image of particle generated from reduced PVA concentration.

FIG. 34

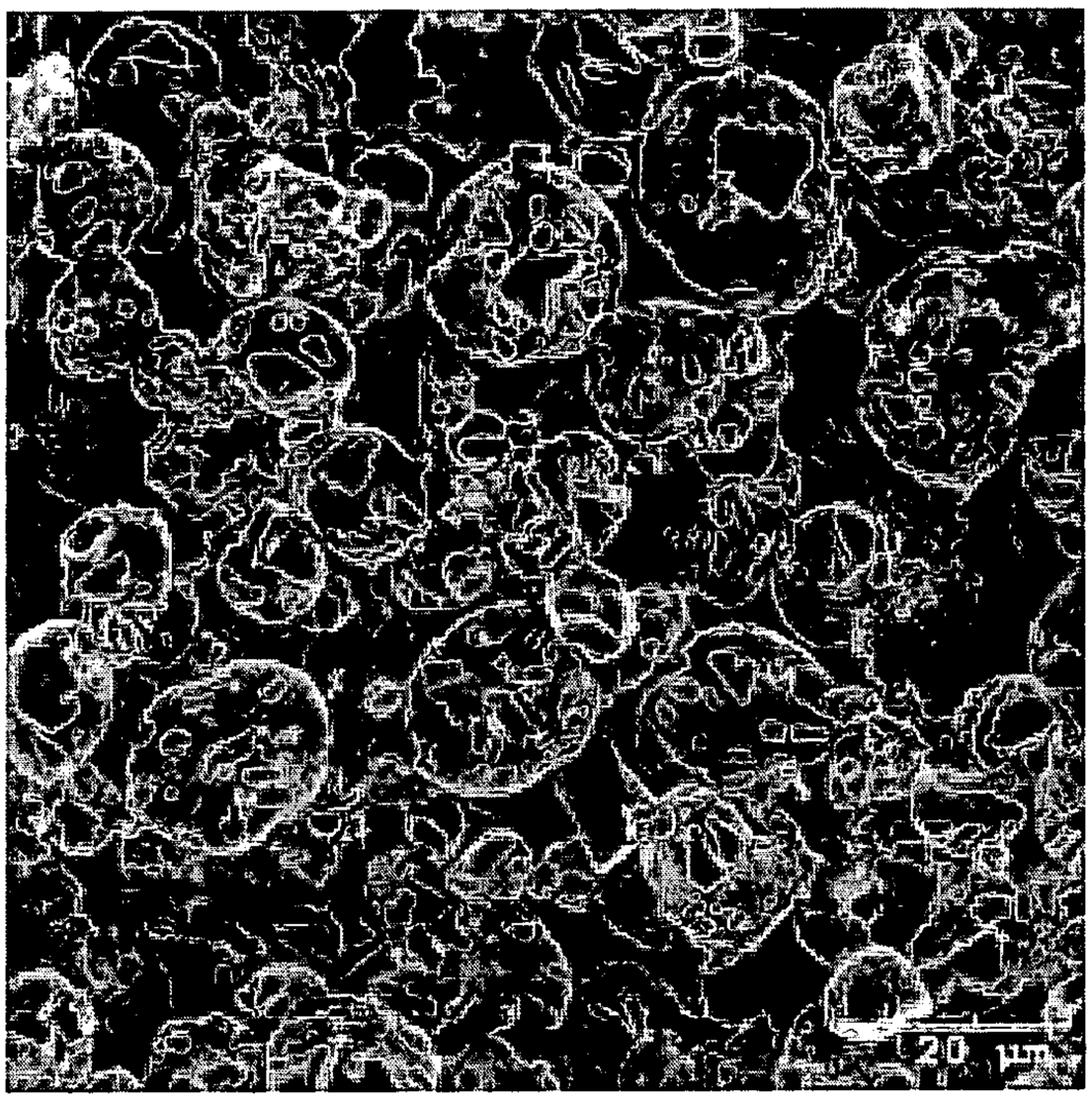

Representative SEM image of alternative porous particles. Addition of N-hexane to the initial dispersion resulted in formation of porous particles. Approximate size of these particles is 10-25 μm.

FIG. 35

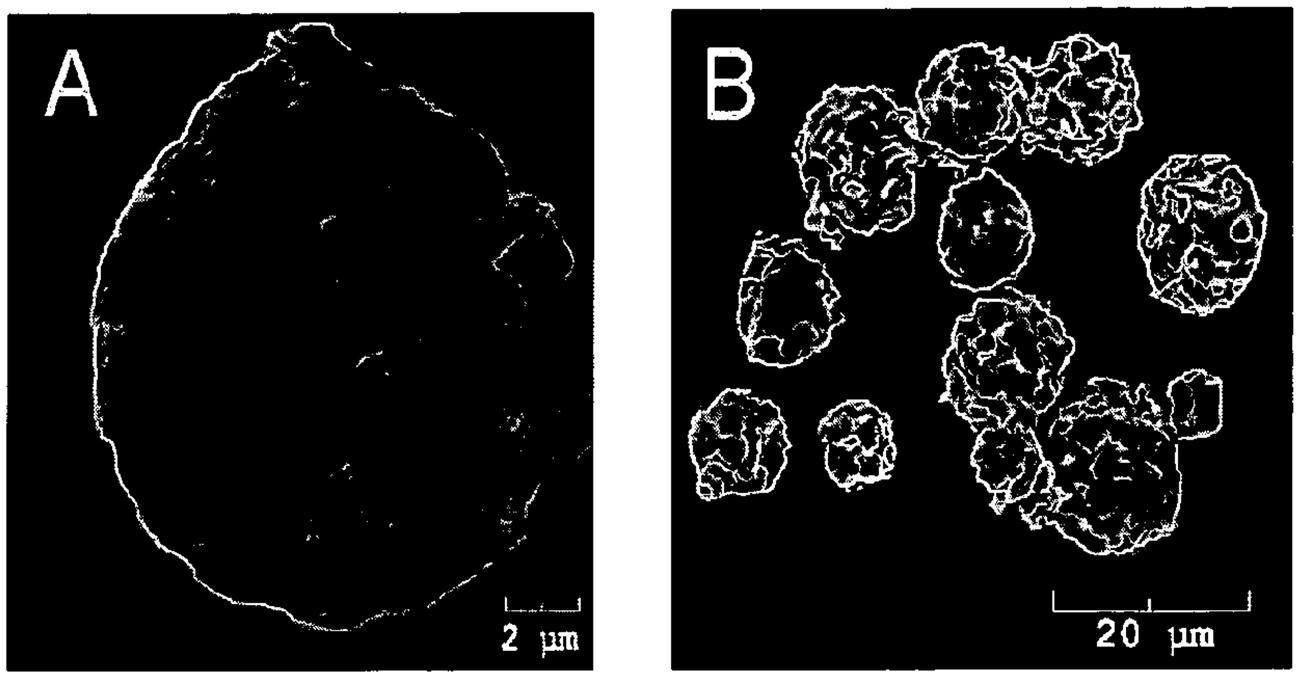

SEM Images of SOD-PKNs
(A) 6000X magnification
(B) 1000X magnification

FIG. 36

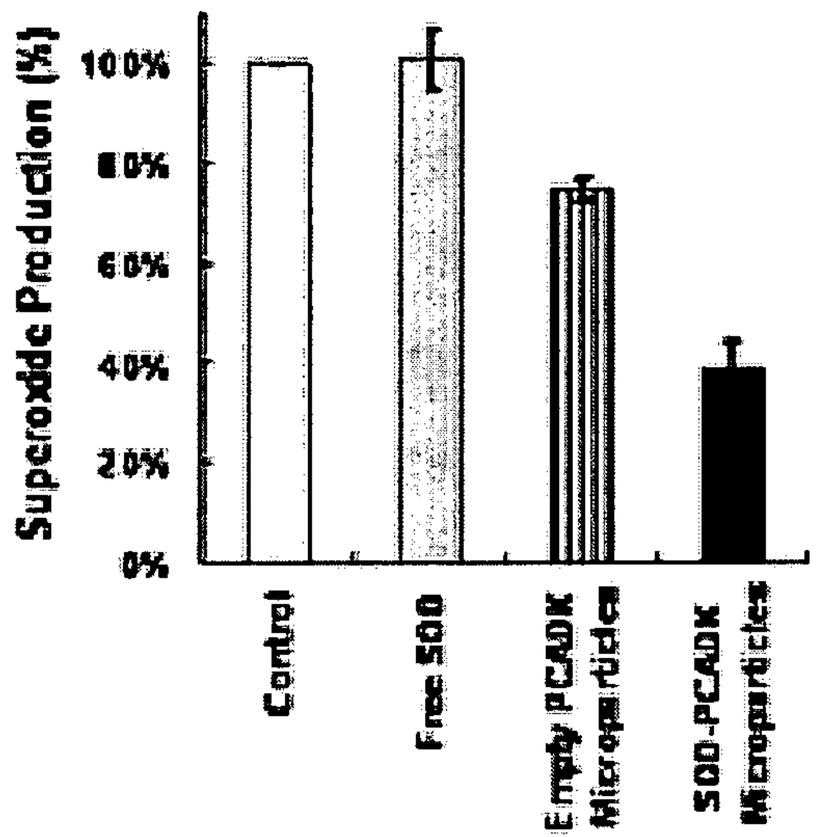

Grouped data from Cultured macrophages pretreated with PK-SOD and stimulated with LPS.

Pretreatment of macrophages with SOD-loaded polyketals resulted in a significant decrease in LPS-stimulated superoxide release as compared to empty PK and free SOD.

FIG. 37

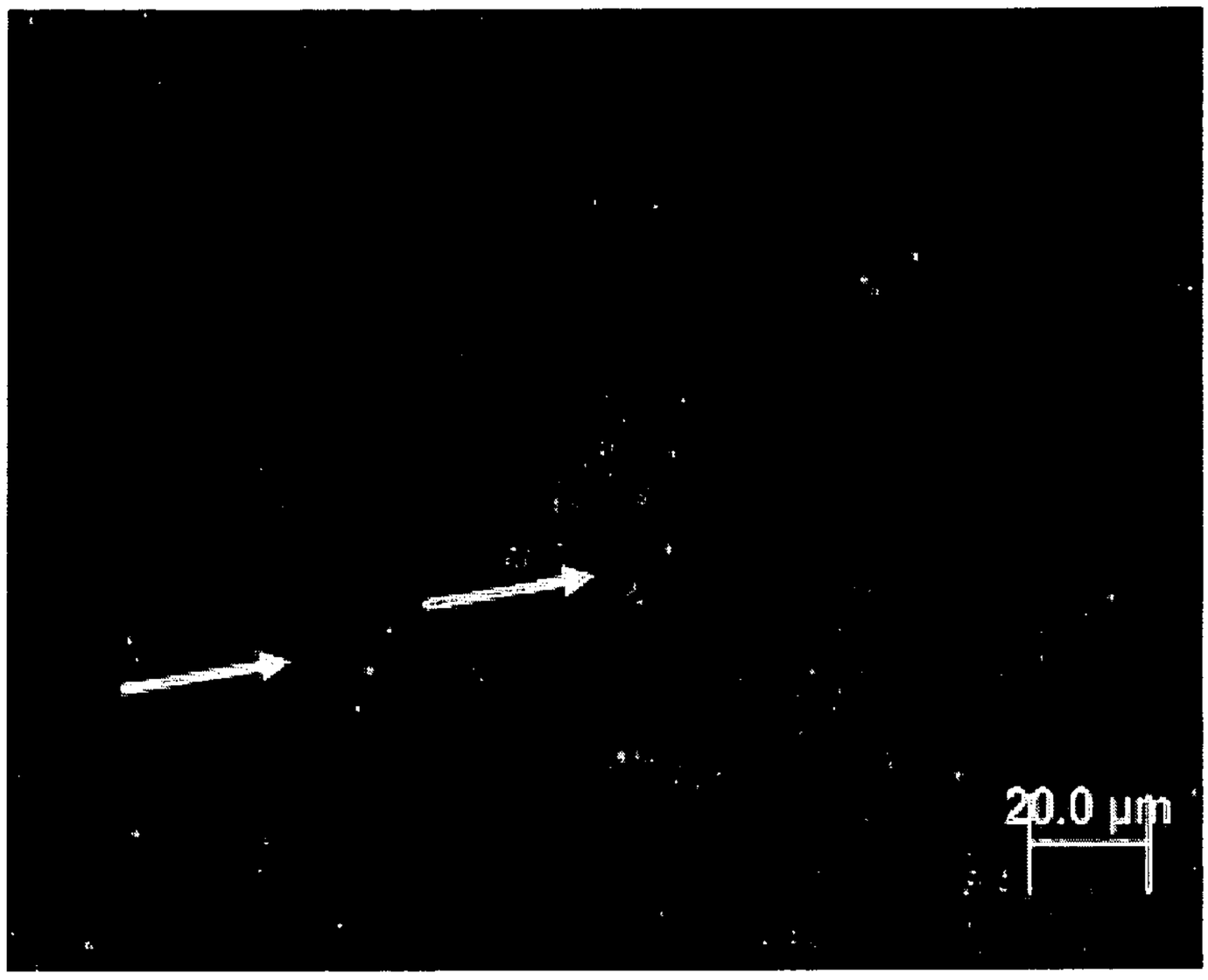

Representative fluorescent image of FITC-loaded polyketals incubated with cultured macrophages. Macrophages were incubated with PK-FITC for 2 hours prior to extensive washing and imaging. Arrows denote cells that have taken up FITC dye. Empty particles can also be seen bound to the surface of macrophages.

FIG. 38

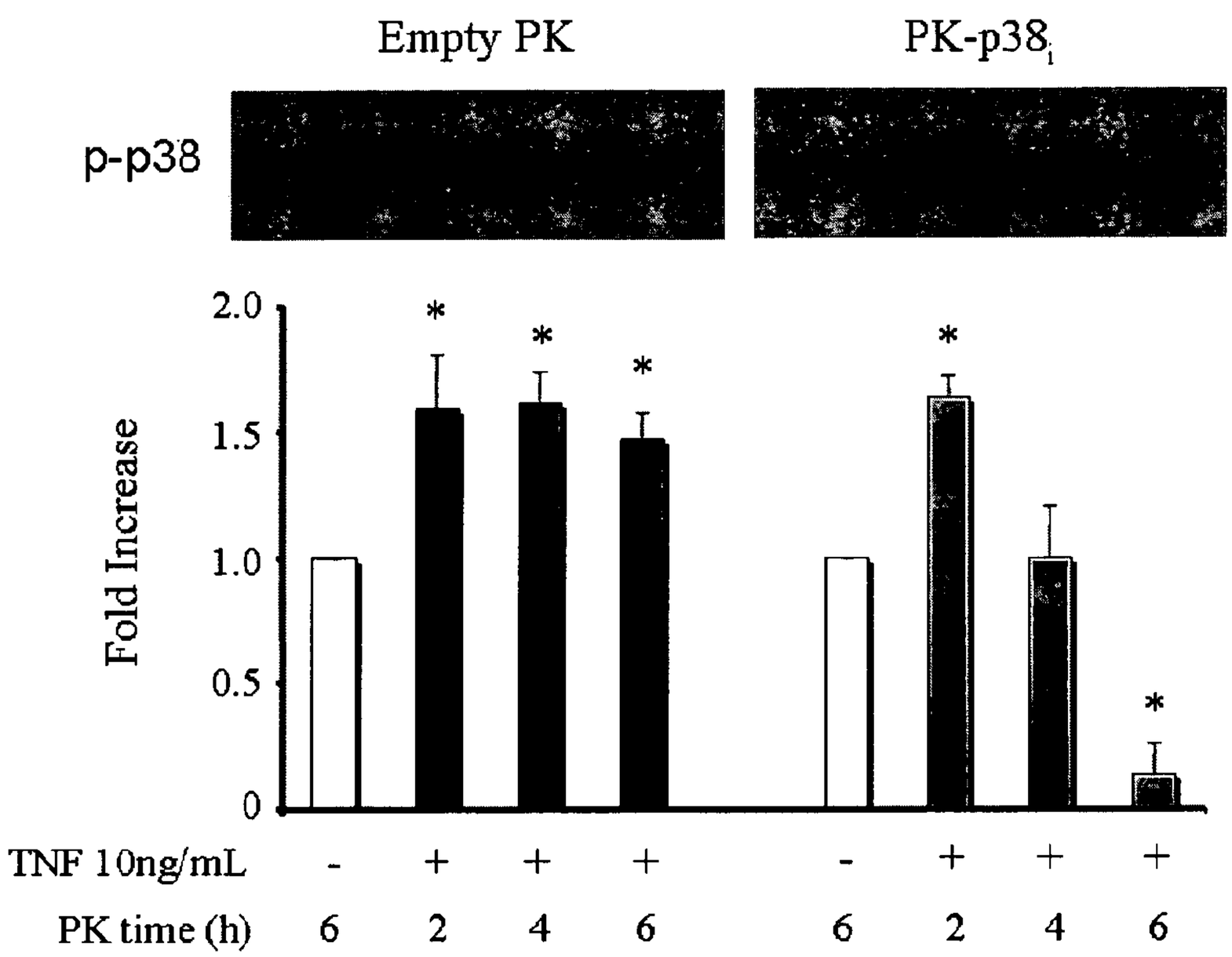
Empty PK
PK-p38i
p-p38
Fold Increase
2.0
1.5
1.0
0.5
0
*
TNF 10ng/mL - + + + - + + +
PK time (h) 6 2 4 6 6 2 4 6

FIG. 39

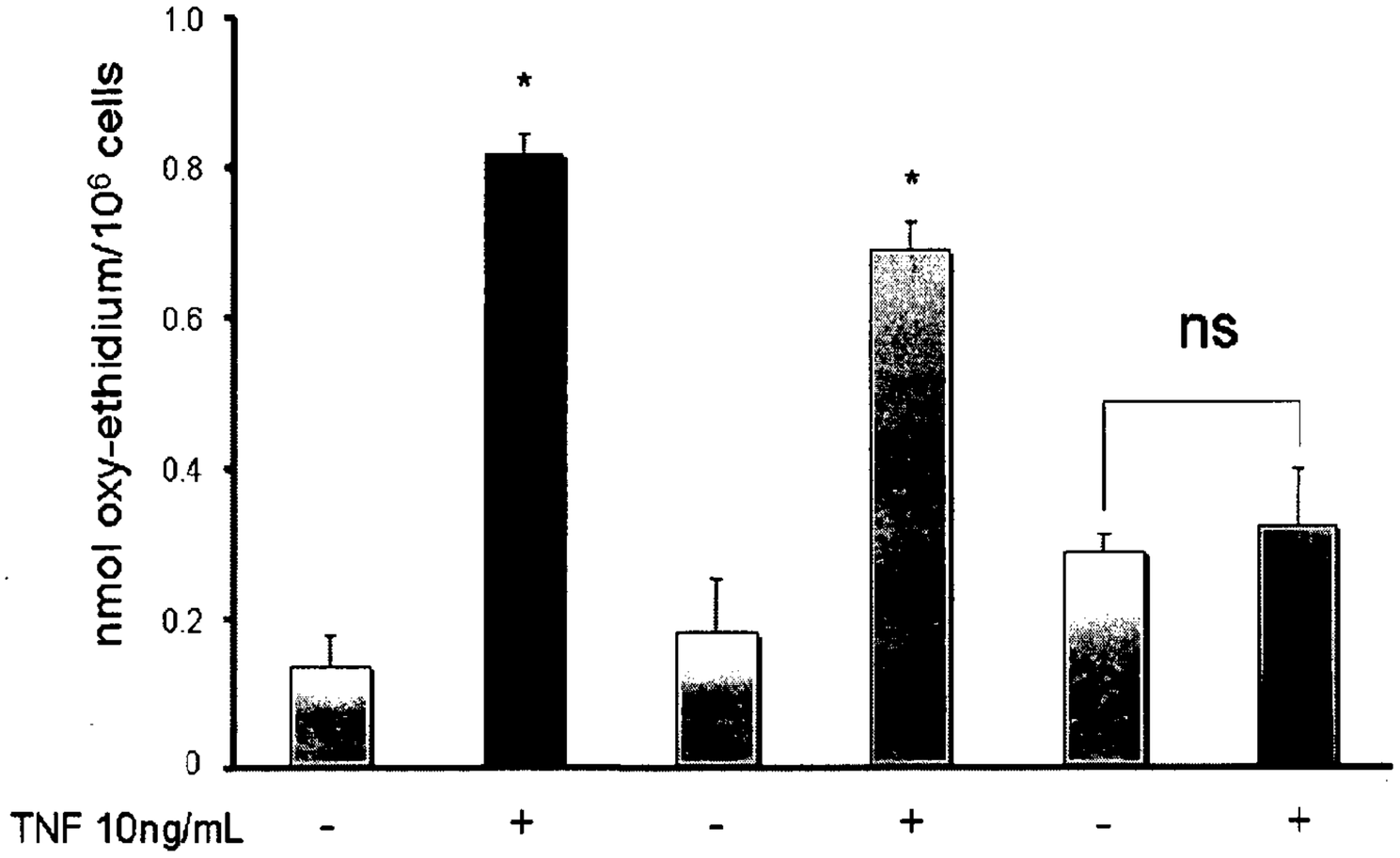

Grouped data from macrophages pretreated with polyketals for 6 hours, stimulated with 10 ng/mL TNF-α for 20 minutes and dihydroethidium for 20 mins. HPLC data demonstrating a significant increase in extracellular superoxide release by TNF-a treatment. This increase was not blocked by empty PK but completely inhibited by PK-$p38_i$ pretreatment (*$p < 0.05$ ANOVA followed by Tukey-Kramer.

FIG. 40

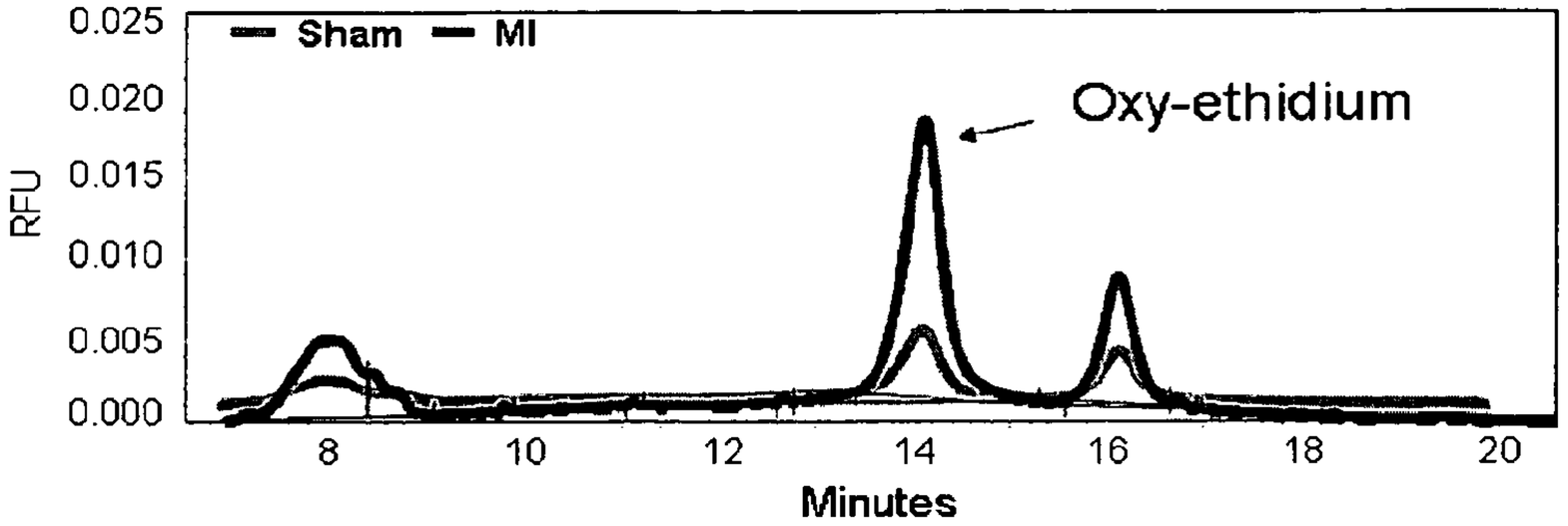
Sham
MI
Oxy-ethidium
RFU
0.025
0.020
0.015
0.010
0.005
0.000
8
10
12
14
16
18
20
Minutes


nM oxy-ethidium/mg tissue
12
10
8
6
4
2
0
Sham
MI

FIG. 41

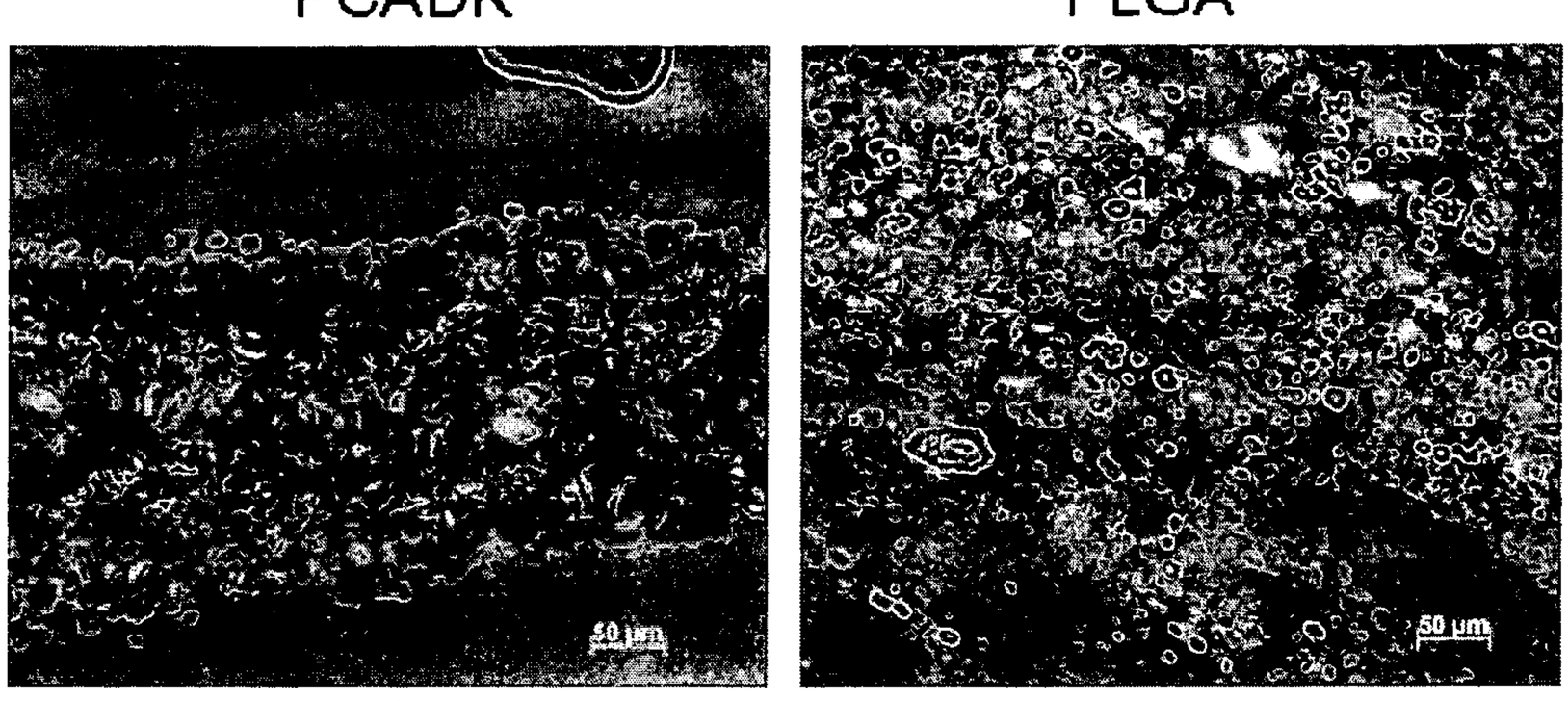

Representative H&E Stain of leg muscle 3 days following injection. In the left panel, PCADK injected forms a defined injection area with little cellular staining outside the borders. PLGA (right) in contrast shows evidence of fibrosis and inflammatory cell population.

FIG. 42

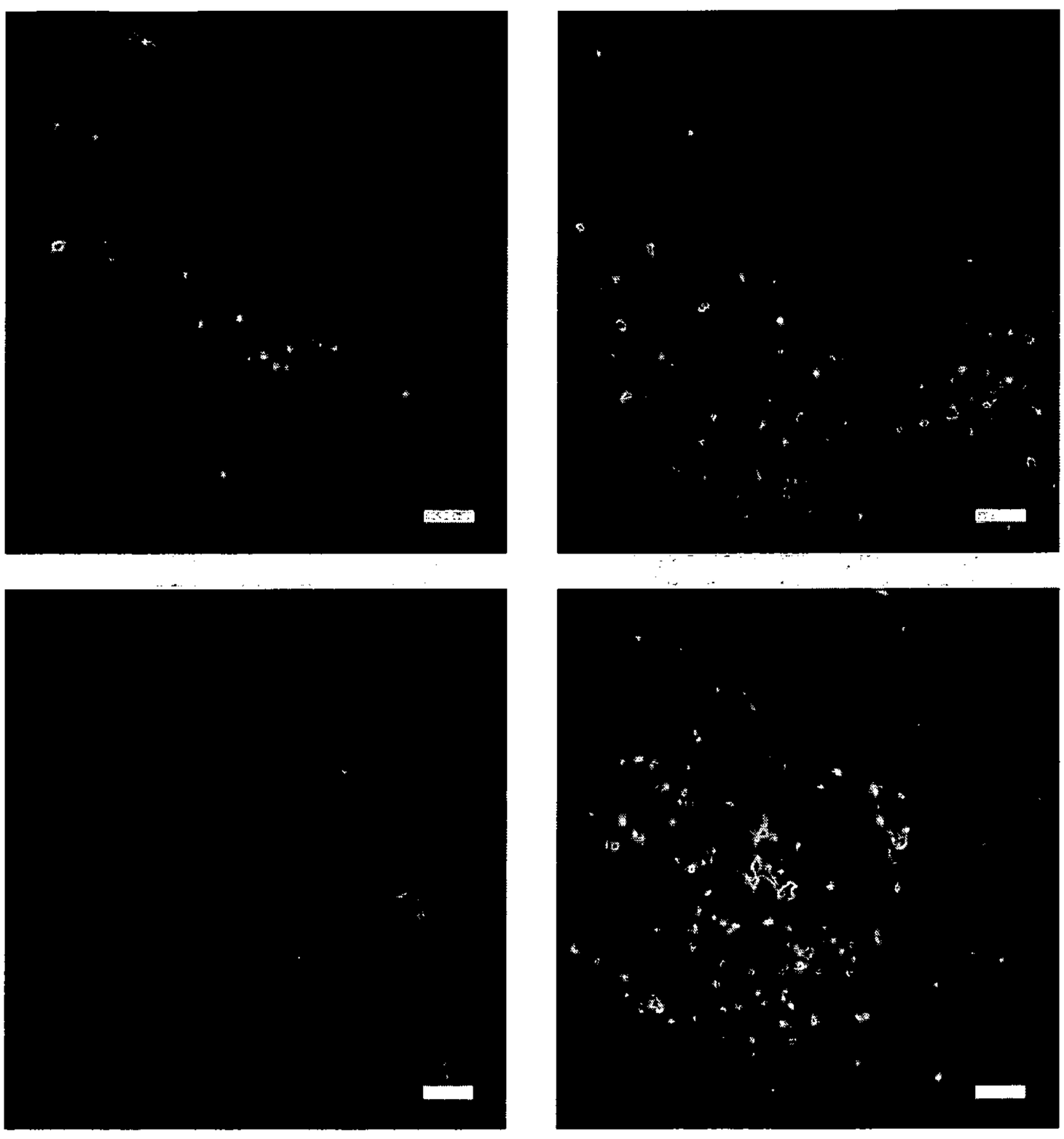

FIG. 43

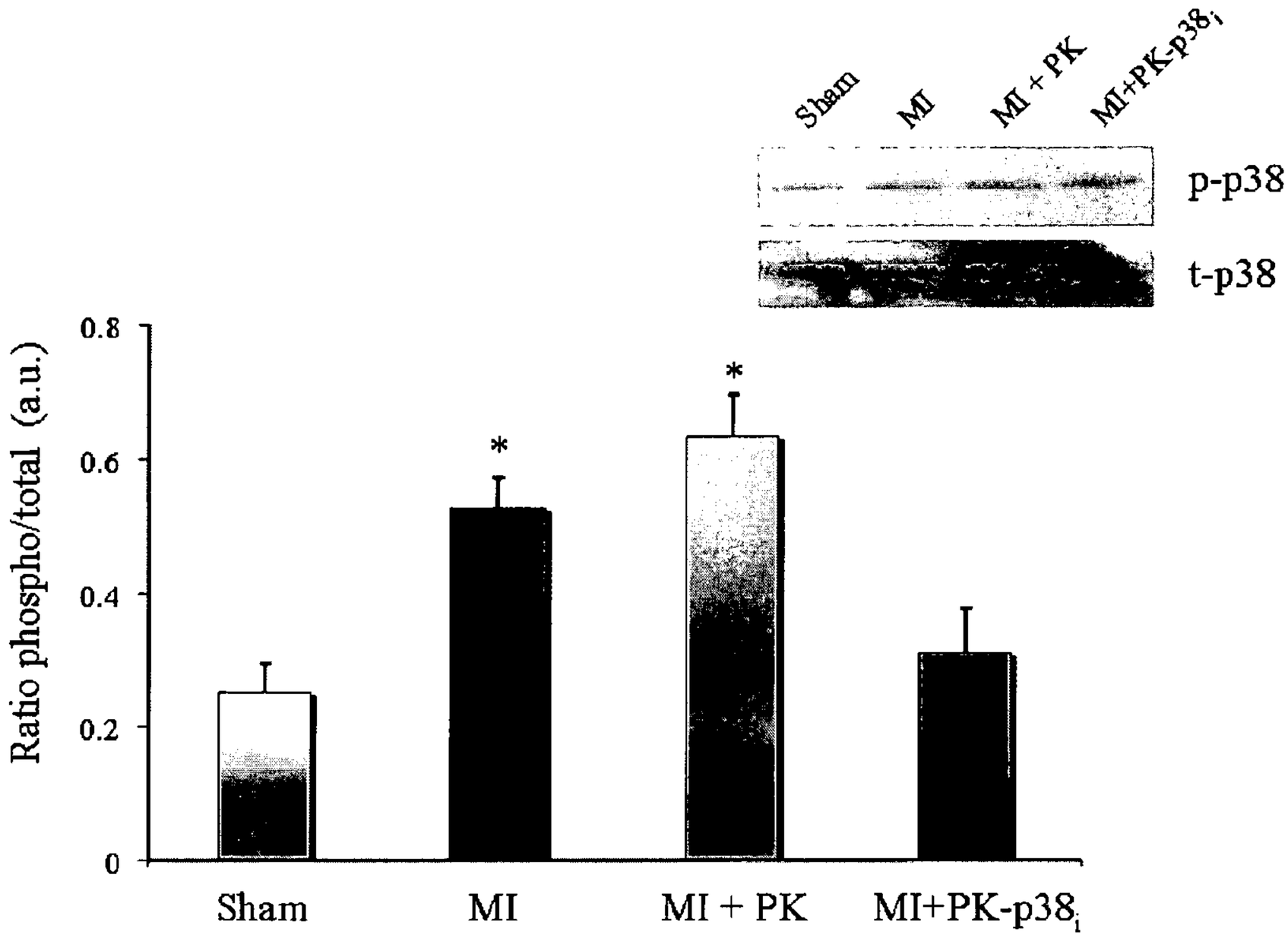
Sham
MI
MI + PK
MI+PK-p38i
p-p38
t-p38
Ratio phospho/total (a.u.)
0.8
0.6
0.4
0.2
0
*
*
Sham
MI
MI + PK
MI+PK-p38i

FIG. 44

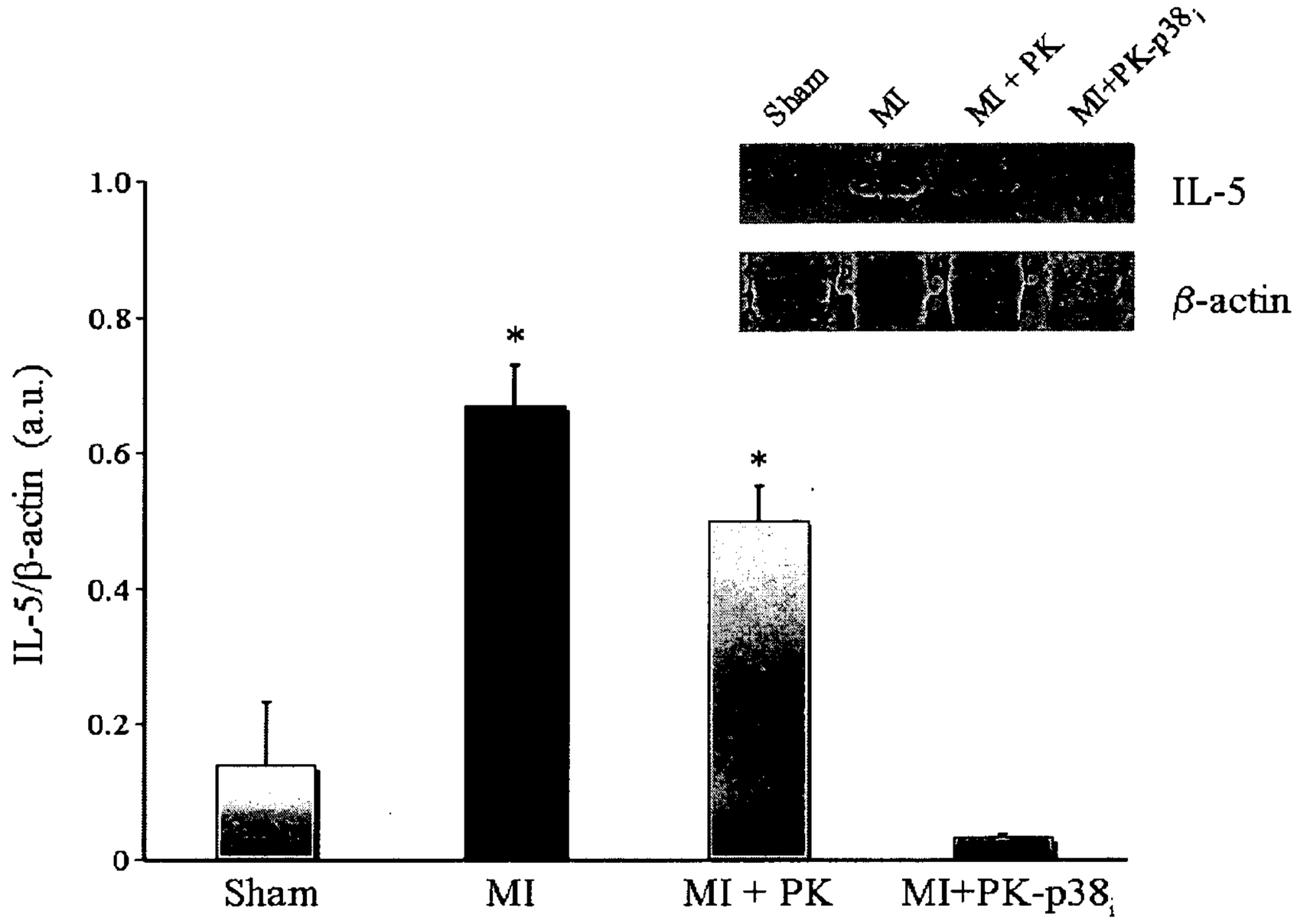
Sham
MI
MI + PK
MI+PK-p38i
IL-5
β-actin
IL-5/β-actin (a.u.)
1.0
0.8
0.6
0.4
0.2
0
*
*
Sham
MI
MI + PK
MI+PK-p38i

FIG. 45

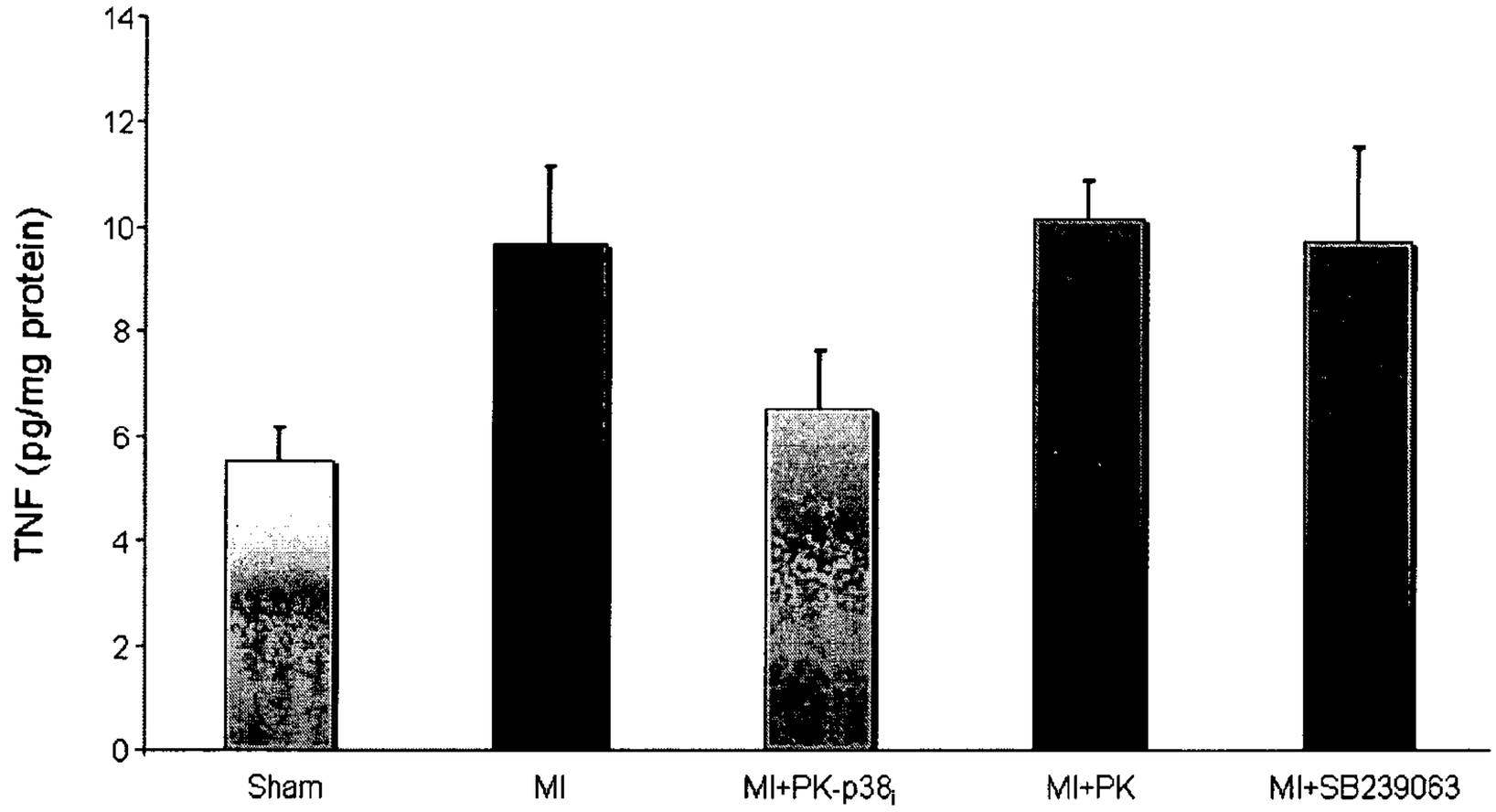
TNF (pg/mg protein)
0
2
4
6
8
10
12
14
Sham
MI
MI+PK-p38i
MI+PK
MI+SB239063

FIG. 46

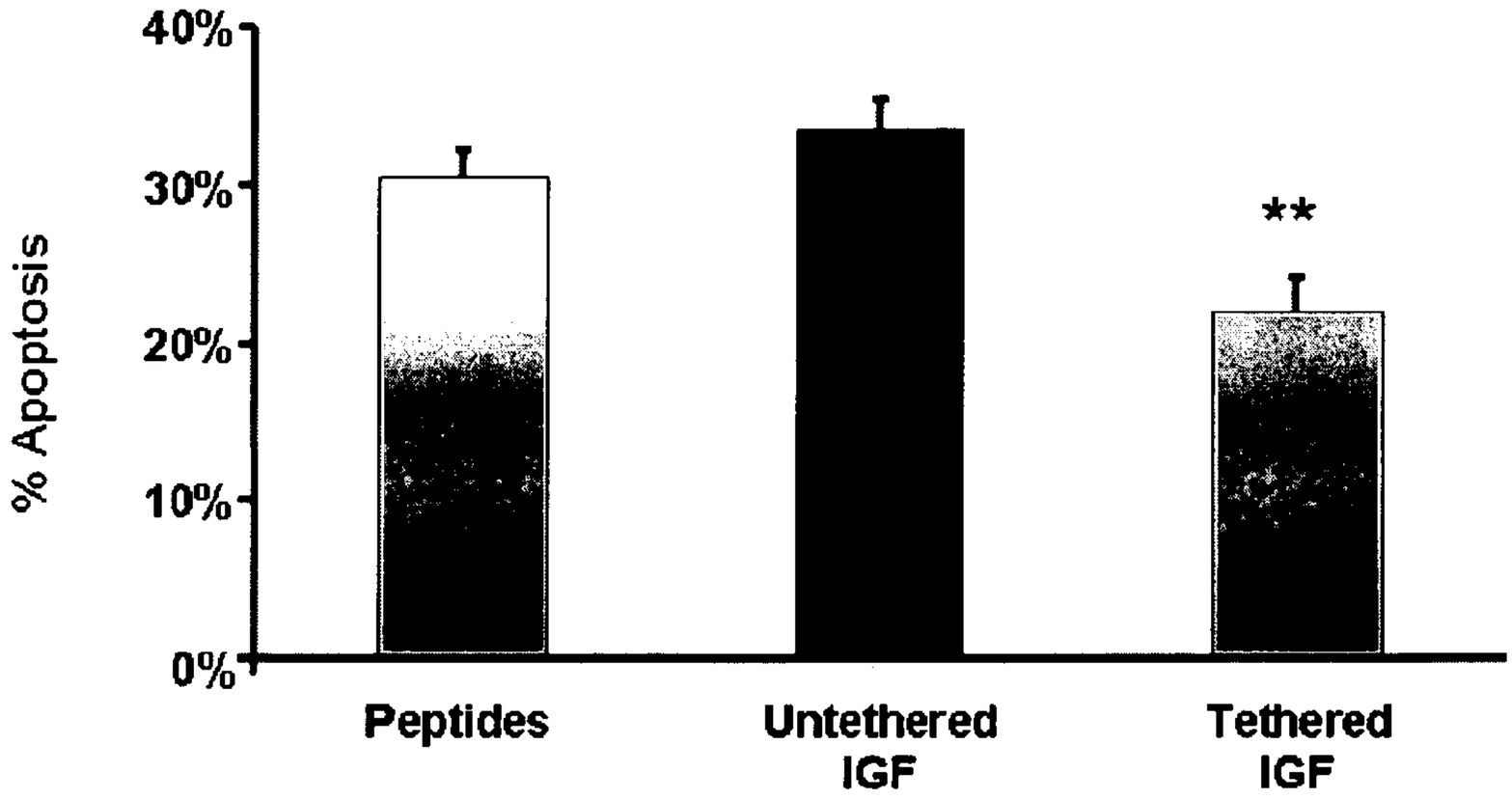

Implanted cell death reversed by sustained growth factor treatment. Neonatal cardiac myocytes were stained with a green membrane dye prior to injection, then stained for cleaved caspase-3 14 days following injection. Data are mean ± SEM from n≥4 animals per group (**p<0.01 vs. peptides alone or untethered IGF).

FIG. 47

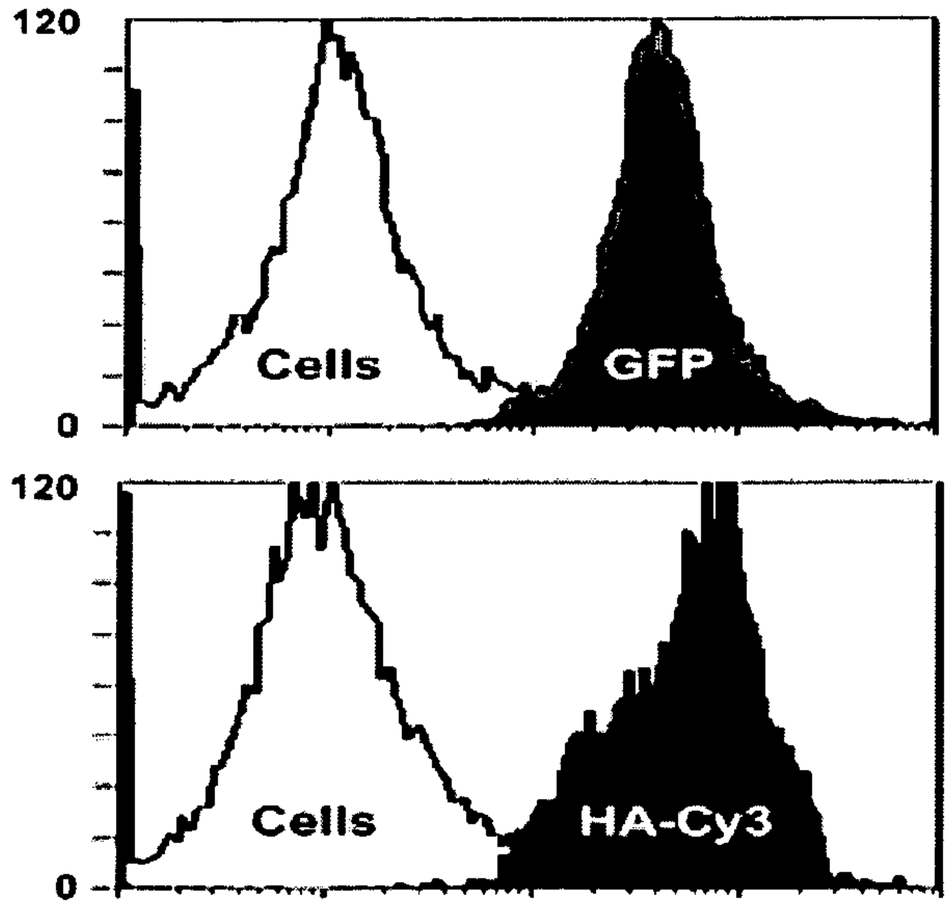

Tracking of cells
Using GFP and HA adenoviruses.
Cells were incubated in suspension with 100 MOI of GFP or hemagglutanin adenoviruses for 2 hours immediately following isolation. Cells were plated for 24 hours and flow cytometry was performed.

FIG. 48

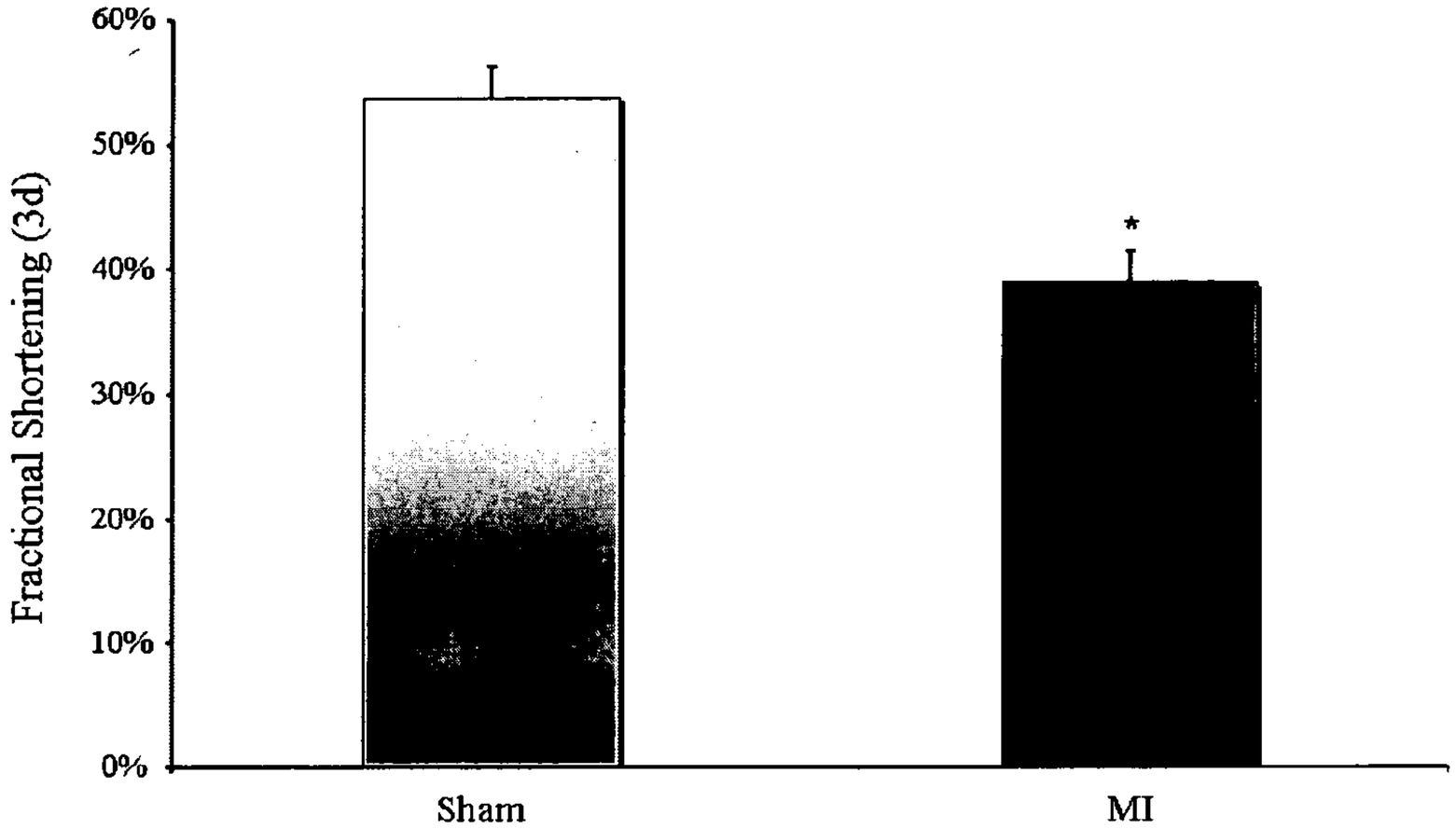

FIG. 49

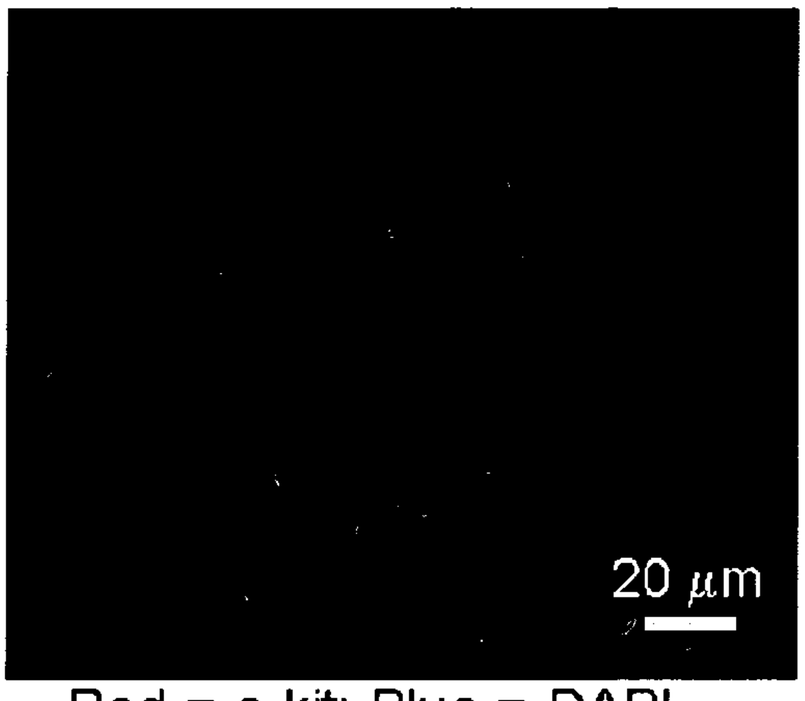

Red = c-kit; Blue = DAPI

Red = CD45; Blue = DAPI

Cardiac stem cell isolation. Cells were isolated as described, fixed in 4% paraformaldehyde and stained with antibodies against the indicated maker followed by a fluorescent secondary antibody.

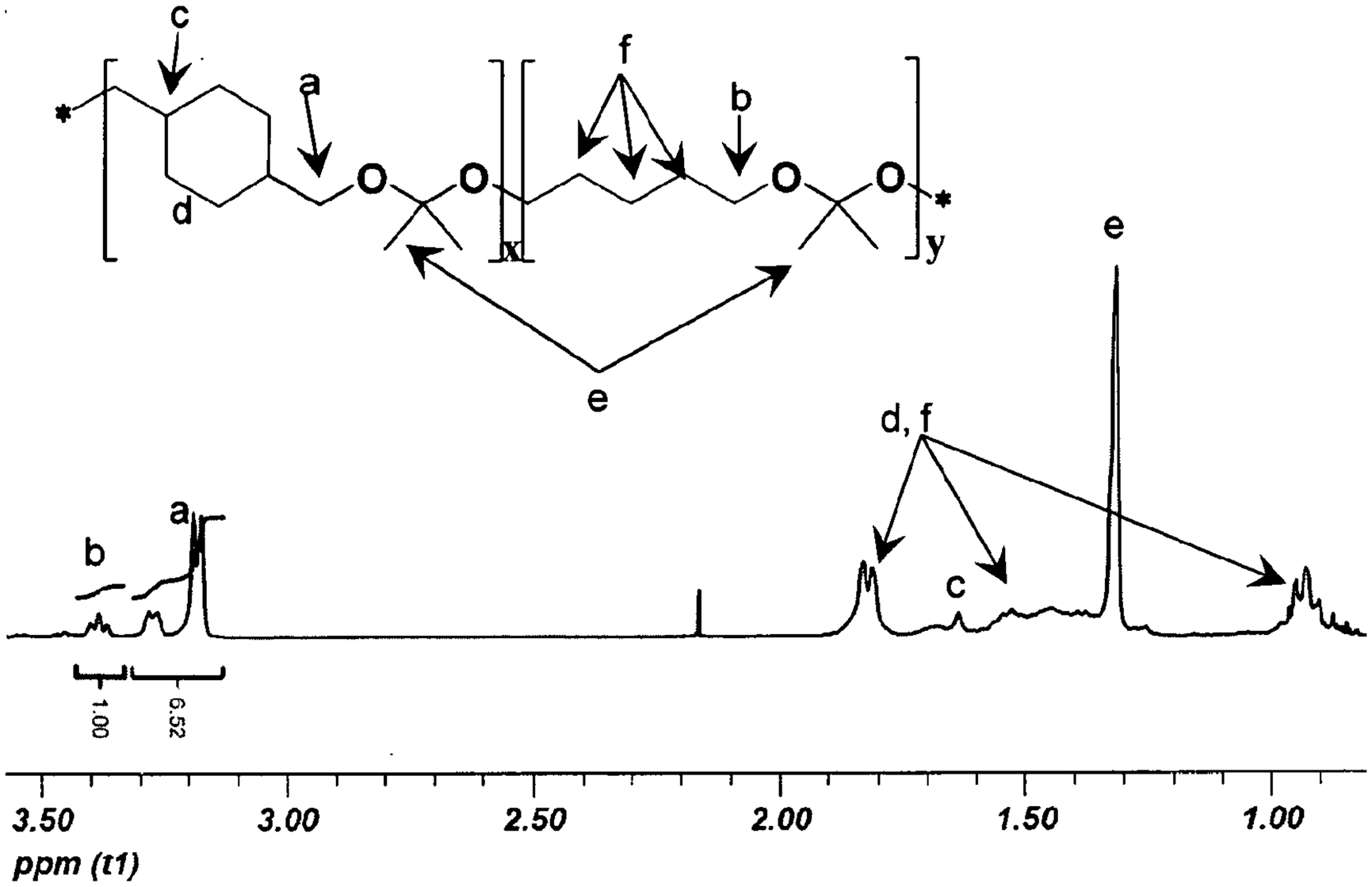

Figure 50. H-NMR spectrum of PK3.

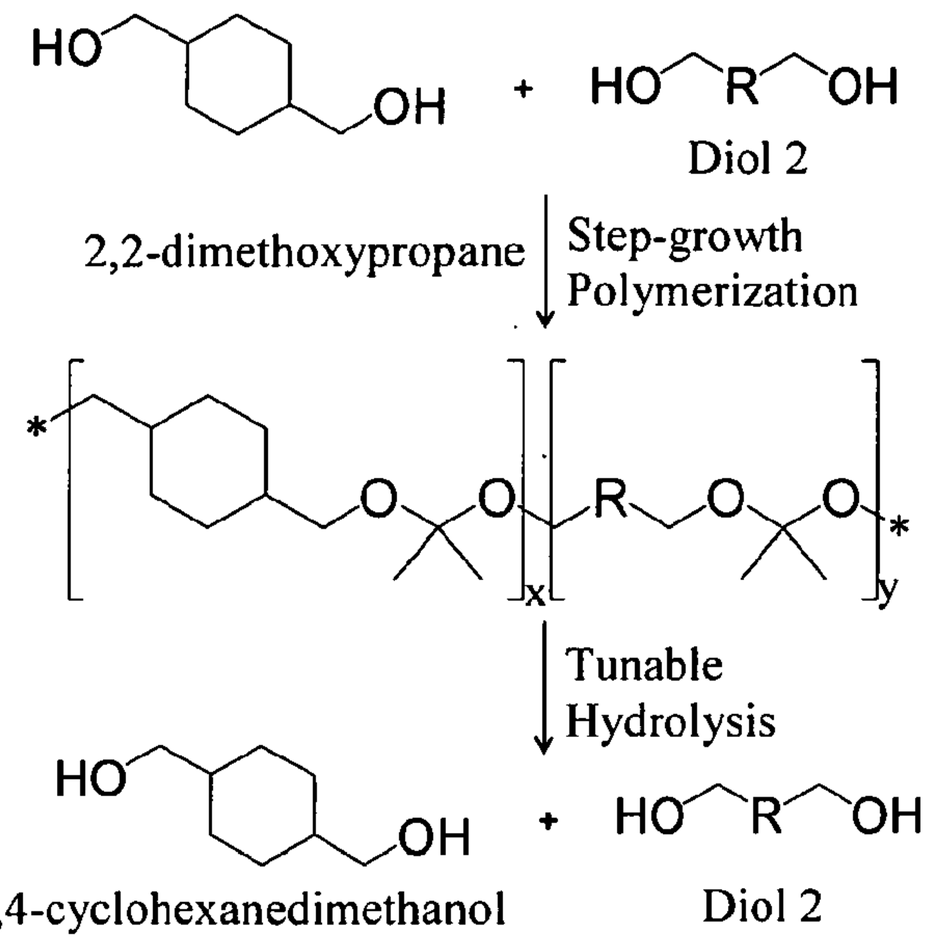

Figure 51 Synthesis of polyketal copolymers from 1,4-cyclohexanedimethanol, a second diol and 2,2-dimethoxypropane.

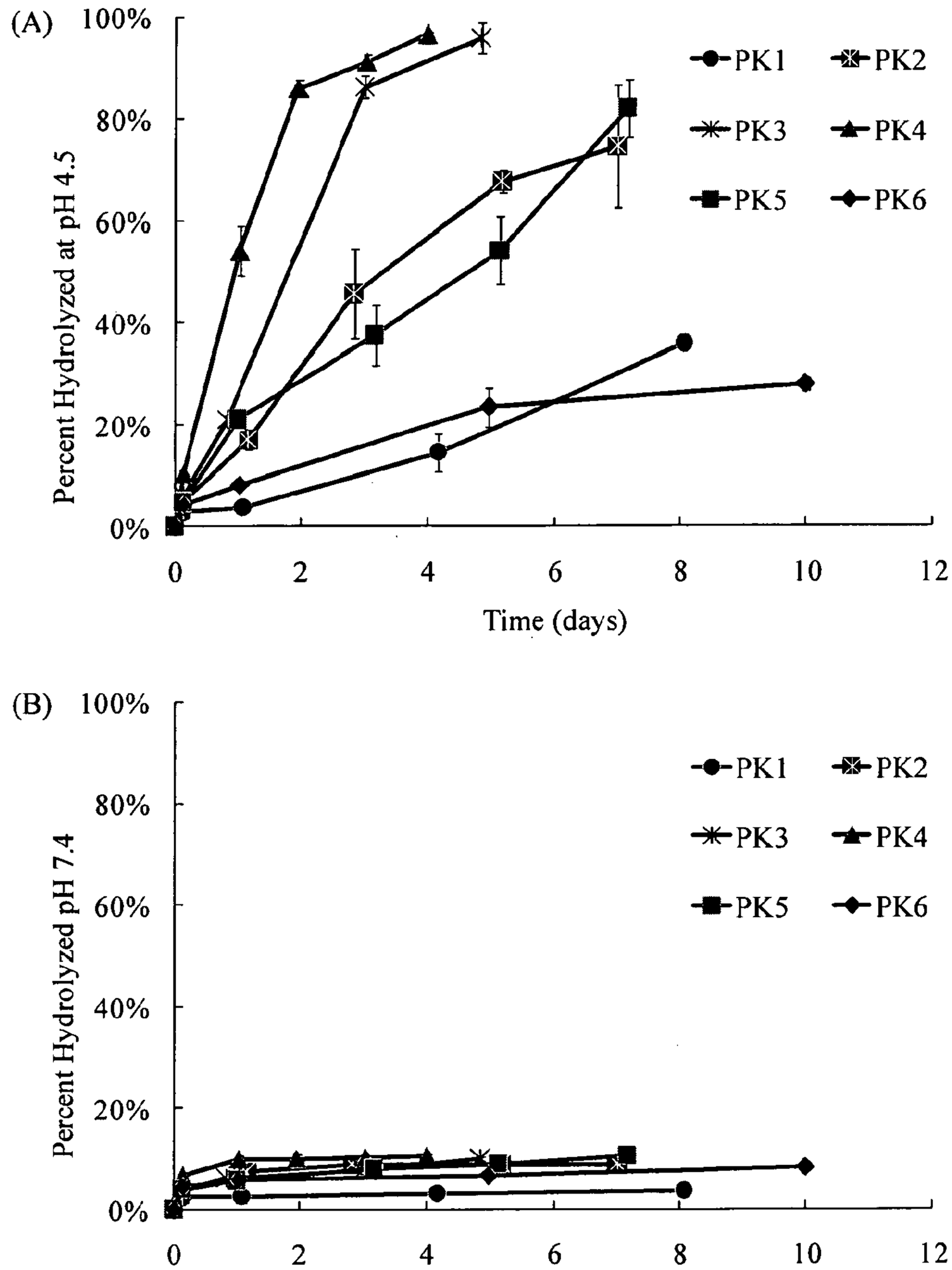

Figure 52. Hydrolysis kinetics of polyketals can be tuned by copolymerization. (A) Hydrolysis profiles of polyketal copolymers PK1 to PK6 in pH 4.5 buffer, and (B) hydrolysis profiles of PK1 to PK6 in pH 7.4 buffer.

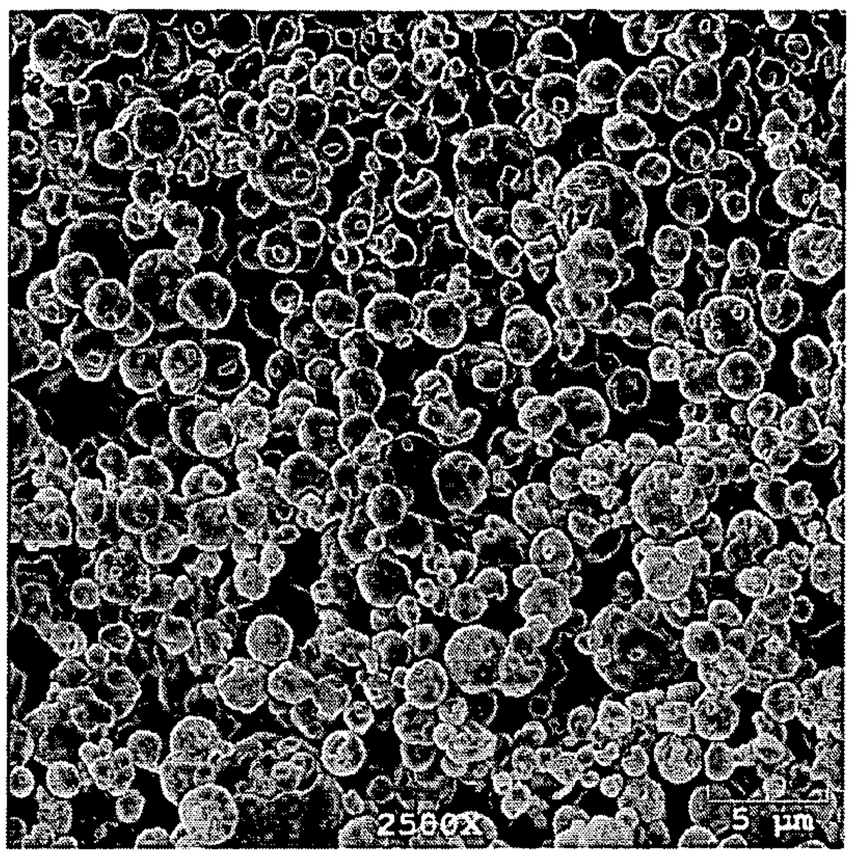

Figure 53. SEM images of particles formulated with PK3. SEM image of empty particles formulated via double emulsion procedures.

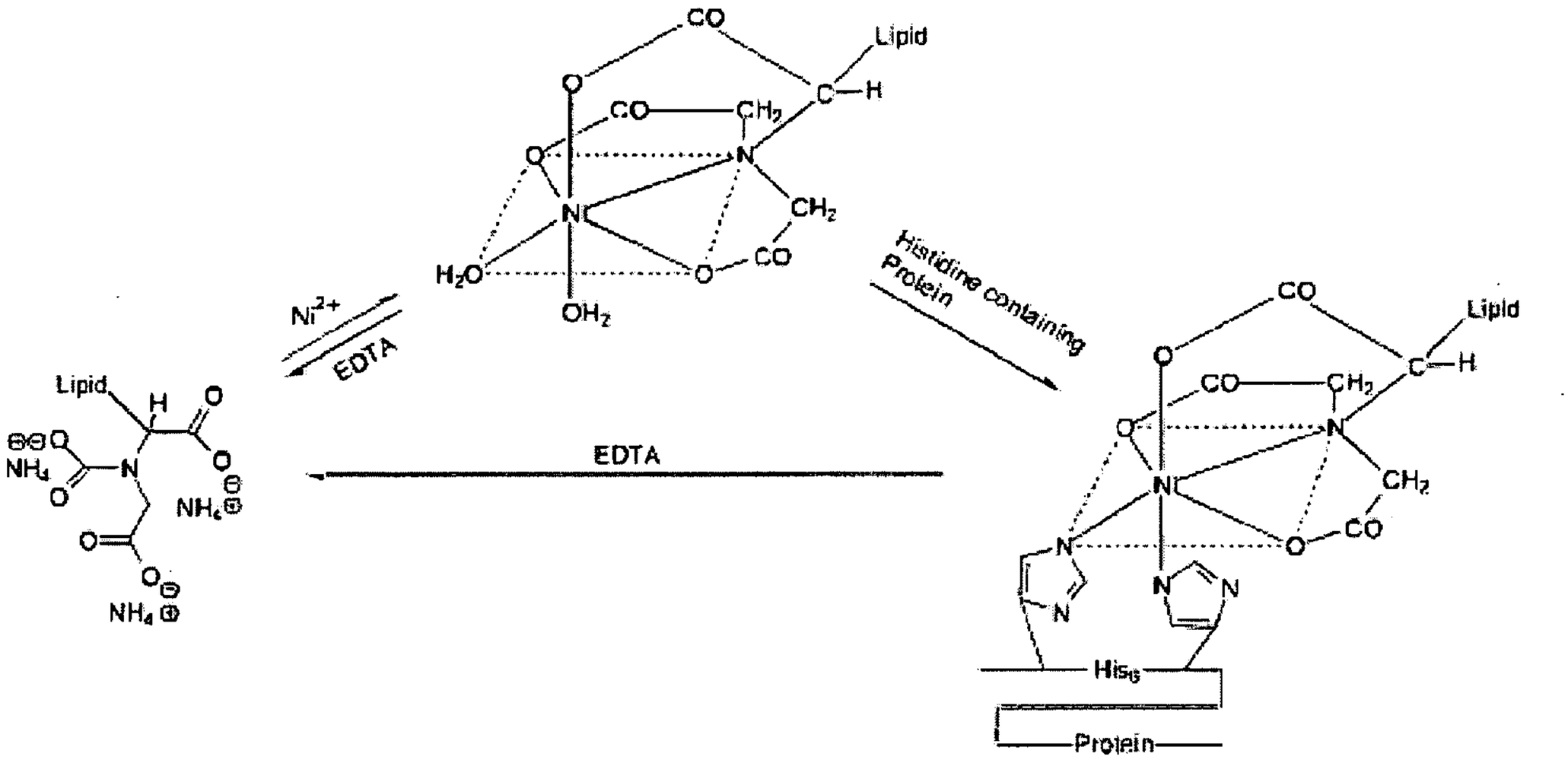
Lipid
CO
CH2
N
H2O
OH2
Ni2+
EDTA
Histidine containing Protein
EDTA
NH4
His6
Protein

Figure 54

A.

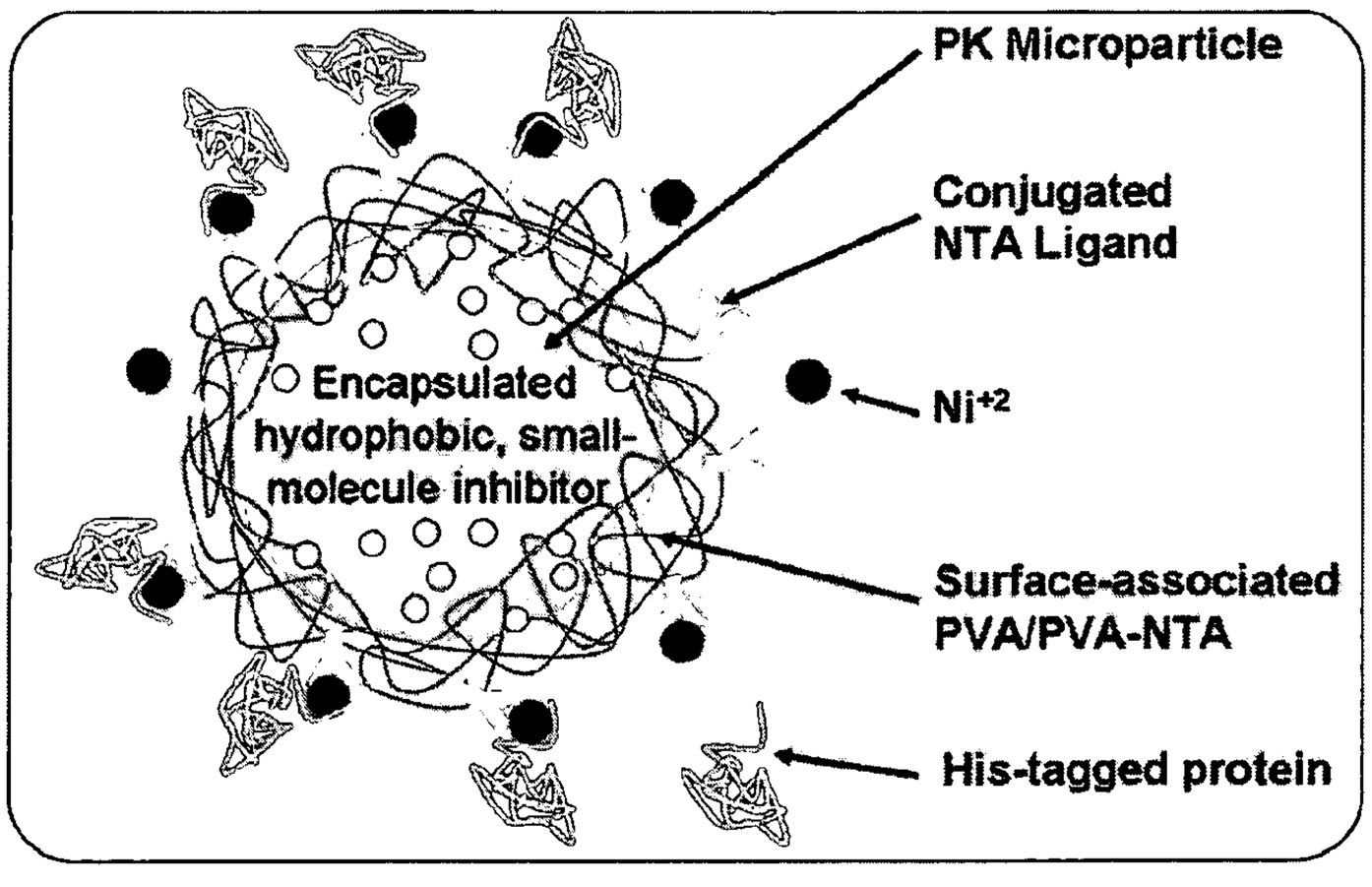

B.

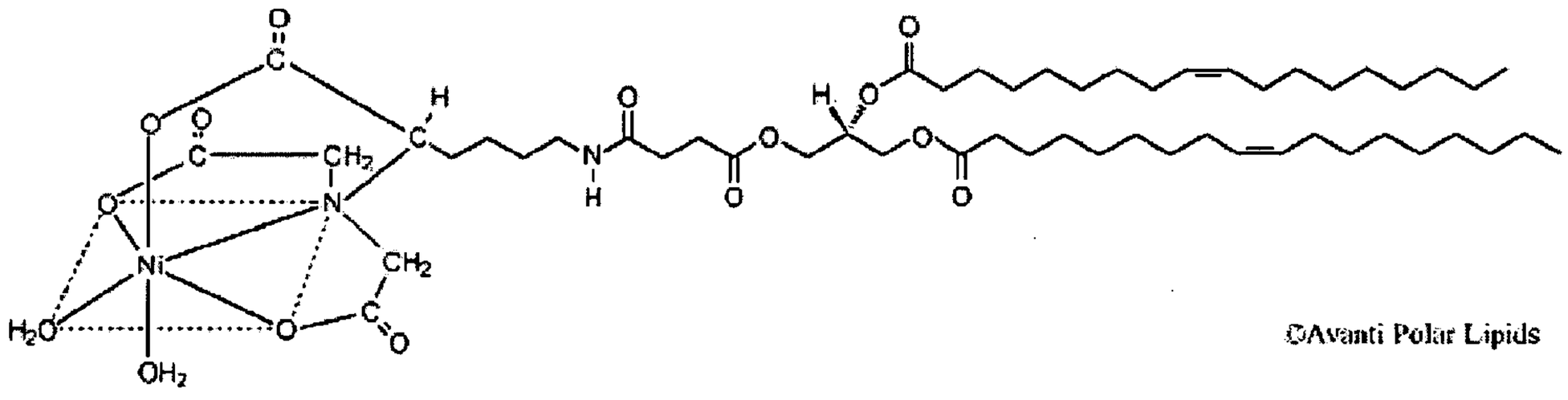

1,2-Dioleoyl-*sn*-Glycero-3-{[N(5-Amino-1-Carboxypentyl)iminodiAcetic Acid]Succinyl}

Figure 55.

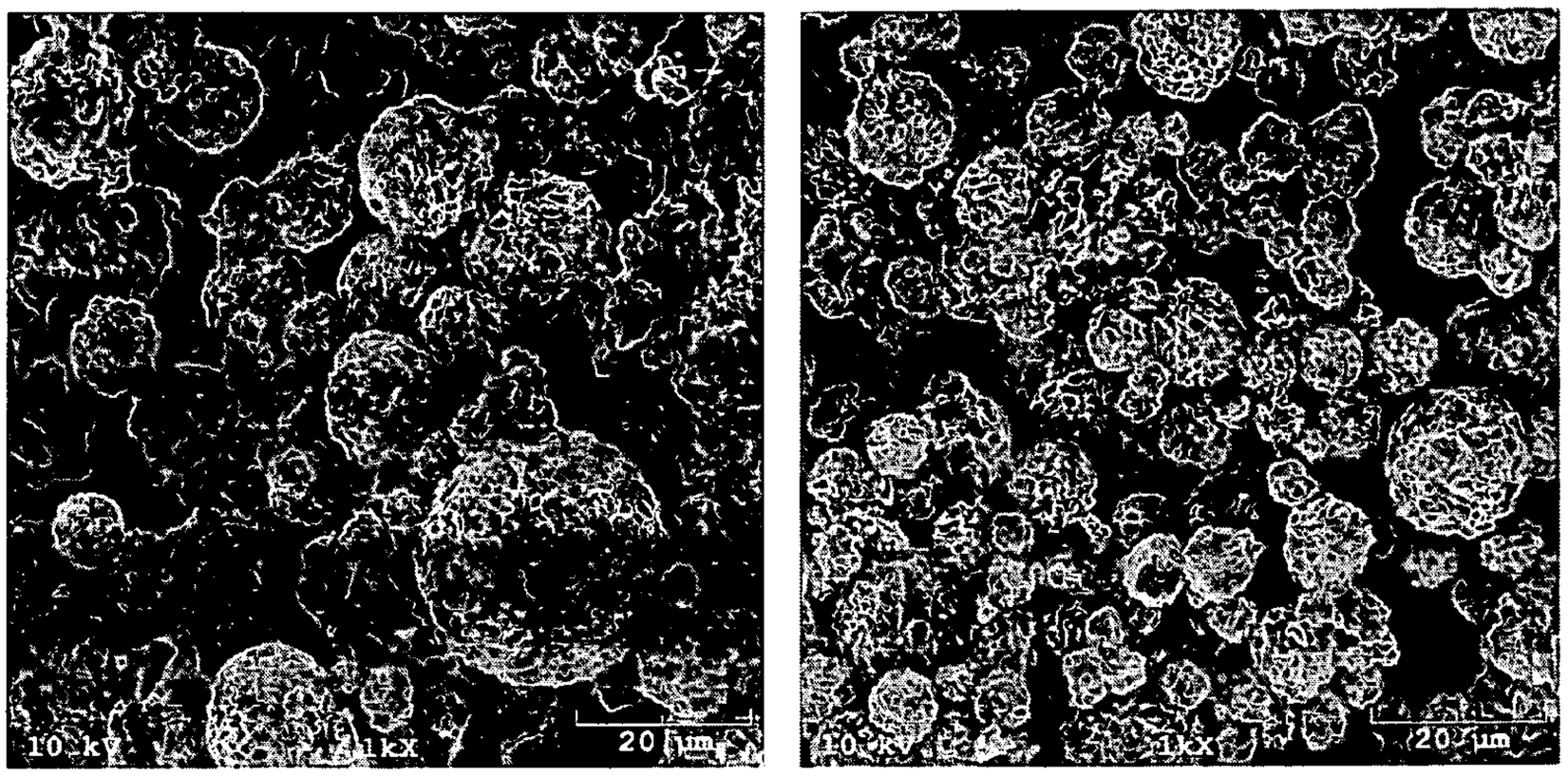

Figure 56. SEM micrographs of 10% NTA PCADK microparticles.

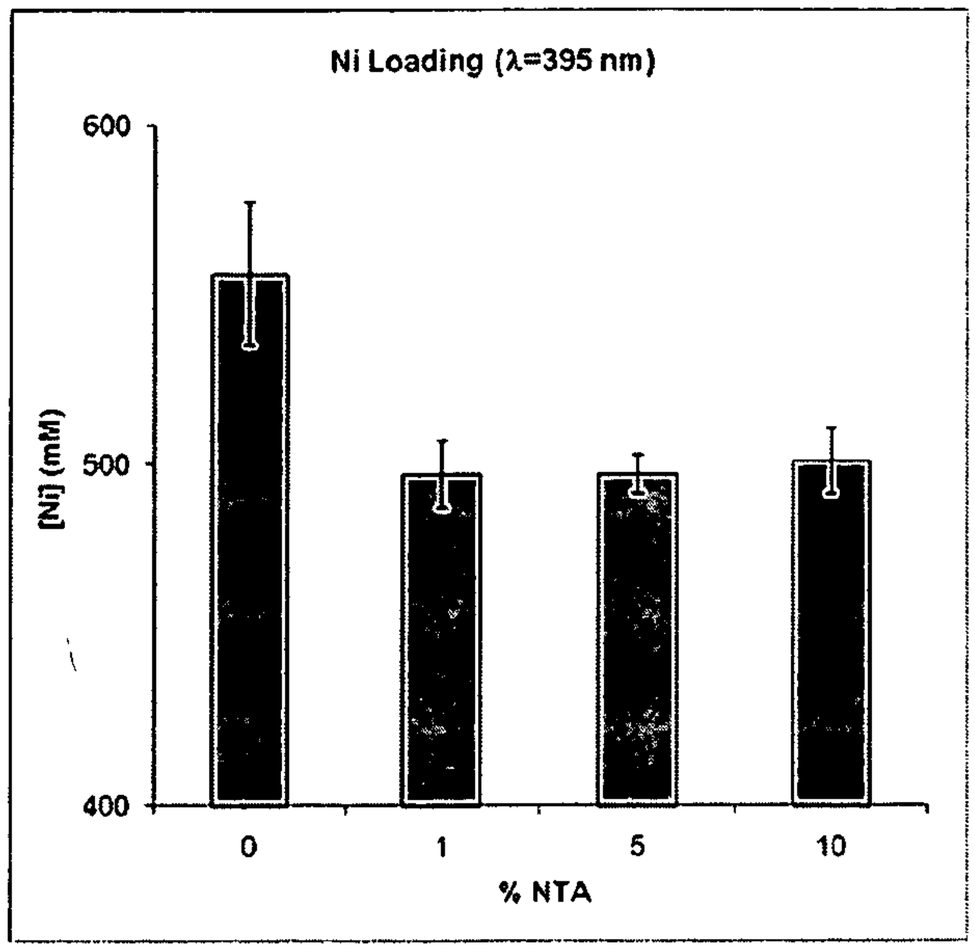

Figure 57. Spectrophotometric determination of Ni depletion in loading solution. PCADK particle with varying concentrations of NTA-ligand (0%, 1%, 5%, 10%) were loaded in $NiCl_2$ solution. After incubating the particles overnight with agitation, solutions were centrifuged and the supernatants analyzed for Ni content spectrophotometrically. The supernatant particles with no NTA-ligand had a nickel concentration of about 550 mM while 1%, 5%, and 10% NTA particles had approximately 500 mM Ni in their supernants. This data suggests that the surface of the particles is saturated with 1% NTA-ligand inclusion. Further quantative testing is currently underway using atomic absorption spectroscopy.

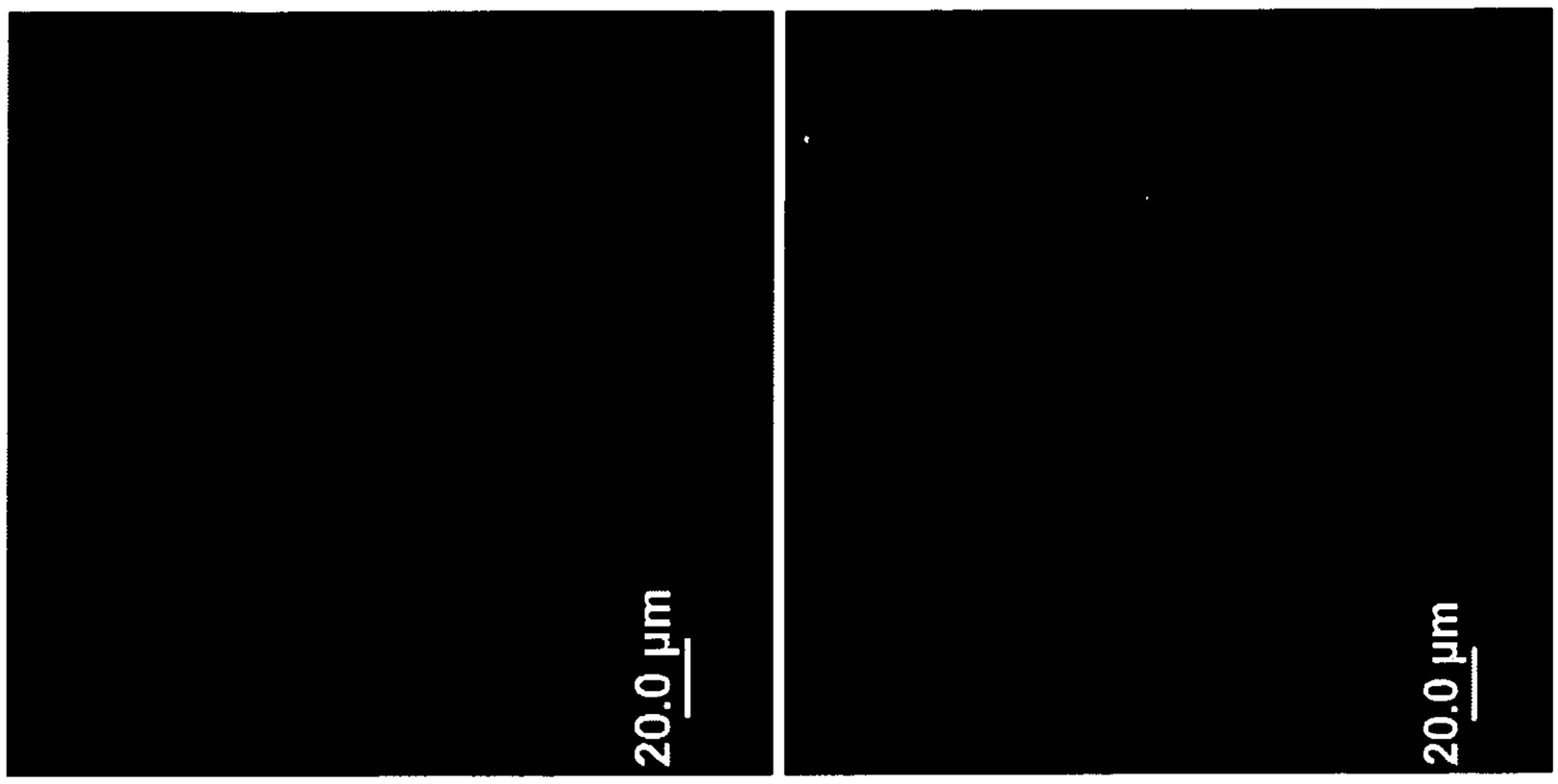

Figure 58. His-tagged Green Fluorescent Protein (GFP) is Ni dependent. 10% NTA particles were charged with Ni, washed extensively and then incubated in a 100 nM solution of His-tagged GFP. Particles were washed extensively with PBS and imaged using fluorescent microscopy. (a) PCADK-NTA particles were loaded in PBS instead of $NiCl_2$. Very little fluorescence from GFP is seen. (b) PCADK-NTA particles loaded with $NiCl_2$ show extensive association with GFP.

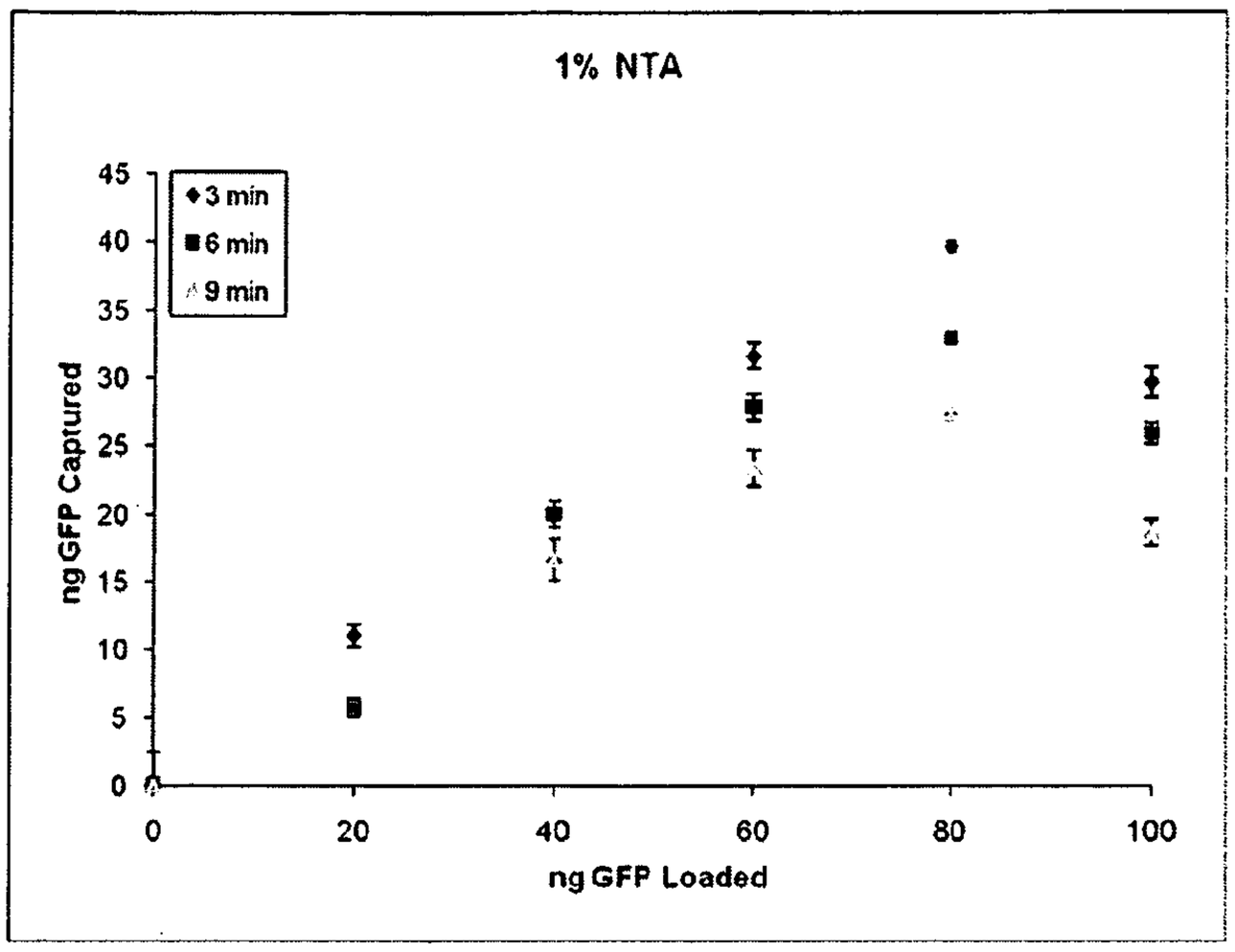

Figure 59. Specific Binding curve for 1% NTA-PCADK particles (On-particle ELISA). 1% NTA-PCADK particles were charged with Ni and loaded with varying concentrations of His-tagged GFP. After extensive washing after GFP loading, horseradish peroxidase (HRP) conjugated GFP antibody (α-GFP Ab) was incubated with the particles (particles suspended at 1 mg particles/ml of PBS-T with a 1:5000 dilution of α-GFP Ab and 1% goat serum) for 2 h at room temperature. Particles were then washed with 3 volumes of PBS-T. Colorimetric determination of HRP activity was done on a plate reader with different amounts of particle per well. 1-step Slow TMB-ELISA substrate (3,3',5,5'-tetramethylbenzidene, Pierce) was used at a substrate and absorbances measured at 370 nm. Readings from 3, 6, and 9 min were compared and shown above. Specific binding curve suggests that 1% NTA particles saturate with GFP when loaded with 60 ng GFP/mg particle.

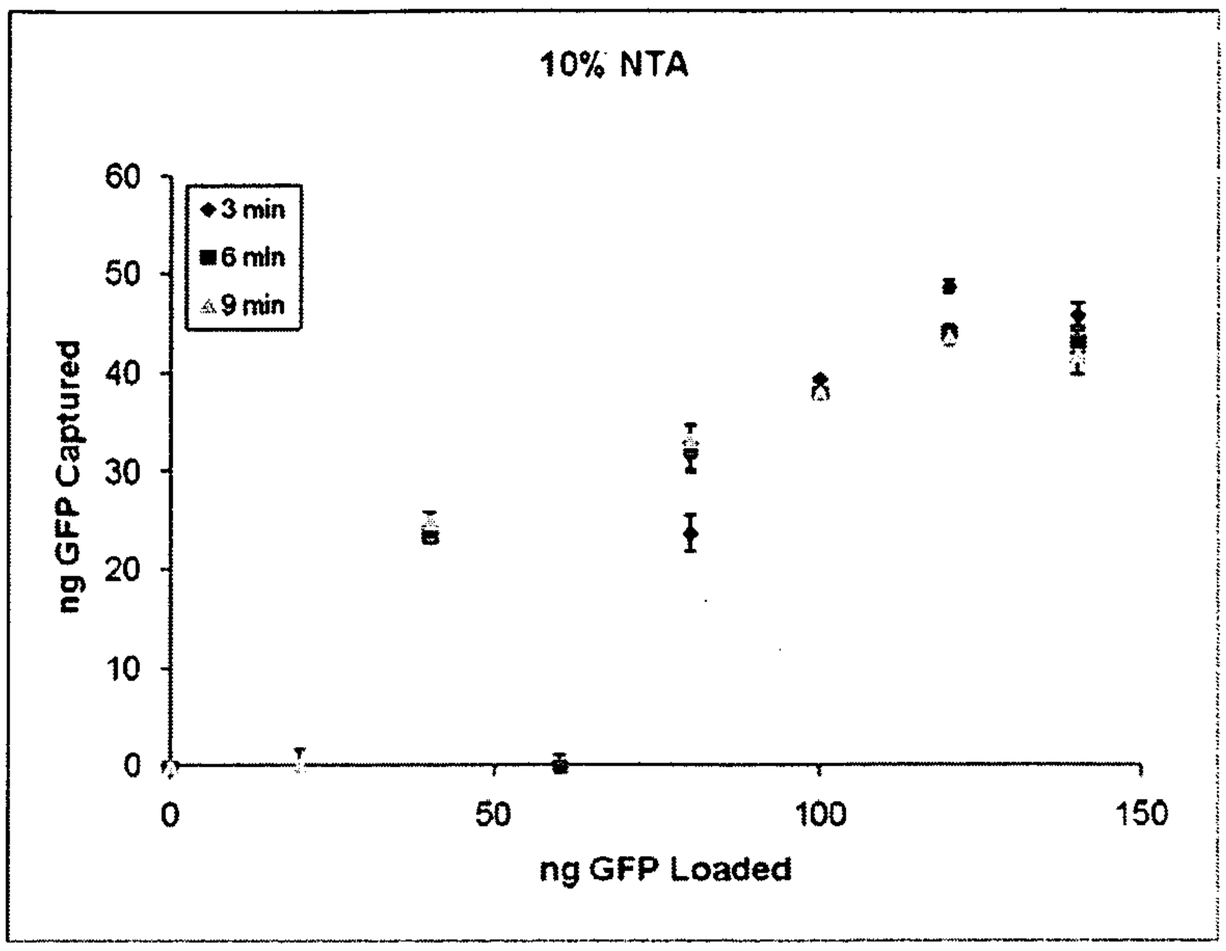

Figure 60. Specific Binding curve for 10% NTA-PCADK particles (On-particle ELISA). 10% NTA-PCADK particles were charged with Ni and loaded with varying concentrations of His-tagged GFP. After extensive washing after GFP loading, horseradish peroxidase (HRP) conjugated GFP antibody (α-GFP Ab) was incubated with the particles (particles suspended at 1 mg particles/ml of PBS-T with a 1:5000 dilution of α-GFP Ab and 1% goat serum) for 2 h at room temperature. Particles were then washed with 3 volumes of PBS-T. Colorimetric determination of HRP activity was done on a plate reader with different amounts of particle per well. 1-step Slow TMB-ELISA substrate (3,3',5,5'-tetramethylbenzidene, Pierce) was used at a substrate and absorbances measured at 370 nm. Readings from 3, 6, and 9 min were compared and shown above. Specific binding curve suggests that 10% NTA particles saturate with GFP when loaded with 120 ng GFP/mg particle.

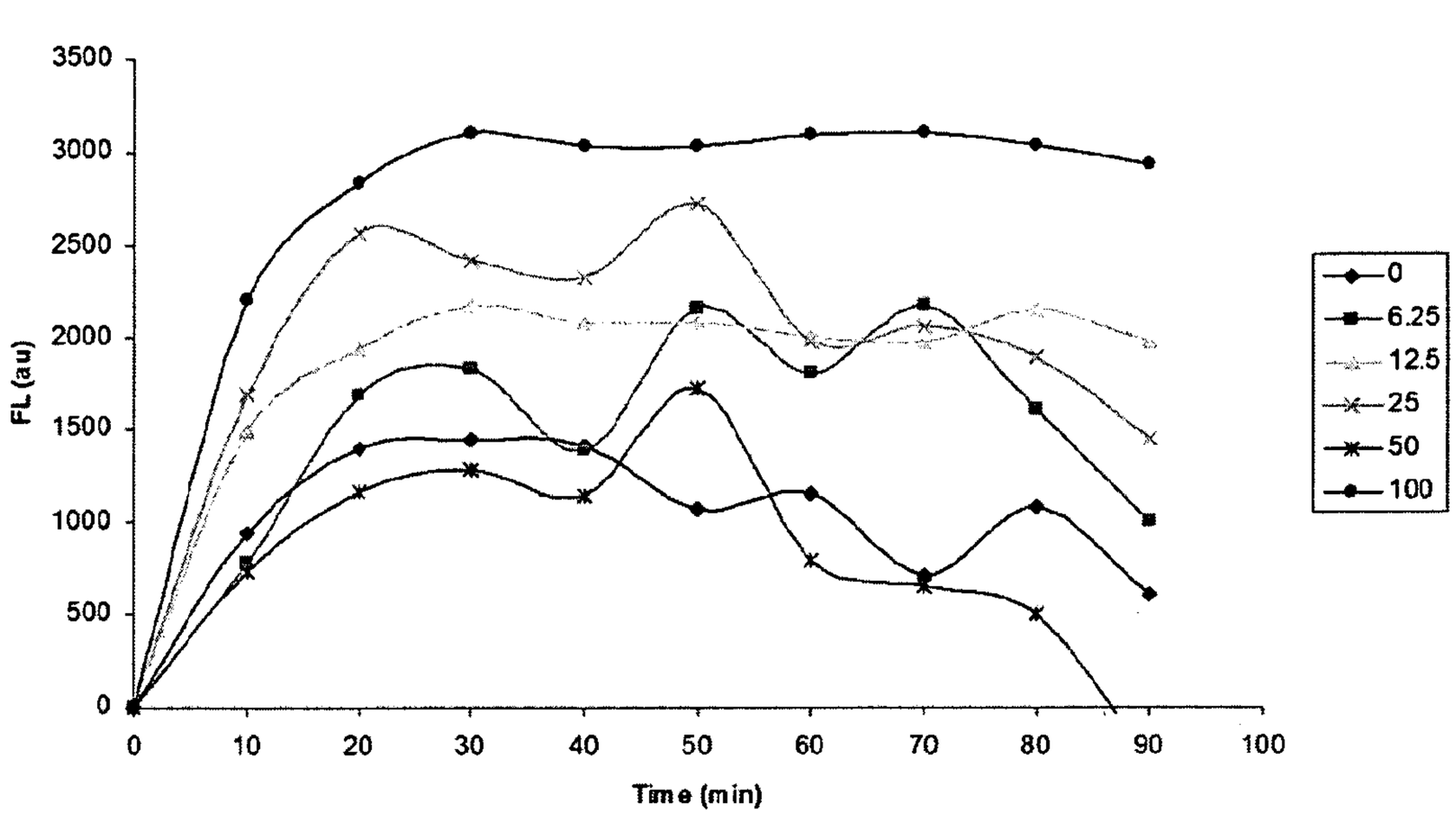

Figure 61. GFP Binding is reversible. Particles loaded with GFP were subjected to a spike of imidazole (200 mM final concentration), a competitive binding ligand to the NTA-Ni complex, and the fluorescence intensity of the supernantant measured as a function of time. Data suggests that GFP is maximally dissociated at 30 minutes in the presence of 200 mM imidazole.

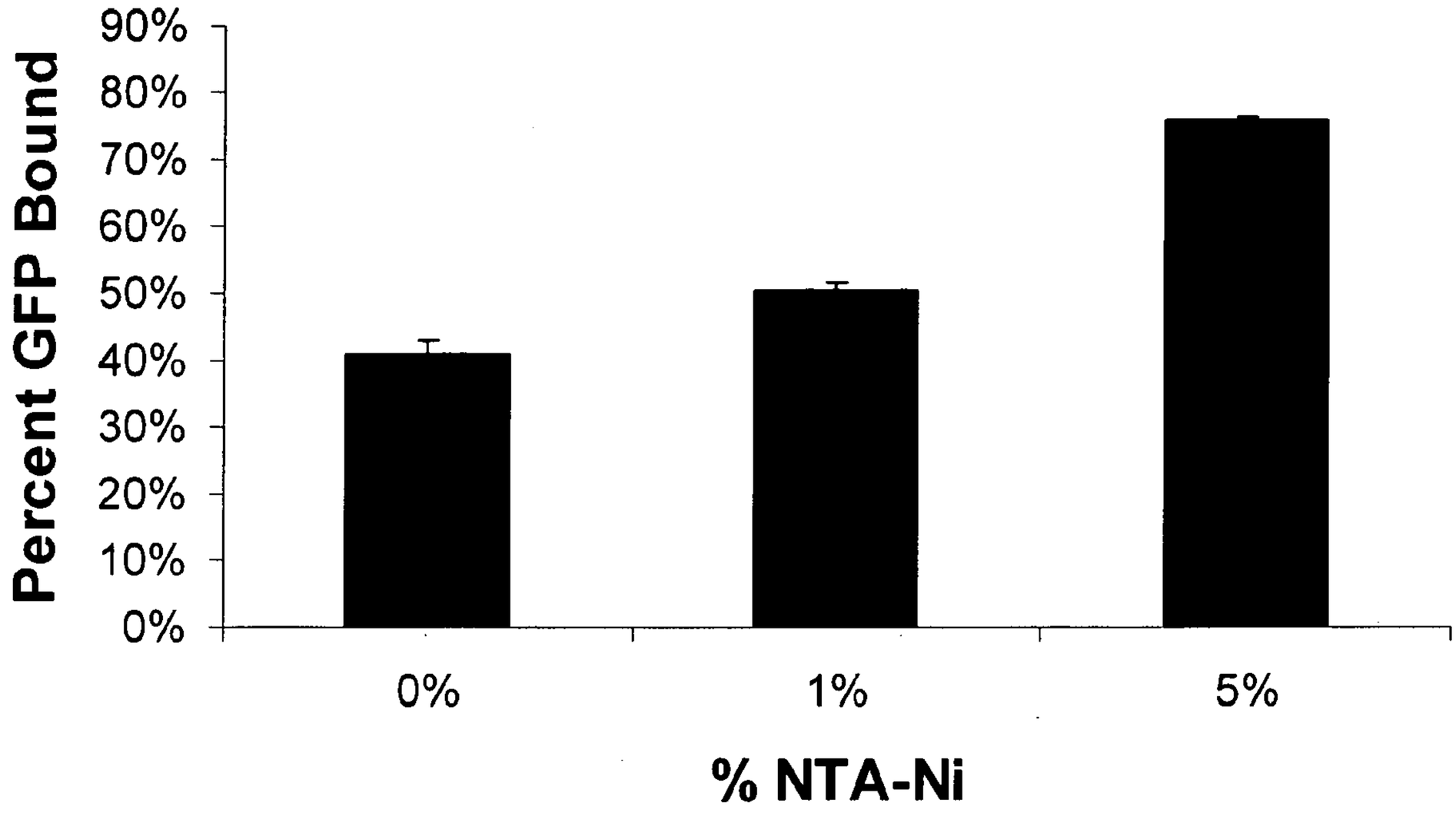

Figure 62

Polyketals from cyclohexane-dimethanol

A

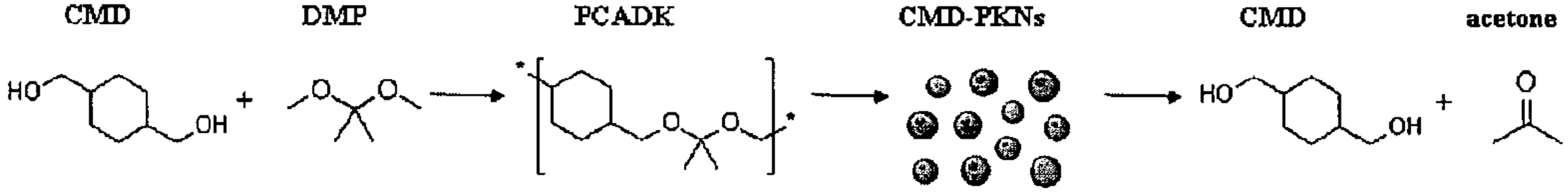

B

Hydrolysis of PCADK

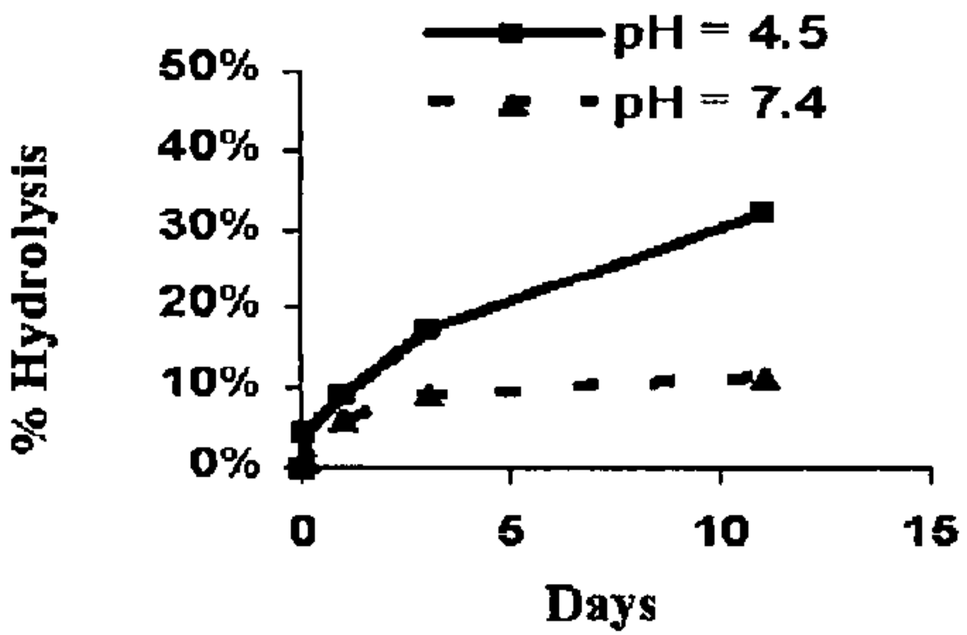

(1) Cyclohexane-dimethanol used in food packaging
(2) Acetone metabolic product of lipids
(3) PCADK Mw = 6,000, PD 1.5
(4) Yield 30-40%

FIG. 19